Open Research Online

The Open University's repository of research publications
and other research outputs

Isotopic Mapping Of Major Himalayan Structures

Thesis

How to cite:

Richards, Andy (2005). Isotopic Mapping Of Major Himalayan Structures. PhD thesis The Open University.

For guidance on citations see FAQs.

© 2005 Andy Richards


https://creativecommons.org/licenses/by-nc-nd/4.0/

Version: Version of Record

Link(s) to article on publisher's website:
http://dx.doi.org/doi:10.21954/ou.ro.0000f632

Copyright and Moral Rights for the articles on this site are retained by the individual authors and/or other copyright owners. For more information on Open Research Online's data policy on reuse of materials please consult the policies page.

oro.open.ac.uk

UNRESTRICTED

"Isotopic Mapping Of Major Himalayan Structures"

A thesis submitted for the degree of Doctor of Philosophy

Andy Richards

MGeol. (Geology) (Leicester)

2004

Department of Earth Science, The Open University

DATE OF SUBMISSION: 16 SEPTEMBER 2004
DATE OF AWARD: 4 FEBRUARY 2005

I

ProQuest Number: C824059

All rights reserved

INFORMATION TO ALL USERS
The quality of this reproduction is dependent upon the quality of the copy submitted.

In the unlikely event that the author did not send a complete manuscript
and there are missing pages, these will be noted. Also, if material had to be removed,
a note will indicate the deletion.

ProQuest C824059

Published by ProQuest LLC (2019). Copyright of the Dissertation is held by the Author.

All rights reserved.
This work is protected against unauthorized copying under Title 17, United States Code
Microform Edition © ProQuest LLC.

ProQuest LLC.
789 East Eisenhower Parkway
P.O. Box 1346
Ann Arbor, MI 48106 – 1346

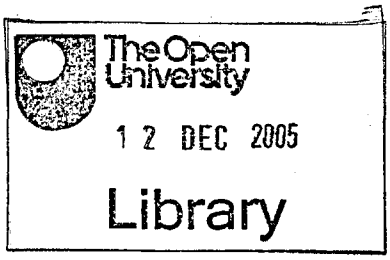

DONATION
T555.496
C

Acknowledgements

A Hungarian tourist approaches the clerk of a tobacconist's. The tourist is reading haltingly from a phrase book:

Hungarian: I will not buy this record, it is scratched.
Clerk: Sorry?
Hungarian: I will not buy this record, it is scratched.
Clerk: Uh, no, no, no. This is a tobacconist's.
Hungarian: Ah! I will not buy this *tobacconist's*, it is scratched...
('The Hungarian Phrasebook' sketch by Monty Python's Flying Circus)

Now read it again replacing the Hungarian with myself and the Clerk with any of my supervisors, that's pretty much analogous to how the past getting-on-for four years (sorry Nigel) have gone.

So firstly, I need to acknowledge my supervisors Nigel, Tom, Randy and Talat, sorry for all the 'Hungarian' type gaffs and thank you for your support, patience and encouragement over the last few years. Thanks are also due to Gav (my unofficial 5th supervisor), Mark and Lauren Godin and Erich Draganits who provided samples which really helped to make this thesis, Mark Fanning and Paul Myrow who provided data, Eduardo Garzanti for exceptionally fruitful discussions on the nature and sources of TSS sediments, Luke 'Woolly' Wooller for the tireless DEM imaging and John Taylor for the cross-section and India figures used in the text. Thanks are also due to everyone at the OU who provided heaps of help: Mabs, PVC, Jo, Lou, Parky, Mouhcine, Craig, Bruce, Nick, Fatima, Kev, Steve, John H., Liz, John W., Janet, Anita, Gill, Dick, Brandon and the cartography Gurus John and Andy (the jury is still out about Illustrator). And a pre-emptive thanks to my examiners Yani and Simon.

Thanks are also due to everyone at NIGL: Steve, Fiona, Quentin, Matt, Adrian, Jane, Ian, Beatrice, Jo, Neil, Aaron, Vanessa and Marcello for their time and endless patience. Thanks also to the 'just visiting' people who I met there, Andy, Richard, Chris and Peter.

In the field, thanks to my travelling companions Tom, Nigel, Randy, Talat, Mark and Gav, and thanks for the logistical support provided by Talat, Sunno, Harri, Namsey Travel (especially Nyima, Tensing and Embe), Mansaslu Trek (especially Cheban, Suresh and Sarba).

Not forgetting everyone else at the OU. Firstly, thanks to all my office buddies past and present: Lee, Jenny, Macca, Severs, Chris, Clive, Kempy (and for scanning

support), Jess and Russ and to everyone who didn't have the pleasure of listening to my music collection (over and over again), Tubs, Jim, Levan, Dela, Marc, Ed, Jase, Basak, Sam, Chris, Kat, Phil, Antonio "I am so ashamed", Diego and Em and thanks to housemates Luke, Nik, Dan, Dan M and Helen. Thanks to you all for helping to make life bearable (or perhaps tepid?) in Milk n' Beans. External to MK thanks to the Stevens and, even more external, the Freyers.

Of course this would all mean nothing if it wasn't for the priceless emotional (and sometimes physical!) support of the following guys, Helen (the best girlfriend in the world!), King, Dunc, Dugs, Dunno, Flobbin', Richie, Ado, Dave and Chris, and Lucy, Jo, Cel, Heike, Karen and Hills; thanks for truly being the best bunch of friends anyone could possibly want.

Due to the unique way PhD students are funded in the UK (some people, like myself, would probably describe it as stupid), I have to thank a few people who without their help, this PhD would not have seen the light of day. So Helen, Mum and Dad and my little sister, thanks for all your support along the way, I really do appreciate everything you've done for me, this is dedicate to you.

Finally, thanks to PG tips, Tea-direct (the way forward in Tea manufacture), Jake Burton and Tom Simms.

Abstract

Analysis of critical radiogenic isotope ratios (Nd and Sr) for bulk samples of metasedimentary formations with clastic protoliths, combined with U-Pb dating of detrital zircons recovered from these formations, have yielded a powerful tool for discriminating between the major lithotectonic units of the Himalayan orogen, thus defining the major tectonic boundaries that divide them in regions where such structures are often obscured by polyphase, high-strain deformation.

In the Sutlej Area, northwest Himalaya, detrital zircon age populations suggest that cratonic India has supplied both a Neoproterozoic source and a Palaeoproterozoic-Late Archaean source that have contributed detritus to the pre-Himalayan depositional basins of the High Himalayan Crystalline Series (HHCS), whereas only the latter source has contributed to the protolith of the northern exposures of the Lesser Himalayan Series (Inner LHS). Whole-rock Nd and Sr isotope systematics confirm the isotopic distinction between the HHCS and the Inner LHS and equate the protoliths of the HHCS and the Outer LHS, thus defining the Main Central Thrust (between the HHCS and the Inner LHS) and the Jutogh Thrust (between the Inner and Outer LHS). Analyses of the enigmatic Haimanta Group broadly suggest correlation with the HHCS, although stratigraphically younger samples appear to have been derived from the older, Palaeoproterozoic-Late Archaean source.

To assess the validity of this technique along strike of the Himalayan orogen, an equivalent study was undertaken in Bhutan (eastern Himalaya). Both zircon and bulk rock isotopic analyses confirm the isotopic distinction between the HHCS and much of the LHS. Although the LHS can be subdivided on isotopic grounds, these subdivisions do not lie in simple Inner/Outer zones as in the Sutlej section. Moreover, a substantial Mesoproterozoic zircon population, unobserved in the western Himalaya, is found within the HHCS. These results provide critical constraints on the evolving palaeogeographic environment within which the Proterozoic and Palaeozoic formations that constitute the core of the Himalayan orogen, were deposited.

Table Of Contents

List Of Figures

List of Tables

List Of Abbreviations

CHUR - Chondritic Universal Reservoir

CT – Chail Thrust

BM - Depleted Mantle

DSG – Daling-Shumar Group

Ga. – Billion years

HHCS - High Himalayan

ILH – Inner Lesser Himalaya

JBF – Jaishidanda-Barsong Formation

ITSZ - Indus-Tsangpo Suture Zone

JT – Jutogh Thrust

KT – Kakhtang Thrust

LA-MC-ICPMS - Laser-ablation Multi-collector Inductively Coupled Mass spectrometer

LHCN - Lesser Himalayan Crystalline Nappes

LHS – Lesser Himalaya Series

Ma. – Million years

MBT – Main Boundary Thrust

MCT – Main Central Thrust

MCTZ - Main Central Thrust Zone

MFT – Main Frontal Thrust

MHT – Main Himalayan Thrust

MSWD - Mean Square Weighted Deviates

NP – Neoproterozoic Population

OL – OutLier

OLH Outer Lesser Himalaya

PPLA – Palaeoproterozoic-Late-Archaean Population

SHRIMP - Sensitive High-Resolution Ion MicroProbe

STDS – South Tibetan Detachment System

THZ - Trans-Himalayan Zone

TSS - Tethyan Sedimentary Series

VT – Vaikrita Thrust

YCS – Yadong Cross-Structure

Chapter 1 - Introduction

1.1 Introduction

Theoretical models for the formation of mountain belts ultimately rely on the geologist's ability to identify the major lithologies, and the structures that deform them, within orogenic belts. Foremost amongst these structures are the thrust faults that provide one of the most important mechanisms for crustal thickening within zones of convergence. Where ambiguity exists in the definition of thrusts, the accuracy and precision of these interpretations are called into doubt. The aim of this chapter is to introduce the reader to the Himalayan orogenic belt and to outline the principal outstanding debate concerning the formation of the Himalaya. Citing previous work, this chapter will also outline how this project will attempt to address this debate.

1.2 The Geology Of The Himalaya

Excellent detailed geological reviews of the geology of the Himalaya are given in Heim and Gansser (1939), Gansser (1964), Le Fort (1975), Le Fort and Upreti (1999), and Hodges (2000); a summary of current knowledge is provided below.

Following two-stage rifting from Gondwana ca. 180 and 130 Ma (Hawkesworth et al., 1999 and references therein), the northward movement of cratonic India led to the closure of the Tethyan Ocean and collision with the Eurasian Plate between 65 and 45 Ma (Beck et al., 1995; Dewey et al., 1988) ultimately leading to the Himalayan orogeny and uplift of Tibet.

DEM images show the sharp contrast between the uplifted Himalaya and Tibetan Plateau (Fig. 1.1) and the low elevation and relief of the Indo-Gangetic plain to the south and the Tarim basin to the north. The Himalayan mountain belt forms a broad arc ca. 2500 km long, anchored, respectively, to the northwest and southeast by the Nanga Parbat (8125 m) and Namche Barwa (7782 m) syntaxes. This arc forms the

southern boundary of the Tibetan plateau (Fig. 1.1) which is 2000 Km wide and is characterised by low internal relief with a mean elevation of 5 Km[1] (Fielding et al., 1994).

Figure 1.1 – DEM image of the Himalayan orogeny and Tibetan Plateau, NP – Nanga Parbat, NB – Namche Barwa, image courtesy of L. Wooller.

[1] All heights in this thesis are measured from present day sea level unless otherwise stated.

Figure 1.2 illustrates the current understanding of Himalayan geology (from Hodges 2000). A remarkable feature of the Himalaya, as demonstrated by Figure 1.2, is that tectonic units and major thrusts can be traced along much of the entire length of the orogenic arc.

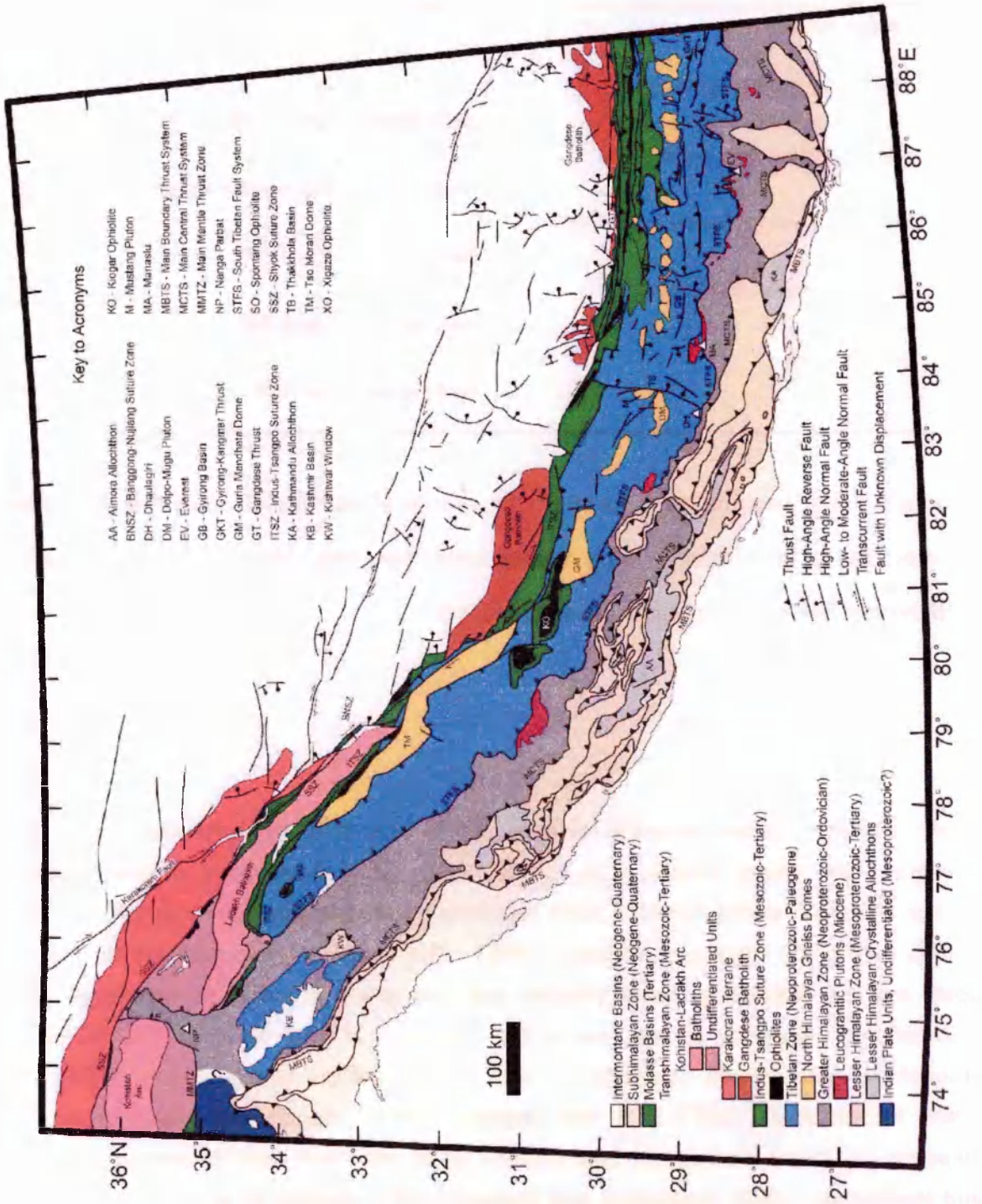

Figure 1.2 – Geological map of the Himalaya; from Hodges (2000).

Since the work of Heim and Gansser (1939) and Gansser (1964) the Himalaya has been divided into six tectonic units, separated by major bounding structures (from north to south):

Tectonic Units	**Major Bounding Structures**
Tibetan Plateau Units	
Trans-Himalayan Zone (THZ)	
	Indus-Tsangpo Suture Zone (ITSZ)
Tethyan Sedimentary Series (TSS)	
	South Tibetan Detachment System (STDS)
High Himalayan Crystalline Series (HHCS)	
	Main Central Thrust (MCT)
Lesser Himalayan Series (LHS)	
	Main Boundary Thrust (MBT)
Sub-Himalaya	
	Main Frontal Thrust (MFT)

Although it will become clear through the course of this project that the Himalayan architecture is undoubtedly more complicated than this, these distinctions will be employed in the following description for clarity.

1.2.1 Tibetan Plateau Units

Tibet consists of three separate terranes, which are, from north to south: Kun Lun, Qiangtang and Lhasa (Dewey et al., 1988), which were successively sutured onto the southern margin of the Eurasian plate following northward movement across the Neo-Tethys during the Mesozoic (Windley, 1995). The underlying mechanisms for plateau uplift are the subject of some dispute, but one group of uplift models invoke the gravitational response to the convective removal of the base of the thickened lithosphere below Tibet, resulting in uplift of the plateau (England and Houseman, 1989; Molnar et al., 1993; Platt and England, 1994). Equally the timing of uplift is disputed, as many models attribute plateau uplift with east-west extension, (England and Houseman, 1989; Houseman and England, 1993; Royden et al., 1997), therefore dating the timing of the initiation of east-west extension is believed to date the age of uplift of the plateau. Estimates vary between Mid to Late Miocene; ca. 8 Ma for cooling histories from central Tibet suggest ca. 8 Ma for the maximum elevation of

Tibet (Harrison et al., 1992, 1995; Molnar et al., 1993), whereas $^{40}Ar/^{39}Ar$ cooling ages from micas (Tibetan Plateau region of north-central Nepal) suggest a minimum age of pre–14 Ma for east-west extension (Coleman and Hodges, 1995; Searle, 1995). A recent investigation into the palaeoaltitude of the plateau using fossil leaves found that the present day elevation of ca. 5000 m in southern Tibet has probably remained unchanged for the past 15 Ma (Spicer et al., 2003).

1.2.2 Trans-Himalayan Zone

The Trans-Himalayan Zone (THZ) lies on the southern margin of the Tibetan Plateau; it is bounded to the south by the Indus-Tsangpo Suture Zone (ITSZ) and can be traced discontinuously for ca. 2500 Km (Windley, 1995). The THZ can be geologically separated into two distinct zones, the Trans-Himalayan Batholith and Kohistan-Ladakh Island Arc.

The Trans-Himalayan Batholith (also referred to as the Gangdese or Kangdese Batholith) is a discontinuous body of intrusions outcropping north of the ITSZ. It represents an Andean-type margin consisting of Ordovician-Cretaceous slates, phyllites, schists, gneisses, amphiboles and migmatites, overlain by volcanic rocks including andesites, dacites, rhyolites and ignimbrites. The supracrustals are intruded by Late Cretaceous to Eocene granodioritic-granitic plutons (Windley, 1995 and references within).

Towards the west, the Karakoram Batholith is separated from the Kohistan-Ladakh Island Arc by the Northern Suture (also known as the Shyok Suture Zone) (Fig. 1.2). This island arc is considered by Coward et al. (1987) to be the most complete section through an exposed island arc yet identified.

The THZ accreted to the southern margin of the Lhasa block prior to India-Asia collision (Searle et al., 1999 and references within), leading researchers to propose a two-stage deformation history for the THZ; initial collision of the Kohistan-Ladakh

Island Arc (soft collision) was followed by collision of the Indian continent (hard collision) (Windley, 1995).

1.2.3 Indus-Tsangpo Suture Zone

The Indus-Tsangpo Suture Zone (ITSZ) (also referred to as the Yarlung-Zangbo Suture) forms the boundary between the THZ and the Tethyan Sedimentary Series (TSS); furthermore, it marks the boundary between the Eurasian and Indian plates. West of Ladakh, the ITSZ narrows and wraps around the Nanga Parbat Syntaxis where it is termed the Main Mantle Thrust, or the Southern Suture, thus differentiating it from the Northern Suture to the north (Hodges, 2000). The ITSZ consists of a melange of incomplete ophiolites and Tethyan sedimentary rocks, including Permian to Triassic limestones, Mesozoic volcaniclastic strata and Cretaceous to earliest Eocene turbidites. Of all the ophiolites, only the Xigaze ophiolite occurs exclusively within the ITSZ; the rest occur as klippen and half klippen (Hodges, 2000; and Fig. 1.2). Recent research by Aitchison et al. (2000) and McDermid et al. (2002) in this complex suture zone have led to discrimination and identification of a number of separate units that will not be considered in detail here.

1.2.4 Tethyan Sedimentary Series

The Tethyan Sedimentary Series (TSS) lies to the south of the ITSZ and to the north of the South Tibetan Detachment System (STDS; or South Tibetan Fault System). Prior to the discovery of the STDS (Burg et al., 1984), the boundary with the underlying High Himalayan Crystalline Series (HHCS) was regarded as a profound unconformity (Gansser, 1964). The TSS is broadly defined as a near continuous, lower Palaeozoic to mid-Eocene, thick (10-15 Km) fossiliferous sedimentary package (Godin, 2003; Hodges, 2000 and references therein) and are regarded as passive margin deposits of the northern edge of India (for example Garzanti, 1999). The TSS has been studied in Zanskar, Ladakh, central Nepal and south-central Tibet; Garzanti

(1999) provides an excellent detailed examination of the TSS in Nepal (Ordovician to Late Cretaceous), separating the succession into six separate units, on the basis of fossil and sedimentary evidence that can be related to the break up and rifting of the Indian craton. Importantly, Garzanti (1999 and references therein) observed noticeable volcanogenic input within certain stratigraphic successions and related these to known coexisting magmatic events including production of the Panjal Traps and Mesozoic arc formation. Furthermore, Godin (2003) provides an excellent study on the structural evolution of the TSS in central Nepal establishing a five phase deformation history, with three phases of folding (D_1, D_2, D_4) and two phases of extension (D_3, D_5); palinspastic bed-length restoration of the TSS implies a minimum of 150% vertical thickening and 43% shortening in the Palaeozoic strata, which is less than previous minimum shortening estimates of Searle et al. (1997a) in Zanskar, Steck et al. (1993) in northwest Himalaya and Ratschbacher et al. (1994) in Tibet. These estimates for vertical thickening and shortening proposed by Godin (2003) are compatible with the structural fan model of Godin et al. (1999; 2001). Neotectonic observations (Ni and Barazangi, 1985) suggest that earthquakes exploit similar structures in the TSS, in the upper reaches of the Sutlej Valley (Himachal Himalaya).

The lowermost TSS as exposed in Zanskar (Gaetani and Garzanti, 1991) lies above a Cambro-Ordovician unconformity (Garzanti et al., 1996; Garzanti et al., 1999; Godin, 2003 and references therein). Underlying this unconformity are metamorphically higher grade rocks, as exposed in the Sutlej Valley (the Haimanta Group; see Chapter 2) and Bhagirathi Valley (the Martoli Formation; Metcalfe, (1993); the Harsil Formation; Prince, (1999), referred to as the Harsil Formation from hereon). The Haimanta Group exhibits vestiges of pre-Himalayan deformation not observed in the younger (Cambro-Ordovician) TSS (Grasemann et al., 1997; Wiesmayr and Grasemann, 2002) whereas the Harsil Formation exhibits similar P-T-t paths to the underlying Vaikrita Formation (HHCS) (Foster et al., 2000). Therefore, the Haimanta Group and Harsil Formation provide complications to the initial definition of the TSS, as these rocks lie above the STDS, but exhibit much higher grade metamorphism than

the TSS *sensu stricto*; therefore, throughout this thesis the term TSS will refer to all rocks lying above the STDS. The Haimanta Group and Harsil Formation support the proposition of Fuchs (1987) who regards the TSS as an autochthonous stratigraphic succession with the lower part metamorphosed to become the HHCS.

1.2.5 High Himalayan Crystalline Series

The High Himalayan Crystalline Series (HHCS) (also referred to as the Greater Himalaya or Central Crystallines) forms the metamorphic core of the Himalayan orogen, and is bounded by the STDS to the north and the Main Central Thrust (MCT) to the south. The HHCS is a continuous body of high-grade metasedimentary and metaigneous rocks intruded by granites and leucogranites. The largest, and arguably the best, exposures of this unit are within central Nepal, where a large number of studies have focused (Hodges, 2000 and references therein; Searle et al., 2003). Within central Nepal Le Fort (1975) proposed that the HHCS can be separated into three formations:

Formation I – The thickness of this unit varies between 1 and 20 Km (Hodges, 2000). The basal portion consists of kyanite to sillimanite – garnet – two - mica banded gneiss of pelitic to arenaceous composition, whereas the upper portion consists of an augen gneiss with quartzite and calcsilicate intercalations. Metamorphic assemblages indicate a metamorphic grade of middle to upper amphibolite facies.

Formation II – The thickness of this unit is relatively consistent, between 2 to 4 Km (Hodges, 2000), with coarse, thick, quartzites at the base, forming a sharp boundary with Formation I. Calcsilicates (with alternating pyroxene calc gneisses and marbles) dominate the lower portion, whilst the upper portion contains more micaceous and finer calcsilicate layers. Metamorphic assemblages are consistent with Formation I (middle to upper amphibolite facies) leading Colchen et al. (1986) to interpret these two formations as a conformable package.

Formation III – The basal portion of this unit is poorly exposed, characterised by a greater proportion of pelitic to greywacke layers, whilst the upper portion consists of ca. 300 m thick coarse augen gneisses, that can be traced over several hundred kilometres from eastern to central Nepal. According to Hodges (2000) this unit is constant with similar lithologies observed at similar structural levels in Bhutan and Zanskar; furthermore, he supports the interpretation of Colchen et al. (1986) and Le Fort (1975) that this unit represents a volcano-sedimentary horizon protolith.

However, along-strike variation within the regional Himalayan context demonstrates the difficulty of tracing these formations outside central Nepal. For example: within the Sutlej Valley (Chapter 2) exposures of the HHCS are considerably thinner and its interpretation is complicated by the presence of high-grade rocks that may represent Lesser Himalaya material (Vannay and Grasemann, 1998; 2001; Vannay et al., 2004; 1999). Within Bhutan (Chapter 4) the HHCS is complicated by internal thrusting (the Kakhtang Thrust; Daniel et al., 2003). Furthermore, correlation of rocks within the higher-grade Nanga Parbat Syntaxis with the formations proposed by Le Fort (1975) proves difficult on lithological grounds (Hodges, 2000).

The HHCS is intruded by a variety of leucogranites that have been studied in some detail by numerous authors (see Hodges, 2000; Singh and Jain, 2003 and references therein). These leucogranites generally form sheeted complexes that display cross-cutting features. They have been subdivided into two-mica, tourmaline-muscovite and tourmaline-two-mica bearing leucogranites (e.g. Inger and Harris, 1993). Although the precise conditions of their formation remains debatable, isotopic studies clearly indicate that these granites are crustal melts, derived from the HHCS during the Early Miocene (Harris and Massey, 1994).

The maximum age of deposition of the HHCS can be constrained from Neoproterozoic detrital zircons derived from Nepal that yield $^{207}Pb/^{206}Pb$ ages of 967 Ma (Parrish and Hodges, 1996) and 833 Ma (DeCelles et al., 2000), whereas the minimum age can be

constrained from intruding Cambro-Ordovician granites, suggesting that the protolith sediments were deposited between the Neoproterozoic and Ordovician. Zircon populations from the stratigraphically younger TSS deposits have a similar age population spectra to the HHCS with an additional Cambro-Ordovician spectra, interpreted by Gehrels et al. (2003) to have also sourced similar protoliths to the HHCS in addition to the Cambro-Ordovician granites. Prior to such isotopic investigations Schelling and Arita (1991) had estimated a Pre-Cambrian age for this unit.

1.2.6 Lesser Himalayan Series

The Lesser Himalayan Series (LHS) (also referred to as the Lesser Himalaya Formation or Lesser Himalaya) is traditionally defined as a tectonic unit bounded to north by the MCT and to the south by the Main Boundary Thrust (MBT); the areal extent of the LHS narrows considerably in eastern Nepal, in contrast to the exposure in the northwest Himalaya (Fig. 1.2). The LHS consists of up to 10 Km of lower-greenschist to lower-amphibolite impure quartzites, psammites, phyllites and schists with infrequent calcsilicates, marbles, dolomites, amphibolites and augen gneisses within a complex fold and thrust system (Hodges, 2000 and references within). Fossils are rare throughout much of the LHS, but a Palaeoproterozoic depositional age has been inferred on the basis of detrital zircons (DeCelles et al., 2000; Parrish and Hodges, 1996). Furthermore Miller et al. (2000) dated zircons from a metabasalt interbedded with the Rampur Formation that yielded a U-Pb evaporation age of ca. 1800 Ma (interpreted by Miller et al. as an extrusion age, discussed further in Chapter 2). In the absence of fossils constraints, Valdiya (1995) separates the LHS into three broad sub-sections:

1. Early Purna sedimentation
2. Middle Purna sedimentation
3. Protean sedimentation

Valdiya (1995) in northwest India terms the Protean (assigning a Neoproterozoic age) as the Outer Lesser Himalaya (OLH) and the Early and Middle Purna (assigning a Mesoproterozoic age) as the Inner Lesser Himalaya (ILH). Srivastava and Mitra (1994) separate these units along the out-of-sequence Tons Thrust (Garhwal Himalaya), which supports the isotopic investigations of Ahmad et al. (2000). Out-of-sequence thrusting in the Nepalese Himalaya has been recognised in eastern Nepal by Schelling (1992), and has been invoked by Harrison et al. (1999) and Robinson et al. (2001) to explain metamorphic and isotopic trends. For example the Mahabharat thrust (Upreti and Le Fort, 1999) is an out-of-sequence thrust that may represent the lateral equivalent of the Tons thrust. High incision rates have produced a number of tectonic windows and half-windows throughout the Himalaya exposing the oldest (Early Purna) sediments such as in the Arun and Sutlej valleys (the Kuncha Group and Rampur Formation (Chapter 2), respectively). A Carboniferous to Permian succession termed the Tansen Group (Amatya et al., 1994) and also referred to as the Gondwana units (Paudel and Arita, 2000), is observed to crop out discontinuously in east Nepal and Sikkim (Gansser, 1964) and overlies the older LHS units unconformably.

Lesser Himalayan Crystalline Nappes

A series of crystalline nappes or thrust sheets have been assigned to the LHS, described here as the Lesser Himalayan Crystalline Nappes (LHCN) (also referred to as Lesser Himalayan Crystalline Allochthons). LHCN have been observed in the western and central Himalaya, and include the Jutogh-Munsiari Nappe in India (Pandey et al., 2004) and the Karnali, Jajarkot, Dadeldhura, Parchauni and Kathmandu nappes in Nepal (Upreti, 1999; Upreti and Le Fort, 1999). There has been considerable debate as to the origin and tectonic rooting of these nappes; Upreti and Le Fort (1999) have reviewed the LHCN in Nepal and conclude that the high-grade gneissic Karnali Nappe is clearly rooted within the HHCS. However, the Jajarkot, Dadeldhura and Parchauni Nappes cannot be rooted to the HHCS and are considered to have a different exotic origin by the same authors. Furthermore, Upreti and Le Fort interpret the Kathmandu

Nappe (Stoecklin, 1980) as two separate terrains that have been juxtaposed by thrusting of the MCT and the later (southern) Mahabharat thrust (both of which they interpret as splays from the same decollement); the upper terrain is interpreted to be rooted in the HHCS, whereas the lower has a similar 'exotic' origin to the Jajarkot, Dadeldhura and Parchauni nappes. Upreti and Le Fort (1999) interpret these exotic terrains to have lain spatially between the LHS to the south and the HHCS (protolith) to the north prior to the Himalaya orogeny and to have evolved with a different geologic history compared to the LHS and HHCS, whereas Vannay and Grasemann (1998; 2001) and Vannay et al. (2004; 1999) interpret the LHCN (Jutogh-Musari Nappe) as Indian basement material (Chapters 2 and 3).

1.2.7 The Sub-Himalaya

The Sub-Himalaya extends laterally along the length of the Himalaya and is traditionally interpreted as molasse sediments that have derived from the eroding Himalayan mountain belt (Gansser, 1964). This unit is over-thrust from the north by the MBT and is separated from the Indo-Gangetic plain to the south by the Main Frontal Thrust (MFT). The Sub-Himalaya thickens northwards and ranges in stratigraphical thickness from between 2 and 10 km. Exposures in the western Himalaya (Pakistan) are stratigraphically separated into Oligocene to lower Miocene siltstones and sandstones of the Rawalpindi Group which underlies the lower Miocene to Pleistocene mudstones, siltstones, sandstones and conglomerates of the Siwalik Group (Hodges, 2000). The Indian Sub-Himalaya is further subdivided as summarised below in Table 2.7 (Najman et al., 1993). In the Nepalese Himalaya the Siwalik Group (or Churia) is separated into lower, middle and upper Siwalik (Mugnier et al., 1999; Upreti, 1999). Incomplete sections are found in the Bhutanese Himalaya (Gansser, 1983).

Investigations within the Sub-Himalaya have implications for the interpretations of the evolution of the Himalaya, including applications to recent exhumation models

(Beaumont et al., 2001; 2004; Jamieson et al., 2004). Detrital micas dated in the Sub-Himalaya suggest that major exhumation of the orogen did not occur until 28 Ma (Najman et al., 1997).

1.3 Formation and Metamorphism of the Himalaya

1.3.1 Pre-Himalayan?

Data supporting pre-Himalayan tectonism and metamorphism (reviewed in Gehrels et al., 2003) include: intrusion of ca. 500 and 1800 Ma granites (Singh and Jain, 2003 and references therein), a ca. 535 Ma Sm/Nd garnet age (Argles et al., 1999; Prince, 1998), bulk rock Sr-isotope homogenisation within the HHCS at ca. 500 Ma (Ahmad et al., 2000) and Cambro-Ordovician uplift and deformation of the Haimanta Group (Grasemann et al., 1997; Valdiya, 1995; Wiesmayr and Grasemann, 2002; Chapter 2). Outcrops demonstrating pre-Himalayan deformation are difficult to identify, as it is likely that metamorphic fabrics have been overprinted by the Himalayan orogenic event itself, but have been recognised in the Nanga Parbat Syntaxis (Wheeler et al., 1995), Sutlej Valley (Marquer et al., 2000) and central Nepal (Gehrels et al., 2003 and references therein).

Hodges (2000) provides an excellent review of the Himalayan structural and metamorphic geological history suggesting separation into three discreet stages:

1. Protohimalayan (*Cretaceous-Early Eocene*)
2. Eohimalayan (*Middle Eocene-Late Oligocene*)
3. Neohimalayan (*Early Miocene-Present*)

1.3.2 Protohimalayan Events

The protohimalayan episode began prior to the collision of Indian and Eurasian plate and concerns deformation in the Transhimalaya, ITSZ and ophiolite obduction. A minimum age for obduction is known from overlying unconformable Early Eocene sediments, whereas late Cretaceous sediments provide a maximum age (Searle et al., 1997a). Protohimalayan blueschist facies metamorphism is observed within the Transhimalaya, ITSZ and Zanskar. High-pressure metamorphism is also observed in the Kohistan-Ladakh Island Arc above the Main Mantle Thrust (Hodges, 2000).

1.3.3 Eohimalayan Events

These events occurred during the period of the India-Eurasian collision, dated to between 65 and 45 Ma (Beck et al., 1995; Dewey et al., 1988; Rowley, 1996). However, the exact timing of this event is dependant on which of several proxies is invoked for collision. These include the transition from marine to non-marine sedimentation and the timing of prograde eclogite metamorphism. Structures attributed to Eohimalayan convergence include fold and thrust nappes in Ladakh, upright folds and steep north-dipping reverse faults within the TSS just south of the ITSZ. Neohimalayan metamorphism is likely to have overprinted Eohimalayan metamorphic fabrics (as described by Lombardo and Rolfo, 2000) and according to Guillot et al. (1999) Eohimalayan metamorphism is more pervasive in the western Himalaya due to rotation of the Indian plate during collision. Examples of Eohimalayan metamorphism include: eclogite facies rocks in the footwall of the Main Mantle Thrust in Pakistan (Pognante and Spencer, 1991) and high-pressure amphibolite to granulite facies metamorphism in Zanskar (Vance and Harris, 1999).

1.3.4 Neohimalayan Events

This period is often described as the main mountain building event that is responsible for the current Himalayan architecture; this period is also responsible for generating some of the main areas of controversy in Himalayan geology, as discussed below. Neohimalayan structures are conspicuous throughout all major Himalayan units, and can be separated into thrust, extension and strike slip.

Major thrust structures include the north dipping, east-west striking, southerly directed major tectonic thrust faults that separate the major Himalayan units described above. Prior to Burg et al. (1984) the STDS was regarded as a thrust (e.g. Gansser, 1964) which was later exploited as a normal fault; Corfield and Searle (2000) interpreted this as a response to gravitational collapse. The MCT is now structurally the highest and oldest of all the major thrusts in the Himalaya, although its existence within the Nanga Parbat Syntaxis is disputed (Pogue et al., 1999; Whittington et al., 1999) and it remains elusive due to poor access to exposures within the Namche Barwa Syntaxis. Excellent exposures of this thrust in Nepal and northwest India contain kinematic indicators that imply a polyphase deformation history for the MCT, which is often referred to as a zone (MCTZ) ranging from meters to kilometres of deformation, developed from a melange of both HHCS and LHS rocks (Hodges, 2000 and references therein). A two-stage deformation history is suggested from Early Miocene (Hodges et al., 1996) and late Miocene to Pliocene (Catlos et al., 2002 and references therein) mineral ages from the MCTZ. Neotectonic observations including thermal springs observed along the current trace of the MCT (Evans et al., 2001) and earthquakes, suggest that this thrust may still be at least locally active. Gansser (1964) estimated displacement along the MCT to be greater than 100 Km, whereas Schelling (1992), using balanced cross sections and field observations, revised this estimate to between 175 and 210 Km.

The MBT lies structurally below the MCT and is marked by breccia ca. 100 m thick. It can be traced for greater distances than the MCT (Fig. 1.2), although is only discontinuously observed in the eastern Himalaya due to poor outcrop. Throw along

the MBT is estimated to be of the order of tens of kilometres (Hodges, 2000). In northwestern India where exposure of this thrust zone is excellent, sedimentation rates and fission tracks suggest that MBT activity was coeval with late stage MCT movement ca. 10 Ma (mid to late Miocene), with displacement rates of ca. 10 mm/year (Meigs et al., 1995). Complimentary sedimentalogical and Ar^{40}/Ar^{39} studies in Nepal suggest the MBT became active in latest Miocene to early Pliocene times (Decelles et al., 1998, 2001).

The MFT is structurally the lowermost south-directed major thrust. Exposure is often poor and the location of the thrust is frequently inferred from neotectonic structures. It represents a decollement and, like the MCT, is a splay of the Main Himalayan Thrust (MHT; also known as the Himalayan Sole Thrust) as inferred from INDPETH seismic profiles (Hauck et al., 1998; Tilmann et al., 2003; Zhao and Nelson, 1993).

Steep, south-dipping, north-directed thrusts are also observed in the Himalaya and confined mainly to the ITSZ and Transhimalaya but are interpreted to have an insignificant role in overall Neohimalayan shortening. However, according to Searle et al., (1997a) similar structures in Zanskar are related to pop-up structures and may account for considerable shortening in the area.

Hodges (2000) separates extensional structures in the Himalaya into five classes. Many of these structures are restricted to Tibet and are associated with gravitational collapse of the Himalaya (e.g. Corfield and Searle, 2000) and gravitational spreading of the Tibetan Plateau (e.g. Molnar et al., 1993). These structures will not be further considered here. Of interest to this project are the extensional structures that occur above and within the HHCS and LHS. A series of low-angle, normal faults, designated the STDS, was discovered in Tibet by Burg et al. (1984) and is now recognised from northwest India to Bhutan. The STDS is defined as at least one low-angle, north-dipping brittle fault, with a 500-1000 m thick zone of mylonites in the footwall (Hodges, 2000). It is spectacularly observed in the southwest face of Everest where

two normal faults (Qomolangma and Lhotse detachments) separate the HHCS from the TSS; minimum displacements of the STDS are estimated to be 40 Km (Searle, 1999; Searle and Godin, 2003). Further examples of STDS related structures include riedel shears in the Sutlej Valley (Chapter 2). Kinematic indicators in northern Nepal suggest polyphase and poly-dimensional deformation along the STDS, including strike-slip and oblique-slip movements (Hodges, 2000). Godin et al. (2001) dated episodic deformation associated with STDS movement in central Nepal at ca. 23 Ma and 11 Ma. Further examples of normal faulting are documented within the Sutlej valley where minor scale normal faults are observed within the HHCS (Karcham Normal Fault: Janda et al., 2003; Chapter 2).

Major strike slip structures within the Himalaya that are of importance to this project include the Yadong Cross-Structure (YCS), located to the northwest of Bhutan. This represents the largest cross-structure discontinuity in the Himalaya, with a sinistral strike-slip off-set of ca. 70 km of the STDS (Wu et al., 1998). The YCS appears to mark an important change in the recent architecture of Himalayan thrusting; east of the structure, out-of-sequence thrusting is observed in the HHCS where the Kakhtang Thrust (Chapter 4) cuts MCT fabrics (Davidson et al., 1997), whereas west of the structure, out-of-sequence thrusting is observed in the LHS (Schelling, 1992; Schelling and Arita, 1991).

Neohimalayan metamorphism within the Himalaya is recorded in structurally higher portions of the LHS and throughout the HHCS. The Tibetan gneiss domes and structurally lower portions of the Transhimalaya also record Neohimalayan metamorphism but will not be considered further in this study. The grade of Neohimalayan metamorphism in both the LHS and HHCS increases structurally upwards towards the MCT and STDS respectively. This phenomenon is known as inverted metamorphism and was first observed by Heim and Gansser (1939). In pelitic rocks of the HHCS estimated peak temperatures range from 500 to 550°C in the roof of the MCT to >650 to 700°C in the upper HHCS, with corresponding metamorphic

zones increasing from kyanite, to sillimanite and muscovite, sillimanite and K-feldspar and finally to sillimanite and K-feldspar and cordierite. Although kyanite-bearing leucogranites are observed in some sections in Nepal, the sillimanite isograd generally represents the first appearance of anatectic leucosomes; as metamorphic grade increases, leucogranite bodies become more frequent. Within the LHS, metamorphic grade increases towards the MCT from the chlorite zone to biotite, then to garnet, with garnet, biotite, muscovite and staurolite assemblages sometimes observed in the footwall of the MCT. Kyanite and sillimanite bearing assemblages at this structural level are interpreted as disrupted slivers of HHCS due to late Neohimalayan slip on the MCT, which resulted in a tectonic melange of LHS and HHCS in the MCTZ.

1.4 Outstanding Debates

1.4.1 Inverted metamorphism

Considerable controversy surrounds interpretations of the Neohimalayan structures and metamorphism. One particular debate is the apparent inverted metamorphic sequences within the HHCS and uppermost LHS (and MCTZ). The above section has described the metamorphic facies that define the inverted metamorphism in the Himalaya. Several models have been proposed to explain the inverted metamorphism as reviewed by Harrison et al. (1999), who distinguishes four general groups of models:

1: Inverted metamorphism developed within the footwall (LHS) of the MCT and anatexis in the hanging wall (HHCS) are spatially and temporally related by thrusting.
2: Thrusting results from HHCS anatexis.
3: HHCS anatexis results from normal faulting.
4: Apparent inverted metamorphism in the footwall (LHS) of the MCT is produced by deformation of two right-way-up metamorphic sequences.

However, none of these models adequately explains all the available observations; most notably, these models fail to take into account the fact that the inverted metamorphic sequences in the HHCS and LHS and anatexis of the HHCS did not occur synchronously.

More recently, Beaumont et al. (2001) proposed a further model that better explains the available data and includes the interpretations of Grujic et al. (1996) who, based on quartz deformation microfabrics, proposed a channel flow model of the HHCS that predicts the highest extrusion velocities are located in the centre of the channel (HHCS). Vannay and Grasemann (2001), based on pure and simple shear kinematic modelling, propose a 'general shear model' that induced a ductile extruding wedge (HHCS). Beaumont et al. (2001), and later Beaumont et al. (2004) and Jamieson et al. (2004), proposed a thermo-mechanical numerical model that suggests ductile extrusion and channel flow of a low viscosity zone are dynamically linked to focused surface denudation and topography of a plateau that is underlain by low-viscosity material (Fig. 1.3). Furthermore the channel flow model is consistent with the findings of Hodges et al. (1992) and Burchfiel et al. (1992) who observed simultaneous Miocene movement on both the STDS (extension) and MCT (compression). Searle et al. (2003) suggests that if the rocks of the hanging wall of the STDS remained fixed whilst the rocks of the footwall were extruded southwards, the STDS does not relate to gravitational collapse or spreading as proposed by Corfield et al. (2000) and Molnar et al. (1993). The Beaumont model is similar in many respects to that of Huerta et al. (1996) who proposed that in a theoretical orogenic belt a wedge of material (rather than a low viscosity, mid-crustal channel, as proposed by Beaumont et al., 2001; Grujic et al., 2002) is extruded to the south; denudation controls the wedge geometry and enhances heating within the upper plate. It seems curious that this work is not recognised by the Beaumont team some five years later.

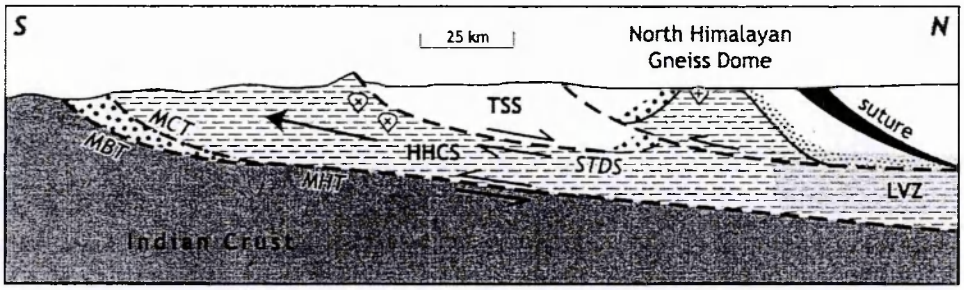

Figure 1.3 - Cross-section of the Himalaya demonstrating the extrusion of the HHCS according to the channel flow model, LVZ; low viscosity zone; see text for further abbreviations, image courtesy of N. Harris and J. Taylor.

1.4.2 The MCT

The location of the MCT is crucial to understanding the thermal evolution and inverted metamorphism of the Himalaya and an important factor in distinguishing between differing mechanisms for burial of the metamorphic rocks. Indeed the significance of theoretical thermo-mechanical mathematical models such as the Beaumont Model rely on the ability to define and test parameters in the field including the location of the MCT and therefore the structural thickness of the extruding channel (Beaumont et al., 2004; Jamieson et al., 2004). Furthermore, precise knowledge of the location of major Himalayan thrusts is paramount to unravelling the tectonic and sedimentary history of the Himalayan orogen. The STDS and MBT are both relatively brittle faults that can be distinguished readily in the field, especially since the STDS frequently is observed to juxtapose high-grade HHCS against low grade TSS along much of its length. However, correct identification of the MCT has caused considerable controversy due to the difficulty of its recognition in the field. A review of the MCT placement and the resulting controversy in the Sutlej Valley is given in Chapter 2. Indeed, it is widely believed that this thrust can be traced laterally across much of the Himalaya (Fig. 1.2) yet there remains a lack of consensus as to how this major thrust is defined; lithological, metamorphic and structural criteria have all been invoked.

Lithologically, the MCT was first defined as the juxtaposition of higher-grade (upper amphibolite) gneisses over lower-grade (lower amphibolite and greenschist) metamorphosed sediments (Heim and Gansser, 1939). Lombardo et al. (1993),

Myrow et al. (2003) and DeCelles et al. (2000), amongst many others, also define the MCT lithologically; furthermore, on the basis of isotopes, DeCelles et al. (2000) interprets the MCT as a terrane boundary invoking large-scale displacement, whereas Myrow et al. (2003), using similar isotopic techniques, regard movement on the MCT on much smaller scale (see later in this section), which supports the balanced cross-sections of Searle (1986). Contrastingly, Pogue et al. (1999) used lithological variations in Pakistan to argue against the existence of the MCT in that area, whereas isotopic data from Whittington et al. (1999) suggests the existence of the MCT in the Nanga Parbat syntaxis area.

Metamorphically, the MCT is defined either using isograds, or by contrasting the metamorphic styles above and below the MCT. The kyanite isograd is often used to demarcate the MCT (Valdiya, 1980; Vannay and Hodges, 1996) although chlorite-out (Inger and Harris, 1992) and muscovite-out in the sillimanite zone have been used (Lal et al., 1981 in Ahmad et al., 2000). Caddick (2004) and Vannay and Grasemann (1998) in the Sutlej Valley, northwest India, contrast the P-T-t paths of the HHCS and LHS and thus define the MCT. However, this approach is restricted to sections where good metamorphic minerals are present in the footwall of the MCT.

Structurally, the MCT is defined by Stephenson et al. (2000) as a large-scale high strain zone of distributed deformation, typically characterised by a single well developed foliation. Stephenson et al. (2000) argue that the MCT can only be defined in a structural sense as definitions based on metamorphic and lithological criteria vary in different sections. However, lithological variations are likely to control both Barrovian metamorphic assemblages and structural deformation due to rheological variations in the deforming rock.

There remains a major controversy in Himalayan literature regarding definitions and placement of the MCT, which can be traced back to Heim and Gansser (1939) who noted the juxtaposition of higher grade (upper amphibolite) gneisses against lower

grade (lower amphibolite and greenschist) metamorphosed sediments when working in Kumaon (northwest Himalaya). They later described the MCT in the following terms: *"Then comes a sudden change, for, after an intermediate layer of phyllite, we suddenly reach a gorge of gneiss dipping gently to the north-north-east. Unquestionably we stand before a great over-thrust coming from the North."*

In addition they separated the rocks in the hanging wall into Upper and Lower Crystalline Units, which Fuchs and Franks (1970) observed to be fault bounded. French workers in Nepal (Bordet et al., 1972; Le Fort, 1975; Pecher and Jest, 1977) located a thrust at a higher structural level than that of Heim and Gansser (1939), but broadly consistent with the thrust observed by Fuchs and Franks (1970) that separated the Upper and Lower Crystalline Units. Hashimoto et al. (1973) and later Arita (1983) proposed a lower MCT (MCT I) and an upper (MCT II) to correspond to the thrusts of Heim and Gansser (1939) and French workers respectively, referring to the material bounded by MCT I and II as the MCT Zone, which included material displaying inverted metamorphism. Valdiya (1980), working in Kumaon, proposed a two thrust geometry referring to the upper thrust as the MCT (as defined by the French Team in Nepal) and the lower thrust as the Munsiari Thrust (previously the MCT as defined by Heim and Gansser, 1939) with the thrusts bounding the LHCN and rooting to the north. Metcalfe (1993), working in a similar area, adopted the term MCT Zone and applied it to the LHCN of Valdiya (1980). Later Ahmad et al., (2000) termed this thrust bounded unit the Inner Lesser Himalaya (Section 1.7). However, in Nepal Upreti (1999) suggested that the term MCT I (Arita, 1983; Hashimoto et al., 1973) is difficult to assign due to lack of metamorphic breaks and structures, although Macfarlane et al. (1992) observed local brittle structures that are coincidental with the MCT I in the Langtang area.

The MCT is now generally regarded as a high-strain shear zone ranging from tens of meters to kilometres in thickness, developed from a tectonic melange of both HHCS and LHS units, that dips northward between 10 to 30°; kinematic indicators suggest

top-to-the-southwest to southeast displacement. Deformation and shearing is inferred to have occurred during and after metamorphism, suggesting a poly-phase deformation history (Hodges, 2000; Kohn et al., 2001; Searle et al., 2003; Simpson et al., 2000). Davidson et al. (1997) termed the wide zone of distributed top-to-the-south shearing as the MCTZ, whereas the MCT is identified with the protolith boundary between the HHCS and LHS. Searle et al. (2003) refers to the MCT as the lowermost plane of high-strain. Metamorphic grade increases sharply within the MCTZ, which can range from chlorite to sillimanite grade and is frequently consistent with a telescoping of metamorphic isograds (Searle et al., 2003). However, although some recent publications accept this general definition, its application in the field still yields further controversy and confusion. For example:

- Searle et al. (2003) disputes Catlos et al.'s (2002) assignment of the Phaplu (Ulleri) Augen Gneiss to the LHS on the basis of lithology, stating it must be "structurally part of the Greater Himalayan Slab (HHCS)";
- Stephenson et al. (2000) insists the MCT can only be defined structurally due to lithological variation throughout the orogen, (which curiously would affect the rheological contrast and therefore structural definition);
- Thakur (1998) fails to assign the MCT to either the Vaikrita or Chail Thrust within the northwest Himalaya.

Thus it is clear that MCT identification is hampered by along-strike lithological variation which can frequently control the rheological contrast and Barrovian metamorphic assemblages in the rocks of both the hanging and footwall. There is clearly a need to discriminate between rocks above and below the MCT which requires an independent approach that does not consider lithological contrasts, metamorphism or structural deformation and furthermore is independent of the tectonic orogenic process.

1.5 Isotopic Definition Of The MCT: A New Approach

So far this introduction has discussed how numerical modelling has proposed a theory that explains a number of observations concerning the metamorphism, anatexis and extrusion of the HHCS. The previous section has demonstrated that attempts to distinguish the lithologies of the HHCS and those of the LHS and to define the MCT on the basis of metamorphism, structural and lithological criteria have led to multiple definitions. The following sections propose a new approach to this ongoing Himalayan debate. Using published examples it will be shown how careful use of selective isotopic systems can be used to define and discriminate between major Himalayan tectonic units and delineate major Himalayan structures. Of primary importance is to set out the underlying assumptions behind this approach which are as follows.

- The metasedimentary rocks used in the study represent metamorphosed clastic sediments which are mixtures of disaggregated portions of igneous, metamorphic and/or older sedimentary rocks that have been exposed, eroded and deposited within the pre-Himalayan depositional basins.
- The isotopic ratios involved are unaffected by diagenesis, thermal or mechanical processes in the crust.

In addition to these assumptions, the approach can only work in defining the location of a fault if the contrasts in the isotopic ratios between lithologies from the footwall and hanging wall of the structure are sufficient to be measurable using the available analytical techniques. This generally means that the protoliths of the two suites of metasediments have been derived from source regions of contrasting age.

If these criteria are met, then isotopes can be used to identify and discriminate between discrete tectonic units and therefore define the structural boundaries that separate them. For the Sm-Nd isotopic system, the evolution of the $^{143}Nd/^{144}Nd$ ratio is dependent on the time elapsed since the sample was at its initial value, and the Sm/Nd elemental ratio of the sample. The isotopic compositions of sediments, or their

metamorphosed equivalents, represent a weighted average of the compositions of the source regions contributing to the sedimentary basin (Arndt and Goldstein, 1987). Importantly, the Nd isotopic ratio is largely unaffected by crustal process after extraction from the mantle and hence Nd isotope ratios are considered to reflect large-scale differences in crustal sources. This robustness allows the reconstruction of depositional basins and their source areas (e.g. Harris et al., 1990).

For these reasons it has been recognised for some years that the Nd isotope system is potentially able to discriminate between tectonic units in geologically complicated areas; examples of its successful application include Dickin and McNutt (1989; 2003) who used Nd model ages to discriminate between tectonic provinces in the Canadian Shield. Furthermore, in orogenic belts where isotopic variations are observed between tectonic units, their erosional history can be constrained in foreland basins using Sm-Nd analysis (e.g. Najman et al., 2000; White et al., 2002). Conventionally, whole-rock Sm/Nd isotopic data are presented as either model ages or as ε_{Nd}.

1.5.1 Nd model ages

The Sm/Nd ratio of a sample changes at the time of extraction from the mantle, as Sm is slightly more compatible than Nd, resulting in the melt (and the crust that it ultimately forms) being more enriched in Nd. This is known as Sm/Nd fractionation. The Nd model age is calculated by projecting the evolution line of the $^{143}Nd/^{144}Nd$ ratio of the sample backwards in time to intersect the evolution line of the mantle reservoir (DePaolo and Wasserburg, 1976b). This is considered to be similar to CHUR (Chondritic Universal Reservoir) and the model age is denoted by T_{CHUR} (calculated using Equation 1, Appendix A). DePaolo (1981) refined this technique using a quadratic curve to show a progressively more depleted mantle that was close to the CHUR evolution line during the Archaean, but diverges progressively to the present day; model ages using this technique are denoted by T_{DM} (calculated using Equation 2, Appendix A). DePaolo (1981) concluded that T_{DM} ages are more accurate crustal formation ages than T_{CHUR} by demonstrating that recalculated data using his method

correspond closer to known geological events. For igneous rocks, the term 'crust formation' age is sometimes used which assumes that only one melting event occurred. However, in igneous rocks where re-melting or contamination has occurred crustal formation ages may be geologically meaningless if they do not correspond to known geological events; in this case the term Nd model age is used (Arndt and Goldstein, 1987). Frequently, the term Nd model age is also used in sedimentary studies as sedimentary basins are likely to source detritus from more than one source or they may recycle sediments within the basin or source detritus from other sedimentary rocks, resulting in the mixing of geologically meaningful crustal formation ages and model ages. Therefore, model age is used in preference to crustal formation age in this study as this study focuses on clastic sedimentary rocks. However, where a sedimentary basin obtains it's detritus from one source (which was formed in a single crustal formation event) then the model age is likely to be geologically meaningful and the term crustal formation age can be used.

1.5.2 ε_{Nd}

ε_{Nd} is calculated using Equation 3 (Appendix A), and is a convenient notation that represents the deviation of the $^{143}Nd/^{144}Nd$ ratio of the sample from CHUR (DePaolo and Wasserburg, 1976a). For igneous rocks, a sample with a positive ε_{Nd} value is considered depleted, requiring a higher Sm/Nd ratio than CHUR; conversely, a sample with a negative ε_{Nd} value indicates that the source was enriched. Furthermore, the deviation between sample and the value of CHUR at a specified time (T) can be calculated as ε_{Nd} (T), using Equation 4 (Appendix A).

To complement this whole rock study Sr isotopes have also been investigated. In contrast to Nd isotopes, the Rb-Sr isotope system is likely to be reset by a range of crustal processes such as thermal events and by fluid flow. Such resetting is often incomplete, resulting in age trends rather than specific isochrons (i.e. where the MSWD of the dataset is greater than 2.5; Rollinson, 1993). In this study, Sr-isotope

ratios have proved useful in revealing the extent, and approximate age, of early metamorphic events in the source regions of the sediments analysed.

Dating detrital zircons using the U-Pb isotopic system, on individual zircons recovered from metasedimentary rocks can provide maximum depositional ages; with sufficient analyses the age of the source rock of the zircons can also be constrained. Typically zircons are unaffected by low grade metamorphism and are known to be highly resistant to sedimentary abrasion during saltation. However, single detrital zircon analysis will typically bias against mafic source areas (which contain few zircons) and against sources that yield zircons with high U contents (>100 ppm) as these crystals are often metamict and do not survive sedimentary reworking. Laboratory processes will further bias towards larger crystals and those that are the least magnetic (e.g. least metamict and inclusion free) (Heaman and Parrish, 1991). Furthermore, sufficient individual zircons need to be analysed to produce a statistically meaningful age distribution, which is both costly and time-consuming. However, recent developments in technology have helped to address this, with relatively high accuracy and precision zircon measurements now performed on Sensitive High-Resolution Ion MicroProbe (SHRIMP) and Laser-ablation Multi-collector Inductively Coupled Mass spectrometer (LA-MC-ICPMS). Examples of the application of SHRIMP analysis of detrital zircon population studies include Van Schus et al. (2003) and Nutman et al. (1994). Zircon data can also be used to independently assess the validity of Nd model age discrimination as exemplified by Dickin (2000), who combined U-Pb zircon ages with Nd model ages to establish a crustal formation map for the Precambrian shield of North America.

1.6 Previous Isotope Studies In The Himalaya

Several published isotopic studies from the Himalaya have assessed the application of the geochemical tracers discussed above to discriminating between the

metasedimentary lithologies of the orogen. Figure 1.4 summarises the locations of these isotopic studies.

Parrish and Hodges (1996) in central Nepal established that U-Pb single zircon ages from LHS and HHCS metasediments have distinct age spectra (1870-2600 and 1000-800 Ma respectively – Fig. 1.5) and that ε_{Nd} ratios from the LHS and the HHCS are also distinct (-21.4 to -25.9 and -14.6 to -18.5 respectively – Fig. 1.6), enabling discrimination between these two tectonic units, and therefore defining the MCT that separates them. U-Pb zircon ages from DeCelles et al. (2000) from a number of localities throughout Nepal found ages greater than ca. 1600 Ma for the LHS (with age distribution peaks at ca. 1860 and 1940 Ma) and ages of 800-1700 Ma (with age distribution peaks at ca. 850 and 950 Ma) for the HHCS (Fig. 1.5), which broadly correspond to the data of Parrish and Hodges (1996).

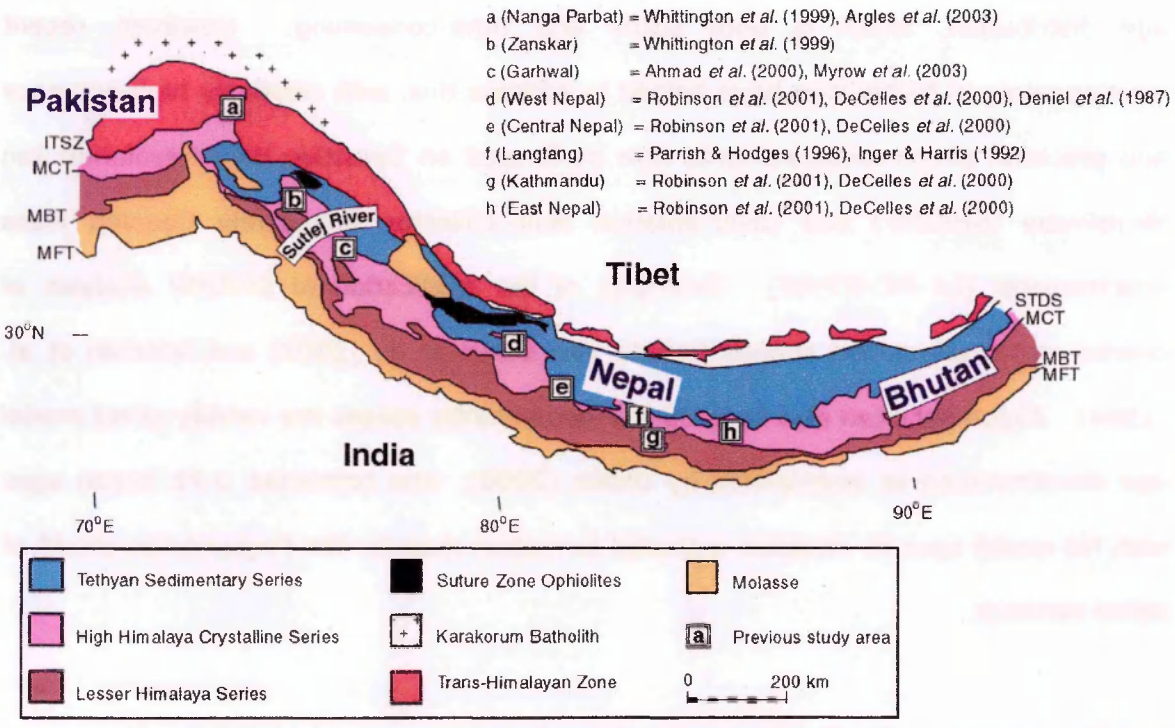

Figure 1.4 - Location map of Himalaya isotopic studies.

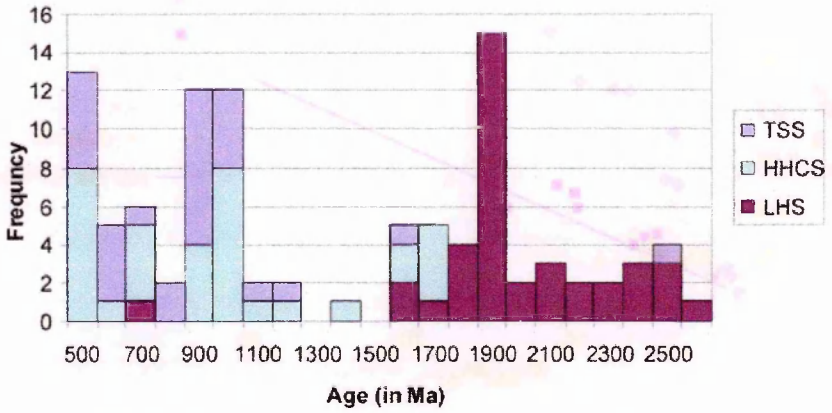

Figure 1.5 - Single zircon age ($^{207}Pb/^{206}Pb$) distribution from published data (Parrish and Hodges, 1996, n=22; DeCelles et al., 2000, n=79).

The distinct ε_{Nd} values for HHCS and LHS sediments across the MCT from the Garhwal region of the western Himalaya has been confirmed by Ahmad et al. (2000) (Fig. 1.6; age corrected to t=500 Ma, discussed at the end of this section). Work in the Nanga Parbat massif (Argles et al., 2003; Whittington et al., 1999; Fig. 1.6) found similar whole-rock Sr-Nd distinctions between groups of clastic sediments that were correlated with the HHCS and LHS. Contrastingly, an alternative study by Pogue et al. (1999) using lithostratigraphical correlations in Pakistan concluded that the MCT was not present in this portion of the Himalaya.

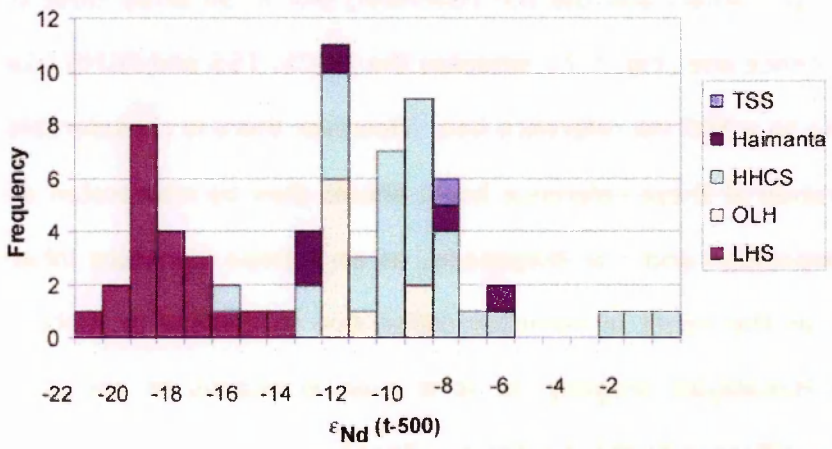

Figure 1.6 - Nd data from constrained localities data from: Ahmad et al. (2000), Parrish and Hodges (1996), Miller et al. (2001), Whittington et al. (1999), Massey (1994), Ayres (1997). All data age corrected to t=500 Ma, discussed at the end of this section.

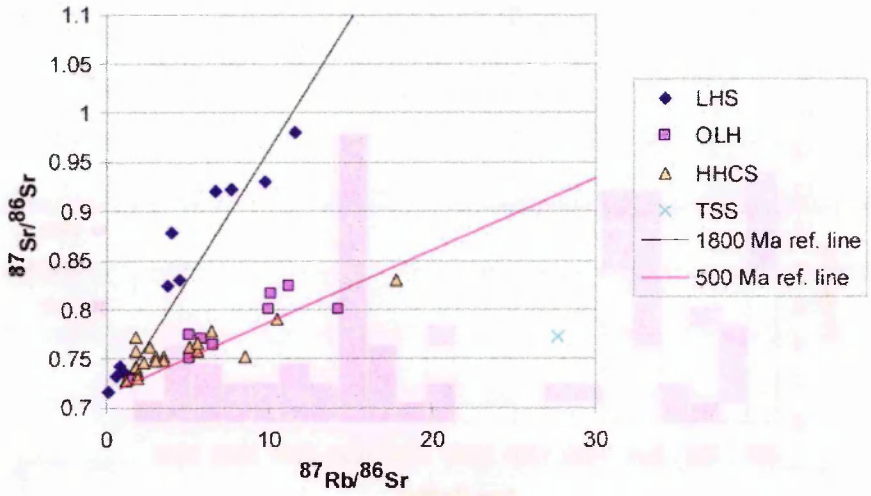

Figure 1.7 - Sr data from constrained localities data from: Ahmad et al. (2000), Parrish and Hodges (1996), Miller et al. (2001), Whittington et al. (1999), Massey (1994), Ayres (1997).

These studies defined the LHS as having a wide range of $^{87}Sr/^{86}Sr$ ratios and older model Nd ages, whereas the HHCS has relatively low and consistent $^{87}Sr/^{86}Sr$ ratios and younger model Nd ages (Fig. 1.7 and 1.8). Ahmad et al. (2000) observed that Neoproterozoic metasediments from the LHS had similar isotope characteristics to the HHCS and TSS (-10 to -19), in contrast to Palaeoproterozoic sediments (-25 to -19) (Fig. 1.6), enabling the LHS in the area to be separated by the Tons Thrust into the Inner Lesser Himalaya (ILH) and the Outer Lesser Himalaya (OLH), as proposed by Valdiya (1995) based on the stratigraphic criteria outlined above. Ahmad et al. (2000) and Argles et al. (2003) used Rb-Sr data to refine the discrimination. They found that the LHS (Nanga Parbat) and the ILH (Garhwal) plot in an array close to a calculated 1800 Ma reference line (Fig. 1.7), whereas the HHCS, TSS and OLHS (Garhwal) plot in an array close to a 500 Ma reference line. However there is considerable debate as to the interpretation of these reference lines: should they be interpreted as representing the age of deposition and / or diagenesis, as an isotope signature inherited from the source area, as the result of homogenisation due to thermal or metamorphic events prior to the Himalayan orogeny, or is it even erroneous to assign *any* geological meaning or significance to these reference lines?

An age of deposition can be dated using Sr isotope ratios (such as in Turnbull et al., 1996) when the rock type is fine-grained and clay minerals such as illite control the

geochemistry of the rock, allowing Sr homogenisation during diagenesis. Given the large scatter of the data in the array around 500 Ma reference line, diagenetic homogenisation may a plausible explanation. Although the high-grade nature of the HHCS would suggest that if these rocks were susceptible to Sr isotope homogenisation during diagenesis then they should also have been reset in the last metamorphic event (the Himalaya orogeny), Figure 1.7 suggests that this is not the case. A provenance age is likely to be recorded if the rock contains a large proportion of detrital Rb-bearing minerals such as mica, K-feldspar, clay minerals etc; considering the broad zircon age spectra of both Parrish and Hodges (1996) and DeCelles et al. (2000) within both the HHCS and LHS this explanation seems less likely. Sr isotope homogenisation can also be associated with thermal, metamorphism or fluid migration events, which may occur separately or as one event. In the presence of high temperatures and fluids Sr is highly mobile and diffuses well, leading to homogenisation of Sr isotopes. This chapter has reviewed evidence for pre-Himalayan metamorphism (section 1.3.1), and there is substantial evidence for thermal events in the HHCS from zircon crystallization ages from granites (ca. 450 to 500 Ma, reviewed in Singh and Jain, 2003). Furthermore, preliminary accessory mineral dating within the core of garnets in the HHCS in the Sutlej Valley have suggested at least one monazite crystallisation event ca. 420 Ma (Caddick, 2004). Therefore, in the light of this information, the most likely interpretation is that at least the 500 Ma reference line corresponds to a thermo-tectonic / metamorphic event in HHCS units that caused partial Sr homogenisation (as suggested by Ahmad et al., 2000) which corresponds to both the age of zircon crystallisation within granite bodies and garnet and monazite crystallization within metamorphic assemblages of the HHCS at ca. 500 Ma. With regard to the 1800 Ma reference line for the LHS metasediments, several granitic bodies associated with the LHS (e.g. DeCelles et al., 2000) have been dated to ca. 1800 Ma, suggesting that Sr homogenisation in these units was coeval with a granite intrusion event in the same way.

Combining whole-rock Sr and Nd isotope systematics with single zircon U-Pb ages, the published work discussed so far suggest that effective discrimination can be made between the HHCS and the LHS through large sections of the Himalaya (at least from central Nepal to Nanga Parbat) and within-unit discriminations of the LHS are possible with the recognition of the ILH and the OLH in Garhwal (Ahmad et al., 2000).

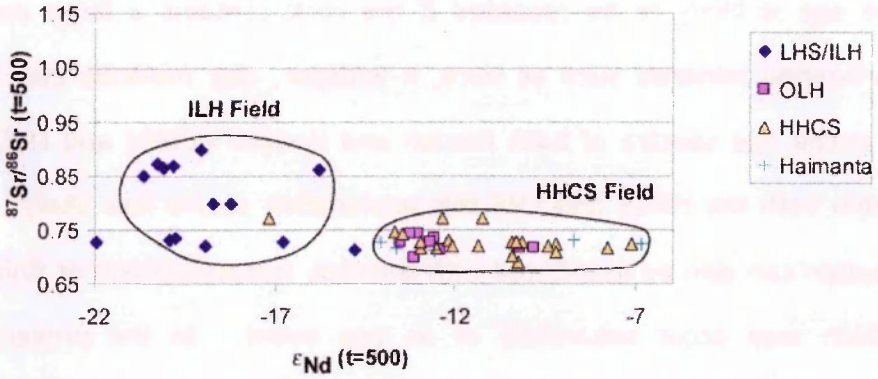

Figure 1.8 - Sr-Nd (age corrected) data from constrained localities data from: Ahmad et al. (2000), Parrish and Hodges (1996), Miller et al (2001), Whittington et al (1999), Massey (1994), Ayres (1997).

However, recent work by Robinson et al. (2001), Miller et al. (2001) and Myrow et al. (2003) argue against any distinction between the LHS and HHCS, on the basis of a considerable overlap in the ε_{Nd} values and model Nd ages of these units. This may be because these authors do not recognise or separate out the ILH and OLH units within the LHS (i.e. Ahmad et al., 2000). In the case of Myrow et al. (2003), the location of the LHS sample yielding overlap with the HHCS field is clearly from the OLH, confirming the findings of Ahmad et al. (2000). Unfortunately, in other cases authors fail to give precise locations for samples or to produce corresponding Sr isotope data. The significance of considering samples with well-constrained field locations can be assessed by comparing Figure 1.6 with Figure 1.9, the latter including all published data, ignoring its location from within the LHS.

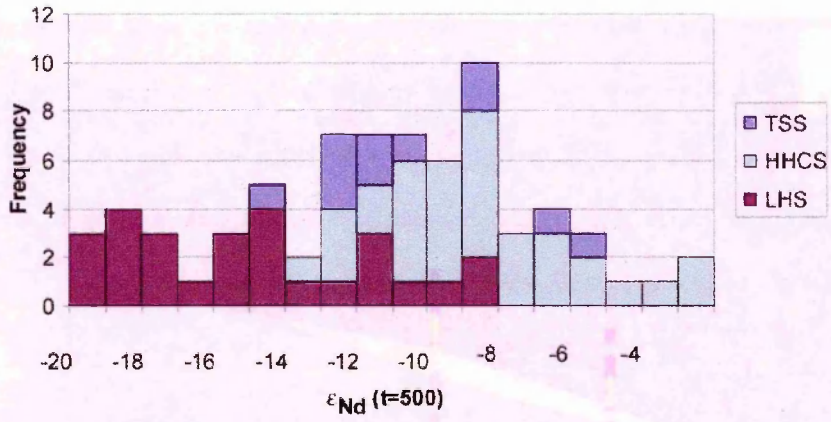

Figure 1.9 - Nd histogram of data from unspecified field locations (t=500Ma), data from: Robinson et al. (2001), France-Lanord et al (1993), Pearson (2002), Deniel et al. (1987).

Ahmad et al. (2000) have shown that ε_{Nd} discriminates Himalayan metasediments better than T_{DM} model ages calculated using the quadratic solution of DePaolo (1981). As Nd model ages are calculated by backwards projection to a time when the sample was extracted from a model reservoir (e.g. T_{DM}) the calculation is sensitive to the $^{147}Sm/^{144}Nd$ ratio, whereas ε_{Nd} (t=0) calculations are independent of this ratio. However, Ahmad et al. (2000) further demonstrates that age-corrected ε_{Nd} (such as t=500) values discriminate better than ε_{Nd} (t=0) as illustrated in Figure 1.10. Age-corrected ε_{Nd} calculations also involve the $^{147}Sm/^{144}Nd$ ratio, but the calculation is less sensitive to the $^{147}Sm/^{144}Nd$ ratio than are Nd model age calculations. The ε_{Nd} (t=500) calculation is therefore less perturbed by thermal and/or metamorphic events that can fractionate the Sm/Nd ratio, such as high-grade metamorphism, migmatisation or granite emplacement events. From plotting the evolution of ε_{Nd} data through time it can be seen that the moist effective discrimination between data sets occurs over the time interval 500 to 800 Ma (Fig. 1.10). This suggests that in the past 500 Ma, Sm/Nd fractionation in the rocks has been negligible. Since 500 Ma marks a known period of magmatism and deformation (Singh and Jain, 2003) the ε_{Nd} (t=500 Ma) ratio has been selected as a potential discriminant. Thus, considering the evidence for Pre-Himalayan metamorphism (Section 1.3.1), ca. 500 Ma granites (Chawla et al., 2000) and monazite ages (Caddick, 2004) in the Sutlej Valley, the 500 Ma discrimination can be related to late extensional stage of the long-lasting Pan-African orogenic events as suggested by Miller et al. (2001).

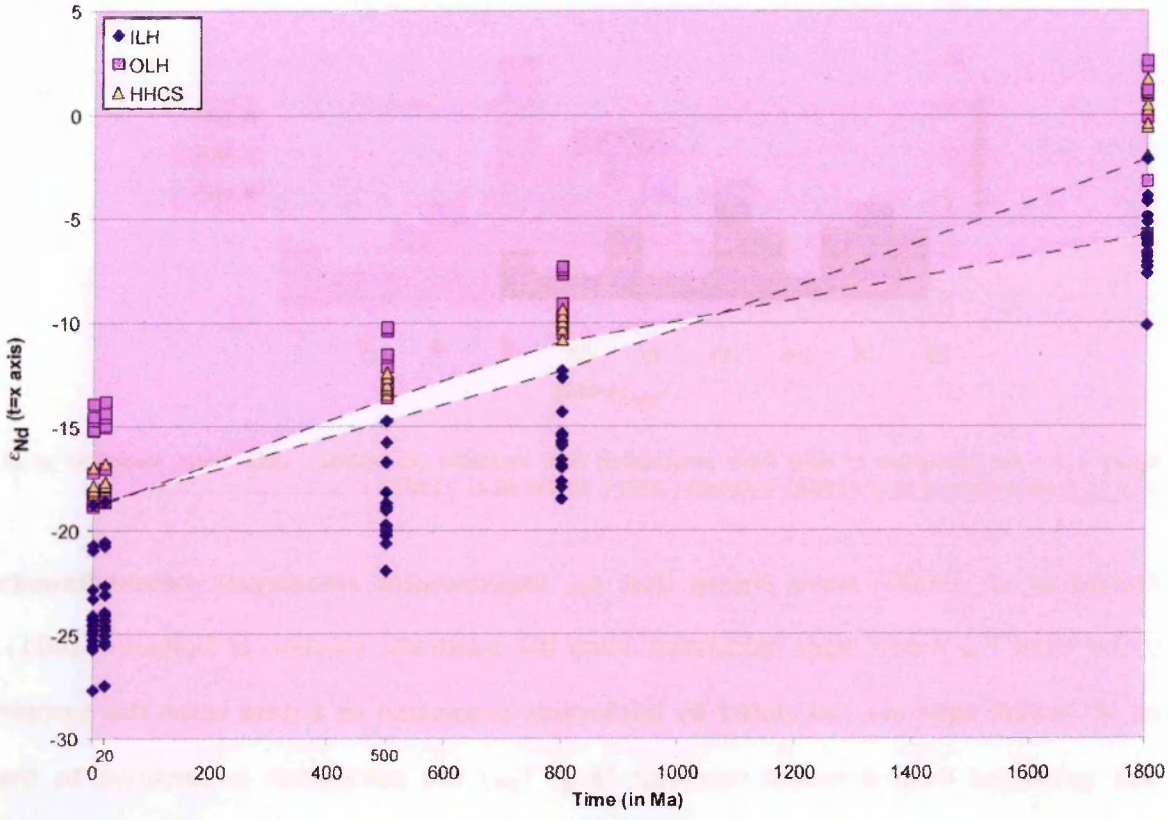

Figure 1.10 – Various age corrected ε_{Nd} data from Ahmad et al. (2000). White polyhedron indicates the extent of ε values that separates the two groups of data. Note that ages ca. 500 to 800 Ma show largest separation of the ILH and HHCS/OLH units. Dashed lines do not represent Nd evolution of individual samples, but simply mark the separation between ILH and OLH/HHCS data group.

1.7 Criteria For The Selection Of Samples For Analysis

When applying the geochemical proxies discussed above the selection of appropriate samples for analysis is of fundamental importance. As discussed below, the ideal samples for Nd bulk rock and for detrital zircon analysis are pelitic and psammitic sediments respectively.

In this study $^{147}Sm/^{144}Nd$ and $^{143}Nd/^{144}Nd$ isotope ratios were obtained from whole rocks. Because REEs are relatively insoluble, and therefore immobile during diagenesis and metamorphism, the REE budget in metamorphosed clastic sediments is largely a reflection of the sedimentary source region. Rocks of pelitic composition were preferred for REE analysis for two reasons. Firstly, Cullers et al. (1987) showed that fine grained, clay-bearing rocks (i.e. pelites) have significantly higher concentrations of REE compared to other sediments, as both quartz and carbonates

were found to effectively dilute the REE concentration. Secondly, the fine-grained nature of a pelitic protolith requires a smaller sample size of the clastic sediment to be representative of the average composition of the source region.

Carbonate-bearing rocks were avoided partly because carbonates will contribute a small component of the REE budget. More importantly, $^{87}Rb/^{86}Sr$ and $^{87}Sr/^{86}Sr$ isotope ratios were also investigated and carbonates provide a major contribution to the Sr-isotope budget. Since carbonates are likely to be derived from seawater, or from crustal fluids during diagenesis, their isotopic composition will not be representative of the source area from which the clastic sediment is derived.

Whereas pelites were preferentially sampled for the whole-rock isotope analysis, medium to coarse grained psammites and quartzites were sampled preferentially for single grain zircon analysis, as the average grain size of a sediment is assumed to reflect the size of the zircon crystals within it, coarse grained rocks are used to extract zircons of a size that allows individual crystal analysis. This study therefore sampled medium to coarse grained psammites and quartzites for zircon analysis and pelites for whole-rock Nd-Sr isotope compositions.

However, occasionally the ideal material was not available due to limited exposure or preferential weathering. Nd studies comparing fine and coarse grained samples provide conflicting results, some studies indicating that grain size does not affect bulk composition (Goldstein et al., 1984) and others suggesting grain size does lead to an apparent difference in the Nd isotope characteristics between coexisting sands and muds (McLennan et al., 1989). Therefore, it is important to explore the possibility that the differences in the Nd and Sr isotope systems observed in the metasediments from the Himalaya is influenced by sampling bias.

McLennan et al. (1989) compared the Nd isotopic composition of modern deep-sea turbidite sands and muds. Their study used coexisting sands and muds and focused

on turbidites with a large volcanogenic input. They found differences between these muds and sands of up to 7 epsilon Nd units, which corresponded to differences of up to 440 Ma in model age calculations. A further detailed study by McLennan et al. (1990) found a similar relationship with modern turbidites; however, they found that Phanerozoic sedimentary rocks have fairly constant model ages of between 1500 to 2000 Ma. A comparative study by Goldstein et al. (1984) used a much broader range of sedimentary protoliths and found no difference in the ε_{Nd} or model age calculations when comparing coexisting sands and muds. In the present study, unlike the work of McLennan et al. (1989; 1990) and Goldstein et al. (1984), volcanogenic clastic rock input to Himalayan sandstones and mudstones is thought to be minimal, suggesting that varying grain size within the whole-rock sample set will not introduce a sampling bias to the results. During the course of this study it will be demonstrated that isotopic characteristics are not correlated with specific lithologies (Chapter 3).

As previously stated, this study will aim to determine whole-rock Sr and Nd isotopes from fine-grained sedimentary rocks, and determine U-Pb zircon ages from coarser sedimentary rocks. Therefore, it is important to consider the source or sources that generate mudstone, siltstone, sandstone and quartzites. Detritus contributing to a simple sedimentary basin will deposit courser grained litholigies proximal to the source and will deposit finer-grained lithologies distal to the source. Sandstones and quartzites that are of equal coarseness will relate more to the maturity of the depositing detritus. However, heavy minerals frequently control the REE budget, and zircon is typically known to be highly resistant to sedimentary abrasion during saltation, this study will demonstrated that isotopic characteristics are not correlated with specific lithologies.

1.8 Aims, Objectives And Structure Of This Thesis

1.8.1 Aims and objectives

The overall aim of the study is to critically assess the application of whole-rock Nd and Sr isotopes and detrital zircon analysis to the discrimination between major Himalayan tectonic units and thereby delineate major Himalayan structures. By applying similar techniques to the western (Sutlej Valley) and eastern (Bhutan) Himalaya these techniques will be used to assess the lateral continuity of these units along the Himalayan orogen. Due to the robust nature of detrital zircons and the Nd whole-rock system that withstands sedimentary recycling and orogenic processes, the results can also constrain novel interpretations of the nature of the source areas of the sediments now overprinted by the Himalayan orogeny, of their depositional basins and of the distribution of pre-Himalayan orogenic events.

1.8.2 Thesis structure

This thesis will describe the field relations and petrology of the Sutlej and Bhutanese Himalayan transects visited during field seasons in 2002 and 2003 (Chapters 2 and 4 respectively). Following the account of each area the elemental and isotopic geochemistry is described and discussed (Chapters 3 and 5). These accounts are followed by an interpretation of the provenance history of Himalayan metasediments and a discussion of the potential source areas involved through a proposed palaeogeographic model (Chapter 6). The results are summarised in the final chapter (Chapter 7).

Chapter 2 - Field Relations And Regional Geology In The Sutlej Area

2.1 Introduction And Aims

The purpose of this chapter is to give a resume of previous work in the Sutlej (or Satluj) area and to introduce and describe the geological units. It is important to fully describe the units and to show an understanding of the underlying complexity of the area as this will be referred to later in this thesis, particularly during the synthesis of the Himalayan story.

The Sutlej River is located in northwest India in the state of Himachal Pradesh (Fig. 2.1), and for the purposes of this study, the Sutlej Area will encompass the Sutlej River drainage basin.

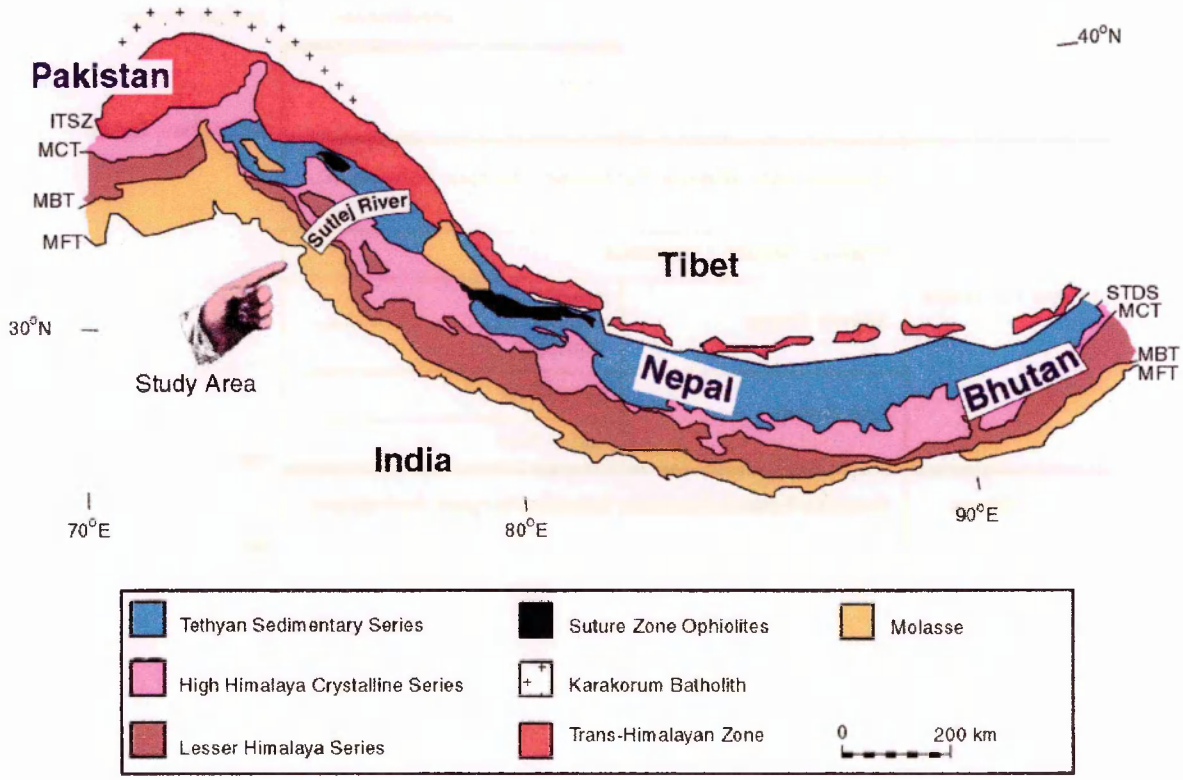

Figure 2.1 - Location map of the Sutlej River.

The geology of the Sutlej Area will be described in this chapter as a geological traverse from the northeast to southwest, i.e. from the High Himalayan mountainous area to

the foothills. The principal lithological units are the TSS, Haimanta Group, High-Grade Crystalline Units, Lesser Himalaya Series and the Sub-Himalaya (Table 2.1; Fig 2.2):

Table 2.1 – Simplified broad-scale field relations in the Sutlej Area.

Major Tectonic Unit	Group / Formation			Major Structures:
High Himalaya	Tethyan Sedimentary Series			
	Haimanta Group	Chamba Fm		
		Manjir Fm		
		Phe Fm		
		Kinnaur Kailas Granite		STDS
	High-Grade Crystalline Series	Vaikrita		
		Karcham Group		Vaikrita Thrust
		Jutogh Group	Wangtu Gneiss complex	
			Jutogh Metasediments	Jutogh Thrust
		Chail Group		MCT/Chail Thrust
Lesser Himalaya	Rampur-Larji Window Formation (Rampur Formation)			
	Shaling-Deoban Limestone			
	Shimla Group	Shimla A		
		Shimla B		
	Krol Group	Inner Krol		
		Outer Krol		MBT
Sub Himalaya	Siwaliks/Kasauli/Dagshai/Subathu/Singtali Formations			MFT

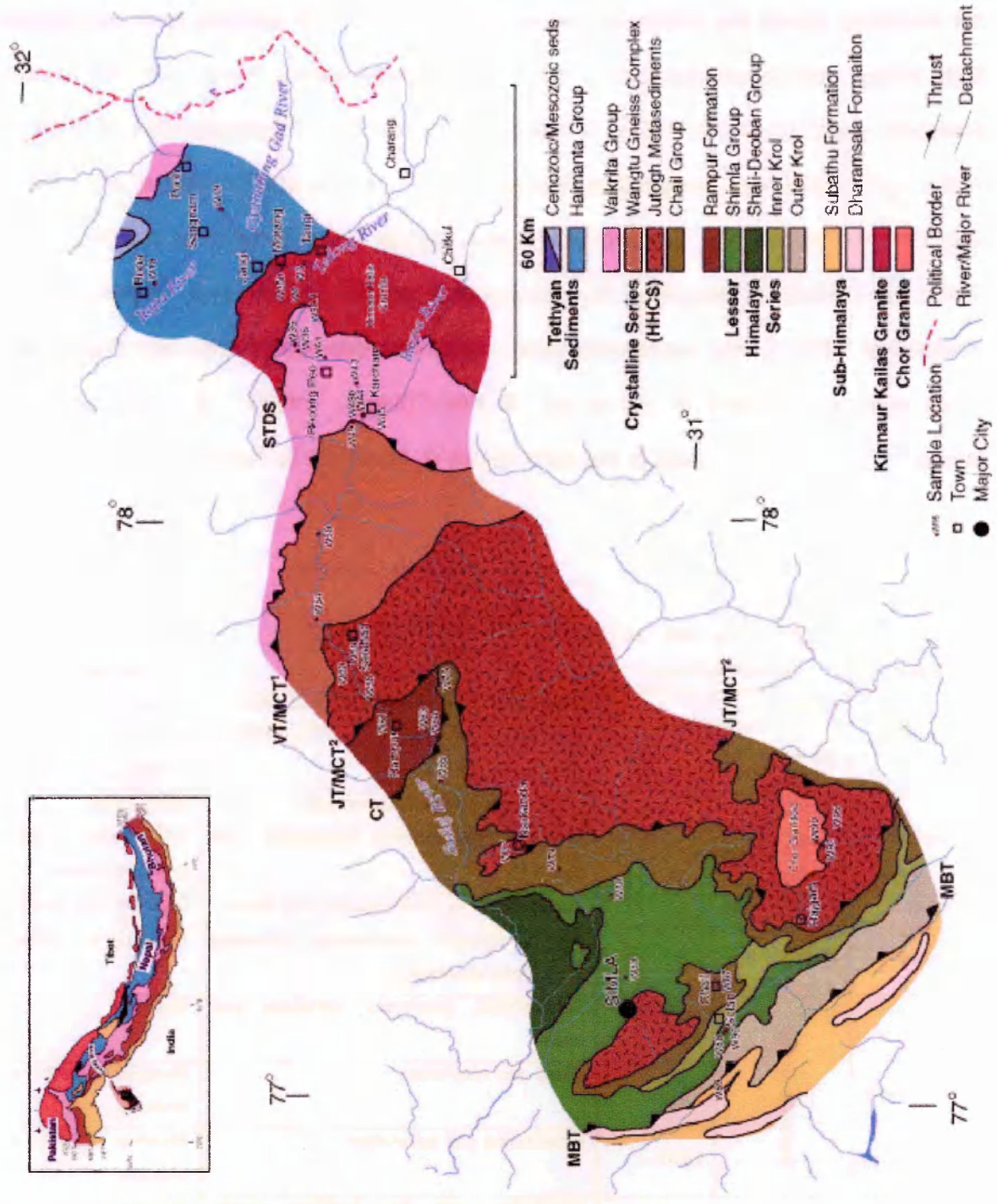

Figure 2.2 - Geology of the Sutlej Area as determined prior to this study (from Thakur and Rawat (1992), Vannay and Grasemann (1998) and Raina (1981); MCT¹ marks the position of MCT as proposed by Vannay et al. (2004, and references therein) and Valdiya (1980); MCT² marks the position of MCT as proposed by Thakur (1992), Manickavasagam et al. (1999), Raina (1981) and Heim and Gansser (1939), VT, Vaikrita Thrust; JT, Jutogh Thrust; CT, Chail Thrust.
Ornament for inset location map, same as Figure 2.1.

2.2 The Tethyan Sedimentary Series

The TSS crop out to the northwest, in the upper reaches of the Sutlej Area close to the border between Tibet and India. Due to logistical and political reasons the TSS was

not observed during the course of this project, although TSS samples from the nearby Spiti Valley and surrounding area have been incorporated, which are the closest accessible outcrops of the TSS to western geologists. The lithostratigraphy of the TSS in the Spiti Valley was assigned by Hayden (1904), and is still broadly in use today. The TSS lies above the Cambro-Ordovician angular unconformity of the Haimanta Group (see below), described by Grasemann et al. (1997) and Wiesmayr and Grasemann (2002), and represents near continuous deposition until late Cretaceous times with a thickness of up to ca. 6 Km (Thakur, 1992). A brief summary stratigraphy of the TSS rocks in the Spiti region is described in Table 2.2:

Table 2.2 - Stratigraphy of the Spiti TSS (Thakur, 1992, after Bagati, 1990).

Age	Formation/Group		Rock type	Important fossils
Cretaceous	Chikkim		Limestones and shales with quartzites	Foraminifera
	Giumal		Quartzites, sandstones with interbedding limestones and shale	Bivalves (scallops, oysters), ammonites
Jurassic	Spiti Shale		Black shale and thin quartzites	Ammonites
	Kioto Limestone		Predominately massive limestones with quartzites	Belemnites, bivalves and gastropods
Triassic	Lilang Group		Huge thickness of limestones and shales	Bivalves and nautilus
Permian	Kuling		Red calcareous sandstones, siliceous shales and sandstones	Brachiopod *productus*
Carboniferous	Kanawar Group	Ganmoch-Idam	Polymictites, quartzites, siltstones and shale	Bivalves
		Po	Shale and quartzites	Bivalves, coral and bryozoa
		Lipak	Limestones and quartzites	Bivalves, coral and bryozoa
Devonian	Muth		Quartzites with cross-bedding, ripple marks and mega cross bedding	Trilobites, bivalves and coral
Silurian	Pin Dolomite		Carbonates, mainly dolomites with shales, siltstones and quartzites	Trilobites, bivalves and coral
Ordovician	Shian Quartzite		Mainly quartz-rich sandstones with some shales and siltstones	Brachiopods and trilobites

2.3 Haimanta Group

2.3.1 Metasediments

The Haimanta Group (Fig. 2.2) was first described by Greisbach (1891) and defined as the rocks overlying the high-grade crystallines of the Vaikrita Group. The term Haimanta was first used by Hayden (1904) to describe the group of TSS rocks that are unfossiliferous (Silurian and older). Srikantia (1981) later separated the group into the Lower and Upper Haimanta; the Manjir Formation diamictite was defined as the upper limit of the Lower Haimanta.

Recently Draganits et al. (1998), after working in the Spiti River area has proposed a further sub-division of the Haimanta Group as follows (from the base upwards; see stratigraphical column, Chapter 3):

Chamba Formation: coarsening-up sequence of mainly metapelites, metasiltstones and metagreywackes with occasional carbonaceous bands; load and flute casts suggest a turbiditic depositional environment;

Manjir Formation: mainly diamictitic with a 'cap carbonate'; a glacial depositional environment is indicated, probably during the Neoproterozoic Marinoan glacial event (ca. 620 Ma);

Phe Formation: a gradual change from metapelites, metasiltstones and metagreywackes to carbonaceous rocks. The Phe Formation (and Haimanta Group) are terminated at the Cambro-Ordovician boundary, where there is a noticeable decrease in the metamorphic grade and strain in the overlying rocks (Grasemann et al., 1997).

In the Sutlej Area, the Haimanta Group is juxtaposed with the Vaikrita Group along the STDS. The Haimanta Group occurs as a broad synformal structure striking northwest-southeast. Approximately 5 Km of Haimanta Group sediments are represented between the Kinnaur Kailas Granite and the village of Pooh; the uppermost ca. 6 Km are absent. A series of steep, north-dipping faults appear to be

present throughout much of the Sutlej section (Fig. 2.3 a); forming riedel shears possibly related to extension along the STDS.

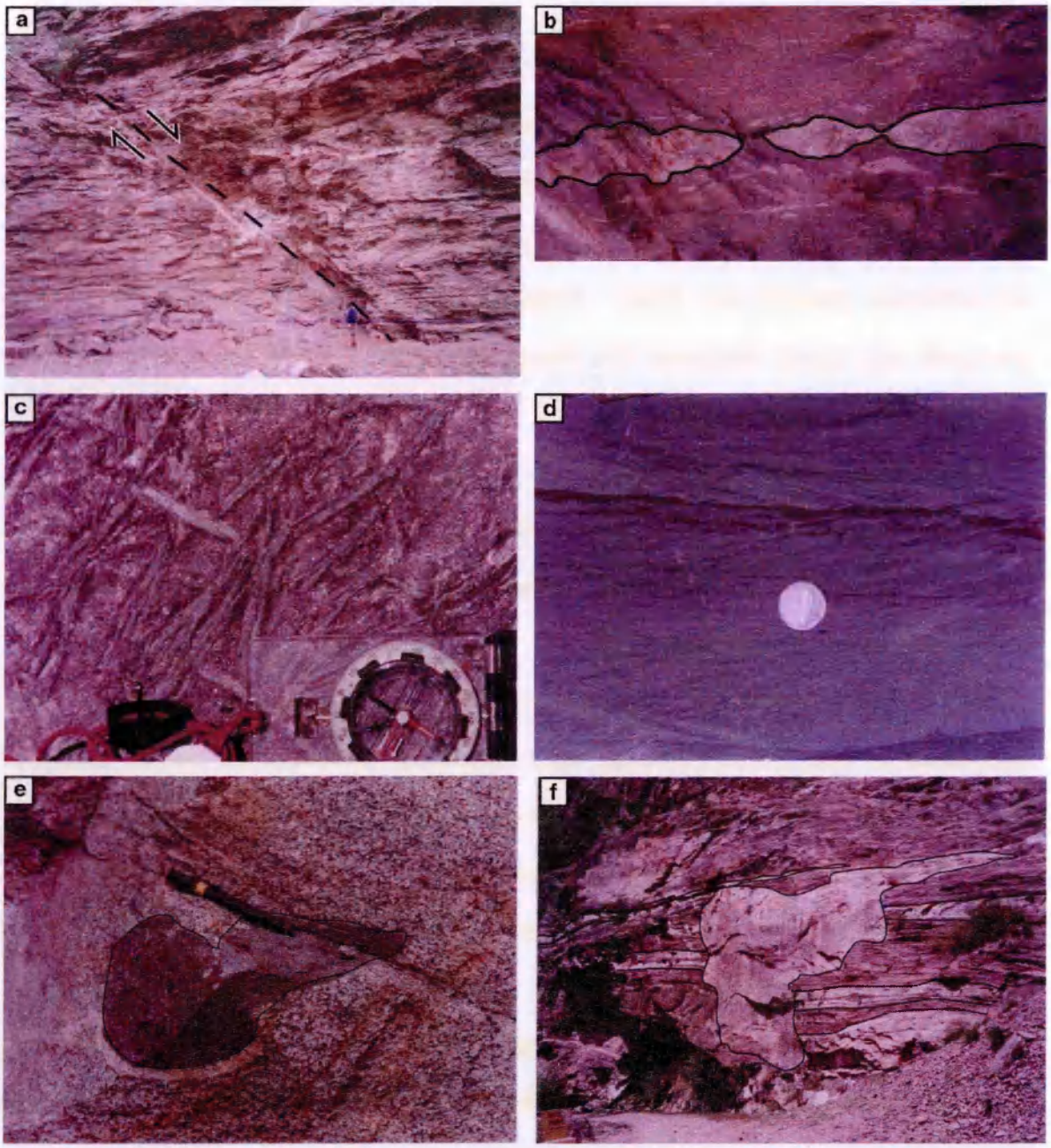

Figure 2.3 a to f – Field relations within the Haimanta and Vaikrita Groups. (a) One of a series of normal faults (riedal shears), looking northwest, related to extension on the STDS, fault gouge and breccia <50 cm; (b) Boudinaged leucogranites and leucosomes within the Haimanta Group, close to the contact with the Kinnaur Kailas Granite; (c) Large randomly orientated porphyroblasts of kyanite crystals within the Haimanta Group; (d) Cross-section of clay drapes seeming to pick-out ripple marks in the hinge of a small parasite fold, Haimanta Group; (e) xenoliths of the host rock (Haimanta) within the Kinnaur Kailas Granite; (f) Leucogranite body cross-cutting migmatites and fabric of Vaikrita Group, close to the STDS.

Close to the contact of the Kinnaur Kailas Granite, northwest of Akpa, the Haimanta Group is represented by a fine to medium-grained quartz biotite graphitic schist which coarsens slightly towards the granite contact. Late, deformed and undeformed, tourmaline-bearing leucogranite melts intrude the Haimanta Group, the greatest

concentration found towards the base of the section in the vicinity of the STDS and the Kinnaur Kailas Granite (Fig. 2.3 b; see next section). At the road bridge near Morang and at the tributary near the village of Tangi large kyanites (>5cm) appear in bands within a schistose fabric. Near Jangi, large staurolites (>1 cm) and kyanites (>5 cm) were also observed in a fine-grained phyllitic matrix, possibly representing a difference in bulk composition (Fig. 2.3 c). Further up section the metamorphic grade decreases and 1-2 Km northwest of Jangi the phyllites and slates coarsen up into psammites. Kyanite and staurolite decrease in abundance, while garnets were observed as far north as Pooh in calc-silicate layers. A few metabasites cut the psammites.

The Ropa River cuts an oblique section through the Haimanta Group in a northwest direction (Fig. 2.2), parallel to the younging direction, as confirmed by fining-upwards quartzites at Sangnam and ripple marks on micaceous bedding plains; best observed in cross-section near hinges of parasite folds (Fig. 2.3 d). The upper reaches of the Ropa River catchment area include part of the Lower Tethyan Sedimentary Series *sensu stricto*; purple psammitic clasts (Silurian) and dark organic rich phyllitic clasts are present in the river debris. The Haimanta Group in the Sutlej section is probably equivalent to the Chamba Formation of the Spiti section.

2.3.2 Intrusives

The Kinnaur Kailas Granite may be divided into three main petrographic facies: 1. Grey, biotite rich, aplitic granite; 2. two-mica, coarse-grained granite; 3. K-feldspar porphyritic granite. Late (Himalayan) aplitic and leucocratic granites cross cut these facies (Chawla et al., 2000; Marquer et al., 2000). Rb/Sr whole rock on the Kinnaur Kailas Granite gives an age of 462 ± 52 Ma and U-Pb zircon analysis gives an age of 459 ± 7.7, which are interpreted as crystallization ages (Chawla et al., 2000).

The Kinnaur Kailas Granite intrudes the lowermost part of the Haimanta Group and is cut by the STDS (Fig. 2.2) which lies directly below and can be tentatively traced as a low angle fault in the Sutlej above the village of Akpa (field observations and Thakur, 1992; Vannay et al., 1999). Marquer et al. (2000) and Chawla et al. (2000) suggest that no structural boundaries are present at the margins of the Kinnaur Kailas Granite. Sharma (1977) described Kinnaur Kailas Granite in the Sutlej as the Akpa Granite. Broad scale field observations reveal the Kinnaur Kailas Granite lies in a northwest-southeast orientation (Thakur, 1992) and is sheared at its margins with the Haimanta Group and the STDS, although it remains undeformed in the centre of the pluton. The sheared margins contain kyanite developed in the fabric. The contact between the Kinnaur Kailas Granite and the Haimanta Group is discordant and contains xenoliths of the host rock (Fig. 2.3 e).

2.3.3 Discussion

The Chamba Formation (lowermost Haimanta Group) is interpreted as having had a turbiditic depositional environment with overlying psammites and quartzites indicating progressive shallowing. In the absence of fossils, the timing of deposition for this formation is difficult to interpret, but the diamictites of the overlying Manjir formation are likely to have been deposited during one of the many Neoproterozoic glaciations and it is speculated that these diamictites are Marinoan (ca. 620 Ma) (Draganits et al., 1998). The termination of the Haimanta Group is at the Cambro-Ordovician boundary. Grasemann et al. (1997) and Wiesmayr and Grasemann (2002) observed that the Haimanta Group has undergone folding that is not observed in the overlying TSS, and the unconformity coincides with the intrusion of the (latest Pan-African) Kinnaur Kailas Granite (460 Ma; Chawla et al., 2000). This therefore implies that the deformation observed in the Haimanta Group is pre-Himalayan (Pan-African) (Miller et al., 2001). Marquer et al. (2000) suggest a continuous section from the HHCS to the Haimanta Group in the Sutlej, and that the contacts of the Kinnaur Kailas Granite are entirely intrusive. They propose the STDS lies 30 Km to the north. However, this study found

shearing at the boundary between the Kinnaur Kailas Granite and the underlying Vaikrita Group gneisses, which suggests that at least one boundary may be tectonic. Chawla et al. (2000) and Marquer et al. (2000) observed that the Kinnaur Kailas Granite cross-cuts the high-grade, pre-Himalayan deformation structures (D2-D3) but is locally affected by Himalayan D4 structures.

The regional correlation of the Chail Group (described later) remains uncertain. In the Lahaul Region, the Lahaul Group is the lateral equivalent to the Chamba Group; they are intruded by the Jispa and Dalhousie 500 Ma Granites respectively. The Chamba Group is interpreted as a westward continuation of the Chail Group, whereas the Lahaul Group is interpreted as a continuation of the Haimanta Group: Thakur (1992) notes that this tectonostratigraphic relationship indicates that the Chail and Haimanta Groups originally belonged to the same tectonic unit, but at present they are located under different tectonic settings.

2.4 The High-Grade Crystalline Series

The high-grade crystalline series refers to the rocks below the STDS and above the MCT (Fig. 2.2, Table 2.1). Below is a review of the field relations of the following units; the Vaikrita Group, the Karcham Group, the Jutogh Group, the Jutogh Klippe and the Chor Granitoid.

2.4.1 Vaikrita Group

The Vaikrita Group is bounded by the STDS to the northwest and Vaikrita Thrust to the southeast at Karcham. The Vaikrita Group represents the HHCS in the Sutlej Himalaya according to Vannay et al. (1999). The Vaikrita Group strikes northwest to southeast and dips 30° to the northwest, with a total thickness of ca. 15 Km. The metamorphic grade decreases from sillimanite migmatites at the top to garnet bearing mylonites, as observed by Vannay et al. (1999).

Broadly, the Vaikrita Group is a high-strain garnet-kyanite-sillimanite paragneiss of psammites and pelites and occasional thin calc-silicates (marbles). Intrusions become more frequent towards the top of the succession and include deformed and undeformed biotite-garnet leucogranites, tourmaline-bearing pegmatites and migmatites (Fig. 2.3 f).

Below the STDS (< 1 Km) the Vaikrita Group appears highly strained with shear fabrics suggesting a shear sense of top to the south (thrusting); sillimanite is present on foliation planes replacing white mica. Thin (<20 cm), occasional calc-silicate (marble) bands are also present. Pelitic gneisses contain garnet, kyanite, sillimanite and tourmaline.

About 5 Km northeast of Karcham a large mylonite zone indicates a marked increase in the strain, this results from movement along Vaikrita Thrust at Karcham (Thakur, 1992). Pre or post-tectonic garnet is present in the more pelitic layers. Conjugate shear sets are present, which are predominately top to the north-northeast, indicating top to the north deformation. Less than 1 Km east from Karcham a series of quartzites and schists crops out; Thakur (1992) assigned these sediments to the Karcham Group and associated them with the Vaikrita Group.

2.4.2 The Karcham Group

According to Thakur (1992), the Karcham Group consists of metasediments, mainly garnet-bearing graphitic schists with intercalated layers of quartzites and thin marbles. The group is highly strained with a noticeable increase towards the top (south) of the group; they lie between the mylonite zone that is associated with the Vaikrita Thrust which separates the Vaikrita Group and the Wangtu Gneiss Complex (part of the Jutogh Group). Late, brittle normal faulting is present in the Karcham Group, described as the Karcham detachment by Marquer et al. (2000) and the Karcham

Normal Fault by Janda et al. (2003) and Hager et al. (2003). Between the Wangtu Gneiss Complex and the Karcham Group Sharma (1977) noted a metamorphic break whereas Virdi (1976) did not. However, the Karcham Group forms only a small outcrop area in the Sutlej Valley and is often associated within the Vaikrita Group, or referred to as either MCTZ material or MCT quartzites (Vannay and Grasemann, 1998). This study considers them as part of the Vaikrita Group.

2.4.3 The Jutogh Group

The Jutogh Group was first described by Pilgrim and West (1928), and is regionally correlated to the Salkhalas of the Western Kashmir Himalaya (Gansser, 1964). According to Sharma (1998) the Wangtu Gneiss Complex corresponds to the Munsiari Formation and the Jutogh Group is correlated with the Almora Group in the Garhwal-Kuman Himalaya.

The outcrop area of the Jutogh Group in the Sutlej Area is large and extends from Karcham in the north to Chor in the south (Fig. 2.2) within the Jutogh Klippe (see below). The Jutogh Group in the Sutlej Area, according to Sharma (1998) consists of:

1. The Wangtu Gneiss Complex –largely the Wangtu Augen Gneiss, and kyanite-sillimanite schists, quartzites, calc silicates and amphiboles;
2. The Jutogh Metasediments – which forms the rest of the group, and are ampibolitised garnet-bearing psammites and pelites, which have a migmatitic fabric.

The Wangtu Gneiss Complex forms a broad domal structure ca. 10 km thick incised by the Sutlej River (Fig. 2.2). The top of the complex is juxtaposed against the metasediments of Karcham Group (assigned to the Vaikrita Group by Thakur, 1992) along the Vaikrita Thrust. There is a large metamorphic contrast between the psammites of the Karcham Group and the Wangtu Augen Gneiss (Caddick, 2004; Sharma, 1977; Valdiya, 1979). The rocks in this zone also appear to be highly

strained, and the strain appears to decrease noticeably in the augen gneiss from the northeast to southwest as the feldspar (plagioclase) augens increase in size from <1 cm at the boundary to > 4 cm ca 1 km from the boundary (see section 2.4.5).

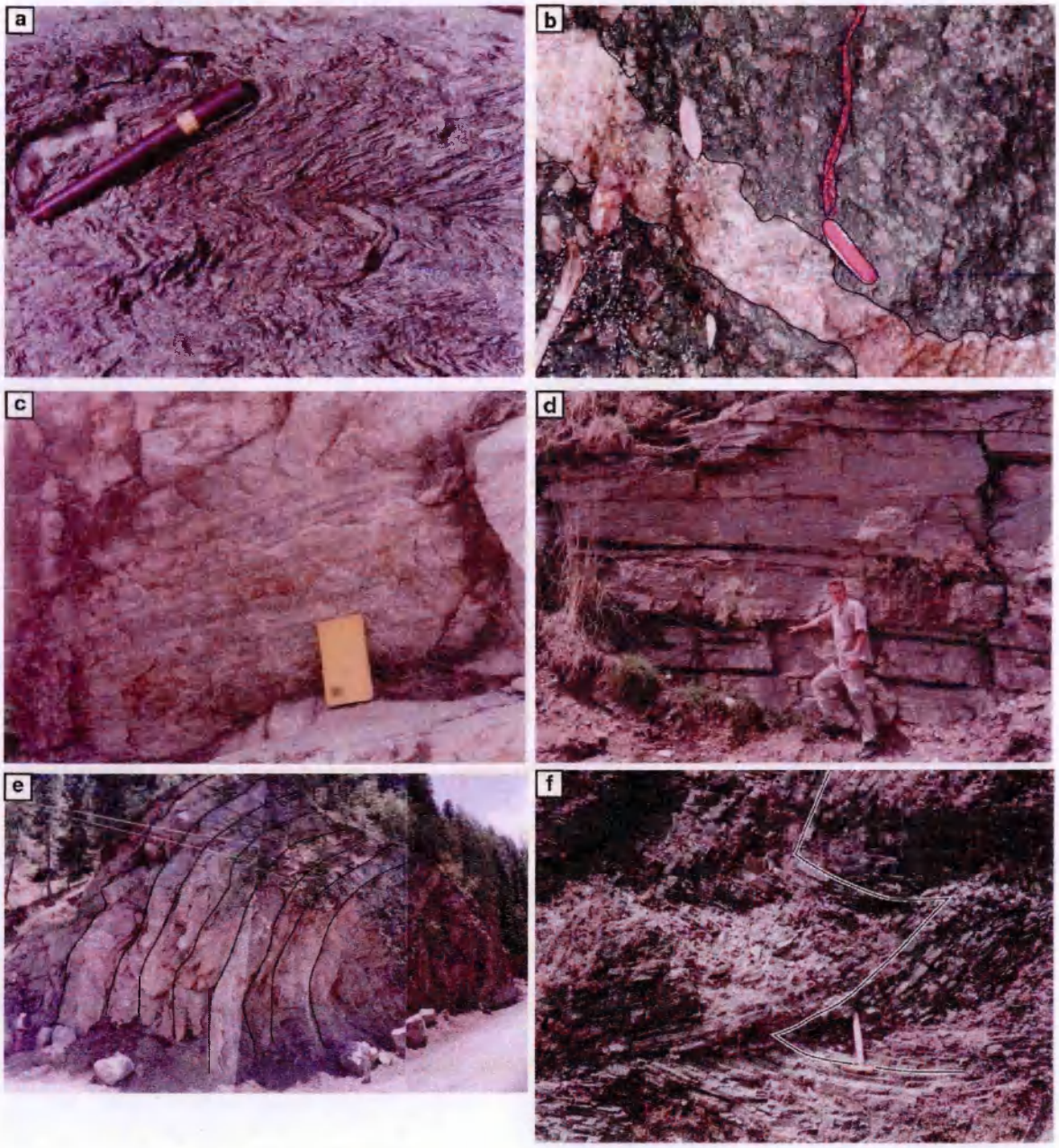

Figure 2.4 a to f – Field relations within the HHCS and LHS. (a) Crenulation cleavage well developed in more micaceous layers, Jutogh Metasediments, near Saharan; (b) Porphyritic texture of the Chor Granitoid, cut by late-stage veining; (c) Recrystallised quartzite, note heavy mineral bands pick out faint cross-bedding in the Rampur Formation; (d) Phyllitic metasiltstones and fine metasandstones, here banded medium-grained sandstones produce minor aquifers, picked out by moss, Shimla Group (Shimla A); (e) Folds in Shimla A, close to the tectonic boundary with Shimla B; (f) Highly deformed near chevron folding in Krol Group.

The nature of the boundary between the Wangtu Augen Gneiss and the Jutogh Metasediments is complicated by mafic and migmatitic intrusions, although it appears to be gradational, and is described as the basal part of the Jutogh Metasediments by Sharma (1998). The Jutogh Metasediments are broadly a medium grade (garnet-

staurolite) metasedimentary sequence of dominantly garnet-mica schists and quartzites, marbles, calc-silicates and graphitic schists (Sharma, 1998; Thakur, 1992). Staurolite-garnet-kyanite schists were observed in Sarahan, where staurolite is aligned along the cleavage. Boudins and crenulation cleavage are well developed in more micaceous layers (Fig. 2.4 a). Within the sequence there are bands of orthogneiss and amphiboles. The Chor Granitoid intrudes the Jutogh Group within the Jutogh Klippe (see below).

To the south, the Jutogh Metasediments are cut by the northeast dipping Jutogh Thrust (Fig. 2.2). The thrust zone contains talc and is highly eroded, and less than 500 metres within the Jutogh Metasediments high-strain zones are observed showing top to the north kinematics.

The Wangtu Gneiss Complex was dated by Kwatra et al. (1986) to 2025 ± 86 Ma using the whole rock Rb-Sr method. However, more recent U-Pb zircon ages give a younger age of 1866 ± 10 Ma (Singh et al., 1994); suggesting that the Rb-Sr age may be geologically meaningless (Miller et al., 2000).

The Jutogh Klippe

Pilgrim and West (1928) first described the rocks around Shimia, which includes crystalline basement material, and identified the structure as the Jutogh Klippe. Gansser (1964) noted that the area was structurally complex and cut by a number of thrusts. The lowermost crystalline unit is the Chail Group; it is bounded at the base by the Chail Thrust, and at the top the Jutogh Thrust separates the Jutogh from the Chail Group.

The Chor Granitoid

Pilgrim and West (1928) recognised that the Jutogh Group within the Jutogh Klippe was intruded by the Chor (or Chaur) Granitoid. The Chor Granitoid is a large, almost circular body ca. 3 Km east from Rajgarh and has an outcrop diameter of ca. 10 km

(Fig. 2.2). It consists of non-foliated homogenous granitoid (dominantly monzogranite and quartz monzonite), porphyritic orthogneiss (Fig. 2.4 b) and biotite orthogneiss (Singh et al., 2002). Garnets are observed in the country rock (Jutogh Group) ca. 1.5 Km from the contact, and increase in size towards the contact, where large garnets (>1 cm are observed), suggesting initial garnet growth due to contact metamorphism. Xenoliths of the Jutogh Group are present within the Chor Granitoid.

Singh et al. (2002) obtained individual U-Pb SHRIMP zircon ages from the Chor Granitoid of 823 ± 5 Ma (analyses undertaken on the SHRIMP II at Curtin University); this age is relatively anomalous compared to most Himalayan granite ages (Singh and Jain, 2003).

Pilgrim and West (1928) interpreted the relationship of the Chor Granitoid as an intrusive laccolith in the core of a large scale recumbent fold (i.e. the Shimla Nappe). Interestingly, Gansser (1964) questioned whether intrusions such as the Chor Granitoid have affected susceptible argillaceous units such as the Jutogh and Shimla units. Later, Kishore and Kanwar (1986) suggest partial melting of the metasediments of the middle to lower crust. Singh and Jain (1996) and Singh et al. (2002) interpreted the relationship between the granitoid and the Jutogh Group as tectonic, based on the presence of strongly developed fabric with orientated (top to southwest) mica, quartz, feldspar and ultramylonites.

2.4.4 Chail Group

The Chail Group according to Thakur (1992) is defined as the lowermost crystalline thrust sheet that is argillaceous-arenaceous in composition, metamorphosed to greenschist facies and underlies the medium to high-grade Jutogh Group. According to Srikantia and Bhargava (1974) the Chail Group is designated the Salkhala Formation and extends from Kashmir to the Shimla Hills. The Chail Group does not outcrop in Munsiari and Pinadari area in Kumaun and so the Jutogh (Munsiari) Group

lies directly on the Deoban Formation along the Jutogh (Munsiari) Thrust. The Chail Group is often described as a nappe as it is bounded above by the Jutogh Thrust and below by the Chail Thrust (Stephenson et al., 2000). Thakur (1992) describes the Chail to be composed of green, grey and silvery phyllitic quartzite, psammitic schist, orthoquartzite, arkose, chlorite schist and occasional limestones metamorphosed in the greenschist facies. Metavolcanics (amphiboles and gabbros) occur sporadically throughout the succession and display geochemical similarities with the mafic rocks of the Jutogh Group (Ahmad et al., 1999). A gabbroic body within the Chail Group collected along the Chail Thrust gives a whole-rock Rb-Sr age of 1907 ± 91 Ma, suggesting that the Chail Group may be older than this intrusion age (Ahmad et al., 1999).

In the Sutlej Valley, the Chail Group outcrops to the southwest of the Rampur-Larji Window and to the north of Narkanda and around Chail (Fig. 2.2) where it is considered as part of the Jutogh Klippe, first described by Pilgrim and West (1928). The Chail Group in the Sutlej Valley is complicated by the under- and overlying thrusts, and an incomplete section is observed. Where exposed, the Chail Group consists of highly weathered, highly strained psammitic and pelitic organic-rich, garnet-bearing mica-schists; cleavage refraction is present and is sub-parallel to bedding. The lowermost part of the Chail Group is exposed to the southwest of the Rampur-Larji Window; a mylonitic augen gneiss crops out close to the Chail Thrust. The mylonitic augen gneiss is between 500-900 m thick, granitic to granodioritic in composition (Thakur, 1992), and is dated as 1200-1400 Ma old by the Rb-Sr whole rock method (Bhanot et al., 1978).

2.4.5 Discussion

According to Heim and Gansser's (1939) classification, the correlations between the various high-grade crystalline units of the area have been a source of considerable confusion. The high-grade crystalline rocks of the Himalaya have, until recently, been

assigned to the High Himalayan sequence. Within the Sutlej Area, this definition has led researchers to the interpretation that all the high grade crystalline rocks in the Sutlej are High Himalayan (Manickavasagam et al., 1999) and therefore the MCT lies between the Jutogh Group and the Rampur-Larji Window (Fig. 2.2, marked as MCT^2); where much higher grade crystalline rocks (Jutogh Group) are thrust over much lower grade rocks (Rampur Formation). However, a metamorphic break at Karcham was discovered by Sharma (1977), and Valdiya (1980) and later Vannay et al. (2004, and references therein), which has led to the distinction and recognition of the Lesser Himalayan Crystalline Units (Jutogh Group), referred to as Lesser Himalayan Basement (Vannay et al., 1999) and High Himalayan Crystalline Units (Vaikrita Group). The work by Valdiya (1980) and Vannay et al. (2004, and references therein) has therefore placed the position of the MCT between these two units (known locally as the Vaikrita Thrust) (Fig. 2.2, marked as MCT^1). Recent work in the Garhwal Himalaya by Ahmad et al. (2000), has led to the discovery of an isotopic distinction between the high-grade rocks of the Vaikrita and Munsiari Groups along a contact also known as the Vaikrita Thrust (Chapter 1). In their interpretation, the Vaikrita Thrust represents the MCT in the Garhwal Himalaya. A detailed Nd isotope study of the high-grade crystalline rocks in the Sutlej Valley may support the work by Valdiya (1980) and Vannay et al. (2004, and references therein) in their interpretation and placement of the MCT (Chapter 3).

2.5 The Lesser Himalaya Series

The formations of the Lesser Himalaya crop out as a broad band northwest to southeast through the Sutlej Area (Fig. 2.2), and are well exposed around the city of Shimla (also known as Simla). The geographical area is described as the Kumaun Hills and is geologically complicated with largely unfossiliferous, complex stratigraphical and lithological successions affected by intense thrusting (Gansser, 1964). According to Thakur (1992) the LHS is separated from the overlying crystalline units by the Chail Thrust (Fig. 2.2), while Pant and Shukla (1999) and Valdiya (1995) describe the Upper

Proterozoic to Cambrian LHS as the Outer Lesser Himalaya. The LHS rocks in the Kumaun Himalaya are described as the Shimla-Krol Belt (Frank et al., 1994; Gansser, 1964).

The following table is a typical stratigraphical succession of the LHS according to Thakur (1992); recent fossil finds have been added where available:

Table 2.3 - Stratigraphy of the Lesser Himalaya, from Thakur (1992) after Tewari (1984). Recent palaeontological/geochronological data replace the previous age constraints.

Tal	Upper	Cambrian	Lower Cambrian (Hughes and Jell, 1999)
	Middle		
	Lower		Pre-Cambrian/Cambrian boundary (Tiwari, 1999)
Krol	E	Pre-Cambrian	'Upper Krol' Ediacara (Late Proterozoic) (Singh et al., 1999)
	D		
	C		
	B		
	A		
Infra Krol			
Blaini Formation			
			Blaini boulder bed, Sturtian (Frank et al., 1994)
Nagthat Formation			
Chandpur Formation Mandhali			Early Vendian Sponge Spicules, Gangolihat Dolomite, (Deoban Formation) (Tiwari et al., 2000)
Deoban	Shali/Larji Gangolihat		
Damta	Rautgara		
	Chakrata *(Shimla Group equivalent)*		Late Riphean (Raha and Sastry, 1982)
Berinag Formation *(Rampur Formation equivalent)*			Early Riphean (Miller et al., 2000)

Described below are the LHS formations from the Rampur Formation (equivalent to the Berinag Table 2.3), the Shimla Group and the Krol Group. These units have been sampled since they are predominantly clastic and represent lower and upper units of the LHS in the Sutlej Area:

2.5.1 The Rampur Formation

The Rampur Formation is exposed within the Rampur-Larji Window (also known as the (Larji–Kullu–Rampur Window), between the Beas and Sutlej Rivers and is correlated with the Berinag Formation. It forms a large antiformal structure and outcrops over a distance of ca. 15 Km in the Sutlej Valley. The rocks within the Rampur-Larji Window are low-grade metasediments and are assigned to the LHS (Thakur, 1992, and references therein) and are tectonically (thrust) bounded by crystalline rocks to the north (Jutogh Group) and south (Chail Group) (Fig. 2.2). The large metamorphic contrast between the low-grade rocks within the Rampur-Larji Window and the high-grade Jutogh Group rocks to the north have, according to Heim and Gansser's (1939) classification, been interpreted as the MCT (Manickavasagam et al., 1999; Thakur, 1992).

The rocks within the Rampur-Larji Window contain the Larji-Shali Formation, the Rampur Formation and the Bandal Granite. It is unclear whether the Rampur Formation unconformably overlies the Bandal Granite or whether the granite intrudes the basal quartzites (Miller et al., 2000). Stromatolites from the Larji-Shali Formation carbonates at the top of the lower sequence suggest a lower to mid-Riphean age, the Rampur Formation is considered the lowermost formation (Miller et al., 2000). However, in the Sutlej Valley, only the Rampur Formation crops out and therefore this succession will be referred to collectively as the Rampur Formation from hereon. The Rampur Formation is predominantly sedimentary with a large proportion of recrystallised quartzites (Fig. 2.4 c), although a suite of metavolcanics (the Rampur Volcanics) occur within the formation. Thakur (1992) describes the Rampur Formation as three members:

Table 2.4 - Lithostratigraphy of the Rampur Formation, after Thakur (1992) and Bhargava et al., (1972).

Member	Lithology
Member A	Cross-bedded and ripple marked quartzitic sandstone
Member B	Grey to green chlorite phyllite with interstratified quartzite and metavolcanics
Member C	Cross-bedded ripple-marked quartzite with chlorite phyllite partings, metavolcanics and paragneiss

The Rampur metabasalts are tholeiitic in composition with a geochemistry indicative of lherzolitic source and relatively high degrees of partial melting (Miller et al., 2000). Sharma (1998) interpreted the quartz dominated lithologies with mineralogical and textural maturity and tholeiitic volcanics as rift-related sedimentation with granitic (source) rocks to the south. The deposition of fine-grained material (now phyllite) within the formation suggests to Sharma (1998) a deepening sequence. Zircons from a metarhyodacite and a metabasalt yielded evaporation ages of 1840 ± 16 Ma and 1800 ± 13 Ma respectively (Miller et al., 2000) suggesting that silicic volcanism and granitic emplacement were coeval. Nd model ages of 2630 Ma from peraluminous granitic rocks suggest recycling of older (Early Proterozoic to Late Archaean) crust (Miller et al., 2000).

2.5.2 Shimla Group

The Shimla Group (also known as the Shimla Slates) crop out in the Sutlej Area near Shimla (Fig. 2.2). The Shimla Group is difficult to constrain stratigraphically as most of the group is bounded by tectonic contacts, and probably represents an allochthonous or para-autochthonous terrain (Gansser, 1964). However, Raha and Sastry (1982), amongst others, found stromatolite-bearing limestones within the group and on this basis assigned an Upper Riphean (early Neoproterozoic) age to the group. A boulder bed overlies the top of the Shimla Group and has been described by many authors (Frank et al., 2001; Frank et al., 1994; Gansser, 1964; Thakur, 1992). Tentative correlations have related this to the Blaini boulder bed. Furthermore, Frank et al. (1994) has related this to the Manjir boulder bed described by Draganits et al.

(1998) which was probably deposited during the Neoproterozoic Marinoan glacial event (ca. 620 Ma).

The Shimla Group broadly coarsens upwards; Srikantia and Sharma (1971) separated the Shimla Formation into several members which are summarised below:

Table 2.5 - Lithostratigraphy of the Shimla Group (from Thakur (1992), after Srikantia and Sharma (1971).

Formation	Member	Lithology	Thickness (in m)
Sanjauli	Upper	Coarse lithology: conglomerates, grits, quartzites, grey and purple shales	1600
Chhaosa	Lower	Greywackes, shales and siltstones interbedding with quartzites Interbedding grey/green/purple shales and siltstones, with greywackes	1300
Kunihar	E	Shale and siltstone interbedding, and limestone	450
	D	Thick bedded, buff/ blue limestone with interbedded shale/marl (local facies)	180
	C	Massive to bedded limestones and dolomites (local facies)	250
Basantpur	B	Shales and siltstones with interbedded lenticular limestone, occasional carbonaceous shale, quartzite and dolomite	600
	A	Grey/white quartzite with occasional conglomerate	190

Thakur (1992) correlates the Shimla Group with the Chakrata Formation (east of the Tons River), part of the Damta Group (Table 2.3), and separates the Shimla Group in to Shimla A and Shimla B for the Sutlej Area:

- *Shimla A* rocks are broadly phyllitic metasiltstones to fine metasandstones with occasional lenticular, medium-grained sandstones (Fig. 2.4 d); a pervasive cleavage is developed.
- *Shimla B* rocks are tectonically separated from underlying Shimla A; folds with wavelengths ca. 10 metres are present close to the boundary (Fig. 2.4 e). Shimla B rocks are more psammitic, consisting of metasandstones and metaquartzites. The slaty cleavage is weaker and less pervasive.

2.5.3 Krol Group

The name Krol was assigned by Medlicott (1864) after Krol Mountain near Solan (Fig. 2.2). An Ediacaran Age (late Neoproterozoic) is assigned to the Upper Krol on the basis of fossil and Re-Os data (Singh et al., 1999). The Krol Group conformably succeeds the InfraKrol and is unconformably overlain by the Chert Member of the Tal Formation which represents the Pre-Cambrian/Cambrian boundary on the basis of microfossils according to Tiwari (1999) or the Lower Cambrian on the basis of trilobites, according to Hughes and Jell (1999). After the work of Medlicott (1864), Auden (1934) separated the Krol into six sub-divisions (Table 2.6):

Table 2.6 - Lithostratigraphy of the Krol Group, after Auden (1934) and Mazumdar and Banerjee (2001).

Formation	Sub-Formation	Lithologies
	E	Argillaceous dolomite, laminated dolomite and grey-black shales
Upper Krol	D	Fenestral, stromatolitic dolomite with chert layers
	C	Limestone, dolomite and laminated algal dolomite
Middle Krol	B	Red shales and minor carbonates
Lower Krol	A	Marlstone and sandstone
	Krol Sandstone	Orthoquartzite, lenses of unconsolidated sandstone, sandstone pellets of phosphate along bedding plane

Thakur (1992) simply divides the Krol Group in the Sutlej Area into the Inner Krol Belt and the Outer Krol Belt though the area is structurally complex:

- *The Outer Krol* - a conglomerate is present between the Shimla Group and the overlying Krol. The conglomerate is polymorphic and contains imbricated clasts of quartzites, mudstones, vein quartz and rare red chert. The Outer Krol near Solan consists of highly weathered phyllites, limestone/dolomites and clastic-rich quartzites. The Outer Krol around Solan may correspond to Auden's (1934) subdivisions E to C.
- *The Inner Krol* is structurally bounded to the Outer Krol. Southeast of Sataun, pelites are highly fractured and folded almost isoclinally (Fig. 2.4 f); quartzites show less structural deformation. Where present, the slaty cleavage is near

parallel to bedding. The Inner Krol may correspond to Auden's (1934) Krol Sandstone.

2.5.4 Discussion

Although punctuated with unconformities, the LHS sediments have had a long depositional history, from the Palaeoproterozoic to the Early Palaeozoic. The Rampur Formation is at least older than 1800 Ma, and possibly as old as 2400 Ma (zircon dating; Miller et al., 2000; Sharma, 1998).

The Shimla Group has been interpreted as having a depositional environment of a prograding muddy delta sequence that formed as result of the collapse of a carbonate shelf (Kumar and Brookfield, 1987). The overlying Blaini Boulder Bed is interpreted as a glacial diamictite deposit coincidental with the ca. 620 Ma Marinoan glacial event. The Latest Neoproterozoic Krol Members are interpreted as a supratidal–intertidal–subtidal depositional environment (Singh, 1979).

Frank et al. (1994) correlates the Blaini boulder bed in the LHS with the Manjir boulder bed in the Haimanta Group (Draganits et al., 1998). Rb/Sr whole-rock dating indicates a maximum depositional age of 700 Ma for the Blaini Boulder bed; whereas both beds have an equivalent model Nd age of 1.8-2.3 Ga. Depositional ages are corroborated by detrital muscovite ages of 865 Ma (Frank et al., 1994) in the Shimla Group; cooling ages for the Aravalli/Delhi System, however, are greater than 1.0 Ga, suggesting that these regions cannot be the source for the material. In addition, Frank et al. (1994) found palaeocurrent direction indicators in the upper Haimanta Group implying a source to the north, rather than to the south as would be expected for an Aravalli source. Indeed, although Rashid (2002) found palaeocurrent directions in the Chakrata (Shimla Group) indicating a southerly direction and a broadly granitoid source region (based on whole rock geochemistry), the Bundelkhand Massif to the south contains U-Pb SHRIMP ages on zircons of >3.2 Ga (Mondal et al., 2002);

whereas no zircons >2.6 Ga have been found in Himalayan metasediments (DeCelles et al., 2000; Parrish and Hodges, 1996), however, this may be due to small sample size as Myrow et al. (2003) after dating 132 zircon fractions has dated two ca. 3.5 Ga zircons from stratigraphically similar rocks in the Garhwal Himalaya.

However, although there are similarities in the depositional ages for the Haimanta Group and Shimla Groups, the Haimanta Group is broadly coarser grained compared to the finer grained Shimla Group (Frank et al., 1992). An alternative explanation is that the Haimanta Group and Shimla groups are proximal and distal lateral facies equivalents respectively within a single basin, but widely separated, which would allow for discrepancies in the palaeocurrent directions.

2.6 The Sub-Himalaya Series

The Sub-Himalaya represents the foreland basin of the deposits of Cainozoic uplift and erosion of the Himalaya; this basin extends across the entire length of the orogen. This unit is located between the MBT to the north, the boundary with the LHS, and the MFT to the south, which is still active and thrusting the older units of the Sub-Himalaya over recent alluvial sediments of the Indo-Gangetic plain (Najman et al., 2000). The units within this group in the Himachal Himalaya are the Subathu, Dagshai, Kasauli and Siwalik Formations and are summarised in Table 2.7.

2.6.1 Siwalik Group

Pilgrim (1910 and 1913) separated the Siwalik into three major sub-units (lower, middle and upper). According to Thakur (1992) the Siwalik Formation in the Sutlej Area is described as follows (from oldest to youngest):

The Lower Siwaliks consists of brown to red massive, hard, coarse medium to fine grained sandstones, and has a total thickness of 1300-1600 metres.

The Middle Siwaliks has a maximum thickness of 1500 metres and consists of medium to coarse sandstones and clays with conglomerates.

The Upper Siwaliks is up to 2300 metres thick and varies from mudstones to conglomerates.

Table 2.7 - Summary of the Late Cretaceous - Tertiary Formations in the Sub-Himalaya, modified from Najman et al. (1993 and 1997) and Burbank (1996).

Formation	Age	Approx age (Ma)	Lithologies	Facies Interpretation
Siwalik	Middle Miocene-Early Pleistocene	Ca. 13 – 1.8 Ma *Burbank (1996)*	Red to brown mudstones, sandstones and conglomerates, broadly coarsening upwards	Fluvial
Kasauli	Lower-Middle Miocene	Ca. 23-10 Ma *Najman et al. (1997)*	Grey sandstones, siltstones and mudstone. Much woody material	Humid Climatic, braided fluvial regime
Dagshai	Mid Oligocene – Upper Oligocene	Ca. 28-23 Ma *Najman et al. (1997)*	Red sandstones, siltstones, mudstones and caliche	Semi-arid climate, meandering fluvial and floodplain regime
Subathu	Late Palaeocene-early Mid Eocene (Lower Lutetian)	Ca. 65-28(?) Ma *Najman et al. (1993)*	Limestones, mudstones and fine sandstones	Shallowing marine
Singtali	Upper Cretaceous-Palaeocene	Ca. 75-65 Ma *Najman et al. (1993)*	Limestones	Shallow marine

2.6.2 Kasauli Formation

The Kasauli Formation is stratigraphically older than the Siwalik Formation and conformably overlies the older Dagshai Formation. Characterised by mainly grey sandstones and mudstones, fossil floral constrain an early to mid Miocene age, while detrital micas from this formation range from 22-32 Ma (Najman et al., 1997).

2.6.3 Dagshai Formation

The Dagshai Formation conformably overlies the stratigraphically older Subathu Formation. It consists of red, friable sandstones, siltstones and mudstones, with

occasional calcite cement. Detrital muscovites give ages from 25 to 32 Ma (Najman et al., 1997).

2.6.4 Subathu Formation

The Subathu Formation is predominantly composed of limestones with mudstones and fine sandstones. Marine fauna assign a late Palaeocene to lower mid-Eocene. Najman et al. (1994) observed that within the Subathu Formation there is little evidence of terrigenous clastic influence and its deposition therefore pre-dates Himalayan uplift. However, Najman and Garzanti (2000) refute this; sandstone petrography reflects a provenance influence from the Indus suture zone suggesting the Subathu Formation is post-collisional.

Chapter 3 - The Geochemistry of the Sutlej Area

3.1 Introduction

The previous chapter explained the complexity of locating tectonic units and structures in the Sutlej area. Previous work (reviewed in Chapter 1) by Parrish and Hodges (1996), Whittington et al. (1999), Ahmad et al. (2000) and Argles et al. (2003) has demonstrated that Sr and Nd whole-rock isotopes and U-Pb dating of individual zircons can be used to define and discriminate between major Himalayan units and therefore the thrusts that divide them. However, some studies claim to refute this distinction (Miller et al., 2001; Myrow et al., 2003). In this study we examine the evidence from both elemental and isotopic compositions of clastic sediments from the Sutlej Area for discriminating between the major Himalayan units (for sample localities see Fig. 2.2).

3.2 Whole-Rock Geochemistry

Elemental abundances of clastic sediments retain information about their source areas. Bhatia (1983) and later Roser and Korsch (1986; 1988) proposed that diagrams based on whole rock major and trace element concentrations can, under some circumstances, be used to discriminate between sediments with contrasting source areas. However, although Ahmad et al. (2000) showed that some correlation did exist, effective discrimination of Himalayan metasediments could not be solely made using these methods. Using discriminate functions of Roser and Korsch (1988), and discrimination diagrams of Bhatia (1983) and Fralick and Kronberg (1997), Figures 3.1 a–d show that no clear discrimination between the major Himalayan tectonics units in the Sutlej can be made; there is considerable overlap of the two units (HHCS and LHS) even when the data is reduced using samples between 60-80% SiO_2 (i.e. those with a 'greywacke' composition). This is because either both groups of sediments are formed in a similar tectonic environment, or because metamorphism has blurred original distinctions. However, the data set plots mainly within the Mafic Igneous Provenance

Intermediate Igneous Provenance fields (Fig. 3.1 a) and plots across most fields in Figure 3.1 b, suggesting a mixed source provenance.

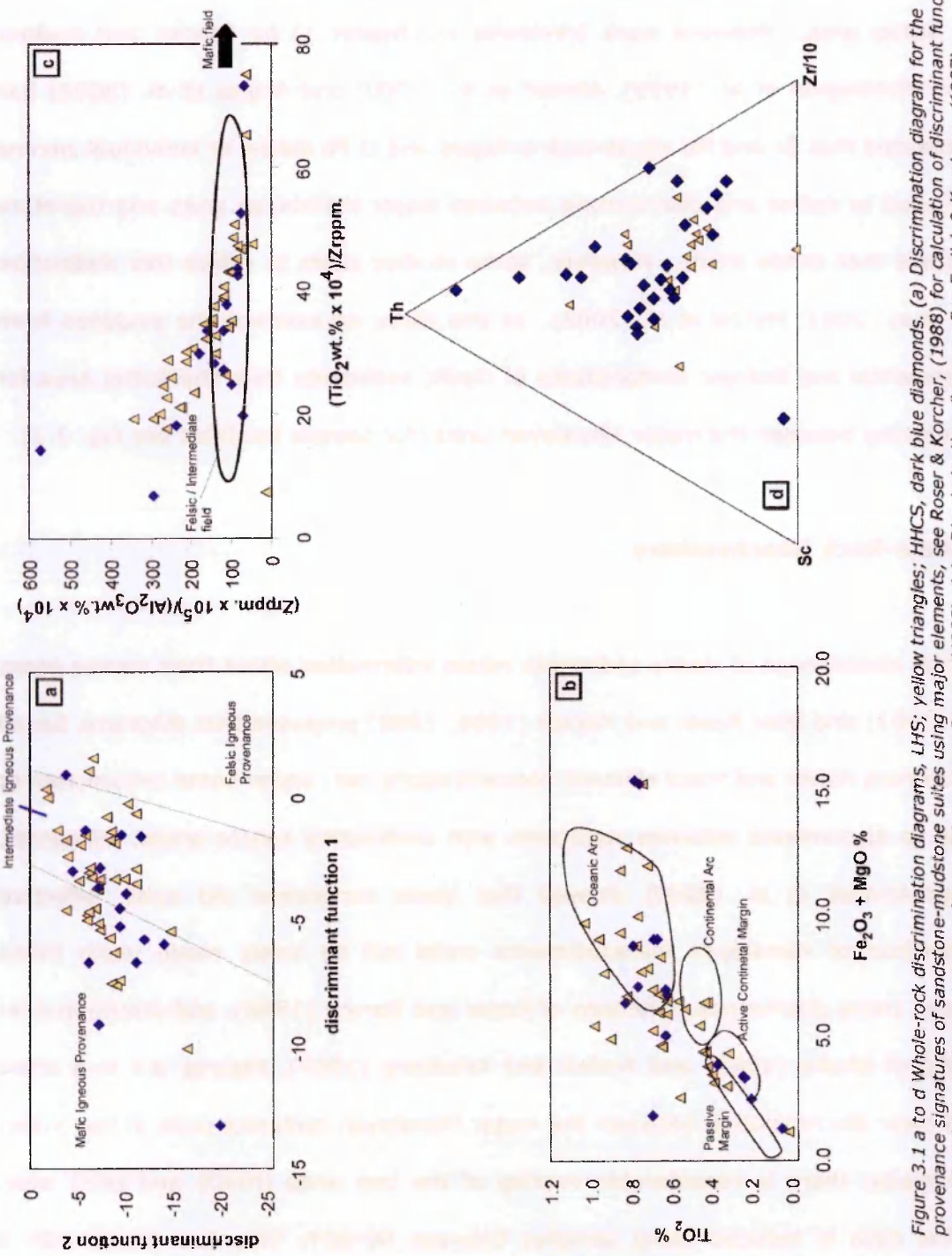

Figure 3.1 a to d Whole-rock discrimination diagrams, LHS; yellow triangles; HHCS, dark blue diamonds. (a) Discrimination diagram for the provenance signatures of sandstone-mudstone suites using major elements, see Roser & Korcher, (1988) for calculation of discriminant function 1 and 2; (b) Discrimination diagram for sandstones after Bhatia, (1983); (c) - Discrimination diagram after Fralick & Kronberg, (1997); (d) Discrimination diagram for Greywackes (after Bhatia & Crook, 1986).

3.3 Isotope Geochemistry

3.3.1 Sr and Nd Isotope Geochemistry - Results

A total of 38 rock samples (Fig. 2.2) were selected for Sr and Nd analysis (plus 14 powdered samples from E. Draganits, Vienna University of Technology) to represent the tectonic units in the Sutlej Area. According to Thakur (1992) the tectonic units in the Sutlej are as in Table 2.1. However, recent work by Vannay et al. (2004 and references therein) designated the Vaikrita Thrust (located at Karcham; Fig. 2.2) as the MCT, thereby subdividing the Crystalline Unit of Thakur (1992) and assigning the Vaikrita Group to the HHCS (hanging wall) and reinterpreting the Jutogh Group (consisting of the Wangtu Gneiss Complex and Jutogh Metasediments) as Lesser Himalayan basement material (footwall).

As demonstrated in Chapter 1 the ε_{Nd} values presented here (Fig. 3.2; Appendix B) are age-corrected to t=500 Ma. This age was chosen because a better discrimination is shown between the Himalayan units, possibly as a result of a tectono-thermal event around this time (Ahmad et al., 2000); other interpretations are discussed in Chapter 1. The ε_{Nd} values from this study (Fig. 3.2) for Thakur's crystalline series appear to cluster into two distinct arrays of -19 to -17 for the Jutogh Group and -13 to -3 for the Vaikrita and Chail Groups (consistent with the ranges for ILHS and HHCS from Ahmad et al., 2000); the unusually low value (-3) for one Vaikrita Group sample may reflect some contribution from mantle-derived volcaniclastic detritus; Inger and Harris (1993) observed low ε_{Nd} values in schists in the HHCS (Langtang). Five outliers are marked 'OL' on Figure 3.2 will be discussed later in the chapter. The observed difference in isotopic arrays is consistent with two major thrusts in the region: the Vaikrita Thrust, which separates the Vaikrita Group in the hanging wall to the Jutogh Group in the footwall, and the Jutogh Thrust, which separates the Chail Group from the overlying Jutogh Group. The Jutogh Thrust is observed to the north of, and is complicated by, the structure of the Rampur-Larji Window. Both the Vaikrita Thrust and the Jutogh

Thrust appear to control aspects of the topography of the Sutlej area; the Vaikrita Thrust is consistent with a sharp change in the course of the Sutlej River, and indeed it appears that the Beas River runs parallel with this thrust for many kilometres, whereas to the south of the Jutogh Thrust the Sutlej Valley appears to widen. The LHS also appears to form two distinct arrays of -19 to -18 for the Palaeoproterozoic sediments of the Rampur Formation (similar to the Jutogh Group), and -12 to -5 for the Neoproterozoic sediments of the Shimla and Krol Groups (similar in isotopic ratio to the Vaikrita and Chail Groups). The metasediments of the Haimanta Group also plot within a similar array to the Vaikrita and Chail Groups, although some overlap with the Jutogh Group and Rampur Formation data occurs (-7 to -18; see discussion). Therefore, the ε_{Nd} (t=500 Ma) histogram appears to define two distinct arrays, similar to the findings of Ahmad et al. (2000), suggesting that the source regions for the Vaikrita, Chail, Haimanta, Shimla and Krol Groups are distinct from those of the Jutogh Group and the Rampur Formation.

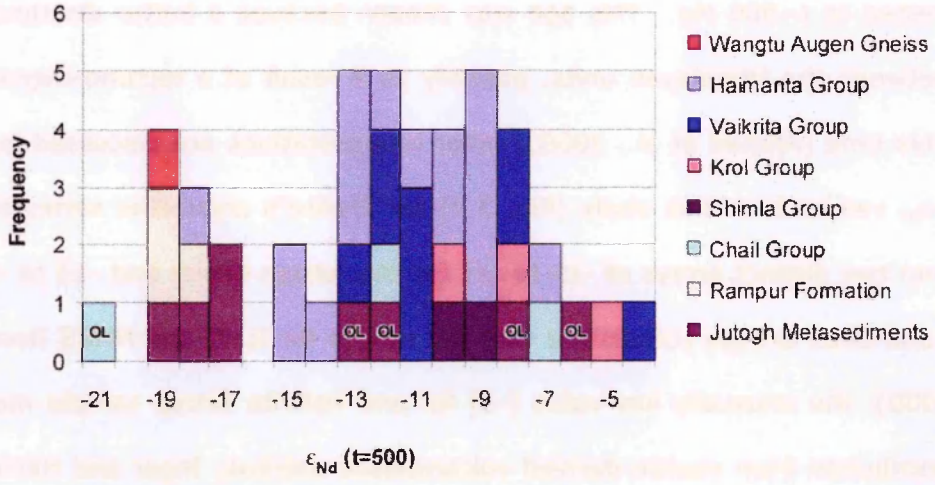

Figure 3.2 – Histogram of isotopic data from the Sutlej Area (this study), presented as ε_{Nd} (t=500 Ma); OL=Outlier.

The Sr data set (Fig. 3.3) shows a similar pattern to that observed in the ε_{Nd} histogram. Published data forms two arrays around calculated reference lines of 1800 and 500 Ma (Fig. 1.7); these form two fields on Figure 3.3 described as a HHCS and a LHS field by Argles et al (2003). For the crystalline unit of Thakur (1992), the Vaikrita and Chail Groups cluster around the 500 Ma reference line (the HHCS field), whereas

the Jutogh Group clusters around the 1800 Ma reference line (the LHS field). The Sr system is more sensitive to geological (e.g. thermal) events than Nd, e.g. one sample from the Vaikrita Group sampled close to the Vaikrita Thrust, near to thermal springs, shows an elevated $^{87}Sr/^{86}Sr$ ratio (>1.250), suggesting perturbation of the system. However, the Vaikrita Group sample with an anomalously high ε_{Nd} value of -3 plots well in relation to the 500 Ma reference line, suggesting that either the perturbation of the Sr system at 500 Ma may have affected the Nd system at the same time, or more likely there is a mafic component to this sample. Within the LHS a distinction can be made which complements the Nd data. The Shimla and Krol Group sediments, like the Vaikrita and Chail Groups, plot around the 500 Ma reference line. The Haimanta Group also plots close to the 500 Ma reference line; this includes the four samples that appear to straddle the two groups on the ε_{Nd} histogram. Although the Rampur Formation data display large variations in both $^{87}Sr/^{86}Sr$ and $^{87}Rb/^{86}Sr$, the data lie close to the 1800 Ma reference line with the exception of one sample collected close to the southern thrust boundary of the Rampur-Larji Window. The outliers identified in Figure 3.2 are also present as outliers on Figure 3.3; again these will be discussed later. Therefore the Sr data strongly complements the Nd data set; distinctive ranges in isotopic ratios can be observed between groups using both isotope systems.

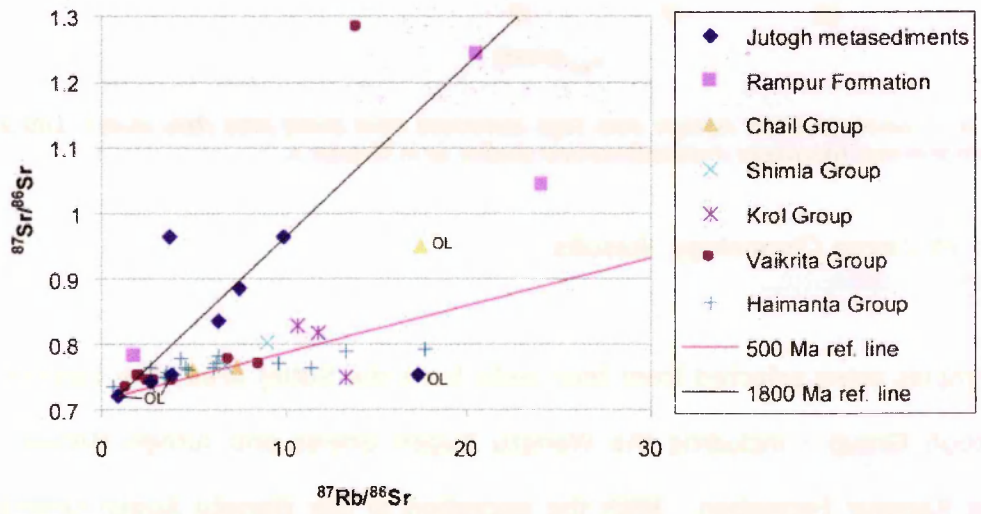

Figure 3.3 - Sr isotopic data from Sutlej Area (this study); OL, outliers, as previously identified in Figure 3.2.

Combining the previously described isotope systems on an age-corrected $^{87}Sr/^{86}Sr$ (t=500 Ma) vs ε_{Nd} (t=500 Ma) plot, the inter-group differences are clarified (Fig 3.4). The Shimla, Krol, Vaikrita and Chail Groups, clearly define one array with characteristically less negative ε_{Nd} values and lower $^{87}Sr/^{86}Sr$ and plot well within the previously defined HHCS field (Fig. 1.8). The Jutogh Group and Rampur Formation with more negative ε_{Nd} values and a greater range of $^{87}Sr/^{86}Sr$ form the second array and plot well within the previous defined LHS field (Fig. 1.8). The HHCS field appears more oblate compared to the 'LHS field' suggesting that the tectono-thermal event that effected the HHCS had little effect on this 'LHS field'. The Haimanta Group broadly plots within the HHCS field which may reflect a tectono-thermal event ca. 500 Ma; indeed the Kinnaur Kailas Granite intrudes the lowermost Haimanta (462 ± 52 Ma, Chawla et al., 2000).

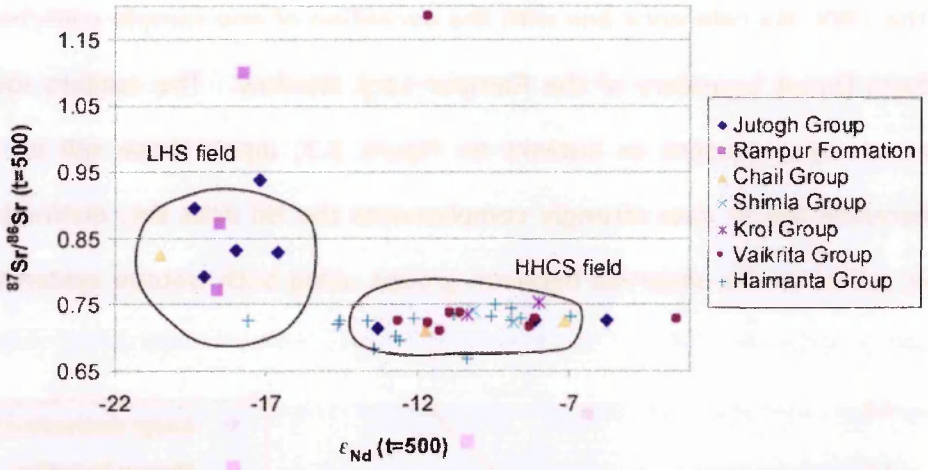

Figure 3.4 - Combined Sr-Nd isotopic data (age corrected) from Sutlej Area (this study); LHS and HHCS fields from previous Himalayan metasedimentary studies as in Chapter 1.

3.3.2 U-Pb Zircon Chronology -Results

Five samples were selected from four units from the Sutlej Area; the Vaikrita Group, the Jutogh Group - including the Wangtu Augen Gneiss and Jutogh Metasediments, and the Rampur Formation. With the exception of the Wangtu Augen Gneiss, these samples are metasediments with sandstone protoliths, and range in metamorphic grade from kyanite to chlorite. All fractions were strongly abraded using the Krogh

(1982) method and photomicrographs of each zircon were taken before and after air abrasion and were analysed by ID-TIMS methods (Appendix A). Conventional ID-TIMS methods gives at least one order of magnitude better SHRIMP or LA-MC-ICPMS accuracy allowing greater geological interpretation as ages have a much greater precision (i.e. they are geologically 'real') allowing greater interpretation when the data is plotted as concordia plots (see below). However, SHRIMP or LA-MC-ICPMS techniques serve as a powerful diagnostic tool when large numbers of minerals need to be analysed (as discussed in Section 1.5), or when minerals have complex core-rim relationships and/or metamorphic overgrowths (which can result in discordance with conventional ID-TIMS methods; see discussion of discordance in section 3.4.2).

The U-Pb zircon geochronological data are presented here as concordia plots (Fig. 3.5 to 3.8; summarised in Fig 3.9 d; Appendix C) and contain a number of concordant to highly discordant measurements. Wetherill (1956) invented the concordia diagram and defined the terms concordance and discordance. Discordance is defined as where a point in the concordia diagram has different calculated $^{207}Pb/^{235}U$ and $^{206}Pb/^{238}U$ ages, conversely concordance is where a point in the concordia diagram has identical $^{207}Pb/^{235}U$ and $^{206}Pb/^{238}U$ ages (Parrish and Noble, 2003). The curve that results from plotting all concordant points through time is termed 'concordia'. Due to the uncertainties in the decay constants for the parent isotopes concordia is in fact a band (Parrish and Noble, 2003; e.g. Fig. 3.7 and 3.8). If concordant to near concordant, the $^{207}Pb/^{206}Pb$ ratio is regarded as a good estimate for the age of crystallisation (Wetherill, 1956), therefore an arbitrary value of 5% discordance will be taken as the maximum value allowing $^{207}Pb/^{206}Pb$ ages to be treated with confidence (Parrish and Hodges, 1996; Ross and Parrish, 1992; Wetherill, 1956). Fractions with 5% discordance or greater will only enable a minimum crystallisation age to be interpreted (Ross and Parrish, 1992) as greater discordance increases the uncertainty of the interpretation, because discordance could be produced by one or more Pb loss event, inheritance or metamorphic overgrowth. In cogenetic zircon populations such as those from magmatic rocks, data can be regressed along a chord using an error

calculation modified from York (1969) (e.g. Fig. 3.7). Using this technique, upper intercept ages are frequently interpreted as corresponding to the crystallisation age of the zircon, whereas lower intercept ages may represent the time of a thermal event, but can be geologically meaningless if they do not correspond to known geological events (Dickin, 1997).

Vaikrita Group (w34z and w43z)

The zircons of the Vaikrita Group samples (w34z and w43z) are fawn/pink in colour and are generally clear with occasional inclusions; they are rounded, mainly anhedral to subhedral and range between 150-300 μm, with some prismatic faces present. There is a small population of elongate zircons (<5%). A broad range of U concentrations is observed (between 82-1191 ppm), although 80% of the population are between 206-675 ppm.

Concordia plots (Fig 3.5 a and b) from the Vaikrita Group (w34z and w43z respectively) demonstrate an older and a younger population (Fig. 3.5 a and b; inset) which are present in both samples. The majority of fractions in the younger population (Fig. 3.5 a and b; inset) have between 2-14% discordance, with $^{207}Pb/^{206}Pb$ ages ranging from 830-897 Ma (although the youngest fraction is 33% discordant). One fraction that is 22.5% discordant yields a $^{207}Pb/^{206}Pb$ of 1126 Ma, which may represent a further population. The older population in both samples are much smaller and are 8-11% discordant; these fractions have $^{207}Pb/^{206}Pb$ ages of between 2515–2574 Ma with one fraction dated to ca. 2085 Ma. These data suggest that a large Neoproterozoic population and a smaller Palaeoproterozoic - Late Archaean population are present within the Vaikrita Group. Furthermore, the maximum age of deposition of these rocks is constrained to 830 Ma. Although it is tempting to interpret this data further using the regression technique of York (1969), a number of uncertainties remain. As these samples are metasediments it is undetermined whether the zircon fractions are cogenetic. Further research, including core and rim observations and dating, is required to ascertain a cogenetic population which would

then enable interpretations that include multiple Pb loss events suffered by the older population related to the crystallisation event of the younger population in the source area.

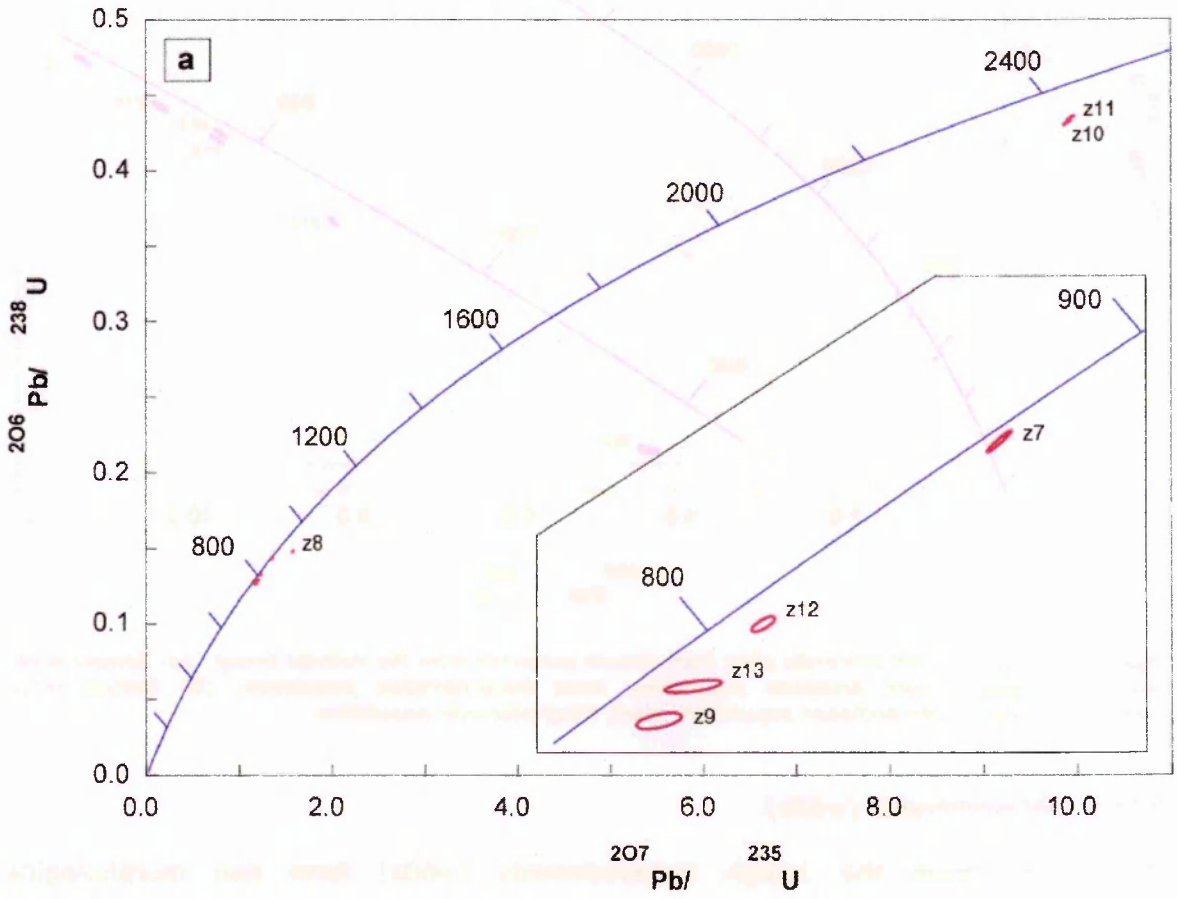

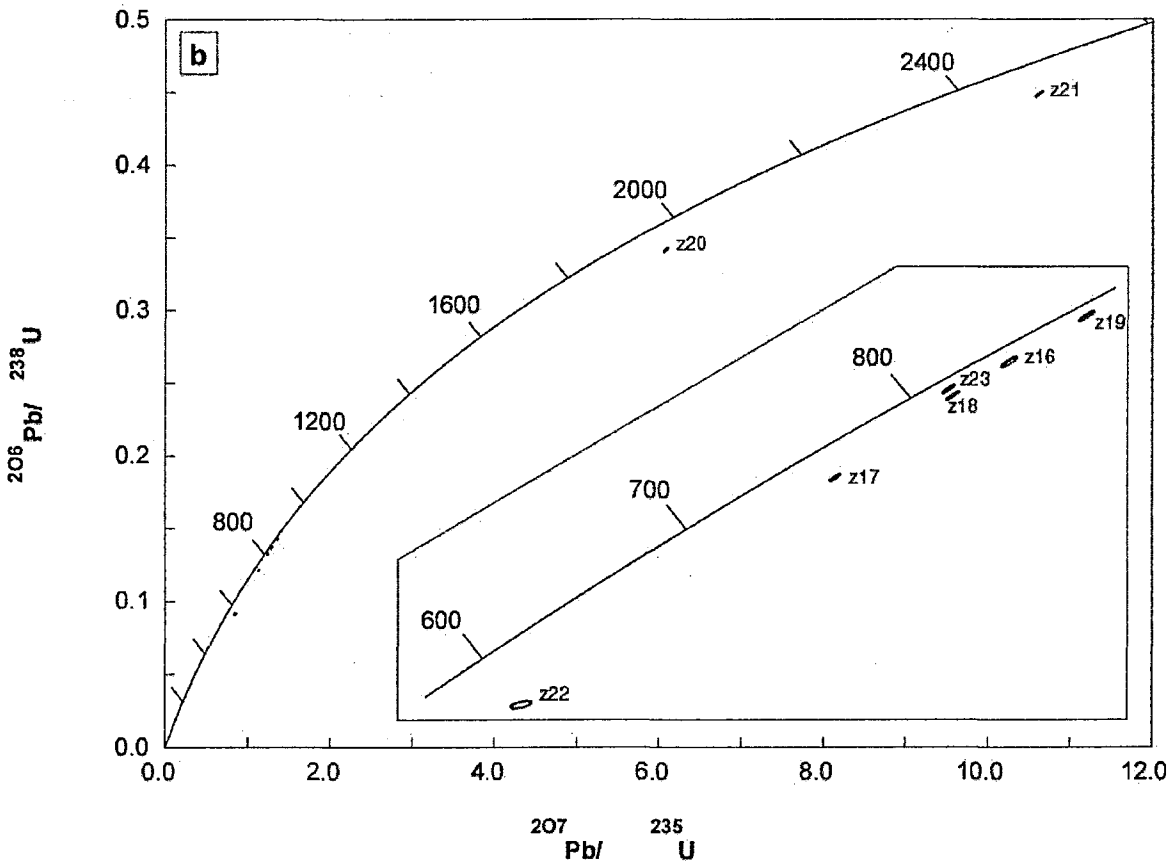

Figure 3.5 a and b - U-Pb concordia plots from zircons extracted from the Vaikrita Group. (a) Sample w34z, Palaeoproterozoic - Late Archaean population; inset Neoproterozoic population; (b) Sample w43z, Palaeoproterozoic - Late Archaean population; inset, Neoproterozoic population.

Jutogh Metasediments (w60z)

The zircons from the Jutogh Metasediments (w60z) form two morphological populations; rounded to sub-rounded detrital grains and elongate prismatic crystals. Both populations range from 200-550 μm and appear colourless and mainly clear; inclusions are infrequent and there is evidence of saltation e.g. pitting. Fractions from the Jutogh Metasediments have concentrations of U between 306-556 ppm.

The majority of zircon fractions from the Jutogh Metasediments (Fig. 3.6) are between 4.8 to 8.5% discordant, with $^{207}Pb/^{206}Pb$ ages of between 2012-2263 Ma; although one fraction (z18) is 46.5% discordant. Although a Palaeoproterozoic - Late Archaean population is present in the Jutogh Metasediments, this group appears different to the Vaikrita Group due to the absence of the Neoproterozoic population. Furthermore, the maximum age of deposition of these rocks is constrained to ca. 2012 Ma. Again, this

sample has a metasedimentary protolith, therefore further interpretations are problematic as the zircon fractions may not be cogenetic.

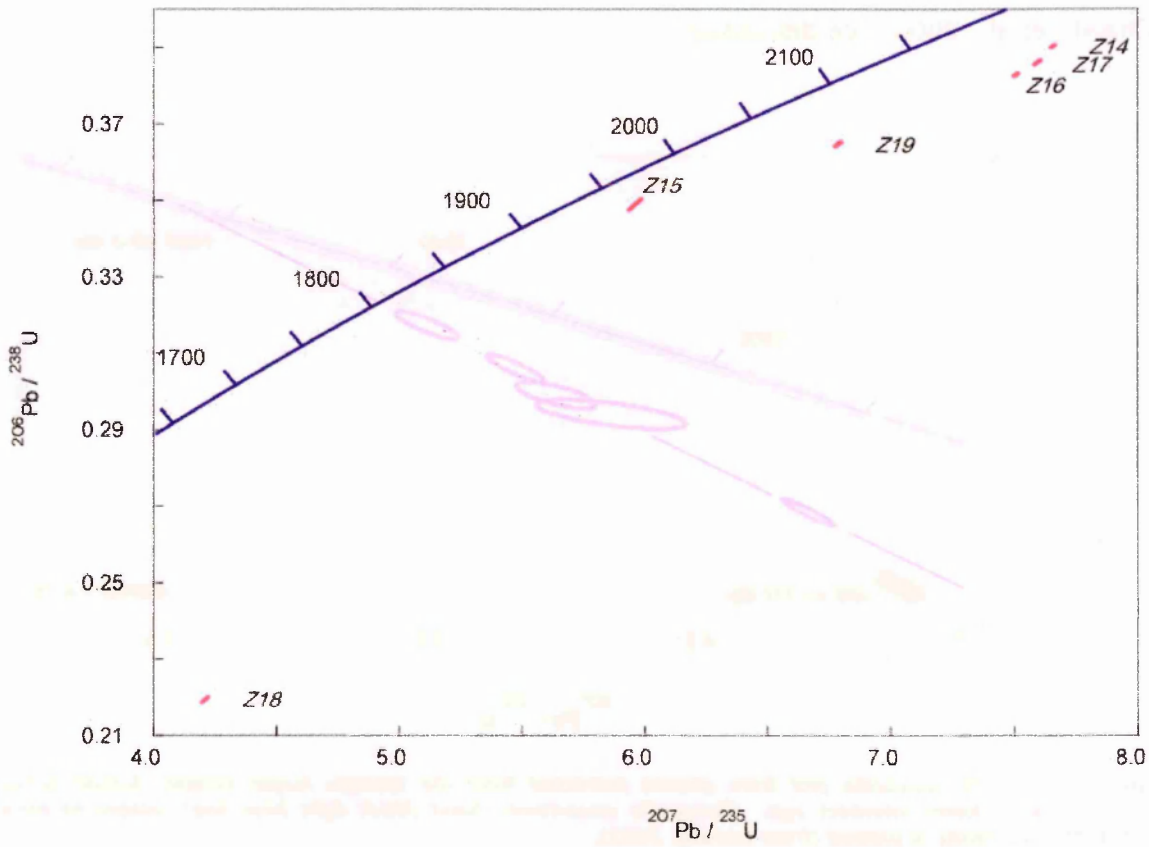

Figure 3.6 - U-Pb concordia plot from zircons extracted from the Jutogh Metasediments, Jutogh Group.

Wangtu Augen Gneiss (w49z)

The Wangtu Augen Gneiss sample (w49z) contains mostly colourless (with some cloudy/metamict) euhedral prismatic zircons with frequent inclusions, which range in size from 200-400 µm. Zircon fractions have U concentrations between 16-358 ppm.

The zircon populations of the Wangtu Augen Gneiss (part of the Wangtu Gneiss complex within the Jutogh Group) are between 2-7% discordant (with $^{207}Pb/^{206}Pb$ ages of between 1846-1858 Ma). The Wangtu Augen Gneiss is assumed to have a granitic protolith and is likely to contain a cogenetic zircon population; therefore the data can be regressed using an error calculation modified from York (1969) with some certainty. The data give upper and lower intersect linear array ages of ca. 1866 ± 6 Ma and ca. 419 ± 104 Ma, respectively and an MSWD of 0.76 (Fig. 3.7). These consistent data

suggest there is no inheritance in the analysed zircon population. The upper intercept age is interpreted as the age of crystallisation, whereas the lower intercept age is within error of the crystallisation age of the Kinnaur Kailas Granite (462 ± 52 Ma, Chawla et al., 2000; see discussion).

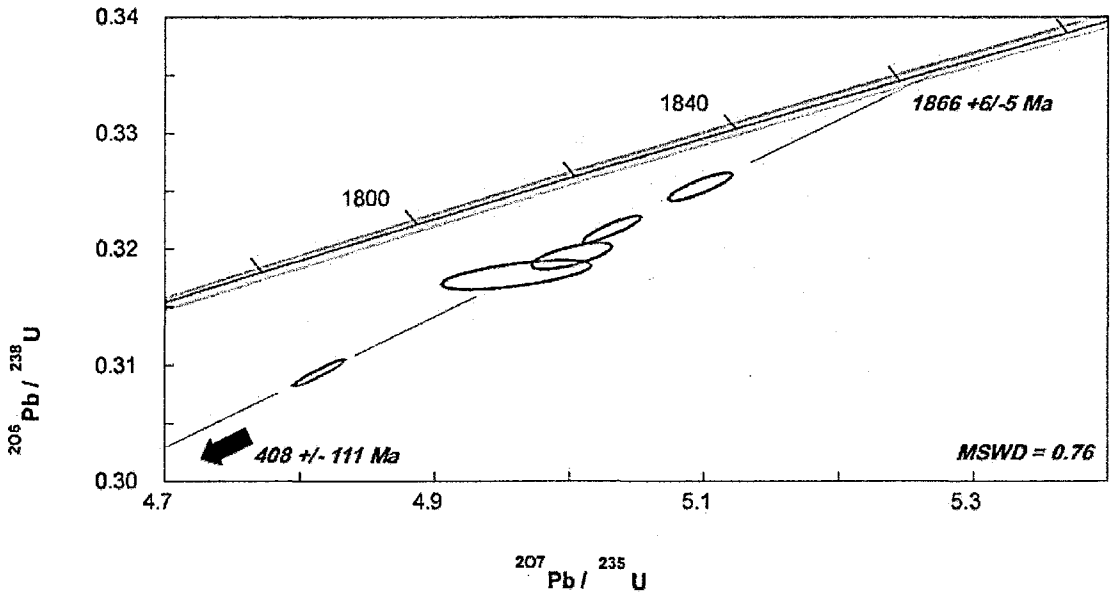

Figure 3.7 - U-Pb concordia plot from zircons extracted from the Wangtu Augen Gneiss, Jutogh Group, arrow point to lower intersect age. Concordia uncertainty band (thick light blue line) related to decay constant uncertainty is plotted (from Ludwig, 2003).

Rampur Formation (w58z)

The Rampur Formation sample (w58z – a recrystallised, massive quartzite; Fig 2.4 c) contains the most sedimentary abraded zircon populations. Two populations may be present; rounded equant grains (some are cloudy/turbid) and rounded elongate grains; although these may be 'end member' morphologies of the same group. No prismatic faces are present; sedimentary abrasion pitting is ubiquitous on every crystal, and they are colourless to off-yellow (possibly due to Fe oxide staining). Zircon fractions have U concentrations between 308-853 ppm. Zircons from the Rampur Formation (Fig. 3.8) are essentially concordant (between 0.2-0.6% discordant) and as a result the $^{207}Pb/^{206}Pb$ age can be regarded as a good estimate for the time of zircon crystallisation; one fraction yielded a $^{207}Pb/^{206}Pb$ age of 1950 Ma, while all other fractions analysed yielded $^{207}Pb/^{206}Pb$ ages of between 1864-1870 Ma, well within error of the 1866 ± 6 Ma upper intercept age (crystallisation age) of the

Wangtu Augen Gneiss (Fig. 3.7). The maximum age of deposition of these rocks is constrained to ca. 1864 Ma.

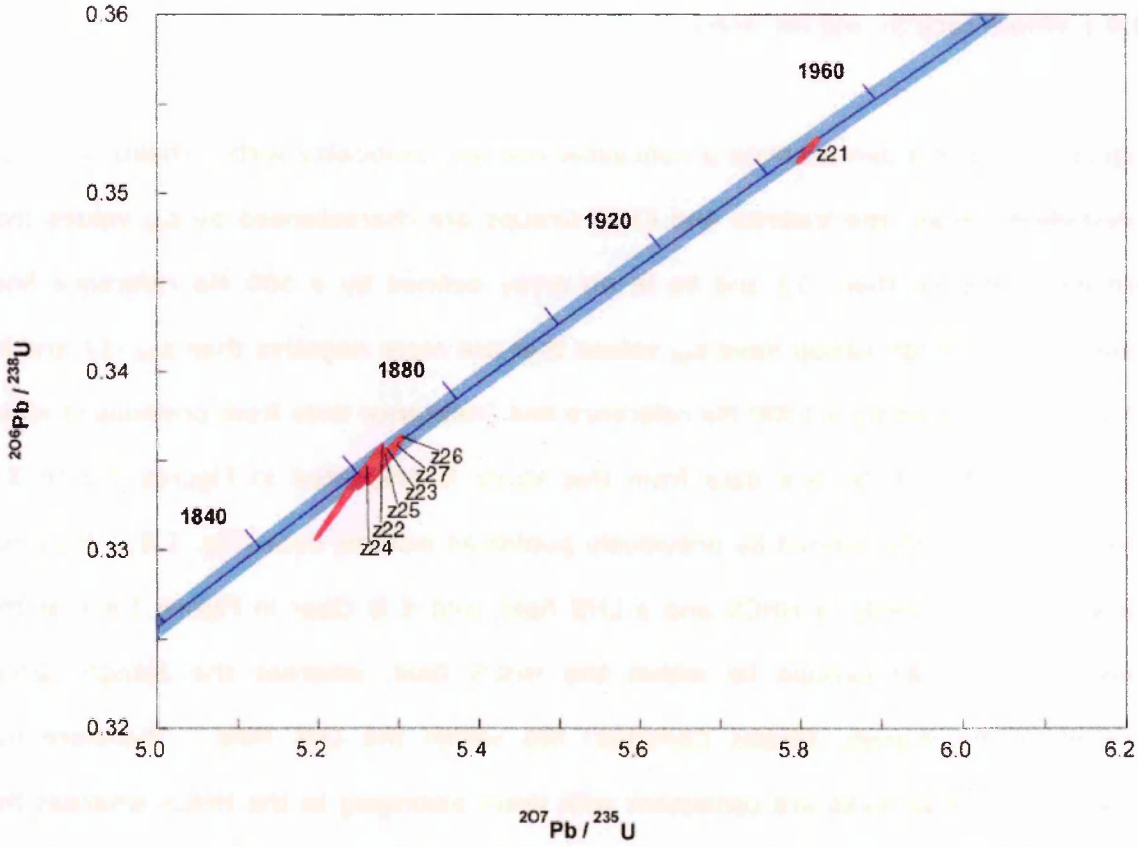

Figure 3.8 - U-Pb concordia plots from zircons extracted from the Rampur Formation, Larji-Rampur Window. Concordia uncertainty band (thick light blue line) related to decay constant uncertainty is plotted (from Ludwig, 2003).

Therefore, as with the Nd-Sr whole-rock data, the Vaikrita Group can be distinguished from the Jutogh Group and Rampur Formation as it contains a large population of Neoproterozoic zircons. All the metasediments analysed contain a Palaeoproterozoic - Late Archaean population, which has implications for the provenance and Palaeogeographic reconstruction of the Himalaya (Chapter 6). The degree of discordance increases with increasing metamorphic grade in the Sutlej Area, as observed by Ross and Parrish (1992), in similarly sized and similarly abraded zircons fractions from the southern Omineca Belt, Canadian Cordillera. Zircons from the chlorite-grade Rampur Formation are between 0.2-0.6% discordant, compared to discordances of 7-9% in the amphibolite grade Jutogh Group and 2-33% in the upper amphibolite grade Vaikrita Group.

3.4 Discussion

3.4.1 Whole-rock Sr and Nd isotopes

Figures 3.2 to 3.4 demonstrate a noticeable isotopic bimodality within Thakur's (1992) Crystalline Series; the Vaikrita and Chail Groups are characterised by ε_{Nd} values that are less negative than -13 and lie in an array defined by a 500 Ma reference line, whereas the Jutogh Group have ε_{Nd} values that are more negative than ε_{Nd} -17 and lie in an array defined by a 1800 Ma reference line (reference lines from previous studies, Fig. 1.7). The whole-rock data from this study is presented in Figures 3.2 to 3.4 together with fields defined by previously published isotopic data (Fig. 1.8). Previous data define two fields, a HHCS and a LHS field, and it is clear in Figure 3.4 that the Vaikrita and Chail Groups lie within the HHCS field, whereas the Jutogh Group (including the Wangtu Gneiss Complex) lies within the LHS field. Therefore the Vaikrita and Chail rocks are consistent with them belonging to the HHCS whereas the Jutogh Group is defined as belonging to the LHS. The MCT is defined as separating the HHCS in the hanging wall from the LHS in the footwall; therefore the MCT is defined in the Sutlej area as Vaikrita Thrust. This distinction supports the finding of Vannay et al. (2004 and references therein) with respect to the location of the MCT and the interpretation that the high-grade rocks of the Jutogh Group are Lesser Himalayan basement material. Considering the Nd measurements, the MCTZ within the Vaikrita Group (previously the Karcham Group) appear to be isotopically indistinguishable, and the presence of perturbed Sr isotope ratios in samples from this zone (Fig. 3.2) show that the Nd system can be used to make robust measurements in high strain orogenic belts. This isotopic data set from the Sutlej Area supports the interpretation made by Parrish and Hodges (1996), Whittington et al. (1999), Ahmad et al. (2000) and Argles et al. (2003) that isotopes can be used to define and discriminate major Himalayan units and the structures that separate them.

Figures 3.2 to 3.4 also show that there is an isotopic distinction within the LHS; the Palaeoproterozoic sediments of the Rampur Formation are characterised by ε_{Nd} values more negative than -18 (t=500 Ma) and lie in an array defined by a 1800 Ma reference line, whereas the Neoproterozoic and younger sediments (the Shimla and Krol Groups) have ε_{Nd} values less negative than -12 and lie in an array defined by a 500 Ma reference line (reference lines from previous studies, Fig. 1.7). Again these data are compared with previous isotopic data, (Fig 3.4); the Palaeoproterozoic LHS sediments lie within the defined LHS field, whereas the Neoproterozoic sediments plot within the HHCS field. This isotopic data set from the Sutlej Area also supports the interpretation made by Ahmad et al. (2000) that an isotopic distinction can be made *within* the LHS. This study uses the same nomenclature as Ahmad et al. (2000) and will refer to the Rampur Formation (and Jutogh Group) as the Inner Lesser Himalaya (ILH), and the Shimla and Krol Group as the Outer Lesser Himalaya (OLH). This nomenclature is used in Figure 3.9 c to illustrate the difference within the Sutlej Area between the ILH field and the HHCS/OLH field.

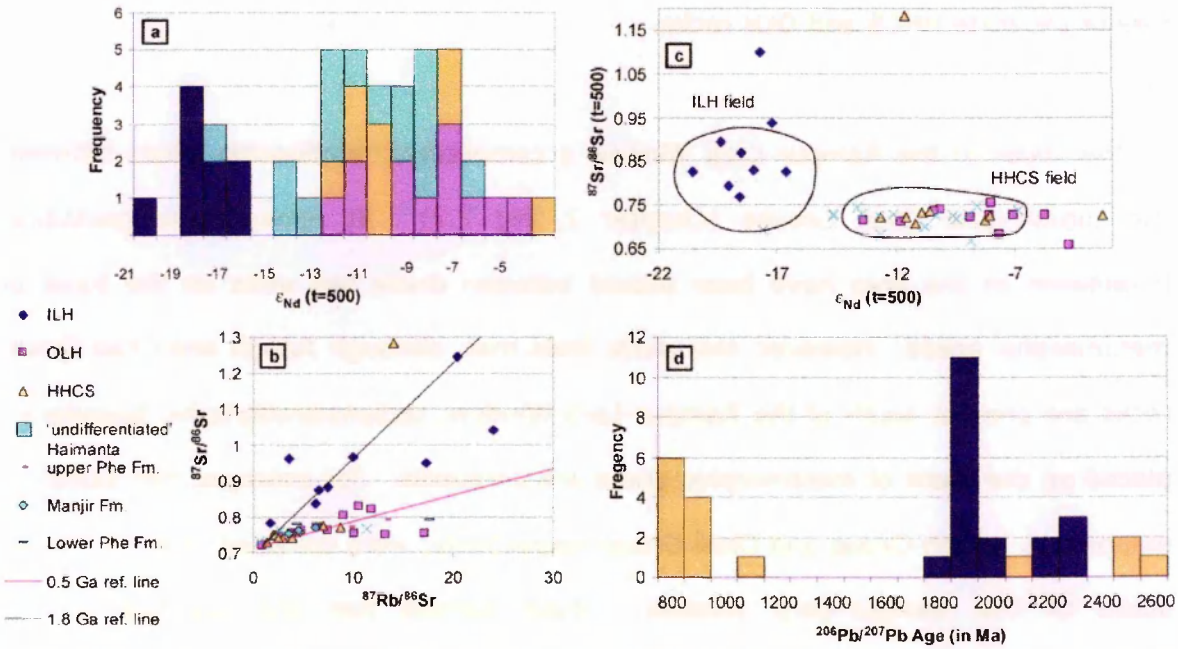

Figure 3.9 a to d - Reinterpreted whole-rock and zircon data from the Sutlej Area (this study). (a) Histogram of isotopic data presented as ε_{Nd} (t=500 Ma); (b) Sr isotopic data from Sutlej Area (this study); (c) Combined Sr-Nd isotopic data (age corrected) from Sutlej Area; LHS and HHCS fields from previous Himalayan metasedimentary studies as in Chapter 1, the term ILH filed is used in agreement with Ahmad et al (2000); (d) Histogram to summarise U-Pb zircon analysis, as $^{207}Pb/^{206}Pb$ showing Neoproterozoic and Palaeoproterozoic – Late Archaean population in the Vaikrita Group (HHCS) and only Palaeoproterozoic – Late Archaean population in ILH units.

Outliers

Eight data are labelled OL (outliers) on Figures 3.2 and 3.3. However, Figure 3.9 a to c shows the reinterpretation (i.e. reassignment to different groups) of these units for the following reasons. This study has already demonstrated that the Sr and Nd isotope systems can be used as powerful stratigraphical tools in areas where metamorphic grade is a poor discriminant (i.e. the definition of the MCT in the Sutlej area). This study was extended to the area around the Chor Granitoid. The 823 Ma Chor Granitoid is believed to intrude the Jutogh Group (Chapter 2; Singh et al., 2002 and references therein) due to metamorphic grade and garnet-bearing characteristics of the host rock amongst other observations. Garnet growth increases rapidly towards the intrusion, an observation that could be taken as further evidence for contact metamorphism. In addition, the Sr and Nd isotope characteristics of the rocks that have been intruded by the Chor Granitoid have a HHCS/OLH affinity (i.e. ε_{Nd} less negative than -13 and lie in an array defined by a 500 Ma reference line), therefore it is reasonable to reinterpret the rocks in this area as those belonging to the Chail Group or high-grade Shimla Group. However, one limitation of this technique is that it cannot separate HHCS and OLH rocks.

To the south of the Rampur-Larji Window a complicated relationship exists between the Jutogh and Chail Groups (Chapter 2, Fig 2.2). It appears the geological boundaries in the area have been placed between these two units on the basis of metamorphic grade. However, this study finds that, although Jutogh and Chail Group rocks are present south of the Rampur-Larji Window, tectonostratigraphic boundaries placed on the basis of metamorphic grade are unreliable. For example, two samples, mapped as Jutogh Group and Chail Group respectively, were collected close to thrusts south of the Rampur-Larji Window. Each sample has the opposite isotope characteristics to that predicted for their mapped unit. Therefore it is possible that local changes in metamorphic grade, such as garnet growth in the Chail Group have lead to inaccurate boundary mapping. A detailed study in this small area may reveal the complicated relationship between the Chail and Jutogh.

The Haimanta Group

Figure 3.2 shows that the Haimanta Group is characterised by a wide range of ε_{Nd} (from -18 to -6) with considerable overlap across both the HHCS/OLH and ILH fields. However, the Sr isotopes from the Haimanta Group (Fig. 3.3) fall on a similar array to the HHCS/OLH field around the 500 Ma reference line. Therefore, a cursory glance at the Haimanta Group data set may lead to an interpretation of a mixed provenance. However, a more detailed study of the Haimanta Group is required and the Nd model ages need to be taken into account first. Closer scrutiny reveals a reverse correlation between the depositional age and the model age, i.e. the stratigraphically older Manjir Formation has model ages between the 1600-1900 Ma, whereas the stratigraphically younger Phe Formation has model ages between 2000-2600 Ma (with the exception of one sample that is located close to the Manjir-Phe boundary). The oldest model ages from the Phe Formation, without exception, are also from the uppermost part *and* are located above the Precambrian/Cambrian boundary (where we place the Upper and Lower Phe Boundary). Further analysis of the data shows the rocks from the Upper Phe Formation are characterised by ε_{Nd} (t=500 Ma) between -13 to -18, whereas the Lower Phe and the Manjir Formation are characterised by ε_{Nd} (t=500 Ma) between -10 to -7 (Fig. 3.10). Therefore, although some overlap in the Nd model ages exists, there is no overlap in the ε_{Nd} (t=500 Ma).

The transition between the Upper and Lower Phe may reflect erosion of a single terrain, where the youngest deposits from the Haimanta Group (Upper Phe) represent the eroded debris of the oldest portion (core) of the terrain (with an isotope signature similar to the ILH), whereas the older sediments (Lower Phe and Manjir Formation) represent a bias towards sediment derived from a younger portion of the terrain (with an isotope signature similar to the HHCS and OLH). These data suggest that as the Haimanta Group youngs, the balance in sources increasingly favours the older source (summarised in Figure 3.10). Therefore the Haimanta Group's geological position above the STDS assigns this group to the TSS, whereas the Sr and Nd isotopes assign

the Lower Phe and Manjir Formation to the HHCS/OLH and the Upper Phe to the ILH (see section 3.4.3 and Figure 3.11).

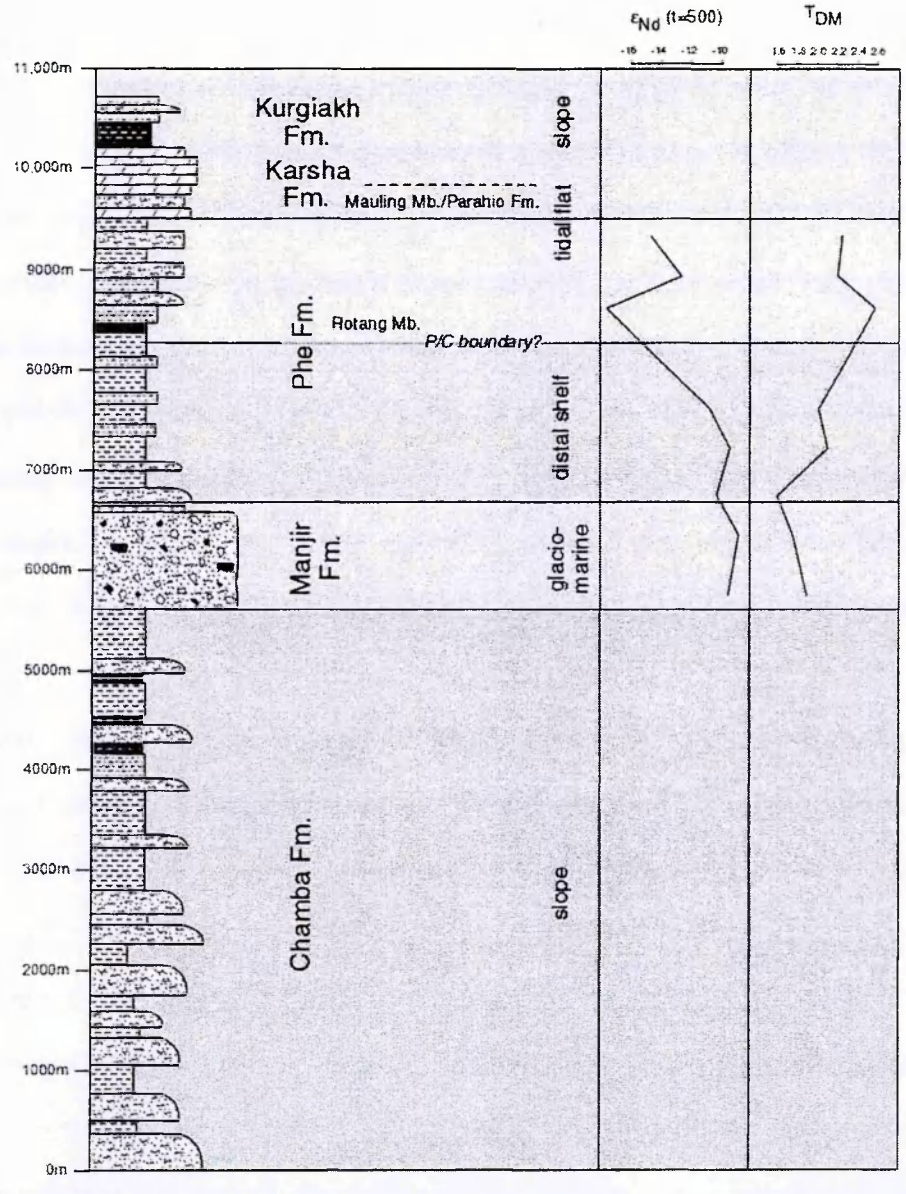

Figure 3.10 - Comparison of ε_{Nd} and Nd model age to stratigraphical height in the Haimanta Group (stratigraphical section from E. Draganits, Figure 3.1 b).

3.4.2 U-Pb Zircon Chronology

Parrish and Hodges (1996) and later DeCelles et al. (2000) established that a discrimination between the LHS and the HHCS can be made on the basis of zircon ages, as a largely Neoproterozoic population component is observed in the HHCS, whereas a largely Palaeoproterozoic - Late Archaean population is observed in the LHS. Myrow et al. (2003; summarised in Fig. 6.1) erroneously used overlapping zircon age

spectra from the OLH (as defined by Ahmad et al., 2000) and the Haimanta Group to interpret that zircon ages can not distinguish Himalayan tectonic units. The work of Ahmad et al (2000) and this study would expect similar age spectra from these units due to isotopic similarities as demonstrated in Figure 3.9 a.

The present study (Fig. 3.5 to 3.8) complements the above findings and demonstrates that within this Himalayan metasedimentary data set, a large Neoproterozoic and a small Palaeoproterozoic - Late Archaean population is observed within the HHCS, whereas only a single Palaeoproterozoic - Late Archaean population is observed within the ILH metasediments (i.e. the Jutogh metasediments and the Rampur Formation). As mentioned above, where discordancy is <5%, the $^{207}Pb/^{206}Pb$ age is regarded as a good estimate for the time of zircon crystallisation, whereas for fractions displaying discordancy >5% the $^{207}Pb/^{206}Pb$ age is taken as a minimum crystallisation age (Ross and Parrish, 1992). These ages are summarised on a histogram in Figure 3.9 d and reflect the above interpretation. Inferred maximum depositional ages can be constrained from the youngest detrital zircon age within a sample (Heaman and Parrish, 1991); therefore within the HHCS a maximum depositional age of mid-Neoproterozoic is constrained, whereas mid-Palaeoproterozoic is constrained for both the Jutogh Metasediments and Rampur Formation. Again these maximum depositional ages reflect the above interpretation.

The Rampur Formation yielded a highly concordant sub-population with $^{207}Pb/^{206}Pb$ ages of between 1864-1870 Ma, very similar to the 1866 ± 6 Ma upper intercept age from the Wangtu Augen gneiss, suggesting that the zircons were mainly sourced from material similar to the Wangtu Augen Gneiss and the Rampur Formation was deposited in a restricted basin environment, such as a rift basin. However, Figure 3.7 demonstrates that the zircon population from the Wangtu Augen Gneiss is discordant and it can be interpreted that this population has experienced lead-loss compared to the Rampur Formation zircons. If these zircons sourced an eroding body similar to the Wangtu Augen Gneiss, the observed difference in discordance in these two units can

be explained by lead loss occurring after deposition of the Rampur Formation due to a thermal/metamorphic event, such as the Himalayan orogeny.

Krogh (1982) demonstrated how air abrasion can produce concordant analysis by removing the outermost layers of the crystal which contain discordant Pb. Indeed sedimentary processes are likely to pre-abrade crystals and also destroy the most damaged (metamict) zircons; further laboratory abrasion and magnetic separation (Appendix A) will bias towards the most concordant zircon crystals. However, all the zircons analysed during the course of this project where abraded similarly. Therefore, it is likely that a combination of both sedimentary abrasion and low-grade (Himalayan) metamorphism has resulted in highly concordant zircon ages from the Rampur Formation. However, the discordant values from the higher-grade units suggest that those units may have suffered significant lead loss compared to the Rampur Formation, as observed by Ross and Parrish (1992) who noted that metamorphic grade appeared to affect zircon discordance. To prove that metamorphic grade is responsible for discordance in the higher-grade units we must first rule out other possibilities. Firstly, as all fractions were strongly abraded, we can rule out insufficient abrasion. Secondly, discordance could be due to substantial metamorphic overgrowth. However, this requires all analysed zircons to have a substantial metamorphic rim. This interpretation is less likely as the analysed zircons appear to have a morphology that is likely due to sedimentary abrasion (Appendix C; compare euhedral crystals from the Wangtu Augen Gneiss with the subhedral crystals from the Jutogh Metasediments and Vaikrita Group). However, to prove with certainty that zircon discordance is due to one or a number of lead loss events rather than metamorphic overgrowth, detailed core-rim investigations are required.

3.4.3 Provenance and discriminating source areas

The Nd data (Figure 3.2 and 3.4) shows that the HHCS/OLH forms a broader array than the ILH array, possibly suggesting a mixed source for the HHCS/OLH and a single,

more restricted source area for the ILH. The zircon data also shows that the age population for the ILH is Palaeoproterozoic (corresponding to Nd model ages of 2400-2800 Ma), whereas the HHCS (and presumably the OLH) has a broader range of Neoproterozoic to Palaeoproterozoic ages from 830-2574 Ma (corresponding to Nd model ages of 1400-2260 Ma). Therefore, the source for the older (Late Archaean – Palaeoproterozoic) population of zircons in the HHCS could be the same as that of the ILH, whereas the younger ca. 800 Ma (Neoproterozoic) population is unique to the HHCS, implying a different (younger) source; this (Neoproterozoic) population shares similar zircon $^{207}Pb/^{206}Pb$ ages with the Chor Granitoid, implying this granitoid is a source of Neoproterozoic zircons. As previously mentioned, one interpretation of these data is that the HHCS/OLH and the ILH sourced the same eroding region (a terrain with Late Archaean to Palaeoproterozoic zircons and ε_{Nd} ca. >-19). However, the HHCS/OLH was also sourced from a second, younger (overlying?) terrain with ca 800 Ma zircons, and ε_{Nd} values <-13 (such as the Chor Granitoid). This model supports the maximum depositional ages interpreted from the zircon data that the HHCS (Vaikrita Group) has a maximum depositional age of Neoproterozoic, whereas the ILH has a maximum depositional age of Palaeoproterozoic, which suggests that the Neoproterozoic source area formed and was eroded into the HHCS/OLH basin after the formation of the ILH units. This model therefore accounts for the two populations of zircon ages, and the less negative, and broader range of ε_{Nd} values compared to the ILH. The Nd whole-rock data show only the average age from the two sources contributing to the HHCS/OLH (summarised in Fig. 3.11). This interpretation would suggest that the Upper Phe Formation (Haimanta Group) may be unique in the Himalaya as it was deposited in the HHCS/OLH basin and was sourced exclusively from the older source terrain whilst detritus from the younger source was reduced (Fig. 6.2, Part 1, Chapter 6, Palaeogeographic reconstruction).

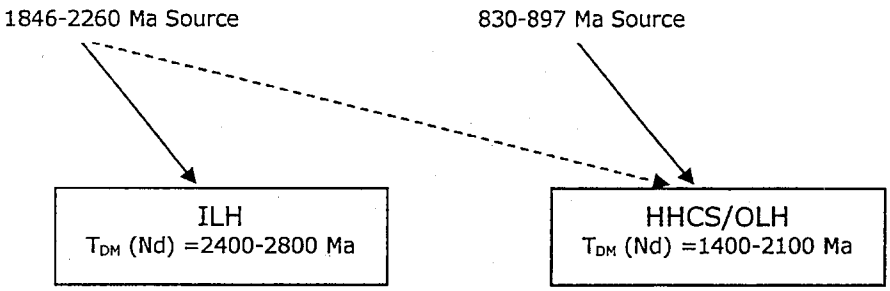

Figure 3.11 – Summary of the interpreted sources for the ILH, OLH and HHCS depositional basins.

3.5 Summary

This study confirms, on the basis of isotopes, that the Jutogh Group lies structurally below the MCT (in its footwall) and is likely to be ILH basement material, as suggested by Vannay et al. (2004 and references therein). Hence the MCT is located near Karcham (Vaikrita Thrust), which is consistent with the available structural information (Chapter 2); furthermore samples from the Vaikrita Group and MCTZ (Karcham Group) are clearly distinguishable from rocks in the footwall which suggests that previous interpretations that the MCTZ is likely a tectonic melange of footwall and hanging wall rocks is inaccurate; the MCT marks a discrete change from footwall to hanging wall material.

The Palaeoproterozoic LHS in the Sutlej Area can be distinguished, on the basis of isotopes, from the Neoproterozoic and younger sediments into the OLH and ILH, supporting the observations by Ahmad et al. (2000), in the Garhwal Himalaya. This project demonstrates that isotopically similar units can display a range in metamorphic grade, and therefore metamorphic grade is a poor basis for separating tectonic units in the Sutlej Area. For instance, the Jutogh Group has been mistaken for the Chail Formation and vice versa to the south of the Rampur-Larji Window, and the previously mapped Jutogh Group schists around the Chor Granitoid have a HHCS affinity and are therefore more correctly described as Chail Group rocks or high-grade Shimla Group, over-printed by contact metamorphism. The confirmed position of the MCT (and therefore respective HHCS and ILH tectonic units) and the reinterpretation of the LHS into ILH and OLH for the Sutlej Area is summarised in Table 3.1 and Figure 3.12.

Table 3.1 – Redefined field-relations in the Sutlej Area after this project.

Major Tectonic Unit	Series/Group	Formation	Major Structures:	Probable Age
High Himalaya	Tethyan Sedimentary Series			Ordovician-Cretaceous
	Haimanta Group	Chamba Fm		Neoproterozoic to Cambrian
		Manjir Fm		
		Phe Fm	STDS	
		Kinnaur Kailas Granite (462 ± 52 Ma)		
	High-Grade Crystalline Series (Vaikrita Group) (Karcham Group - MCT Zone)			Neoproterozoic to Cambrian
Inner Lesser Himalaya	Crystalline series (Jutogh Group)	Wangtu Gneiss Complex (1866 ± 6 Ma)	MCT/ Vaikrita Thrust	Palaeoproterozoic
		Jutogh metasediments		
	Sedimentary Series	Rampur-Larji Window/ Rampur formation	?Jutogh Thrust?	
Outer Lesser Himalaya	?Chail Group?		?Chail Thrust?	Neoproterozoic to Cambrian
	Shaling - Deoban Limestone			
	Shimla Group	Shimla A		
		Shimla B		
	Krol Group	Inner Krol	MBT	
		Outer Krol		
Sub Himalaya	Siwaliks/Kasauli/Dagshai/Subathu/Singtali Formations		MFT	Tertiary

By combining whole-rock Nd and Sr data with detrital zircon ages, this study has determined that whilst the ILH has been derived from a Palaeoproterozoic source terrain (with ca. 1800-2300 Ma zircons) the HHCS and OLH appear to be sourced from two terrains, the first equivalent to that of the ILH (possibly reworking itself) and the second Neoproterozoic in age (ca. 800-1000 Ma), possibly granitoid protoliths equivalent to the Chor Granitoid.

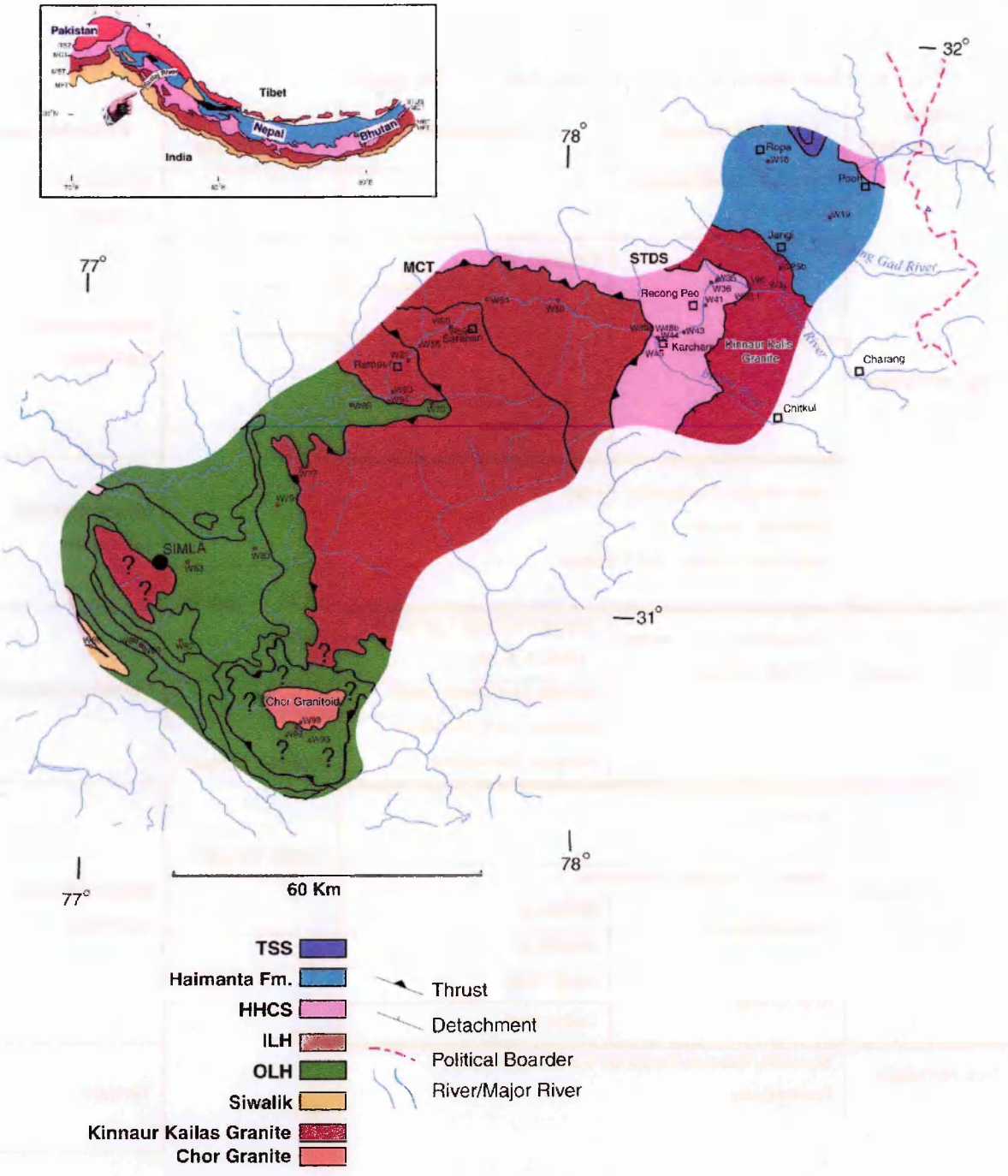

Figure 3.12 - Geology of the Sutlej Area as determined after this study (modified from Raina, 1981; Thakur and Rawat, 1992; Vance and Mahar, 1998); which confirms the position of the MCT as proposed by Vannay et al. (2004, and references therein) and Valdiya (1980) and the distinction of the OLH and ILH as proposed by Ahmad et al. (2000);question marks represent uncertainty of interpretations; Ornament for inset location map, same as Figure 2.1.

Chapter 4 - Field Relations And Regional Geology In Bhutan

4.1 Introduction And Aims

The purpose of this chapter is to give a resumé of previous work in Bhutan and to introduce and describe the geological units. It is important to understand the underlying complexity of the area before a synthesis of the Himalayan story can be attempted.

Bhutan is located to the east of Sikkim and to the southwest of the Namche Barwa syntaxis (Fig. 1.1 and inset map Fig. 4.1). The Bhutanese sector of the eastern Himalaya is unique in a number of ways. For example, the topographical relief in Bhutan is unlike any other area in the Himalaya; although there are no mountains above 8000 m as in central and eastern Nepal, steep gorges result from the fast incision rates related to the high rainfall on the eastern Himalaya. Moreover there is a much smaller lateral extent of foothills, e.g. near Chasilakha (central Bhutan) a 4070 m peak lies only 25 Km from the MFT (Duncan et al., 2003).

Until the geological expeditions of Gansser in the 1960s and 1970s (Gansser, 1983), the geology of Bhutan had scarcely been studied; only Godwin-Austen (1868), Mallet (1875), Pilgrim (1906), Hayden (1907) and Lahiri (1941) had published on the area. To this day, due to visa restrictions and the difficulty and cost of travel, the geology of Bhutan is still relatively unknown. In this chapter the geology of the Bhutan is described from north to south; i.e. from the High Himalayan mountainous area to the floodplains of the Brahmaputra. Due to the difficult nature concerning studying field relations in Bhutan the following description in this chapter is based largely on (but not entirely) the work of Gansser (1983), Grujic (1996; 2002), Daniel et al. (2003) and Davidson et al. (1997) with additions from this study where cited. The principal lithological units are the TSS, HHCS, LHS and the Sub-Himalaya Formations (Table

4.1). Figure 4.1 represents the most up to date geological map of Bhutan, which is based mainly on the work of Gansser (1983), with revisions from this study and Grujic et al. (1996; 2002). As geological investigations in the Bhutan Himalaya are relatively infrequent, large additions to these maps have even occurred recently, such as the addition of the Sakteng Klippe (Grujic et al., 1996) and Ura Klippe (Grujic et al., 2002).

Table 4.1 – Table summarising the tectonic series in the Bhutan Himalaya. KT=Kakhtang Thrust.

Major Tectonic Unit	**Group / Formation / Unit**		**Major Structures:**
TSS	Upper Mesozoic (Lingshi Formation) Lower Mesozoic Palaeozoic in General (=Tang Chu Basin Sediments) Chekha Formation		STDS
High Himalaya	HHCS above the KT	Paro metasediments: Lunana Metasediments Northeastern Metasediments	KT
		Crystalline Units: Northern Crystalline (Takhtsang Gneiss)	
	HHCS below the KT	Paro Metasediments: Bumthang-Djule La Metasediments Paro Metasediments Cändebi Metasediments	
		Crystalline Units: Sure Crystalline Unit Tashigang Crystalline Unit Chasilakha Crystalline Unit	MCT
Lesser Himalaya	Daling-Shumar Group (with concordant granitoids) Duiri Formation Baxa Formation Damudas		MBT
Sub Himalaya	Siwaliks		MFT

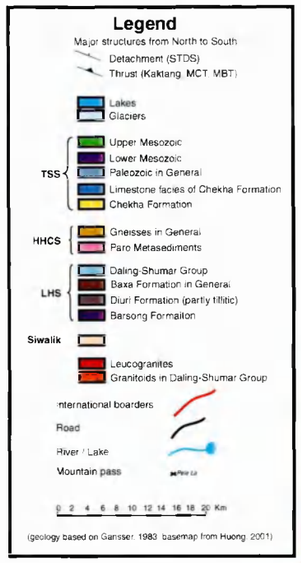

Figure 4.1 Geological map of Bhutan, basemap from Huong (2001), geology based on Gansser (1983) with revisions from Grujic et al. (1996; 2002) and this study; sequence of major structures from north to south: STDS; Kahktang; MCT; MBT; MFT; LB, Lingshi Basin; TK, Tang Chu Klippe; BK, Black Mountain Klippe; UK, Ura Klippe; SK, Sakteng Klippe. Localities marked on larger scale maps Appendix D. Ornament for inset location map, same as Figure 2.1.

4.2 The Tethyan Sedimentary Series

The TSS crop out in the proximity to the border with Tibet, in the geographical High Himalaya, as well as in a series of outliers further south (Fig. 4.1). Gansser (1983) describes the TSS outcrops in Bhutan as a series of basins and belts that are conformable with the underlying HHCS. Burchfiel et al. (1992) and recently Edwards et al. (1999) suggested that a tectonic contact (STDS) exists between the TSS and the underlying HHCS; Edwards et al. (1999) found Mesozoic slates juxtaposed against the Gophu La leucogranite in the Gonto La area (part of the Mönlakarchung - Passalum Leucogranite, northwestern Bhutan; see Fig. 4.1) (Castelli and Lombardo, 1988; Dietrich and Gansser, 1981).

On the basis of existing mapping, the Lingshi basin in the far west of Bhutan is the largest outcrop of TSS, and is described in detail by Gansser (1983). The highest grade member of the TSS outcrops above the tourmaline-bearing Chung La leucogranite (Blattner et al., 1983) as porphyroblastic schists. Metamorphism decreases in extent up section, together with an increase in phyllites, quartzites and calc-schists, described as the Chekha Formation by Jangpangi (1978). The upper part of the Chekha Formation, which is particularly well exposed in the Wang Chu Gorge (near Shodu; Fig. 4.1), is associated with an increase in carbonate abundance. These limestones and marbles were termed the Dando Gömpa facies by Gansser. The Chekha Formation is folded throughout and intruded by the tourmaline-bearing Chung La leucogranite. Overlying the Chekha Formation is a series of thin pink quartzites and grey shales, grading into greywackes topped by a pebbly horizon, interpreted by Gansser (1983) as tillite of possible late Precambrian or Carboniferous age. Towards the centre of the Lingshi basin, northwest from the Wang Chu gorge and above the possible tillite, lie the youngest sediments in Tang Chu basin, which are affected by the Yale La antiform. Gansser (1983), on the basis of fossil evidence, separates the predominately limestone sediments (with occasional intercalations of slates and

phyllites) in the core of the Lingshi basin into the Lower Mesozoic (mainly Jurassic and Triassic) and the Upper Mesozoic (mainly Cretaceous), assigning the latter to the Lingshi Formation. These Mesozoic sediments are evidently not observed in any other part of Bhutan.

Unlike the Sutlej Area, several TSS basins crop out south of the STDS, and are located in south central and eastern Bhutan (Edwards et al., 1996; Gansser, 1983; Grujic et al., 1996; Fig. 4.1). Grujic et al. (2002) interprets these outcrops as klippen, suggesting they mark the southernmost extent of the STDS, noting the tectonic contact between the TSS and the underlying Crystallines. Grujic et al. (2002) described two further klippen in eastern Bhutan: the Ura Klippen (possibly an extension of the Black Mountain Klippen) and Sakteng Klippe. Top-to-the-north shear sense indicators are located at the base of these klippen suggesting that this contact shows similarities with the STDS. Grujic et al. (2002) place the boundary at the base of the Chekha Formation, whereas Edwards et al. (1996) suggest Devonian limestones (from the Tang Chu klippe) directly overlie the STDS.

In this study, sampling of the TSS was restricted to the Ura, Black Mountain and Tang Chu Klippen due to logistical restraints that prevented sampling in northern Bhutan. The largest of these is the Tang Chu klippen, located in central Bhutan around Pele La (3400 m). Gansser (1983) describes the Tang Chu klippe as a synformal basin that is structurally and stratigraphically similar to the top of the Kathmandu klippe (Stoecklin, 1980). It is underlain by HHCS sillimanite ± garnet two-mica gneisses, schists and migmatites; kinematic indicators, including top-to-the-north movement inferred from boudinaged leucogranite sills and dykes, overprint top-to-the-south shear sense indicators. Metamorphic grade and tectonic deformation decrease towards the top of the klippe (Grujic et al., 2002). The base of the Chekha Formation consists of biotite ± garnet porphyroblastic schists and quartz conglomerate, that are Intruded by tourmaline-bearing leucogranites (Fig. 4.2). Above a series of calc-schists (possibly equivalent to the Dando Gömpa facies) of the Chekha Formation lie dark fossiliferous

slates, containing Middle to Upper Devonian corals and brachiopods (Termier and Gansser, 1974). Gansser (1983) distinguishes the Chekha Formation from these slates, describing them as "Palaeozoic in general", (Fig 4.1) and in this case, referring to them as the sediments of the Tang Chu basin. The slates are succeeded by a series of thick limestones and slates overlain by a further unit of slates (exposed at Belu; Fig. 4.1) and a final layer of limestone containing crinoidal fragments (Gansser, 1983). The succession continues into the Tang Chu valley, north of the Pele La; Gansser observes a slight increase in metamorphic grade towards the centre of the klippe, and similar tourmaline-bearing leucogranites intrude schists of the Chekha Formation which marks the extent of the Tang Chu klippe. The Chekha and Palaeozoic sediments are suggested by some authors to extend further to the south towards the Black Mountains, nearly doubling the size of the Tang Chu klippe (Singh, 1973).

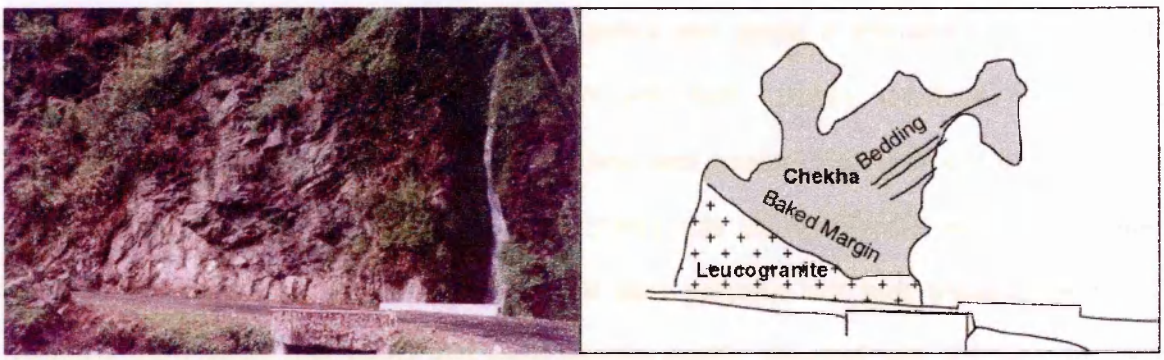

Figure 4.2 Contact of leucogranite with basal Chekha Formation, note baked margin.

Proterozoic and younger sediments, as described in the Tang Chu basin, have so far not been discovered in any other TSS klippen. The Ura and Sakteng klippen consist of garnet ± biotite-schists, pelites and quartzites and are interpreted as belonging to the Chekha Formation (Grujic et al. 2002, and this study). Within the Sakteng klippe, near Radi, some sedimentary structures, including cross-bedding, persist suggesting that the klippe upright. River float in the Gamri Chu (and its tributaries; Fig. 4.1) includes amphibolitised ultramafic rocks with micaceous books. A deformed leucogranite dyke at the base of the Chekha Formation within the Sakteng klippe gave a crystallisation age of 17-22 Ma (Daniel et al., 2003) interpreted as a maximum age of north-directed shearing (Grujic et al. 2002).

4.3 The High Himalaya Crystalline Series

The HHCS dominate the outcrop in most of Bhutan: only the Kuru Chu-Shumar Half Window allows extensive exposure of the LHS (Fig. 4.1). Gansser (1983) separates the HHCS of Bhutan into three distinctive units; Paro metasediments, Gneisses and Leucogranites. However, Swapp and Hollister (1991) identify the Kakhtang Thrust as a major tectonic break within the HHCS; according to Grujic et al. (2002) after Gansser (1983), Swapp and Hollister (1991) and Davison et al. (1997), the Kakhtang Thrust can be traced from east to west across most of Bhutan (Fig. 4.1) and is responsible for effectively doubling the thickness of the HHCS exposure to the east of the Yadong Cross-Structure, located to the northwest of Bhutan (Chapter 1).

The division of the HHCS along the Kakhtang Thrust is based on the recognition by Swapp and Hollister (1991) that the hanging wall shows higher temperatures compared to the footwall; indeed the HHCS in the hanging wall contains sillimanite-bearing gneisses (Davidson et al., 1997; Stuewe and Foster, 2001), Grujic et al. (2002) suggested that the hanging wall lithologies are from a lower structural level than the HHCS in the footwall. Observations from this study and those from mapping by Gansser (1983) confirm that migmatites and large leucogranite bodies are more common above the thrust. The Kakhtang Thrust is located structurally above the TSS klippen (Fig. 4.1) and has been inferred to postdate the north-directed shearing on the STDS (Grujic et al., 2002). The following description of the HHCS in Bhutan follows Grujic et al. (2002), whilst lithological units are after Gansser (1983):

4.4.1 – The HHCS below the Kakhtang Thrust

The HHCS below the Kakhtang Thrust is divided into crystalline units (predominantly gneisses) and Paro metasediments (predominantly metasediments).

The Crystalline Units

The Chasilakha Crystalline Unit is located north of Phuntsholing (in western Bhutan) between Wangu Chu and Amo Chu (rivers) and extends for ca. 30 km towards Paro. Gansser (1983) correlates the Chasilakha Gneiss with the Darjeeling Gneiss. The MCT is placed by Gansser at the base of the first major gneiss layer of the Chasilakha granitic gneiss. This unit appears to form a wide, basin-like, syncline which consists of several sheets of garnet-bearing two-mica granitic gneisses separated by lenticular quartzites and garnet-bearing amphibolites. The gneisses in this section are similar in composition, and are well banded, layered and appear sheared into migmatitic zones; schists, quartzites, marbles and fine-grained garnet-biotite granulites are associated with the northernmost granitic gneiss (Gansser, 1983).

The Sure Crystalline Unit is separated from the Chasilakha Crystalline Unit by north-south faulting, and is located to the north of Geylegphu (central Bhutan). The unit consists of migmatitic garnet-bearing two-mica granitic gneiss, similar to the Chasilakha Gneiss (Gansser, 1983). Kyanite-bearing biotite schists overlie the granitic gneiss which are frequently cut by coarse-grained pegmatites; these schists decrease in metamorphic grade and degree of strain to biotite porphyroblastic schists that grade into the Sangsing La Formation. This formation consists of schists grading upwards into phyllites, which Gansser correlates with the Chekha Formation.

The Tashigang Crystalline Unit is located in the east of Bhutan, near Tashigang, and is separated from the Sure Crystalline Unit by the Kuru Chu-Shumar Half Window (Fig. 4.1). Gansser (1983) arbitrarily delimits the northern extent of this unit at Yangtse Dzong. However, following Grujic et al. (1996; 2002) the extent of the unit is limited in this study to the footwall of the Kakhtang Thrust. Above the MCT, south of Tashigang, feldspar-rich gneisses are strongly sheared and dip north-northeast; an increase in metamorphic grade around Tashigang is indicated by the development of kyanite-bearing migmatites (Daniel et al., 2003; Stuewe and Foster, 2001), while medium to coarse grained granites appear cut by fine mafic intrusives (Fig. 4.3). To

the north of Tashigang, Gansser (1983) and Grujic (1996; 2002) observed a series of large synforms and antiforms with similar amplitude and axial traces running east southeast to west northwest (Fig. 4.1), fine grained quartzitic biotite schists are exposed in the cores of antiforms with biotite gneisses in the limbs which grade northwards (towards the Kakhtang Thrust) into biotite granitic gneisses and well-bedded two-mica gneisses, further intrusives include massive hornblende diorites, 1-2 km thick (Gansser, 1983).

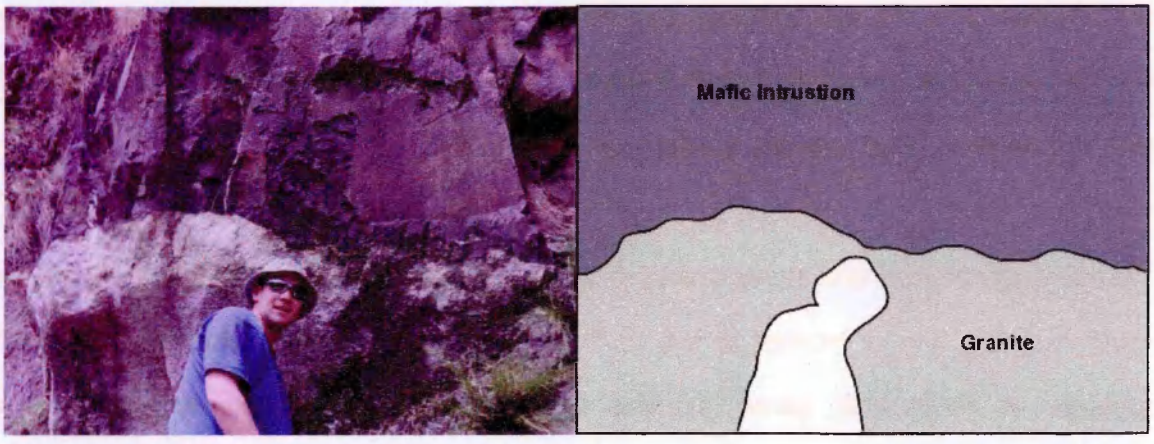

Figure 4.3 - Intrusive contact between medium to course grained granite and fine grained mafic rock within HHCS, close to MCT. Recrystallisation not observed in granite margin, some scaly textures in mafic intrusive close to contact suggesting chilled margin.

The Paro metasediments

The Paro metasediments form the largest exposure of the medium-grade metasediments associated with the HHCS around Paro, their type locality. Garnet-staurolite two-mica schists are the dominant rock type with a north-northeast to northeast regional dip. Exposure of the Paro Metasediments is excellent along the road between the confluence of the Paro and Wang Chu and Thimphu Rivers. The metasediments here are a weathered series of garnet-staurolite, two-mica schists, marbles, quartzites and granitic gneisses. Their regional dip to the northeast is disturbed locally by small-scale folding. The Takhtsang Gneiss overthrusts these metasediments along the Kakhtang Thrust. Gansser (1983) describes a series of marble zones, located near Chapcha, (interbedded with garnet-bearing schists, calc-silicates and boudinaged quartz veins) separated by quartzites, which may be structurally repeated. Above these marbles, quartzites show an increase in

metamorphic grade towards the overlying gneiss. Two granitic gneiss domes are exposed along the Wang Chu and Paro valleys comprising biotite-garnet and biotite augengneiss respectively.

The Paro Metasediments are probably correlated with metasedimentary units further east. These include: (i) the Cändebi metasediments exposed to the east of the Tang Chu Basin, near the village of Cändebi, comprising a sequence of carbonate and pelitic metasediments within a faulted antiform and surrounded by highly strained crystallines intruded by tourmaline-bearing leucogranite intrusions and (ii) the Bumthang-Djule La Metasediments that outcrop as a belt east of Bumthang and northwest towards the Djule La area above the Kakhtang Thrust (Fig. 4.1). Gansser (1983) notes that the dominant facies of these metasediments comprises two-mica, garnet schists with biotite-psammite gneisses increasing in abundance towards the centre of the unit. There is a noticeable increase in the abundance of steeply dipping sillimanite-bearing schists towards the northern margin of the unit (Djule La area); marbles and dolomites also appear more common. The northern margin of the unit is cut by the Kakhtang Thrust and is particularly well observed near Kakhtang.

4.4.2 – The HHCS above the Kakhtang Thrust

The HHCS above the Kakhtang Thrust can also be separated into crystalline units (predominantly migmatitic gneisses with a greater extent of leucogranite intrusion) and Paro Metasediments (predominantly marbles, calc-silicates and dolomites).

The Crystalline Units

The HHCS above the Kakhtang Thrust is described as the Northern Crystalline Unit by Gansser (1983). This study sampled a small proportion of this unit that dominates the northern reaches of Bhutan (Fig. 4.1). Due to logistical restraints, the Northern Crystalline Unit was only accessible below the Takhtsang monastery (West Bhutan), the type locality for the Takhsang Gneiss, and south of Yangtze Dzong (East Bhutan).

The Takhtsang Gneiss consists of banded sillimanite-garnet-biotite gneiss with quartz and aplite seams; gneisses become migmatitic locally. The Takhtsang Gneiss contains lenses of calc-silicate, garnets, feldspars and pyroxenes (Gansser, 1983). To the north, coarse, interbedded quartzites and garnet-sillimanite-biotite schists occur within the gneiss. In eastern Bhutan, near Yangtze Dzong, the Northern Crystalline Unit appears as a biotite augen gneiss alternating with coarse-grained biotite gneiss; neither sillimanite nor migmatites were observed at this locality.

The Paro metasediments

The Lunana metasediments lie in north-central Bhutan, ca. 50 Km to the northeast of the Tang Chu basin. They form a belt of metasediments interspersed with migmatitic-gneisses, that are cut by two large tourmaline-bearing leucogranites, known as the Gophu La and Western Leucogranites (Castelli and Lombardo, 1988; Dietrich and Gansser, 1981). Th-Pb measurements yielded a 12.5 ± 0.4 Ma monazite crystallisation age for the Gophu La leucogranite (Edwards and Harrison, 1997). The predominant facies of the Lunana metasediments comprises phlogopite ± diopside marbles and calc silicates that are intruded by minor biotite amphibolites (Gansser, 1983).

The Northeastern Metasediments have a similar outcrop pattern to the Lunana metasediments, and are intruded by sills, dykes and massive tourmaline-bearing leucogranites of the Mönlakarchung leucogranite body (Blattner et al., 1983). A further similarity to the Lunana lithologies is the dominance of carbonates (mostly phlogopite ± diopside ± garnet marbles, calc silicates and dolomites).

4.4 The Lesser Himalaya Series

The LHS throughout the Himalaya is bounded to the north by the MCT and to the south by the MBT. Exposure of the LHS is limited to a narrow band through most of the southwest and south of Bhutan. However, the Kuru Chu-Shumar Half Window in

southeast Bhutan allows a large exposure of the LHS (Fig. 4.1). The LHS in Bhutan consists of a series of thrust stacks as seen in other parts of the Himalaya, such as the Krol Belt and the Jutogh Klippe in the Sutlej Area (Chapter 2). Table 4.2 summarises the different units and thrusts within the LHS. Due to political and logistical restraints not all the units in Table 4.2 were sampled during the course of this study.

Table 4.2 - Summary of the LHS units and their tectonic relationships (modified from Ray et al. 1989 and Jangpangi, 1974).

	Age (according to Jangpangi, 1974):
Thimpu Group (HHCS)	Precambrian
————*Thimpu Thrust (MCT)*————	
Barsong Formation	Gansser (1983)
Daling-Shumar Group (with concordant granitoids)	Precambrian
————*Shumar Thrust*————	
Diuri Formation	Carboniferous-Permian
Baxa Formation	
————*Buxa Thrust*————	Lower Palaeozoic-Precambrian
Damudas, Gondwana	Carboniferous-Permian
————*MBT*————	
Siwalik Group	Tertiary

4.5.1 The Damudas

Gansser (1983) describes this group as tectonically disturbed sediments, comparable with the Damudas of the Darjeeling area. Within the India Subcontinent, Mid-Jurassic coal-bearing facies may be correlated with the many Gondwanan coal seams throughout Asia (Gosh, 1993; Ray and Chakraborty, 2002 amongst others). They consist of low-grade sandstone, shale, slate, limestone and dolomite; of particular interest are the sandstone coal-bearing beds (Gansser, 1983). Due to their thin outcrop pattern and highly tectonically disturbed nature, outcrops are often covered in scree.

4.5.2 The Diuri Formation

The Diuri Formation crops out to the southeast of Bhutan and south of the Kuru Chu-Shumar Half Window. According to Gansser (1983) the Diuri Formation consists of a 2000 m thick sedimentary package, comprising of a basal conglomerate overlain by pebbly shales, slates and quartzitic bands within a partly faulted synform. The conglomerate within the Diuri Formation is tentatively correlated with the Blaini boulder bed (Chapter 2), unfortunately not sampled in this project. Lineations within the slates and phyllites are overprinted by kink bands that parallel the Kuru Chu-Shumar Half Window (Gansser, 1983). The Diuri Formation is assigned an age that is older than that of the Damudas due to "the lack of coal, great thickness and rare gritty quartzite intercalations as well as the incipient metamorphism" (Gansser, 1983), this interpretation is consistent with the stratigraphical age of the Blaini boulder bed within the Sutlej Area (Late Neoproterozoic; Chapter 2).

4.5.3 The Baxa Formation

The Baxa Formation is widely exposed in south-central and southwestern Bhutan. Although the Krol Group (described in Chapter 2) has been correlated with the Baxa Formation Gansser (1983) questions this correlation in the light of poor biostratigraphical markers. Gansser (1983) further limits the Baxa Formation to those rocks that are predominately made up of dolomites, limestones, calcareous shales, gypsum and basal quartzites. The ferruginous quartzites pass upwards into dolomites and limestones, which are cut by thrusts carrying Daling phyllites (Gansser, 1983). The dolomites and limestones of the Phuntsholing section have been thrust out of the section, leaving only the ferruginous quartzite horizons exposed; quartzites are also observed in the thrust imbrications, whereas, north of Narphong, the Baxa Formation forms a strongly sheared tectonic wedge consisting of dolomites between north-dipping phyllites and quartzites of the Daling-Shumar Group, (Gansser, 1983).

4.5.4 The Daling-Shumar Group

The Daling-Shumar Group forms the largest LHS thrust sheet in Bhutan, achieving its maximum thickness in the east, and thins westwards due to either tectonic or sedimentary processes. This group dominates the Kuru Chu-Shumar Half Window that forms a complex northwards striking antiform, cut by a series of east-west trending faults and thrusts. The inverted metamorphic gradient associated with the MCT reaches its highest grade within the half window (Gansser, 1983; Stuewe and Foster, 2001).

Gansser (1983) describes the Daling-Shumar Group as one of the most complex sedimentary groups of the whole Himalaya. The Daling-Shumar Group may be broadly described as a series of unfossiliferous phyllites, slates and quartzites, of which the quartzites dominate the group and are responsible for the majority of outcrop exposure in the Daling-Shumar Half Window. They are often referred to as the Shumar Quartzites which are massive recrystallised quartzites (Fig. 4.4 a) with weak sedimentary features picked out by heavy mineral banding (Fig. 4.4 b) and are excellently observed in the cliffs between Morang and Lhuntsi. Gansser (1983) assigns the name Daling-Shumar as tentative correlations can be made with both the Daling sediments in Sikkim and the Shumar of Nautiyal et al. (1964). Due to the complex nature of the group, a complete stratigraphical section is not known. However, Ray et al. (1989), separate the group into "system A" and "system B" within a series of mapped thrusts. System B, representing the upper part, consists of a repetitive sequence of phyllites and quartzites, with thin discontinuous marbles beds enclosed within phyllites; the two uppermost quartzite bands are thin (100-250 m), but continuous for ca. 30 Km along strike. System A, separated from system B by thrusting, consists of a series of sheared granitic gneisses, phyllites and quartzites.

Within the Phuntsholing section, the Daling-Shumar Group outcrops as strongly folded, sheared and faulted phyllites with interbedded thin quartzites. Towards the MCT amphibolite dykes become more common (Gansser, 1983).

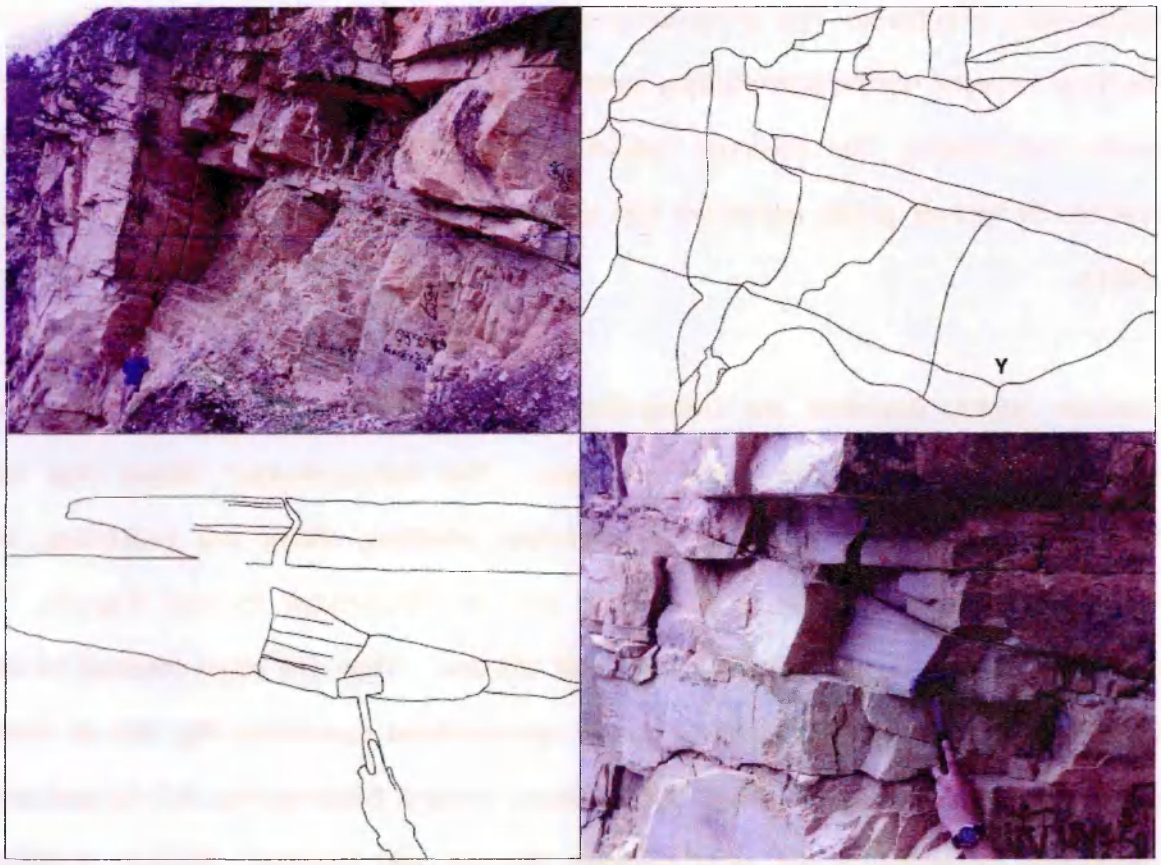

Figure 4.4 - Shumar Quartzite, Daling-Shumar Group (a) Recrystallised massive Shumar Quartzite, point 'Y' corresponds to close up of b; (b) Detail of heavy mineral bands picking out weak bedding, cross-bedding occasional and very weak.

4.5.5 The Barsong Formation

According to Gansser (1964) the Barsong Formation is located structurally below the MCT and the overlying augen gneisses of the HHCS (Fig. 4.5). The Barsong Formation outcrops as a single thin sliver with an aerial extent of less than 1 Km thick and ca. 10 Km wide in the eastern Bhutan (Fig. 4.1). It consists of thick quartzites and layers of shale, with a maximum thickness of 500m. The quartzites are pure, and preserve weak sedimentary features such as cross bedding and ripple marks. The organic-rich calcareous shale layers contain a number of reworked Palaeozoic microfossils and Upper Jurassic (Oxfordian) dinoflagellate cysts (Gansser, 1983). Gansser speculates

that due to its unique depositional age this may represent a remnant of an intermediate facies that is usually faulted out by the overlying crystalline thrust sheet above the MCT.

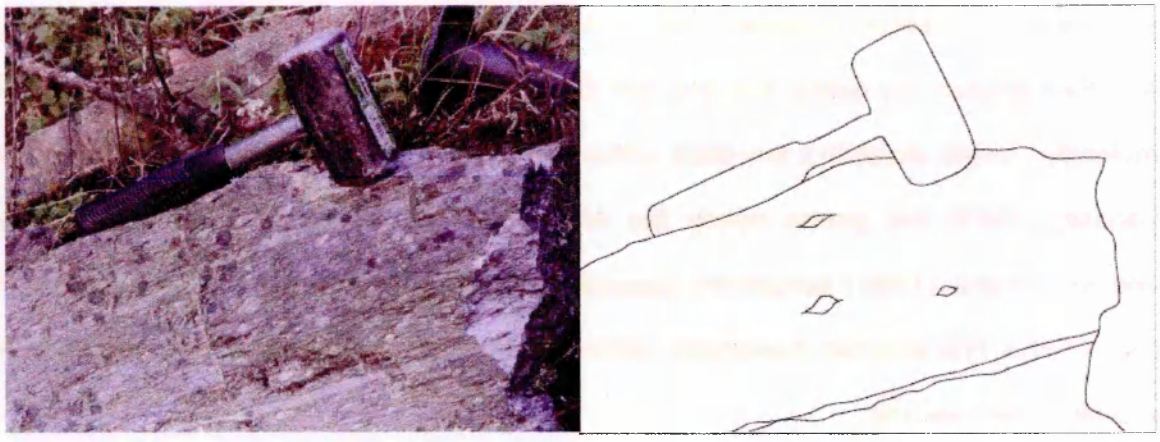

Figure 4.5 - Augen gneiss, HHCS; strained augens in gneissic fabric with weak boudinaged veins, close to MCT, near Barsong.

4.5.6 The Jaishidanda Formation

The Jaishidanda Formation (Daling Phyllites, Gansser, 1983) is a series of garnet-bearing phyllites and schists between 30-600 m thick which overlie the Daling-Shumar Group across much of Bhutan (Dasgupta, 1995); its sedimentation age is uncertain. The Jaishidanda Formation lies in a similar structural position to the Barsong Formation, although contrastingly forms a continuous unit across much of Bhutan. The assignment of the Jaishidanda Formation is controversial: according to Dasgupta (1995) lithologically this formation is "broadly akin" to the underlying Daling-Shumar Group, whereas Jangpangi (1974) assigns the Jaishidanda Formation as a portion of the overlying HHCS. This formation also appears to lie at a similar structural position to the Karcham Group (Chapter 2); the application of whole-rock isotopes may help resolve this issue.

4.5.7 Intrusives

A series of five large granitic gneisses has been mapped within the Kuru Chu-Shumar Half Window extending over several kilometres (Fig. 4.1). It consists of two-mica

granitic gneisses and augen gneiss with sheared tectonic contacts within the Daling-Shumar Group (Fig 4.1); no evidence for contact metamorphism was observed. These intrusives are distinct from the granites that intrude the HHCS due to the absence of associated migmatites (Gansser, 1983). A confusing study of the Kangpar Gneiss (Fig. 4.1, East Bhutan) by Sinha-Roy and Sen Gupta (1986) described the orthogneiss as a mylonitic, single sheet 2-3 km-thick within the Baxa Formation, although according to Gansser (1983) this gneiss clearly lies within the Daling-Shumar Group. Sinha-Roy and Sen Gupta (1986) tentatively suggest that this anatectic granite may represent part of the Precambrian basement, although they then state that the granite was emplaced tectonically.

4.5 The Sub-Himalaya Series

The Sub-Himalaya in Bhutan is described as the Siwaliks (molasse) by Gansser (1983). The Siwaliks are bounded to the north by the MBT and to the south by (recent) alluvial deposits which overlie the MFT. Unlike many other sectors of the Himalaya, the Siwaliks is largely missing along much of the Bhutan sector allowing recent alluvial deposits to reach the MBT (Fig. 4.1). Where present, Siwalik deposits are predominately siliciclastic, ranging from conglomerates to mudstones, dipping to the north and over-thrust by the LHS along the MBT. Thrust repetition, as observed in Nepal, is uncommon in the Bhutan Siwaliks (Gansser, 1983). Unfortunately, political and logistical restraints prevented this study from venturing into the sub-Himalaya.

Chapter 5 – The Geochemistry The Bhutan Himalaya

5.1 Introduction

This project has shown that Sr, Nd and U-Pb isotope systems can be used to distinguish major Himalayan units and structures within the Sutlej Area (Chapter 3). To test whether effective discrimination observed in the Sutlej could be traced eastwards along the Himalayan mountain belt, samples were collected and analysed from the Bhutanese sector of the eastern Himalaya. The previous chapter explained the tectonic units and structures in Bhutan; this chapter concerns the geochemical data obtained from this project. As in Chapter 3, both elemental and isotopic compositions of clastic metasediments are examined for discriminating between major Himalayan units.

5.2 Whole-rock geochemistry

To enable comparison with the Sutlej Area, similar plots using the discrimination criteria of Bhatia (1983), Roser & Korsch (1988) and Fralick & Kronberg (1997) were used.

Figures 5.1 a-d demonstrate that this geochemical dataset shows broad overlaps between the HHCS, LHS and TSS units and therefore no clear discrimination can be made; this pattern was also observed in the Sutlej data set (Chapter 3.2). However, the discriminate function diagram of Roser & Korsch (1988) (Fig. 5.1 a) shows that many of the HHCS, LHS and TSS samples plot within the mafic igneous provenance field, although a number of LHS samples plot towards the left of this field. A number of mainly HHCS and TSS samples plot within the intermediate and felsic igneous fields. Figure 5.1 b shows the LHS has a greater affinity for sediments derived within passive

or active continental margin settings, whereas the HHCS and TSS plot closer to the oceanic and continental arc fields, although the data show a large amount of scatter.

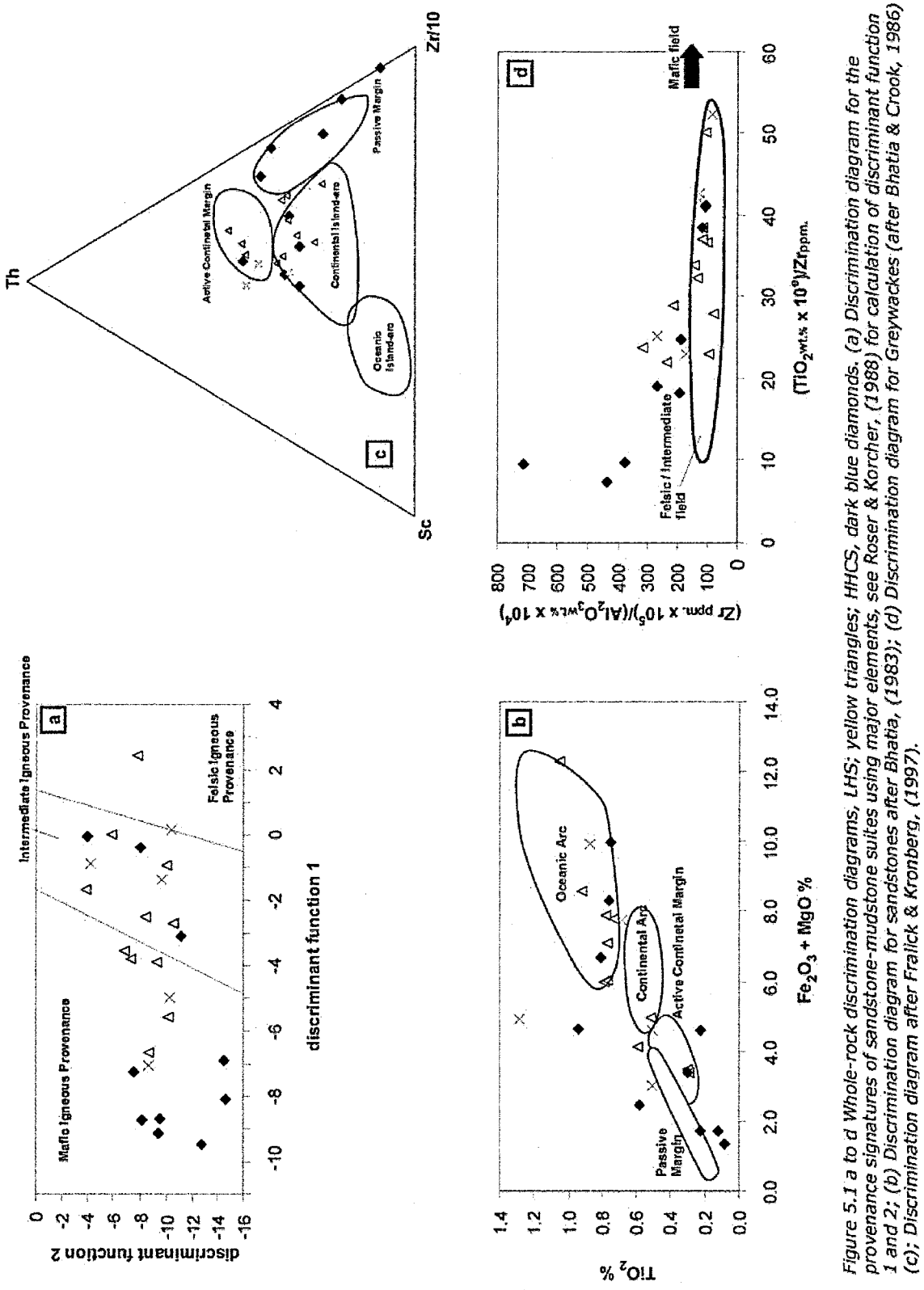

Figure 5.1 a to d Whole-rock discrimination diagrams, LHS; yellow triangles; HHCS, dark blue diamonds. (a) Discrimination diagram for the provenance signatures of sandstone-mudstone suites using major elements, see Roser & Korcher, (1988) for calculation of discriminant function 1 and 2; (b) Discrimination diagram for sandstones after Bhatia, (1983); (d) Discrimination diagram for Greywackes (after Bhatia & Crook, 1986) (c); Discrimination diagram after Fralick & Kronberg, (1997).

Figure 5.1 c shows that many of the LHS samples plot within or near the passive margin to continental-island arc fields whereas most of the HHCS and TSS samples plot within or near to the continental-island arc to active continental margin fields. Figure 5.1 d demonstrates that felsic/intermediate rather than mafic sources have contributed to all these sediments. However, due to elevated Zr/Al_2O_3 ratios many of the LHS samples plot outside the felsic/intermediate field, whereas most of the HHCS and TSS samples plot within this field. The inconsistencies between Figures 5.1 a and 5.1 d perhaps suggest a non-igneous source for this rock suite. Given the lack of clear discrimination offered by any one plot, no firm conclusions can be drawn from the element geochemistry of these clastic sediments.

5.3 Isotope Geochemistry

5.3.1 Previous Isotope Studies

The large number of previous isotope studies from the Nepalese, Indian and Pakistani Himalaya have been reviewed in Chapter 1 (Argles et al., 2003 and references therein). These establish that Sr and Nd whole-rock isotopes and U-Pb dating of individual zircons can be used to define and discriminate between major Himalayan units (Fig. 1.5 to 1.8). However, only a small number of isotope studies have so far been undertaken in Bhutan, including one on the emplacement of granitic bodies and leucogranites within the HHCS (Edwards and Harrison, 1997) and another that dated formation and metamorphism of the Bhutanese Himalaya (Daniel et al., 2003). Conclusions drawn from published U-Pb monazite and xenotime ages from Bhutan include: (i) the age of initial penetrative thrust-related deformation and metamorphism within the LHS and lowermost HHCS (MCTZ) is constrained to at least 22-20 Ma; (ii) metamorphism of kyanite-bearing migmatites is dated at 18-16 Ma; and (iii) syn-tectonic leucogranites situated below the Kakhtang Thrust were emplaced at ca. 18-13 Ma (Daniel et al., 2003). Th-Pb monazite ion microprobe measurements have constrained the crystallisation of the Kula Kangri Granite (Gophu La leucogranite,

Chapter 4), located above the Kakhtang Thrust, to 12.5 ± 0.4 Ma (Edwards and Harrison, 1997). However, in contrast to studies from the Nepalese, Indian and Pakistani Himalaya, metasedimentary whole-rock Sr and Nd studies are unknown in the limited literature from the Bhutan Himalaya, or indeed anywhere in the eastern Himalaya eastwards of the Everest transect.

5.3.2 Sr and Nd Isotope Geochemistry - Results

A total of 26 rock samples were selected for Sr and Nd analysis to represent the Bhutanese Himalaya as described in Chapter 4 and outlined in Table 4.1. A further 6 samples (called TSS Regional) from L. Godin, (Queen's University, Canada) and N.B.W Harris (The Open University) collected from central Nepal (Annapurna) and south eastern Tibet (Kangmar gneiss dome) respectively, were added to the TSS suite from Bhutan, where sampling was limited by logistical constraints (Chapter 4). These additional samples are treated as a single group, termed the TSS (regional), in contrast to the TSS (Bhutan).

As for the Sutlej database (Chapter 3) the ε_{Nd} values presented here (Appendix B) for the Bhutan dataset are age-corrected to t=500 Ma. Figure 5.2 shows that the HHCS data from Bhutan define a group (ε_{Nd} = -12 to -7) similar to the HHCS from the Sutlej Area. As for samples from the Sutlej and Garhwal regions of the western Himalaya, the LHS samples from Bhutan form two distinct groups: the first (ε_{Nd} = -22 to -20) represents the majority of samples from the LHS in Bhutan, the Daling-Shumar Group; the second (ε_{Nd} = -14 to -7) coincides with the HHCS data. The latter group comprises samples from the Barsong Formation and the Jaishidanda Formation. As already discussed (Chapter 4), the Barsong Formation appears anomalous due to its Mesozoic sedimentation age (Gansser, 1983), whereas the Jaishidanda Formation is a more persistent unit that overlies the Daling-Shumar Group in the MCTZ across much of Bhutan (Dasgupta, 1995); its sedimentation age is uncertain. The TSS (regional) and TSS (Bhutan) data also lie within a similar range (ε_{Nd} = -12 to -8) to the HHCS

data, although a few samples from this group produced uncharacteristically more positive ε_{Nd} as observed in the Sutlej (this study) and Nepal (Robinson et al., 2001). These more positive ε_{Nd} values, termed outliers in the following discussion, may reflect local volcanogenic input as suggested by Garzanti (1999).

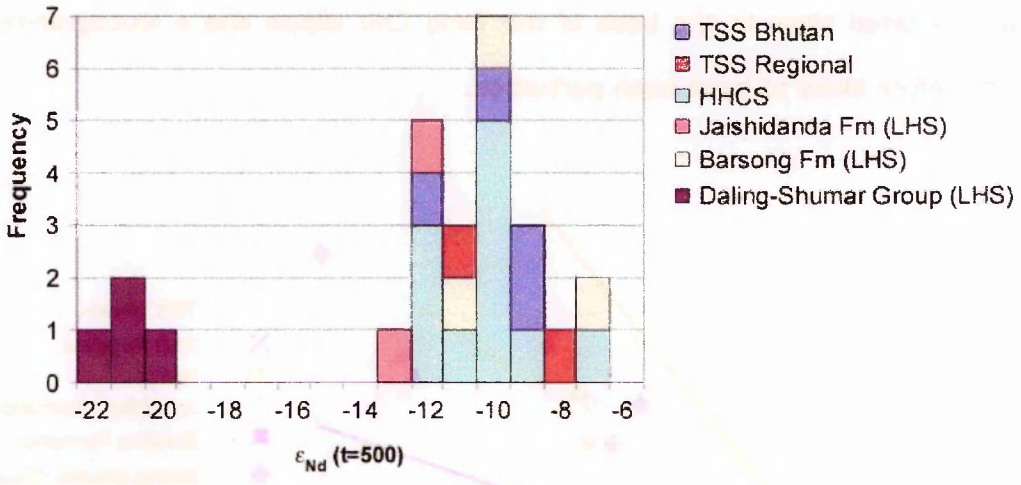

Figure 5.2 - Nd isotopic data from Bhutan(this study), presented as ε_{Nd} (t=500 Ma).

The Sr isotope plot of Chapter 3 (Fig. 3.3) demonstrates that the HHCS from the Sutlej, (and a number of samples from the OLH with similar ε_{Nd} values) plot as an array around a 500 Ma reference line, whereas samples from the LHS that are characterised by more negative ε_{Nd} values, plot around an 1800 Ma reference line. A similar pattern is observed in the Bhutan dataset (Fig. 5.3); the HHCS both above and below the Kakhtang thrust, together with the samples from the Barsong and Jaishidanda Formations, plot as an array along a 500 Ma reference line, whereas the LHS samples with more negative ε_{Nd} plot as a steeper array on the $^{87}Sr/^{86}Sr$ Vs $^{87}Rb/^{86}Sr$ plot (Fig. 5.3). A possible difference between the Bhutan and Sutlej datasets is that these LHS samples plot closer to a 1000 Ma rather than a 1800 Ma reference line. However, the Sr data complements the Nd data as similarities observed with the Nd data are reflected in the Sr data; this relationship is also observed in the Sutlej study (Chapter 3). Two outliers with elevated $^{87}Sr/^{86}Sr$ ratios (marked 'OL' on Fig. 5.3) from the HHCS array are likely to have been perturbed as these two samples (from the Jaishidanda and Barsong Formations) are located immediately below the MCT and may have experienced fluid movement along the thrust zone (as proposed in

Fig. 3.3). The TSS (regional) and TSS (Bhutan) samples plot close to the HHCS array in Figure 5.3, but most samples plot below the 500 Ma reference line. Low $^{87}Rb/^{86}Sr$ values for all TSS samples from this suite do not allow a robust lower age reference line to be plotted due to inadequate anchor data points. One TSS sample (from Bhutan; marked 'OL' Fig. 5.3) plots close to the 1000 Ma reference line; however, the sample is located close to the base of the Tang Chu klippe and a leucogranite body and is therefore likely to have been perturbed.

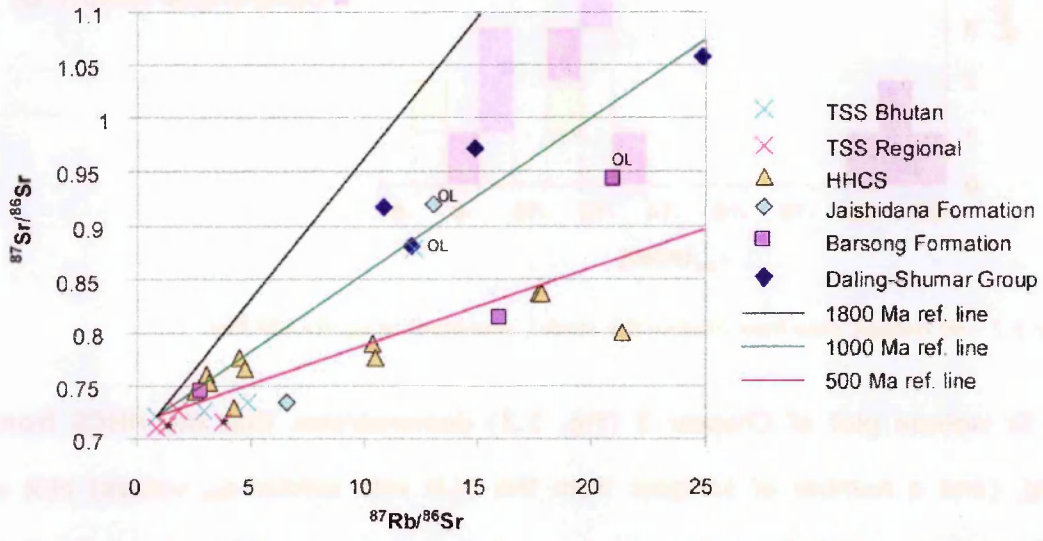

Figure 5.3 - Sr isotopic data from Bhutan (this study); asterisked (*) samples explained in section 5.4.1; OL=outlier.

Fig. 5.4 combines the Sr and Nd data, which are both age-corrected to t=500 Ma. This plot exemplifies the inter-group differences already discussed above. The two fields shown on this plot are defined by previous isotopic studies (Chapter 3, Fig. 3.4 and 3.9 c); the first array (described as the ILH) is defined by low ε_{Nd} values and a high $^{87}Sr/^{86}Sr$; the second array (described as the HHCS) is defined by high ε_{Nd} values and low $^{87}Sr/^{86}Sr$. The LHS of Bhutan can be clearly separated into these two isotopically distinct arrays: samples from the Daling-Shumar Group lie within the ILH array, whereas samples from the Jaishidanda and Barsong Formations lie within the HHCS array. Samples from the HHCS, TSS (Bhutan) and TSS (regional) also plot within the oblate HHCS array suggesting that the proposed ca. 500 ma thermal event

(see Chapter 1) was widespread, extending along strike across the entire length of HHCS and TSS outcrop in the Himalaya.

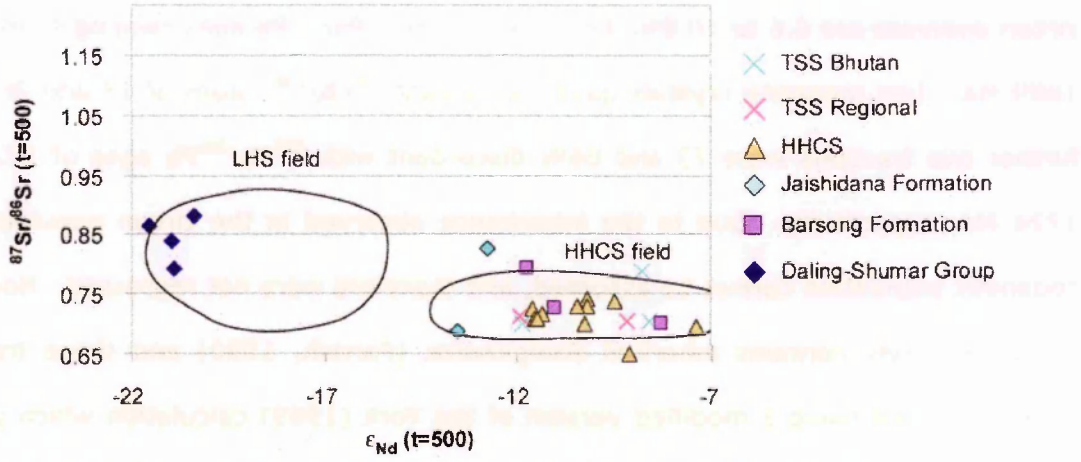

Figure 5.4 - Combined Sr-Nd isotopic data (age corrected, t = 500 Ma) from Bhutan (this study); fields defined by previous isotopic studies (Fig. 1.8, Chapter 1).

5.3.3 U-Pb Zircon Chronology

To enable comparison with the Sutlej U-Pb zircon dataset, samples were recovered for zircon dating from the HHCS, LHS (Daling-Shumar Group) and Barsong Formation of the Bhutan Himalaya. These samples included metaquartzites from the HHCS, Daling-Shumar Group and Barsong Formation, augen gneisses from the HHCS and Daling-Shumar Group and a metarhyolite from the Daling-Shumar Group; psammites and quartzites are uncommon to the Jaishidanda Formation and were therefore not sampled for zircon analysis (as discussed in section 1.7). Photomicrographs of each zircon were taken before and after air abrasion (Krogh, 1982) (see Appendix C.2). The data presented here build on a previously unpublished data set analysed by K Thimm (2000; see Appendix C).

Daling-Shumar Group: Metarhyolite (RP109)

This metarhyolite yielded well-developed prismatic zircons which are pink to clear; some appear turbid, broken or cracked. Imaging these zircons reveals core-rim morphology, suggesting an inherited core whilst the rim is likely due to rhyolite crystallisation. Once abraded, U concentrations have moderate differences of 264-494 ppm. Both zircon and monazite crystals were successfully extracted and analysed

from the metarhyolite; single grain zircon analyses are between 1.8 to 12.6% discordant, with $^{207}Pb/^{206}Pb$ ages ranging from 1788-1819 Ma, whereas multi-grain zircon analyses are 0.6 to 10.8% discordant, with $^{207}Pb/^{206}Pb$ ages ranging from 1819-1889 Ma. Two monazite crystals gave concordant $^{206}Pb/^{238}U$ ages of 18 and 20 Ma, a further two fractions were 73 and 66% discordant with $^{207}Pb/^{206}Pb$ ages of 1727 and 1724 Ma respectively. Due to the inheritance observed in the zircon populations, a cogenetic population cannot be assumed, and therefore were not regressed. However, monazite rarely contains inherited components (Parrish, 1990) and these fractions were regressed using a modified version of the York (1969) calculation which yielded an upper intercept age of 1755 +60/-59 (MSWD = 41) and a lower intercept age ca. 20 Ma (Fig. 5.5); this younger age can be interpreted as lead loss due to the Himalayan orogeny.

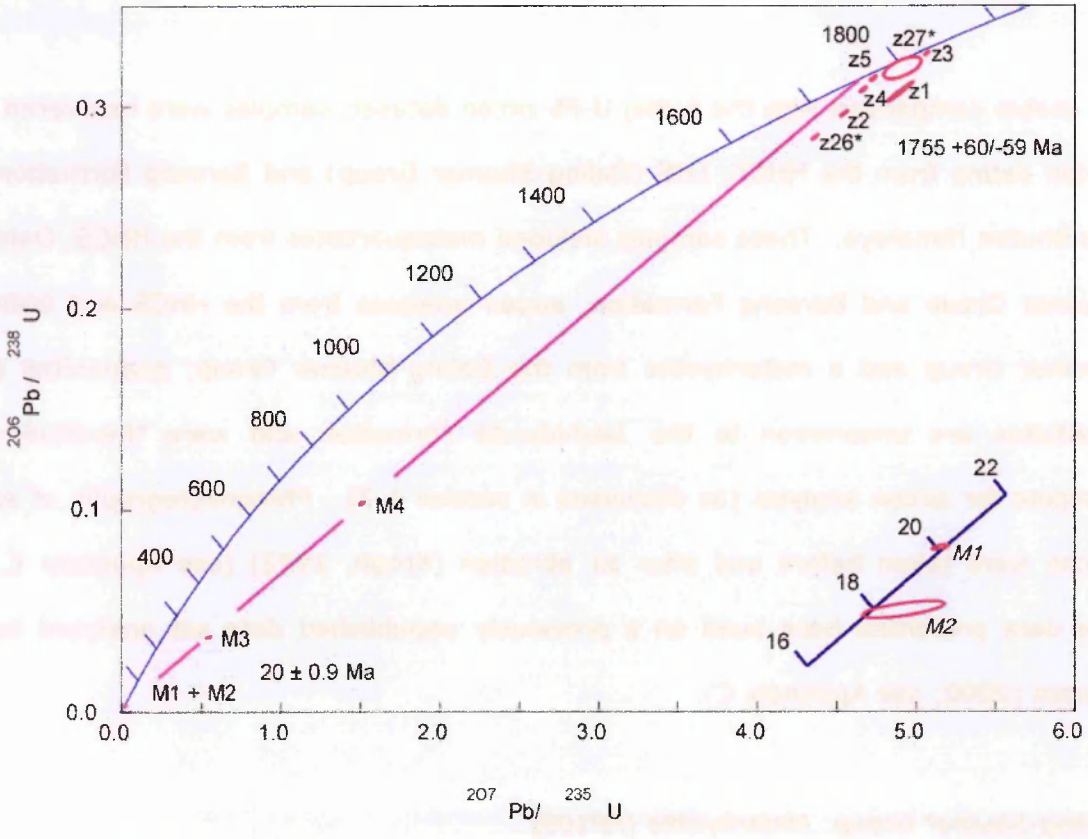

Figure 5.5 - U-Pb concordia plots of zircons extracted from Daling-Shumar Group, LHS, metarhyolite. Asterisked (*) fractions indicate analysis during this study, included for comparative purposes.

Daling-Shumar Group: Biotite Augen Gneiss (RP110)

The zircons extracted from this biotite augen gneiss have similar morphologies to the metarhyolite described above; this sample contains a single population of zircons

which are <120 µm, with well developed prismatic faces; they are clear to pink in reflected light; some are turbid, and inclusions are present. Imaging also reveals that these zircons contain a core-rim morphology. U concentrations are larger than those from the metarhyolite (above) with variations of 57-865 ppm. Zircon-only fractions were analysed from this sample, with single crystal analyses between 2.4 and 16.8% discordant giving $^{207}Pb/^{206}Pb$ ages ranging from 1715-2253 Ma, whereas multi-grain zircon analyses are 3.3 to 24.3% discordant, with $^{207}Pb/^{206}Pb$ ages ranging from 1791-1958 Ma (Fig. 5.6). A number of fractions yield $^{207}Pb/^{206}Pb$ ages similar to zircons from the metarhyolite. The zircon fractions in both the metarhyolite and biotite augen gneiss strongly suggest inheritance and are in contrast to the unimodal zircon population in Wangtu Augen Gneiss (Fig. 3.7). The relatively broad range in $^{207}Pb/^{206}Pb$ ages suggest that the source of inheritance is unlikely to be from a cogenetic source such a granite, but may suggest melts formed from a sedimentary source.

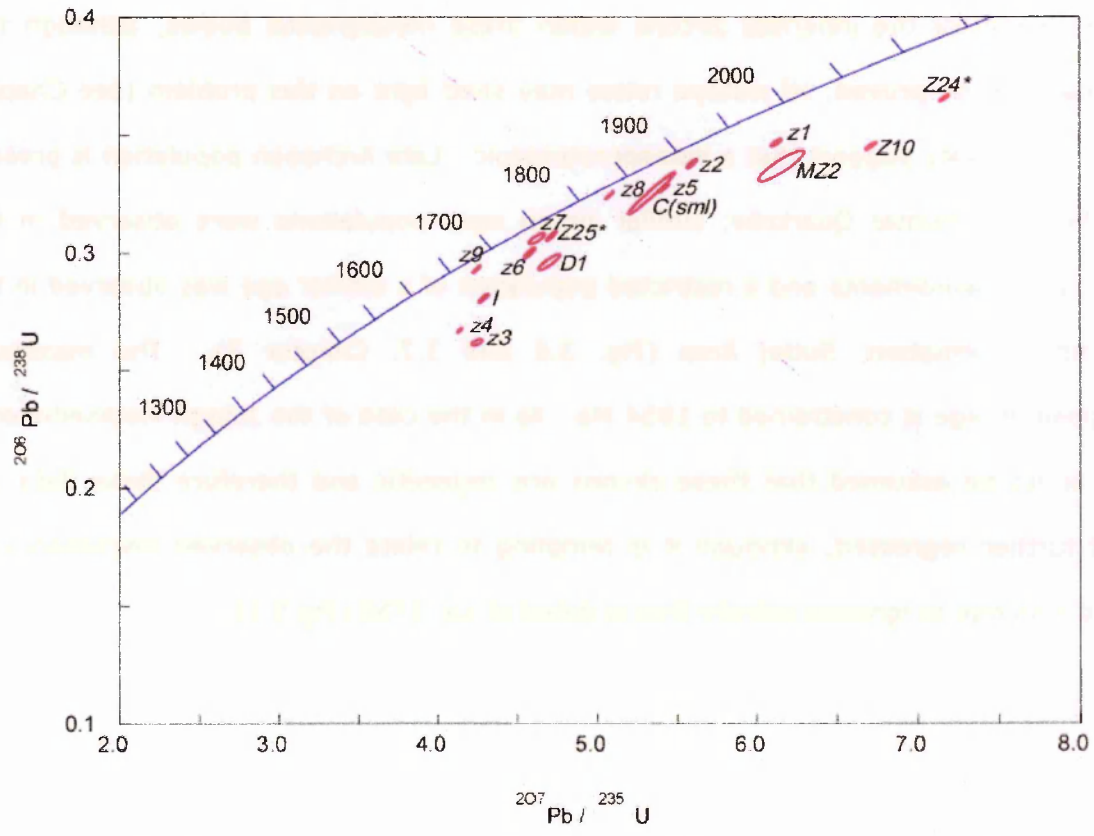

Figure 5.6 - U-Pb concordia plots of zircons extracted from Daling-Shumar Group, LHS, Augen Gneiss. Asterisked (*) fractions indicate analysis during this study, included for comparative purposes.

Daling-Shumar Group: Shumar Quartzite (B75z)

Zircons were extracted from a massive, recrystallised quartzite, located stratigraphically below the metarhyolite and biotite augen gneiss. Two morphological zircon populations were observed; the first comprises colourless, prismatic euhedral to subhedral crystals, most of which are rich in inclusions, while the second population is detrital with well-rounded, anhedral, pitted crystals. Two types of zircon morphology (rounded equant and rounded elongate) are observed in this latter population; both appear inclusion-free and are fawn to light yellow, with some turbidity. Moderate U concentrations were recorded of 41-423 ppm. A total of 14 single-grain zircon analyses (Fig. 5.7) were 1.7 to 7.8% discordant, which yielded $^{207}Pb/^{206}Pb$ ages that appear to represent two populations between 1854 and 2000 Ma (12 fractions) and 2449 and 2545 Ma (the remaining 2 fractions); there appears to be little correlation between discordance and $^{207}Pb/^{206}Pb$ age. The large and relatively younger population is comparable with the zircon populations within the previously mentioned metarhyolite and augen gneiss (Fig. 5.5 and 5.6 respectively). This quartzite may be the source for the inherited zircons within these metaigneous bodies, although this remains to be proved; Hf isotope ratios may shed light on this problem (see Chapter 7). These data suggest that a Palaeoproterozoic - Late Archaean population is present within the Shumar Quartzite; similar zircon ages populations were observed in the Jutogh Metasediments and a restricted population of a similar age was observed in the Rampur Formation, Sutlej Area (Fig. 3.6 and 3.7, Chapter 3). The maximum deposition age is constrained to 1854 Ma. As in the case of the Jutogh Metasediments it cannot be assumed that these zircons are cogenetic and therefore these data are not further regressed, although it is tempting to relate the observed discordance to lead loss due to igneous activity that is dated at ca. 1755 (Fig 5.5).

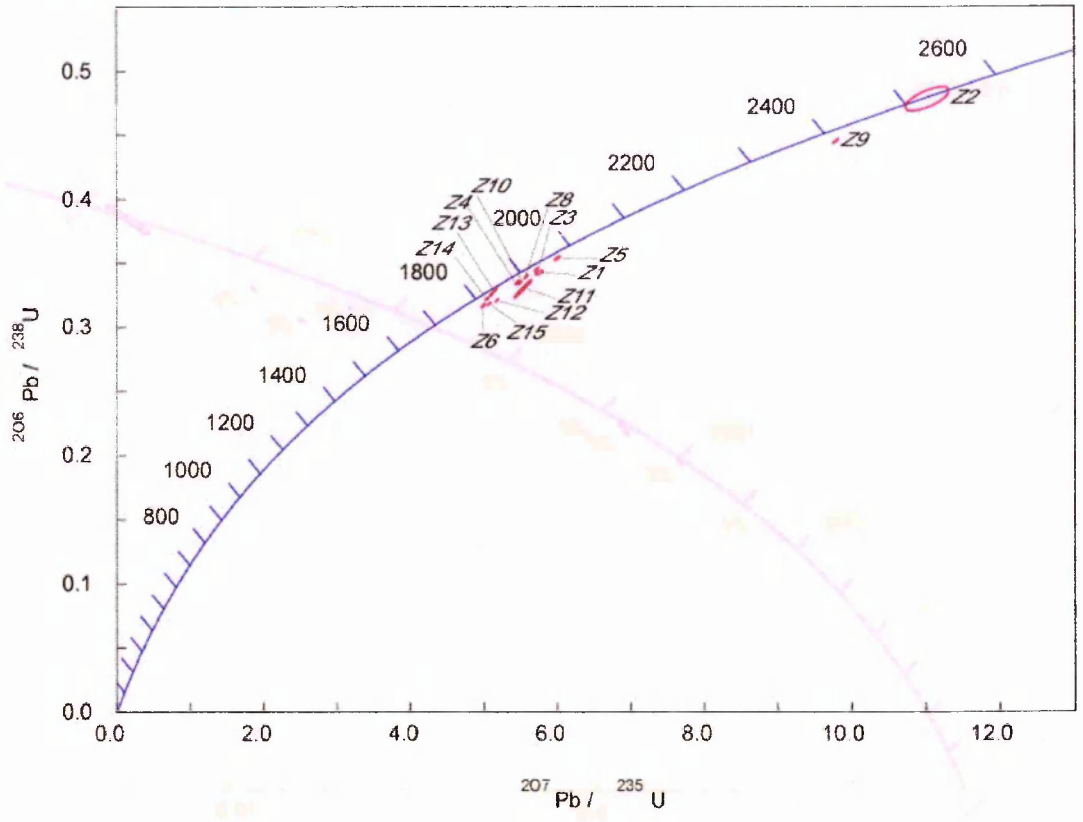

Figure 5.7 - U-Pb concordia plots of zircons extracted from Daling-Shumar Group, LHS; Recrystallised Shumar Quartzite.

Barsong Formation: Quartzite (RP52)

A recrystallised quartzite from the Barsong Formation contains zircons characterised by well-rounded, mainly anhedral, equant to elongate morphologies. A total of 9 single detrital zircon fractions yielded a broad range in U concentration of 110-1871 ppm. The observed discordance of 9 fractions from this formation ranges from nearly concordant (0.1%) to 15.7 % discordant (6 fractions were less than 5% discordant), $^{207}Pb/^{206}Pb$ ages are evenly distributed from 1371 to 2557 Ma (Fig. 5.7). Again, these data cannot be assumed to be cogenetic and therefore regressions have not been applied to this data set. These fractions may represent the previously observed Palaeoproterozoic - Late Archaean population (as observed in the Shumar Quartzite) and a previously unobserved Mesoproterozoic population. The maximum depositional age is therefore constrained to 1371 Ma, whereas Gansser (1983) dated Mesozoic palynomorphs. Furthermore this formation is observed to have whole-rock isotope characteristics of the HHCS/TSS. Clearly this unit appears to be anomalous and will be discussed in section 5.4.

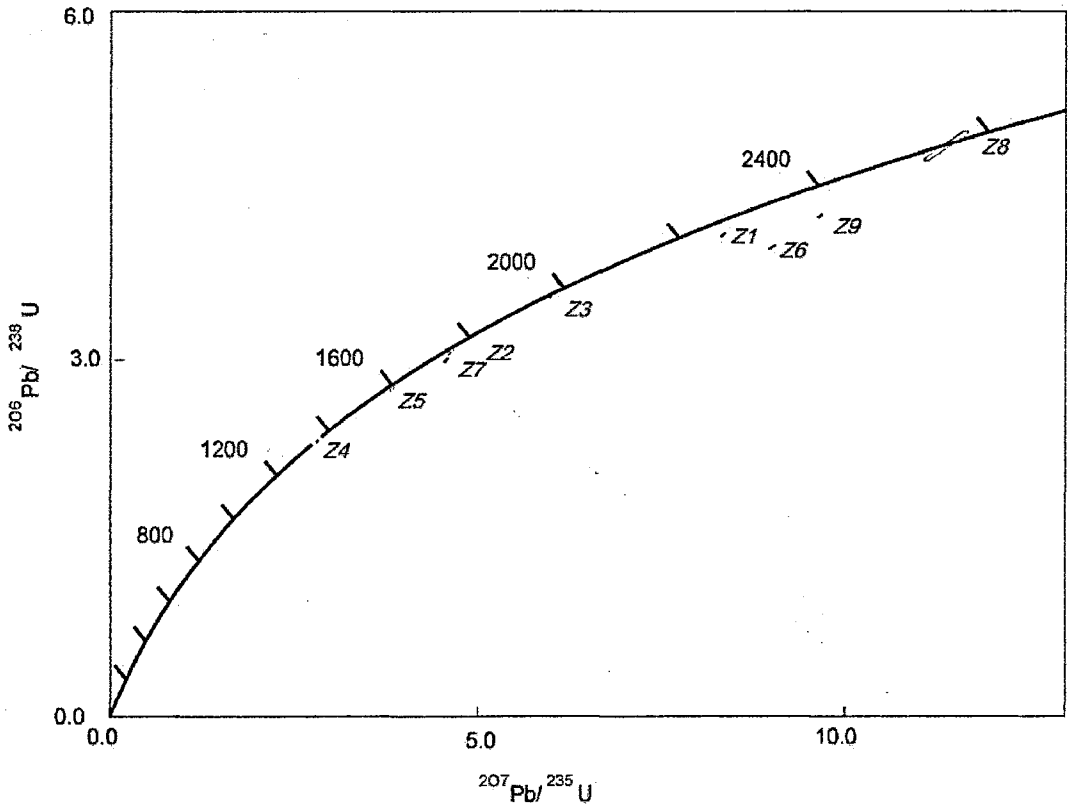

Figure 5.8 - U-Pb concordia plots of zircons extracted from a quartzite, Barsong Formation.

HHCS: Augen Gneiss (RP 69)

Analysis of the augen gneiss (located above the Kakhtang Thrust) included both monazite and zircon crystals. Variations in U were recorded within the augen gneiss from 304 to 533 ppm. A total of three single grain zircon fractions from the augen gneiss were between 8.5 and 13.3 % discordant, whereas a multi-grain fraction gave a highly discordant analysis of 33.7%. No relationship is observed between U concentration and discordance. $^{207}Pb/^{206}Pb$ ages of the single-grain fractions range between 827-847 Ma; the multigrain analysis gave a similar $^{207}Pb/^{206}Pb$ age of 820 Ma (Fig. 5.9). Seven single grain monazite fractions yielded U concentrations between 1571-5788 ppm; 3 fractions were 60.7, 74.3 and 93.5 % discordant with $^{207}Pb/^{206}Pb$ ages of 788, 791 and 439 Ma respectively. The remaining 4 fractions were near concordant with $^{206}Pb/^{238}U$ ages of between 14-15 Ma. When regressed the zircon and monazite crystals produce an upper intercept at 826 ± 0.7 Ma (MSWD = 6.7) (crystallization age), the lower intercept (ca. 14 Ma) suggest the Himalayan orogeny is the event responsible for lead loss in the crystals (Fig. 5.9).

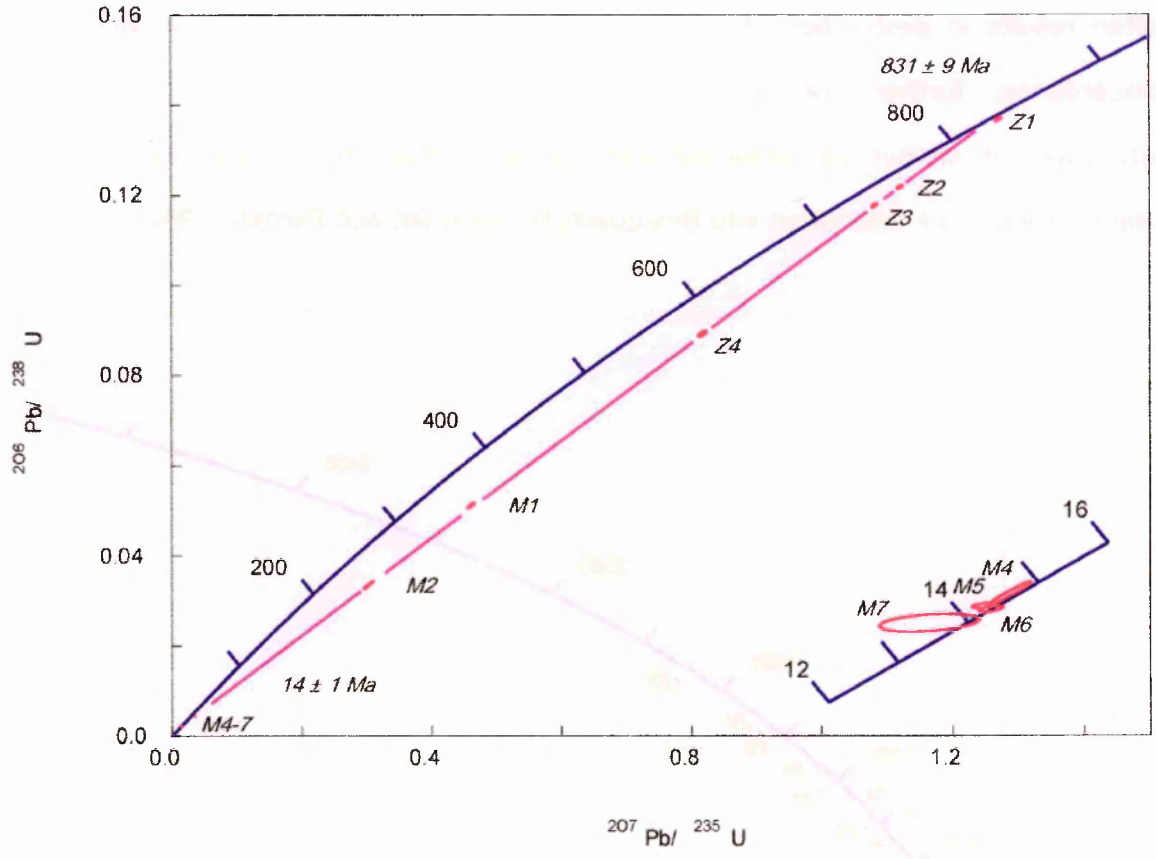

Figure 5.9 - U-Pb concordia plots of zircons extracted from an augen gneiss, located above the Kakhtang Thrust, within the HHCS.

HHCS: Quartzite (RP 71)

The quartzite contains zircon morphologies that display less sedimentary abrasion than those from the Barsong Formation quartzite. Moderate variations of U concentrations of 193-517 ppm were recorded from zircons from the metaquartzite. A total of 9 single grain fractions from the metaquartzite gave between 0.4 and 25.2 % discordance. The zircons analysed may form two populations, as $^{207}Pb/^{206}Pb$ ages are evenly distributed between 978-1578 Ma, whereas one zircon fraction (with a $^{207}Pb/^{206}Pb$ age of 1824 Ma) may represent a Palaeoproterozoic population (Fig. 5.10). Further analyses are required to fully identify the populations within this quartzite; again, these data cannot be assumed to be cogenetic and therefore regressions have not been applied to this data set. However a maximum depositional age is given at 978 Ma. One thorite grain gives a $^{207}Pb/^{206}Pb$ age of 785 Ma (68.7 % discordant), this age is considerably younger than the oldest zircon so far dated from this sample.

However, thorite minerals contain large amounts of U (in this case 16339 ppm) which often results in destruction of the crystal structure and therefore large amounts of discordance; furthermore, as thorite minerals can be susceptible to low-grade alteration, it cannot be assumed with certainty that this crystal has remained unperturbed since deposition into this quartzite (Heaman and Parrish, 1991).

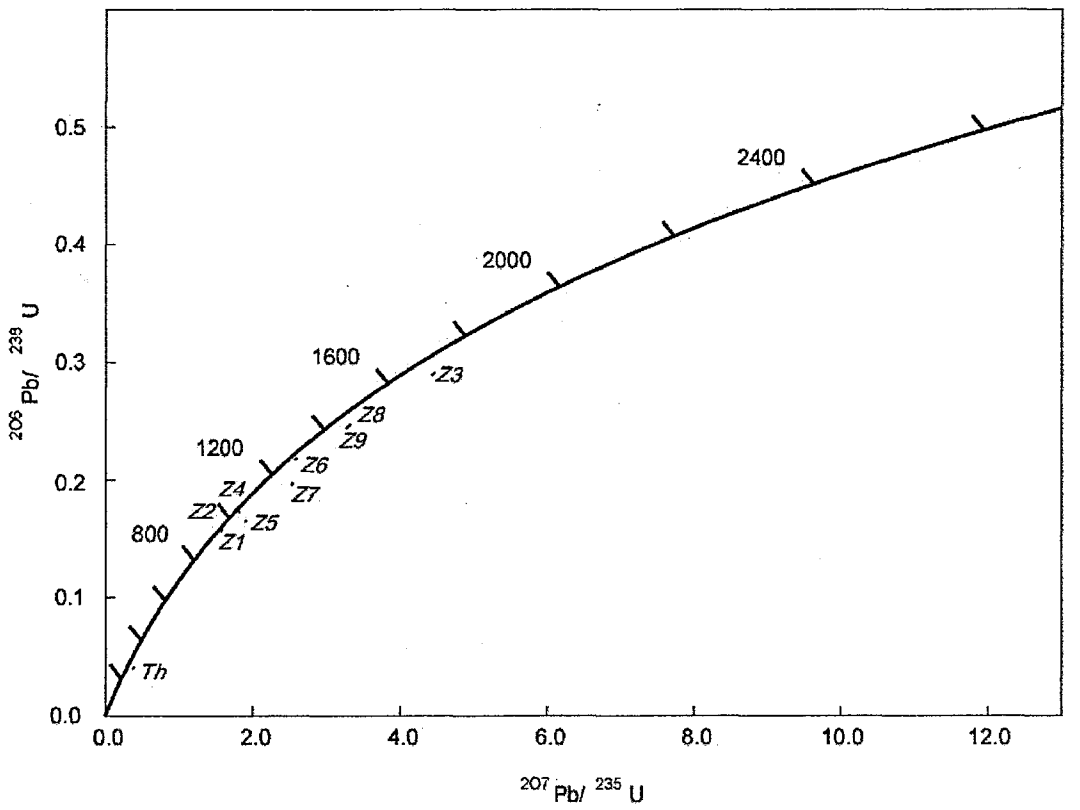

Figure 5.10 - U-Pb concordia plots of zircons extracted from a quartzite, located below the Kakhtang Thrust, within the HHCS.

5.4 Discussion

5.4.1 Whole-rock Sr and Nd isotopes

Figures 5.2 and 5.3 demonstrate that within the LHS the Daling-Shumar Group is isotopically distinct from the Jaishidanda and Barsong Formations. Figure 5.4 demonstrates that the Daling-Shumar Group data fall within the ILH field, whereas the Jaishidanda and Barsong Formations data lie within the HHCS field. This pattern is observed within the Sutlej Area; sediments structurally below the MCT and defined within the HHCS array were described as the Outer Lesser Himalaya (OLH). The

Jaishidanda and Barsong Formations both appear to be isotopically equivalent to the OLH units in the western Himalaya. However, in contrast to the OLH in the Sutlej/Garhwal region which occupy a position in the outer parts of the orogen, the Jaishidanda and Barsong Formations in Bhutan are restricted to the MCTZ (Dasgupta, 1995; Chapter 4). Therefore the terms ILH and OLH are inappropriate due to the spatial distribution of these samples. Instead the term JBF (Jaishidanda and Barsong Formations) is used to describe samples with OLH isotope characteristics as defined in the western Himalaya, whereas the term DSG (Daling-Shumar Group) is used to describe samples with ILH characteristics. The structural position of the JBF is possibly due to the development of the late stage out-of-sequence Kakhtang Thrust within the HHCS, whereas within the Sutlej section out-of-sequence thrusting was accommodated to the south of the MCT along the Jutogh Thrust (Chapter 3). An alternative interpretation is that as the JBF (and particularly the Jaishidanda Formation) bears strong resemblance to the Karcham Group in the Sutlej (both isotopically and in its geological location), these rocks represent the MCTZ in both the Sutlej and Bhutan. In the Sutlej section the MCT is placed at its basal contact with the Wangtu Gneiss, suggesting that the lowermost Jaishidanda Formation marks the MCT in Bhutan, supporting Jangpangi (1974) who assigns the Jaishidanda Formation to the HHCS.

These findings so far suggest that whole-rock isotopes can be used to characterise the DSG/ILH along large parts of the Himalayan orogen, with the proviso that well-characterised units that are conventionally mapped as part of the LHS, and generally have Phanerozoic deposition ages, share the same source regions as do samples from the HHCS. Furthermore, as with the Sutlej Area, samples from the DSG (ILH) of Bhutan describe a narrow ε_{Nd} array, whereas samples from the HHCS, TSS and OLH/JBF form a much broader ε_{Nd} array (Fig. 5.2), which may be due to provenance from multiple source areas (see Chapter 6 for further discussion).

Samples from the HHCS both above and below the Kakhtang Thrust lie within the defined HHCS field (Fig. 5.4) and form an array along the 500 Ma reference line (Fig. 5.3); which suggests that the Bhutan HHCS shares whole-rock isotopic characteristics with the HHCS as recovered from the central and western Himalaya (Chapter 1; Fig. 1.4 to 1.8). Furthermore, although a metamorphic change is apparent across the Kakhtang Thrust, there is no isotopic change suggesting that this thrust thickened the same portion of the HHCS in Bhutan (Grujic et al., 2002).

Figure 5.4 shows that the TSS samples appear isotopically similar to the HHCS field. In the Sutlej Area, the Haimanta Group is separated from the TSS by an unconformity (Chapter 2), yet the two units are isotopically similar (Chapter 3), suggesting that throughout the ca. 500 Ma event that led to the uplift and erosion of an unspecified portion of strata of the Haimanta Group (Grasemann et al., 1997; Wiesmayr and Grasemann, 2002), deposition continued sourcing a similar terrain, possibly even the uplifted upper (?) Haimanta Group. Figure 5.3 shows that many TSS samples lie below the 500 Ma reference line, even though their depositional age post-dates 500 Ma, suggesting that the source of these sediments (possibly the Haimanta Group, as suggested above) had been perturbed by this event prior to erosion (previously explained in Chapter 1). The TSS suite from Bhutan contains a number of samples from the Chekha Formation, which lies above the STDS in Bhutan (Grujic et al., 2002). The Chekha Formation, unlike much of the TSS throughout the Himalaya (Godin, 2003; Hodges, 2000 and references within) is metamorphosed and tentative correlations can be made with the Haimanta Group in the Sutlej Valley. Indeed the Chekha Formation has many characteristics of the Haimanta Group; isotopically they have similar ε_{Nd} isotope values and plot close to the 500 Ma reference line on Sr isotope plots. In outcrop they are folded and frequently intruded by tourmaline-bearing leucogranites. Moreover a pebbly horizon towards the top of the formation (Wang Chu basin) is interpreted by Gansser (1983) as a tillite which may correspond to the Neoproterozoic Marinoan glacial event (ca. 620 Ma) as observed in the Manjir Formation of the Haimanta Group (Chapter 2 and Fig. 3.10). However, the Chekha

Formation lacks the following features of the Haimanta Group: (i) an overlying unconformity with the TSS; (ii) a 'cap carbonate' observed above the tillite in the Manjir Formation; and (iii) a ca. 500 Ma granite that intrudes the lower Haimanta (Chawla et al., 2000). A larger data set from the Chekha Formation would properly assess a possible correlation between the Chekha Formation and the Haimanta Group. Recognition of an equivalent unit in the intervening Nepalese sections remains equivocal; for example within the Annapurna region, the lowermost TSS, the Sanctuary Formation, is below garnet-grade (Godin, 2003).

Minor differences are however present between the Sutlej and Bhutan data sets; the DSG in Bhutan, unlike the ILH in the Sutlej Area, plot scattered around a 1000 Ma reference line (Fig. 5.3); although it remains uncertain whether this is statistically significant. In addition the separation between the HHCS and DSG Groups using ε_{Nd} (Fig. 5.2) is much greater in Bhutan compared to the Sutlej, possibly due to different provenance of the source areas (Chapter 6).

Figure 5.11 demonstrates that once the JBF is distinguished from the remaining units of the DSG, discrimination can be made between the HHCS and LHS on the basis of trace elements (samples have been labelled according to the array they lie within), however, the interpretation that the JBF is part of the HHCS tectonic unit reduces the DSG data set. In general the findings of this study suggest that whole-rock isotopes can be used to describe and discriminate between the major tectonic units along large parts of the Himalayan orogen.

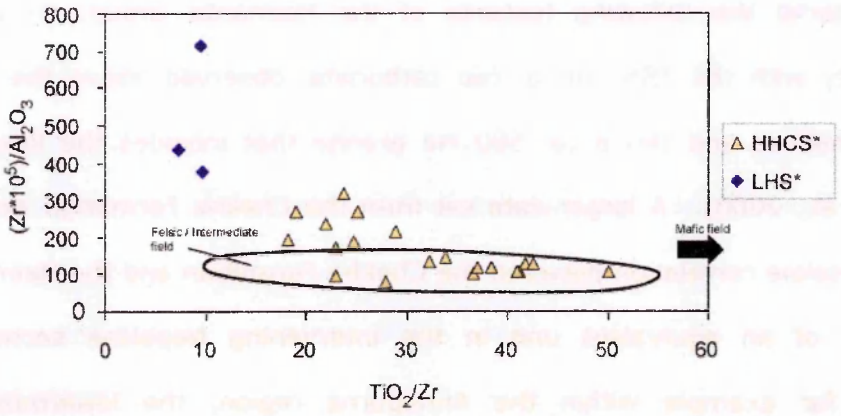

Figure 5.11 - Discrimination diagram after Fralick & Kronberg, (1997). Asterisked (*) labels explained in section 5.4.1. The DSG data presented here are from pure quartzites; low Al_2O_3 and possibly TiO_2 should be expected relative to the HHCS samples.

Despite this general conclusion there remain isolated anomalies (outliers). Elevated $^{87}Sr/^{86}Sr$ ratios from the TSS and the OLH have been explained by the close proximity of these samples to leucogranite intrusions or fault activity, which can both perturb the $^{87}Sr/^{86}Sr$ (as observed in the Sutlej, Fig. 3.3). Two TSS samples marked with an asterisk (*) on Figure 5.3 lie below the 500 Ma reference line as characteristic for the TSS samples, but these samples are Mesozoic and have uncharacteristically high (more positive) ε_{Nd} values, whereas the Devonian and Permo-Carboniferous samples have characteristic (more negative) ε_{Nd} and $^{87}Sr/^{86}Sr$ values and lie within the HHCS array (Fig. 5.4). The effect of basalt contamination on ε_{Nd} has already been demonstrated in the ILH of the Sutlej region (Chapter 3), and a relationship within the TSS may exist between the depositional age of samples with apparently perturbed ε_{Nd} values and magmatic events. Indeed these perturbed ε_{Nd} samples were deposited after known magmatic events including the early Permian Panjal Traps (ca. 258-275 Ma; Noble et al., 2001) and Mesozoic arc formation (Aitchison et al., 2000; McDermid et al., 2002). Therefore it is possible that TSS samples that have been deposited more recently than the early Permian contain basaltic detritus, thus inducing a variable isotopic component of higher ε_{Nd}. However, Figure 5.1c shows that the TSS samples are geochemically similar, whether pre or post-Permian in age, suggesting that Nd contamination from basaltic sources is small, but sufficient to perturb the ε_{Nd} values.

5.4.2 U-Pb Zircon Chronology

Metasediments

Figure 5.12 summarizes the metasedimentary $^{207}Pb/^{206}Pb$ zircon age populations in Bhutan. The detrital zircon ages ($^{207}Pb/^{206}Pb$, 1854-2239 Ma) from the Shumar Quartzite (Daling-Shumar Group) are comparable to the detrital zircon ages from the ILH in the Sutlej (1864-2260 Ma); no zircons younger than ca. 1800 Ma have been dated from either group. A maximum depositional age from the Shumar Quartzite is constrained to ca. 1854 Ma and is comparable with the maximum depositional ages from ILH units in the Sutlej, where maximum depositional ages are constrained to between 1864 and 2012 Ma.

Zircons recovered from the HHCS metasedimentary sample are comparable with similar HHCS samples from the Sutlej Area (Chapter 3) as these both contain zircons younger than ca. 1800 Ma; furthermore maximum depositional ages are comparable with ca. 978 for Bhutan and ca. 840 Ma for the Sutlej Area. However, in terms of zircon populations, the HHCS sample from Bhutan does not share a number of characteristics with the Sutlej Area HHCS data set. These include the absence of late Archaean zircons (although one fraction was dated to ca. 1824 Ma, which may represent at least a Palaeoproterozoic population) and a significant Mesoproterozoic population. These discrepancies may result from small sample populations; Parrish & Hodges, (1996) and DeCelles et al., (2000) produced age populations similar to those derived from the Sutlej HHCS samples (this study) from fractions containing 7 and 27 zircons respectively, whereas Myrow et al. (2003; Fig. 6.1) studied metasediments with HHCS isotopic characteristics and demonstrated that 134 zircon ages formed a broad population from ca. 600 to 2600 Ma, with a small distinct Archaean population (3000 to 3500 Ma); if further fractions were analysed from both HHCS sections a similar age spectra to Myrow et al. (2003) might be observed.

However, although there are discrepancies between the two data sets, zircons recovered from the Bhutan HHCS metasedimentary sample can be distinguished from zircons recovered from the Bhutan DSG metasedimentary sample by the presence of zircons younger than ca. 1800 Ma, which is comparable with zircon populations in the Sutlej Area (Chapter 3). These discrepancies could be resolved by dating larger numbers of zircons.

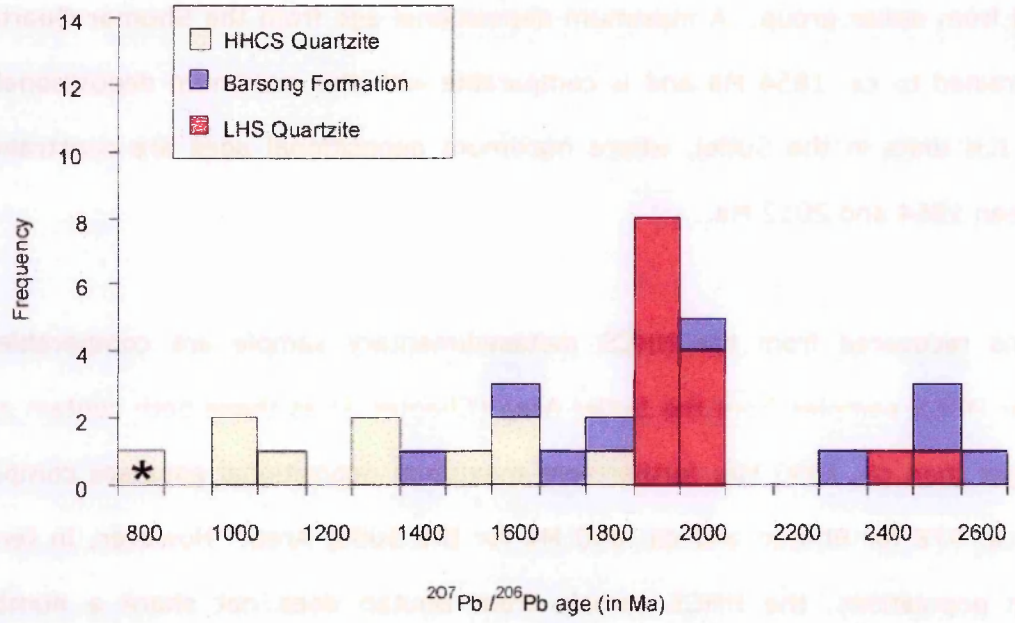

Figure 5.12 – Summary of the metasedimentary $^{207}Pb/^{206}Pb$ zircon age populations in Bhutan. Asterisked (*) indicates a single thorite analysis.

The ε_{Nd} and Sr-isotope characteristics of the Barsong Formation indicate characteristics that are quite distinct from other lithologies from the DSG/JBF in Bhutan yet similar in many respects to the isotopic characteristics of the HHCS. However, the zircon age population (1371 to 2557 Ma; summarised in Fig. 5.12) reveals a curious anomaly compared to other HHCS zircon populations in that these typically extend to younger ages than 1371 Ma. However, the distribution of zircon ages within the HHCS metaquartzite from below the Kakhtang Thrust suggests a bias towards the older components in the population (Fig. 5.10), although Late Archaean ages were not observed in the HHCS, but a similar Mesoproterozoic age spectrum is observed in both samples. A total of only 9 fractions were analysed for this sample and it is therefore likely that if more fractions were analysed a younger component

might be found. The location, outcrop size, isotopic characteristics and Mesozoic palynomorphs (Gansser, 1983) are equivocal. Should we regard this unit as a sliver of TSS that became incorporated within the MCTZ, or is it erroneous to assign the quartzite sample (RP 52) to the same unit that Gansser (1983) observed Mesozoic palynomorphs? Alternatively, the anomalous Mesozoic age of the palynomorph study may suggest (laboratory?) contamination as this age has not been independently verified by any other palaeontological study, or a repeat analysis. Therefore, on the basis of isotopic mapping, the Barsong Formation could be considered the same as the Jaishidanda Formation. Clearly more work is required to fully characterise this remarkable and anomalous Himalayan formation.

Intrusives

Although inherited components were not observed in the Wangtu Augen Gneiss (Sutlej Area; Fig. 3.7), the broad range of ages, variable discordance and imaging from the augen gneiss from within the Daling-Shumar Group suggest a significant inherited component within this population (Fig. 5.6); when inheritance is observed, it cannot be assumed that a cogenetic population is present therefore the data cannot be regressed. However, although the metarhyolite also appears to show inheritance in the zircon population, monazites recovered from this sample enable a chord to be regressed through the monazite data producing an upper intersect age of 1755 +60/ -59 Ma (interpreted as an age of crystallisation); and a lower intercept age of 20 ± 0.9 Ma, which suggests that discordance is likely due to lead loss during the Himalayan orogeny (Fig. 5.5). If inheritance is assumed for these metaigneous rocks, the source of these zircons is less likely to come from a cogenetic body such as a granite. A more probable interpretation may be that these igneous bodies derived their inherited zircons from a sediment, such as the Shumar Quartzite itself.

Within the Bhutan HHCS the augen gneiss located above the Kakhtang Thrust yielded monazites and zircons that can be regressed through a chord that produces an upper intercept of 826 ± 0.7 Ma (interpreted as a crystallisation age) and a lower intercept

of ca. 14 Ma (related to lead loss during the Himalayan orogeny). The crystallisation age of ca. 826 Ma is unusual for granitoids within the Himalaya; however this is comparable to the Chor Granitoid (described in Chapter 2) and is within error of the 823 ± 5 Ma U-Pb shrimp zircon ages from that body (Singh et al., 2002).

5.4.5 Summary

The aim of this study of clastic sediments from the lithologies of the Bhutan Himalaya is to test whether the discrimination criteria established from the Sutlej study could be applied further east along the Himalayan mountain belt; the following interpretations can be drawn from this data set:

(i) Whole-rock Sr and Nd isotopes and U-Pb zircon analysis support isotopic studies from the central and western Himalaya and hence show that isotopic mapping can define and discriminate between major Himalayan units and structures from Nanga Parbat to Bhutan.

(ii) The Barsong and Jaishidanda formations of what has been previously mapped as the LHS are isotopically distinct from other units within the LHS and may be correlated with the HHCS, suggesting either that they lie within the MCTZ, or that they represent an out-of-sequence thrust slice comparable with the OLH of the Sutlej region. Of even greater significance is that if these units demarcate the lower plane of the MCT (as does the Karcham Group in the Sutlej), then the MCT is now mapped below the JBF, supporting the interpretation of Jangpangi (1974). Furthermore this also refutes suggestions that the MCTZ represents a zone of tectonic intermingling of the LHS and the HHCS (described in Chapter 1).

(iii) Although a metamorphic break is observed within the HHCS across the Kakhtang Thrust, metasediments from the footwall and hanging wall are isotopically indistinguishable, suggesting that this thrust is intra-formational within the HHCS of Bhutan (Grujic et al., 2002).

(iv) Sr isotope-ratios of bulk rock from the TSS generally lie below a 500 Ma reference line on a $^{87}Sr/^{86}Sr$ Vs $^{87}Rb/^{86}Sr$ plot. Nd isotopes suggest that samples stratigraphically younger than eruption of the Panjal traps may have become contaminated by basaltic material during deposition.

(v) The Chekha Formation is isotopically similar to, and is tentatively correlated with, the Haimanta Group. Erosional products of these rocks at ca. 500 Ma may have been deposited in the TSS basin.

(vi) Zircon populations suggest further mixing of detritus derived from the DSG/ILH and HHCS source areas during deposition of the HHCS. The lack of <1800 Ma zircons within the DSG suggest that detritus from this group did not derive from a HHCS protolith, or simply that this unit was already lithified during the deposition of the HHCS, as suggested by the maximum depositional ages and intercalated igneous rocks.

Further studies are required to characterise other units within the DSG that were not sampled in this study, to investigate the effect of basaltic material contamination on the TSS, to extend the detrital zircon data set within the HHCS and Barsong Formation, and to examine further the relationship between the Chekha Formation and the Haimanta Group.

Chapter 6 – Provenance And Palaeogeography

6.1 Introduction

The application of the whole-rock Sr and Nd isotopic systems and single zircon U-Pb dating have been used to successfully define and discriminate between major Himalayan units and structures. These two independent approaches can also shed light on the various source areas (provenances) of the metasedimentary formations. Combining the Nd and U-Pb isotopic data provides essential constraints on the ages of the terrains from which the sediments were sourced (e.g. Dickin, 2000). If multiple sources are involved, however, these interpretations are less straightforward. Nonetheless important palaeogeographic reconstructions can be inferred from combining bulk-rock data with detrital mineral ages. For example, for a refractory mineral like zircon that is resistant to metamorphism and deformation, the youngest age in a population of detrital grains can constrain the maximum age of deposition (Heaman and Parrish, 1991).

The aim of this chapter is to identify the provenance of clastic sedimentary formations described in Chapters 2 and 4 and to constrain the environments and timing of their deposition using the isotopes presented here (Chapters 3 and 5), in order to attempt a palaeogeographic reconstruction of the major Himalayan units. It will be shown that shifts observed in the isotopic compositions of the analysed Himalayan metasediments are related to contemporaneous tectonic activities that have influenced the sedimentary record, as suggested in Chapter 1.

6.2 Provenance And Deposition

6.2.1 Sutlej

Interpretations from whole-rock data

Figure 3.4 (a combined Sr-Nd isotope plot) shows that LHS metasediments plot within either the HHCS or the ILH field, enabling the LHS to be subdivided into the ILH and the OLH, whereas HHCS samples plot solely within the HHCS field; the Haimanta Group also broadly plots within the HHCS field (to be discussed later). Therefore, these data imply that at least two source areas, with distinctly different Sr and Nd (and U-Pb) isotopic signatures, were actively eroding and their detritus was being deposited into pre-Himalayan basin(s).

Of considerable significance is the observation from the Nd dataset that samples from the HHCS form a much broader array than samples from the ILH (Fig. 3.2 and 3.4). These differences can be explained if it is argued that deposits derived from a single source (that is assumed to be isotopically homogeneous) will define a tighter isotopic array than do deposits derived from multiple sources. It may therefore be reasonable to interpret a mixed provenance for the HHCS field in contrast to a single source for the ILH field. If a mixed provenance is implied for the HHCS, then (using Nd isotopes as an example) the simplest model that explains the existing data is to invoke mixing of two 'end members', one with more negative ε_{Nd} than the HHCS array and the other with more positive ε_{Nd} than the HHCS array. As the relative contributions from these two sources vary through space and time a broad ε_{Nd} array is obtained that lies between these two end members. One possible model to account for the isotopic signatures of most Himalayan metasedimentary formations is that of two distinct source regions; a Palaeoproterozoic – Late Archaean source (PPLA) that provides the provenance of the ILH, and a Neoproterozoic source (NP) that combines with detritus from the PPLA source to provide the provenance of the HHCS.

Figure 3.2 shows that the Haimanta Group is characterised by a wide range of ε_{Nd} (from -18 to -6) with considerable overlap across both the HHCS and ILH fields suggesting a greater contribution from the PPLA source in this group compared to the HHCS. However, the Sr isotopes from the Haimanta Group fall on a similar array to the HHCS field around the 500 Ma reference line (Fig. 3.3). A more detailed examination of the Haimanta Group (summarised in Fig 3.10) reveals a reverse correlation between the depositional age and the Nd model age. For example the older Manjir Formation has Nd model ages between 1600-1900 Ma, whereas the younger Phe Formation has Nd model ages between 2000-2600 Ma (with the exception of one sample that is located close to the Manjir-Phe boundary). The oldest model ages from the Phe Formation, without exception, are from the youngest units and are located above the Precambrian/Cambrian boundary (which is placed between the Upper and Lower Phe Formation). Further analysis of the data shows the rocks from the Upper Phe Formation are characterised by ε_{Nd} values of -13 to -18, whereas the lower Phe and the Manjir formations are characterised by ε_{Nd} between -10 and -7 (Fig. 3.10). Therefore, although some overlap in the Nd model ages exists, there is no overlap with regards to ε_{Nd}.

This systematic change within the Haimanta Group could be explained by a model where a composite terrain containing rock masses with different ε_{Nd} values is being eroded (i.e. two 'end members'). In terms of Sr and Nd isotopes, this terrain consists of material with NP characteristics in the outer or upper parts (i.e. younger material), whereas the core or underlying parts (i.e. older material) contains material with PPLA characteristics. The eroded products are deposited into the Haimanta Group basin. As the terrain begins to erode, a greater proportion of the erosional products deposited in the basin have NP characteristics. Through time, the outer/upper portion of this terrain diminishes and a greater proportion of the erosional products deposited in the basin have PPLA characteristics. The transition between sediments dominated by the NP source and sediments dominated by PPLA source occurs either at or close to the boundary between the lower and upper Phe Formation.

The OLH is isotopically indistinguishable from other lithological units in the HHCS field. Indeed, apart from its geographical location, the OLH shares many similarities with the Haimanta Group (Chapter 2); the significance of this isotopic and stratigraphical similarity will be evaluated during the discussion of the palaeogeography later in this chapter. However, at this point the OLH can be inferred to have a similar provenance history to the Haimanta Group, and according to the above model a stratigraphical age that post-dates ILH deposition, which is consistent with the palaeontological observations (Chapter 2 and Table 2.5).

The deposition of the Haimanta Group ceases at a Cambro-Ordovician unconformity which is correlated with the intrusion of the Kinnaur Kailas Granite (Grasemann et al., 1997; Wiesmayr and Grasemann, 2002; Chapter 2). The Sr isotopes from the Sutlej traverse (Fig. 3.3) show an alignment of the HHCS, OLH and Haimanta Group samples along a 500 Ma reference line implying Sr homogenisation by a thermal event (Ahmad et al., 2000), whereas the ILH data form a rough alignment along an 1800 Ma reference line. The 500 Ma thermal event is coeval with the intrusion of the Kinnaur Kailas Granite (amongst other ca. 500 Ma granites, reviewed in Singh and Jain, 2003), which suggests that the ILH were situated far enough away from the other units not to be perturbed by this ca. 500 Ma thermal event. Post-intrusion sedimentation is represented by the TSS. Due to the Sr and Nd isotopic similarity of the HHCS and Haimanta Group (with the exception of the Upper Phe), it has already been suggested (Chapter 5) that the source of the TSS may be the remnants of uplifted portions of one or both of these groups. Furthermore, there is tentative evidence for Pre-Himalayan metamorphism in the Sutlej Valley (reviewed in section 1.6) which supports this proposed model that the TSS sourced detritus that contains a ca. 500 Ma thermo-metamorphic event.

Thus far, the model developed from the whole-rock Sr and Nd isotope data set explains the provenance of the HHCS and ILH fields. Whereas sediments that lie in

the ILH field were derived from a single source (PPLA), at least two source regions contributed to the deposition of sediments within the HHCS field (PPLA and NP). This is demonstrated by the Haimanta Group where stratigraphically old deposits plot within the HHCS field, and stratigraphically younger deposits show an increase in the flux of detritus from an PPLA source, up until the ca. 500 Ma thermal event.

Interpretations from zircon data

Zircon studies were undertaken on the Vaikrita Group (HHCS), the Jutogh Group, including samples from the Wangtu Augen Gneiss and Jutogh Metasediments (ILH basement) and the Rampur Formation (ILH sediments). Zircon populations (summarised in Figure 3.9 d) from the HHCS of the Sutlej traverse demonstrate that both a Neoproterozoic and a Palaeoproterozoic - Late Archaean population are present, whereas a single Palaeoproterozoic - Late Archaean population is observed from zircons recovered from the ILH metasediments (i.e. the Jutogh Metasediments and the Rampur Formation; as previously discussed, although a significant Late Archaean population is not observed due to the small data set, further analysis are likely to show this component in the population). This confirms the role of PPLA and NP sources inferred from the Nd isotope data.

The Wangtu Augen Gneiss is interpreted to have intruded the Jutogh Metasediments (Chapter 3) ca. 1866 Ma (zircon crystallisation age), leading to what is now considered the Jutogh Group (Chapter 2.4.3 and Table 2.1). ε_{Nd} data from the ILH indicates that the Rampur Formation is isotopically distinct from the Jutogh Metasediments, and shares many characteristics with the Wangtu Augen Gneiss. This interpretation is in agreement with the zircon $^{207}Pb/^{206}Pb$ age populations (Chapter 3), where most detrital zircons from the Rampur Formation have concordant ages of ca. 1868 Ma compared with zircons from the Wangtu Augen Gneiss that yield an upper intercept age of 1866 Ma, which supports the notion of a restricted source for the Rampur Formation (corresponding ε_{Hf} values from zircons from the Wangtu Augen Gneiss and

Rampur Formation are required to confirm this relationship). In contrast, zircons from the Jutogh Metasediments have discordant age populations between 1888 to 2260 Ma.

The available isotopic constraints suggest that the Jutogh Metasediments were intruded by the Wangtu Augen Gneiss (creating the Jutogh Group), which was closely followed by development of a basin and deposition of detritus derived from the Wangtu Augen Gneiss as the Rampur Formation. A rift-related basin/passive margin depositional environment is suggested by whole-rock geochemistry (Fig. 3.1 a-d and Miller et al., 2000). The youngest detrital zircon from the Rampur Formation provides a maximum age of deposition (1864 Ma) whereas intercalated and intrusive metabasalts constrain the minimum age of deposition to 1800 ± 13 Ma (Miller et al., 2000). Therefore the deposition of the Rampur Formation is bracketed to between ca. 1864 and 1800 Ma. The Jutogh Metasediments are constrained to have been deposited before ca. 1866 Ma (prior to the intrusion of the Wangtu Augen Gneiss). Due to the tightly constrained age population within the Rampur Formation (1864 to 1870 and 1950 Ma), a major source for the Rampur Formation zircons is likely to be granitic body with a zircon crystallisation age between 1864 and 1800 Ma (a body similar to the Wangtu Augen Gneiss), a potential source for the Jutogh Metasediments is yet to be identified (but see below). However, the source material for the Jutogh Group is constrained by ε_{Nd} values between -19 to -17, with detrital zircon ages older than 1866 Ma, and (discordant) $^{207}Pb/^{206}Pb$ age populations between 1888 to 2260 Ma.

According to the proposed dual-provenance model, sediments from the HHCS, OLH and Haimanta Group are assumed to have been derived from varying proportions of detrital fluxes with PPLA and with NP characteristics. This model agrees with the detrital zircon populations observed in the Vaikrita Group (HHCS). Considering the distribution of $^{207}Pb/^{206}Pb$ ages, the source for the Palaeoproterozoic - Late Archaean population in the HHCS may be the same as that of the Jutogh Metasediments (Fig. 3.5 a and b and Fig. 3.6, respectively). A maximum age of deposition of the HHCS is constrained by the age of the youngest zircon from the Neoproterozoic population at

830 Ma. Further research into these populations might enable interpretations that include multiple Pb loss events suffered by the older population related to the crystallisation event of the younger population in the source area; this would agree with the proposed model that suggests material of NP characteristics was eroded from a terrain with PPLA characteristics after deposition of the Rampur Formation and prior to deposition of the HHCS, OLH and Haimanta Group. Thus, as this terrain was being eroded and deposited in the HHCS basin (ca. 830 Ma), both material with PPLA and NP characteristics were being sourced by either directly eroding terrain or recycling the material in the sedimentary system. The significantly larger Neoproterozoic population suggests that the younger contributing source is dominant.

In summary (Fig. 6.3 Part I and Section 6.4 Stages 1 to 6), the zircon and whole-rock Nd-Sr data support each other in identifying key events in the source areas of Himalayan sediments. These data support a model that suggests that the HHCS and the ILH were derived from the same eroding region (the PPLA terrain with Palaeoproterozoic - Late Archaean zircons and ε_{Nd} more negative than -19, Fig. 6.3 Part I, Stage 1). However, the HHCS was also partly derived from a second, younger terrain (NP) contributing Neoproterozoic zircons, and ε_{Nd} values less negative than -13 (Fig. 6.3 Part I, Stage 3). This model accounts for the two populations of zircon ages, and the less negative, and broader range of ε_{Nd} values in the HHCS compared to the ILH. The Nd whole-rock data show only the average model ages from the two sources contributing to the HHCS. Within the Haimanta Group, the Upper Phe Formation is unique in that it was deposited in the HHCS basin and was sourced dominantly from the older PPLA source terrain during a period when the flux of detritus from the younger NP source region was reduced (Fig. 6.3 Part I, Stage 4).

6.2.2 Bhutan

Interpretations from whole rock data

The combined Sr-Nd plot of Bhutan metasediments (Fig. 5.4) shows similarities with the Sutlej data set; the HHCS (both above and below the Kakhtang Thrust), Chekha Formation and the TSS lie within the previously defined HHCS field and the LHS has components that have characteristics of the ILH and HHCS fields. However, as discussed in Chapter 5, the terms ILH and OLH are inappropriate due to the spatial distribution of these samples. Instead the term JBF (Jaishidanda and Barsong Formations) is used to describe samples with OLH isotope characteristics as defined in the western Himalaya, whereas the term DSG is used to describe samples with ILH characteristics. As with the ILH of the Sutlej transect, the DSG of Bhutan is constrained in a narrow ε_{Nd} array (Fig. 5.2), whereas samples in the HHCS, JBF and the TSS of Bhutan form a much broader ε_{Nd} array (although this array is two ε_{Nd} units narrower than the comparable dataset from the Sutlej transect). For the Sutlej data (Fig. 3.2), the separation between the two groups is of the order of one ε_{Nd} unit, whereas for the Bhutan data the separation between the HHCS and DSG groups (Fig. 5.2) is of the order of six ε_{Nd} units. However, this may reflect a smaller data set compared to the Sutlej transect.

To enable comparisons with the two data sets, the proposed model so far suggests that the Rampur Formation is sourced almost exclusively from a single province (the Wangtu Augen Gneiss), whereas the Jutogh Metasediments are sourced from an older, unspecified source area (evidenced by the Palaeoproterozoic - Late Archaean zircon population). Following the ca. 850 Ma event associated with magmatic intrusions such as the Chor Granitoid (that may have led to formation of the NP source), the source of the Jutogh Metasediments (PPLA) contributed a small amount of material to the HHCS basin, whereas the larger component contributing to the HHCS basin consisted of younger material that was likely to have been formed by the ca. 850 Ma event (NP). However, within Bhutan, the ε_{Nd} data suggests that there was a smaller contribution

into the HHCS basin from the older PPLA source (characterised by the Palaeoproterozoic - Late Archaean zircon population). Furthermore, the ILH ε_{Nd} array is less negative than the DSG ε_{Nd} array, suggesting a different provenance. For the reasons discussed in Chapter 1, homogenisation of the Sr isotopes is attributed to thermal resetting events; the ILH samples plot around an 1800 Ma reference line (Fig. 3.3), whereas the DSG plot around a 1000 Ma reference line (Fig. 5.3), which may be interpreted as thermal resetting events in the respective source areas, or a spatial relationship due to proximity of the thermal events. However, it must be made clear these are minor differences in source regions, and the general model developed so far is consistent with the general isotopic relations from both the western and the eastern Himalaya. It is likely that a Palaeoproterozoic - Late Archaean terrain will have been constructed from a number of smaller terrains, as demonstrated in the Canadian Shield (Dickin, 2000).

The Chekha Formation, which is assigned to the TSS in Bhutan, shares many similarities with the Haimanta Group (Chapter 5). However, the Chekha Formation does not display the large variations in ε_{Nd} that has been invoked as evidence for mixing between the dual source regions; one interpretation may be that uplift in the eastern portion of the pre-Himalayan basin due to granitic intrusion was less Stoecklin, (1980) observes no Cambro-Ordovician unconformity in Nepal or that variations in the thickness of the eroding younger NP source resulted in contrasts along strike in the Himalaya. In the Sutlej transect this source may have been somewhat thinner, and therefore resulted in the upper Phe Formation being derived from the older and underlying PPLA material. Conversely, in the eastern Himalaya (Bhutan), the terrain may have been thicker resulting in the erosion and deposition of mainly NP material. However, a complete stratigraphical section from the Tang Chu basin would be required to confirm this interpretation; logistical restraints prevented this study from sampling this section (Chapter 4).

The TSS (Fig. 5.2 to 5.4) is isotopically indistinguishable from other samples that plot within the HHCS field. It has already been suggested that a tectonic event coincident with ca. 500 Ma intrusions in the Sutlej Area produced uplift and the Cambro-Ordovician unconformity between the underlying Haimanta Group and the TSS (Grasemann et al., 1997; Wiesmayr and Grasemann, 2002; discussed in Chapters 2 and 3). Prior to deposition of the Upper Phe Formation, the Haimanta Group shares isotope characteristics with the HHCS field. It has been suggested that the Upper Phe Formation may represent a time when the PPLA source area dominated the clastic flux in the Haimanta basin. Therefore, with this apparent bias towards the PPLA source, the younger sediments, as represented by the TSS, should appear to be dominated by a source region with isotopic characteristics of the PPLA source; however, this is not observed, as the TSS has similar isotopic characteristics to the HHCS field, suggesting that the TSS may represent a recycled component of the HHCS: it is therefore possible that the uplifted portion of the Haimanta Group (and possibly the HHCS itself) has been eroded and deposited to form the younger TSS. The Sr isotope plot supports this interpretation in generating an array around the ca. 500 Ma reference line (Fig. 5.3), despite being obtained from sediments deposited during the Mesozoic, suggesting further still that the TSS is a recycled component of the HHCS. Although many of the Nd data points from the same samples plot within the HHCS array, a number of late-Palaeozoic/Mesozoic samples have been shown (Chapter 5) to plot with ε_{Nd} values more positive than -3. Ahmad et al. (2000) attributed some of these perturbed isotope values to high carbonate contents, but it was suggested in Chapter 5 that such values may be caused by basaltic contamination from sources such as the Panjal Traps (ca. 258-275 Ma) (Noble et al., 2001) and Mesozoic arc formations (Aitchison et al., 2000; McDermid et al., 2002) as observed by Garzanti (1999 and references therein). Prior to these magmatic events, ε_{Nd} for the TSS is unperturbed, and samples plot within the HHCS array. Therefore, as well as being derived partly from a NP source region, some younger TSS samples can be interpreted as also having a basaltic input. However, Fig. 5.2 to 5.4 demonstrates that the basaltic

detritus did not dominate the TSS basin since some stratigraphically young (Mesozoic) samples remain unperturbed and plot within the defined HHCS field (Fig. 5.4).

The JBF lies within the HHCS field (Fig. 5.4) so it is tentatively correlated with the OLH and is therefore interpreted to have a similar provenance. However, unlike the OLH, the Barsong Formation is assigned a Mesozoic stratigraphical age (Gansser, 1983) whereas within the OLH the youngest sediments are Upper Cambrian (Chapter 2). Therefore, despite its geographical location, the Barsong Formation has stratigraphical and isotopic characteristics similar to the TSS. The Barsong Formation may represent a slice of the TSS, imbricated during movement on the MCT. However, this interpretation is unlikely to apply to the Jaishidanda Formation since it is a more persistent unit that overlies the Daling-Shumar Group in the MCTZ across much of Bhutan and it is also metamorphically distinct from the Barsong Formation (mylonitic garnet-mica schist; Dasgupta, 1995); indeed the Jaishidanda Formation shares many characteristics with the Karcham Group (Chapters 2 and 3).

Interpretations from the zircon data

Detrital zircon populations from the HHCS (Fig. 5.10) can be distinguished from detrital zircon populations from the DSG (Fig. 5.7) by the presence of zircons with $^{207}Pb/^{206}Pb$ ages younger than 1800 Ma, whereas zircons analysed from the DSG samples contain a significant Palaeoproterozoic-Late Archaean population.

Zircon ages from the Rampur Formation (Sutlej section) support the interpretation that this formation has a Wangtu Augen Gneiss provenance. However, in the Bhutan data set, the zircon populations are discordant and have large $^{207}Pb/^{206}Pb$ age ranges within the Daling-Shumar Group, probably reflecting multiple provenances in the quartzite and inheritance in the metarhyolite and augen gneiss (Fig. 5.5 and 5.6 respectively). The quartzite, located stratigraphically below the metarhyolite, contains two populations; an older, smaller population between 2449 to 2545 Ma, which suggests a provenance similar to the Jutogh Metasediments (PPLA), and a younger,

larger population between 1854 to 2071 Ma, which constrains the maximum deposition age to 1854 Ma, compared to 1864 Ma in the Rampur Formation. This maximum deposition age is older than the youngest zircons in the augen gneiss and the metarhyolite (1715 and 1788 Ma, respectively), suggesting that these metaigneous rocks post-date quartzite deposition, especially since no zircons of 1715 to 1788 Ma age are found in the quartzite. This agrees both with the stratigraphical observations and with the interpretation that zircons from these rocks contain inheritance. Therefore two sources are suggested; an older, less significant source (similar to the source for the Jutogh Metasediments) and a younger, dominant source containing zircon populations between ca. 1854 to 2071 Ma. This broadly agrees with the suggestion that the older eroding craton is comprised of a number of distinct terrains, as inferred from the ε_{Nd} DSG array (Fig. 5.2).

The Neoproterozoic HHCS zircon population from the Bhutan dataset is also consistent with the model proposed for the Sutlej section. However, one apparent inconsistency between the two sections is that the Palaeoproterozoic - Late Archaean zircon population is not observed in the HHCS from Bhutan, although this may reflect the relatively small data set. However, the ε_{Nd} array suggests a much smaller input of (older) material into the HHCS basin of the eastern Himalaya, compared to the Sutlej, possibly due to a thicker, younger terrain in Bhutan.

The quartzite from the Barsong Formation is constrained to a maximum depositional age of 1371 Ma. Zircons from this formation have low discordancy and $^{207}Pb/^{206}Pb$ ages range from 1371 to 2557 Ma. However, the distribution of zircon ages with the HHCS metaquartzite from below the Kakhtang Thrust suggests a bias towards the older components in the population (Fig. 5.10). A total of only 9 fractions were analysed from this sample and it is therefore possible that if more fractions were analysed a younger component would be found. Indeed, it may be significant that a maximum depositional age of 1371 Ma is obtained from a unit that has been assigned a Mesozoic stratigraphical age, which appears anomalous compared to other TSS

zircon populations (e.g. DeCelles et al., 2000; Fig. 1.5). This quartzite therefore may belong to the Jaishidanda Formation, placing the correct geological boundary between Jaishidanda Formation and the Barsong Formation above this quartzite, not below it. Alternatively, (as discussed in 5.4.2) the anomalous Mesozoic age of the palynomorph study may be due to laboratory contamination, this age has not been independently verified by any other palaeontological study, or a repeat analysis. Therefore, on the basis of isotopic mapping, the Barsong Formation could be considered the same as the Jaishidanda Formation.

6.3 - Potential Source Regions

Table 6.1 summaries the interpretations made so far for the source regions of the Himalayan lithologies investigated in this study. The Rampur Formation may be unique in that the characteristics of its source region can be correlated with an exposed lithology in the section, namely the Wangtu Augen Gneiss, although further work is required to confirm this. The two main source regions remain unidentified. Firstly, the Neoproterozoic population (derived from the NP source) which contributes to the HHCS and, secondly the Palaeoproterozoic - Late Archaean population (derived from the PPLA source) which contributes to both the HHCS and the ILH and probably is also the source of detritus to the Daling-Shumar Group and the Jutogh Metasediments. Both the PPLA and NP sources are interpreted to contribute varying amounts of material to the OLH and Haimanta Group, but are at present isotopically indistinguishable; these units will be separated accordingly later.

Table 6.1 - Summary of ages and provenance characteristics from studied Himalayan sections.

	Tectonic Unit	Group / Formation	Deposition age	Provenance characteristics	Provenance located?
Sutlej	ILH	Jutogh Metasediments	<2012 Ma[d]	PPLA:2012-2260 Ma[z] ε_{Nd} = -19 to -17	Unknown[1]
	ILH	Wangtu Augen Gneiss	1866 Ma[c]	1866 Ma ε_{Nd} = -19	N/A
	ILH	Rampur Formation	1864-1800 Ma[d]	1864-1859 Ma[z] (1948 Ma) ε_{Nd} = -19 to -18	Wangtu Augen Gneiss
	HHCS	Vaikrita Group metasediments	<840 Ma	PPLA: 2085-2574 Ma[z] ε_{Nd} = -19 to -17	Unknown[1]
				NP: 830-897 Ma[z] εNd = <-11	Unknown
	OLH	Chail, Shimla and Krol Groups	<840 Ma and after HHCS depostion	ε_{Nd} = -19 to -17	Unknown
Bhutan	DSG	Daling-Shumar Group - Quartzite	1755-1854 Ma[d]	1854-2449 Ma[z] ε_{Nd} = -22 to -20	Unknown[1]
	DSG	Daling-Shumar Group - Metaigneous	1755 Ma[c]	1755 Ma[c]	Inheritance from DSG Quartzite?
	JBF	Jaishidanda and Barsong Formations	<1371 Ma[d]	1371-2557 Ma ε_{Nd} = -7 to -14	Unknown[1]
	HHCS	HHCS metasediments	<987 Ma[d]	NP: 987-1824 Ma ε_{Nd} = -7 to -12	Unknown
	TSS	Sanctuary Formation	< HHCS deposition	εNd = <-12	Unknown

Key: PPLA, Palaeoproterozoic - Late Archaean population, NP, Neoproterozoic population; [d], depositional age (implies max. depositional age); [c], crystallisation age; [z], zircon age spectra; [1], same provenance.

The Neoproterozoic Provenance (NP)

When comparing the Neoproterozoic zircon population in the Bhutan and Sutlej HHCS Himalaya, there appears to be a number of discrepancies related to the zircon age populations. In particular, large age ranges in the Bhutan HHCS are present (978-1824 Ma; suggesting the existence of a Mesoproterozoic source), compared to the Sutlej HHCS where detrital populations yield two $^{206}Pb/^{207}Pb$ age populations of 811-1127 and 2084–2572 Ma. These discrepancies may relate to inhomogeneity in the source area or more likely the result of small sample sizes; Parrish and Hodges,

(1996) and DeCelles et al., (2000) published age populations based on 7 and 27 zircon fractions respectively (Fig. 1.5) that generated age populations which are similar to those derived from the Sutlej and Bhutan HHCS samples in this study (summarised in Fig. 3.9 d and Figs 5.5 to 5.10). However, Myrow et al. (2003) studied metasediments with HHCS isotopic characteristics and demonstrated that 134 zircon ages formed a broad population from ca. 600 to 2600 Ma (Fig. 6.1), with a small Middle to Early Archaean population (3000 to 3500 Ma). This age distribution illustrates that a small number of zircon analyses may only identify ages that dominate the population, thus explaining the apparent difference in age populations between the Bhutan and Sutlej data sets.

In order to identify possible sources for the main sedimentary lithologies discussed in this study, it is necessary to review potential Precambrian exposures of India (Fig. 6.2). The Eastern Ghats mobile belt lies to the south-east of India between Kolkata and Maharashtra. The craton consists of largely high-grade igneous and metamorphic rocks (Naqvi and Rogers, 1987). Recent investigations suggest that this craton consists of a series of terrains with different U-Pb and Sm-Nd ratios. However, Shaw et al., (1997) have noted four age clusters, ca. 1450, 1000, 800 and 550 Ma (based on U-Pb SHRIMP investigations); the ca. 800 and 500 Ma events are interpreted as metamorphic events, whereas the ca. 1450 and 1000 Ma events are interpreted as magmatic events. Rickers et al., (2001) observed values of ε_{Nd} less negative than -5 for this craton. These data suggest that this craton is a potential Neoproterozoic (NP) source. Indeed, Ar-Ar data support a thermal resetting event in this craton at ca. 500 Ma (Mezger and Cosca, 1999), which supports the observations from the Sr isotope data (Fig. 3.3 and 5.3). The Eastern Ghats is described as a mobile belt that is thrust over an Archaean craton along its margins (Naqvi and Rogers, 1987) consistent with the proposed model that requires the Neoproterozoic source region to overlie the Palaeoproterozoic - Late Archaean source region.

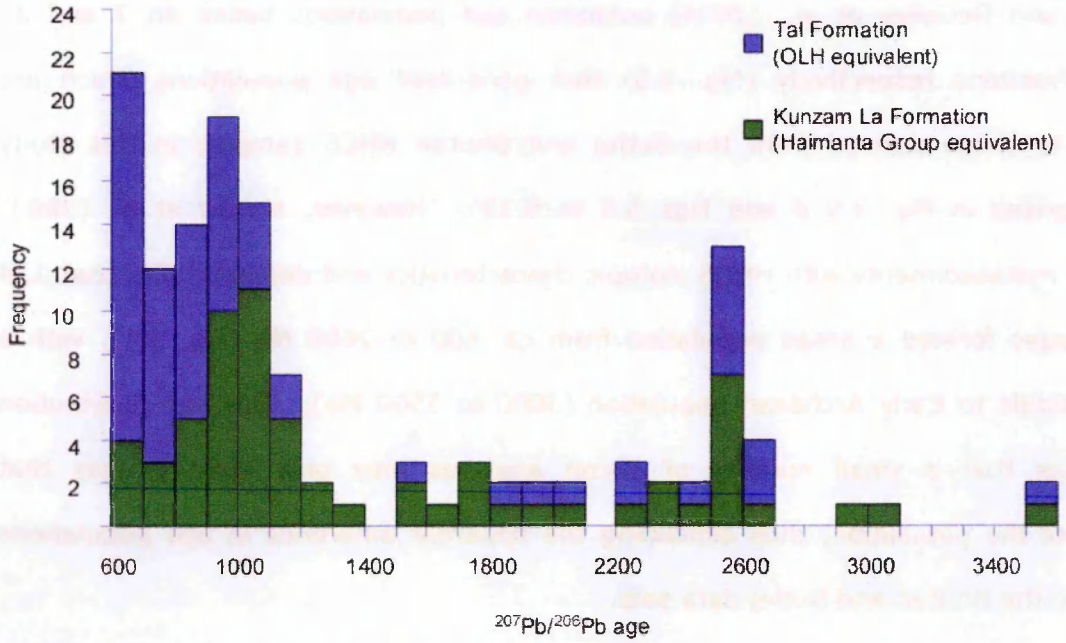

Figure 6.1 - Histogram of $^{206}Pb/^{207}Pb$ ages from Myrow et al. (2003).

The Palaeoproterozoic - Late Archaean Provenance (PPLA)

A number of terrains and granites in the Indian foreland have recently been dated and tentative correlations can be made regarding potential source areas of Palaeoproterozoic – Late Archaean age for the Himalayan sediments. The Bundelkhand Massif lies within the Aravalli craton in the north-west of India (Naqvi and Rogers, 1987, see fig 6.2); zircon ages range from 1900-3200 Ma, with a large population at 2500 Ma (Deb et al., 2001; Mondal et al., 2002; Pandit et al., 2003, amongst others). Nd model ages from Bundelkhand Massif granites (2500 Ma; Gopalan et al., 1990) support the inference that this craton is a potential Palaeoproterozoic - Late Archaean source area. However, since other lithologies from the Aravalli craton provide zircons age ranging from 800 to 3300 Ma (Wiedenbeck et al., 1996), it is unlikely this craton was the Palaeoproterozoic - Late Archaean provenance as this source is defined as containing no zircons younger than 1800 Ma (Table 6.1). However, the proposed model implies that at ca. 850 Ma the NP and PPLA source areas were juxtaposed (as suggested by the variations in the Haimanta Group), therefore the Aravalli craton may be equivalent to this terrain.

The large age ranges found in zircon populations extracted from units from the Eastern Ghats mobile belt and Bundelkhand Massif indicate that these regions would not provide homogenous protoliths during their erosion; indeed they may be amalgamations of a series of smaller belts and cratons, as observed by Dickin (2000). To account for the isotopic variations such as in the Haimanta Group, the proposed model (above) takes inhomogeneity within the source areas into account.

Himalayan Granitoids

Within the Himalaya there are a number of granitoids that correspond to the zircon ages found in detrital grains from the metasediments. For example, this study has shown that the Wangtu Augen Gneiss is a likely source for the Rampur Formation. A potential source for the 800 Ma zircons observed in the HHCS metasediments could be Neoproterozoic granites such as the Chor Granitoid, dated at 823 ± 5 Ma (Singh et al., 2002), which is within error of the 826 ± 0.7 Ma crystallisation age for the HHCS augen gneiss in Bhutan (Chapter 5). However, such potential sources could not explain the large age ranges of detrital zircons in these metasediments, suggesting that a larger cratonic region is a more likely source. Although good evidence is presented for the 500 Ma event overprinting the Neoproterozoic source region, this event could be attributed to the same thermo-orogenic event that led to a number of ca. 500 Ma granite intrusions observed within the HHCS throughout the Himalaya (Singh and Jain, 2003 and references therein).

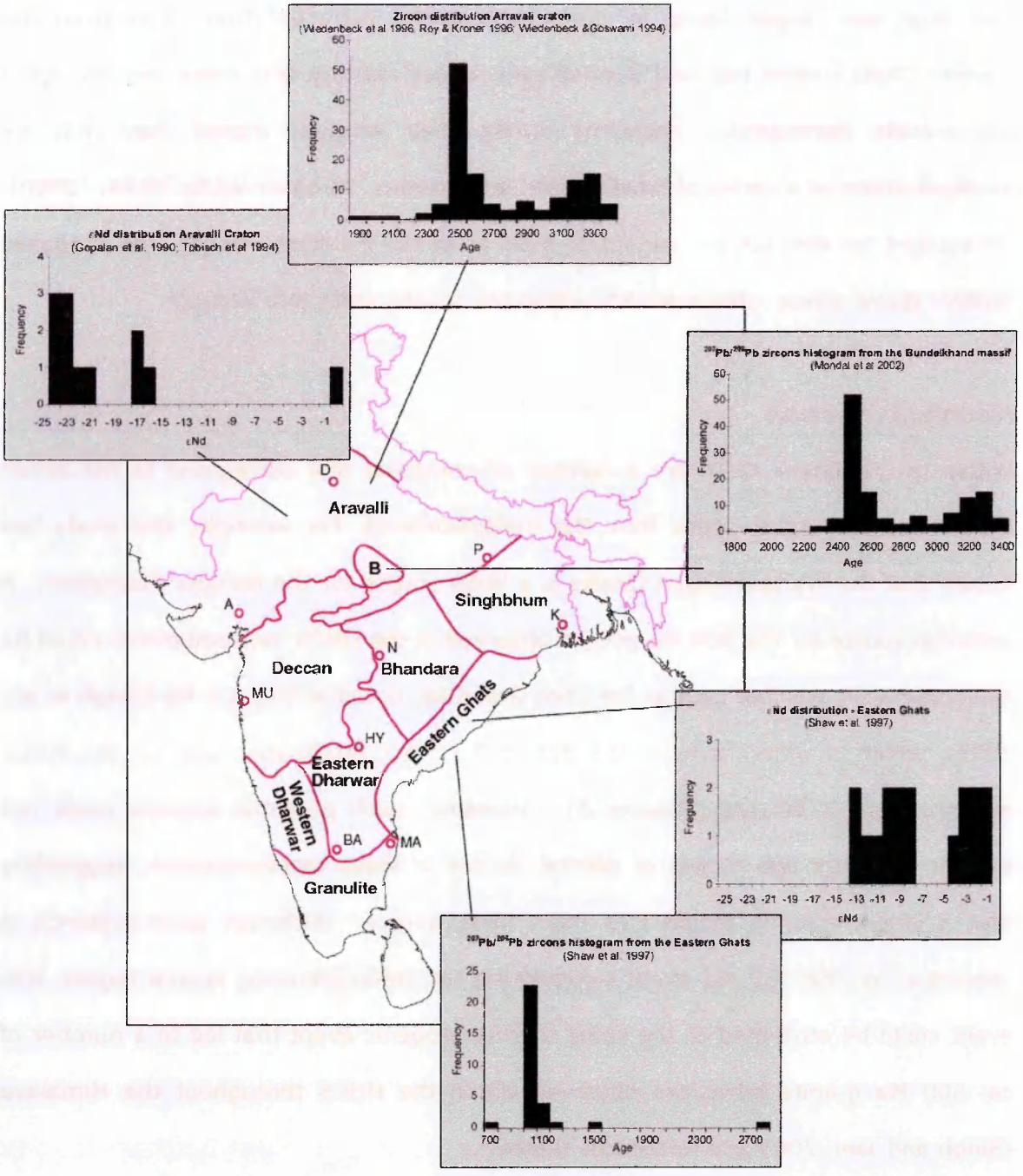

Figure 6.2 - Selected cratons and subdivisions of India; B, Bundelkhand Massif. Locations include; D, Delhi; P, Patna; A, Ahmedabad; K,Kolkata; N, Nagpur; MU, Mumbai, HY, Hyderabad; MA, Madras; BA, Bangalore. (adapted from Naqvi and Rogers, 1987; India image courtesy of J. Taylor).

6.4 Palaeogeography (Fig. 6.3)

Combining the data and field observations described within the previous four chapters, and building on the models proposed earlier in this chapter, a palaeogeographic reconstruction of the principal Himalayan formations and the depositional

environments of the component clastic sediments is outlined below. The following description is illustrated by Figure 6.3 part I and II, and is described in an evolutional sequence, beginning with the formation of the Palaeoproterozoic - Late Archaean source region, and ending with the formation of the Himalaya in their present configuration:

Figure 6.3 Part I:

Stage 1 - Archaean-Proterozoic craton (PPLA) intruded at 1800 Ma

An Archaean-Proterozoic craton (such as, perhaps, the Bundelkhand Massif), is characterised by zircon populations between 1.8-3.5 Ga and $\varepsilon_{Nd\ (t=500\ Ma)}$ of more negative than -21.

Stage 2 – Development of and deposition of Rampur Formation and Jutogh Metasediments within ILH basin(s).

Thermal events during stage 1 lead to basin formation either by failed rifts within the craton or a marginal rift that did not form the final sea floor spreading, leading to the development of a passive margin/rift basin and sedimentary deposition (Miller et al., 2000). Whole-rock geochemistry indicates that the Rampur Formation and Daling-Shumar Group sediments may be examples of rift-related basin (or passive margin deposits) (Chapters 3 and 5; Miller et al., 2000). The Rampur Formation is derived mainly from erosion of granitic material emplaced during Stage 1, as is indicated by the dominance of zircons of similar age (ca. 1866 Ma) and by corresponding ε_{Nd} values in the bulk rocks. The youngest concordant $^{206}Pb/^{207}Pb$ age of 1864 Ma constrains a maximum depositional age, whereas basalt intrusion at ca 1800 Ma constrains the minimum age of deposition (Miller et al., 2000). The Jutogh Metasediments may also have been deposited about this time; the broader range in zircon ages and psammites and pelites in this unit suggest a more distal depositional environment and less restricted source.

The large and discordant zircon age populations and ε_{Nd} values from the Daling-Shumar Group suggest a more cratonic source, such as the Bundelkhand Massif. Its deposition is bracketed by the youngest detrital zircon age (1854 Ma) and the age of the overlying (meta)rhyolite (1755 Ma). Discordance of zircons within the (meta)rhyolite and biotite augen gneiss reflect inheritance.

Stage 3 – Deposition of HHCS sediment

The available isotopic evidence requires a contributing source for the HHCS that contains units characterised by zircons younger than 1800 Ma and bulk-rock values less negative than ε_{Nd} -10 (i.e. younger, Neoproterozoic Nd model ages; shown in Fig. 6.2 as a series of units that are juxtaposed on top of the gneisses). A potential source is provided by a mobile belt such as the Eastern Ghats that is juxtaposed with the source similar to the Bundelkhand Massif that is now not exposed, possibly by strike-slip tectonics, prior to deposition of the HHCS sediment, at ca. 850 Ma (early Pan-African?). Once uplifted, erosion of such a belt, in conjunction with a relatively minor sedimentary flux from older cratonic material would result in deposition in the HHCS basin of detritus of appropriate isotopic characteristics. The conclusion that the HHCS is derived from a larger proportion of the younger (NP) rather than older (PPLA) cratonic material is demonstrated by the bias towards a younger ca. 800-900 Ma zircon population in the Sutlej HHCS, and within the Bhutan HHCS the younger material is even more dominant. However, due probably to inhomogeneity in the younger source, its contribution to the Bhutan HHCS is less biased towards a ca. 800-900 Ma population, although all zircons are younger than 1800 Ma. Indeed the dominance of younger cratonic input within the Bhutan HHCS explains the less negative ε_{Nd} array and larger separation in ε_{Nd} values from the DSG. Ergo, the HHCS is derived from mixed sources.

Stage 4 – Deposition of the Haimanta Group / Outer Lesser Himalaya

The OLH formations and Haimanta Group are generally isotopically indistinguishable. It is only during the Himalaya orogeny that these units experienced differing

geological histories. Their depositional regime and source material are similar to the HHCS, being characterised by ε_{Nd} between -15 and -8; zircon populations from these two units also suggest the same provenance (Myrow et al., 2003; Fig. 6.1). However, as the younger material (e.g. Eastern Ghats mobile belt) becomes more eroded, more of the older cratonic material is exposed and contributes detritus to the sedimentary basin. This is observed within the Haimanta Group as progressively younger units are increasingly dominated by the older source (Fig. 3.10), as is observed in the upper Phe Formation with excursions towards a PPLA source. Deposition of the OLH and Haimanta Group post-date the HHCS, as indicated by maximum depositional ages of 525 and 830 Ma respectively, together with Cambrian fossils from the OLH (Chapter 2; Table 2.5). Indeed the presence of suspected Marinoan diamictites may also suggest similarities between the OLH and Haimanta Group (Chapter 2).

Stage 5 – Ca. 500 Ma (late Pan African) deformation, granitic intrusion uplifting, folding and eroding the Haimanta Group / Outer Lesser Himalaya

The deposition of the Haimanta Group / OLH appears to continue up to a Cambro-Ordovician unconformity (ca. 500 Ma, late Pan African), which is coincidental with a number of ca. 500 Ma intrusions (Singh and Jain, 2003 and references therein) including the Kinnaur Kailas granite 459 ± 7.7 Ma (Chawla et al., 2000). The episode that includes intrusion of ca 500 Ma granites is interpreted by Grasemann et al. (1997) and Wiesmayr and Grasemann (2002) to be instrumental in the uplift and deformation of the Haimanta Group, leading ultimately to the unconformity that separates the Haimanta Group from the undeformed overlying TSS. The ca. 500 Ma tectono-thermal event impacts significantly on the Sr isotope ratios of some bulk-rocks. Whereas older formations from the Sutlej area (including the Rampur Formation) are not perturbed, the Sr systematics of equivalent units in Bhutan suggest partial resetting. However, the HHCS and Haimanta Group / OLH show complete resetting of the Sr isotope ratios thus constraining the spatial distribution of this event, which may have resulted from metamorphism (as suggested by ca. 420 Ma

monazites in the cores of garnets; Caddick, 2004 and Argles et al., 1999; Marquer et al., 2000) that was later overprinted in high-grade rocks (pers. com., M. Caddick).

Stage 6 – Deposition of the TSS

The Uppermost Haimanta Group suggests a shift in provenance with an increased flux from older cratonic material (i.e. increase erosion of the PPLA source). However, data from the TSS suggest that the younger NP source (the Eastern Ghats mobile belt for example) dominates the sedimentary flux into the TSS basin, suggesting that the uplifted portion of the Haimanta Group could have provided the source material for the TSS. This depositional regime explains how stratigraphically younger sediments form an array along a 500 Ma reference line on Sr isotope plots (Fig. 5.3). Deposition of the TSS continues until late Cretaceous; sediments stratigraphically younger than early Permian frequently show mafic (basaltic) contamination (Garzanti, 1999 and reference therein) and in their elevated ε_{Nd} characteristics, possibly related to post-Panjal traps magmatism (ca. 258-275 Ma; Noble et al., 2001) or Mesozoic arc formations (Aitchison et al., 2000; McDermid et al., 2002). Therefore, the TSS is isotopically characterised by ε_{Nd} between -15 and -8, with excursions towards less negative values, with Sr isotopes plotting on or below a 500 Ma reference line; detrital zircons from the TSS contain both Neoproterozoic and Palaeoproterozoic - Late Archaean age populations similar to populations from the HHCS (DeCelles et al., 2000). Two-stage rifting from Gondwana ca. 180 and 130 Ma (Hawkesworth et al., 1999 and references therein) (i.e. between cratonic India and Africa), ultimately leads to the closure of the Tethyan Ocean and the Himalayan orogeny.

Figure 6.3 Part I

south north

Stage 1 - Archaean-Proterozoic craton (PPLA) intruded at 1800 Ma
- deposition of ILH sediment, 1800 Ma zircons constrains upper limit for the depositional age

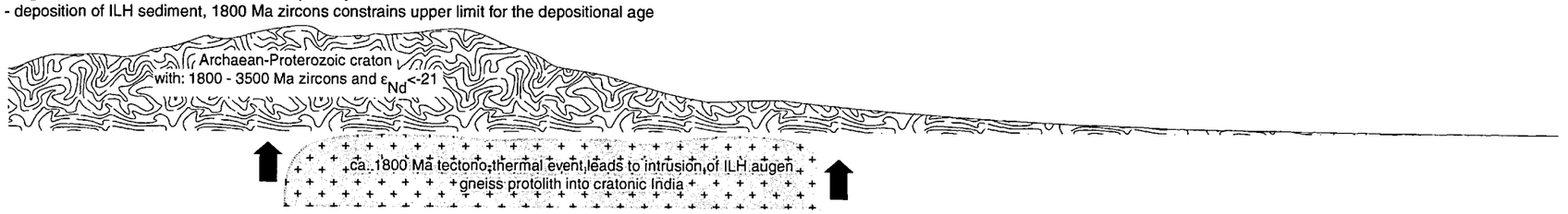

Stage 2 - Development of and deposition of Rampur Formation and Jutogh Metasediments within ILH basin(s).
- deposition of ILH sediment, 1800 Ma zircons constrains upper limit for the depositional age

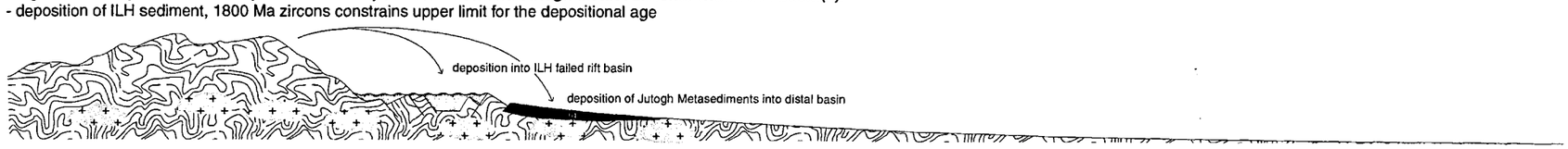

Stage 3 - Deposition of HHCS sediment
- Neoproterozoic material is emplaced over the Archaean-Palaeozoic craton
- deposition of HHCS sediment (protolith); sourced mainly from the Neoproterozoic, but also from the craton, ca. 800 Ma zircons constrains upper limit for the depositional age

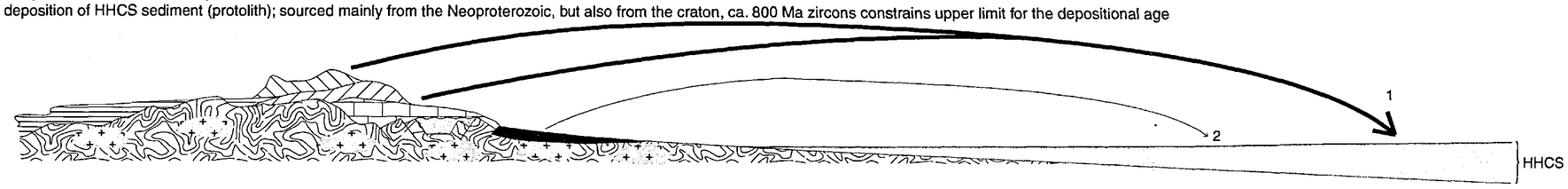

Stage 4 - Deposition of the Haimanta Group / Outer Lesser Himalaya
- deposition of the Haimanta Group, more Archaean-Proterozoic Craton is eroded and deposited in Haimanta basin, resulting in older model ages for younger sediments

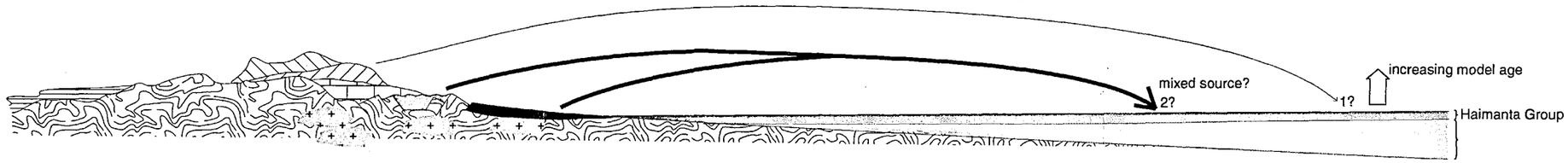

Stage 5 - Ca. 500 Ma (late Pan African) intrusion
- ca. 500 Ma (late Pan African?) deformation, granitic intrusion uplifting and folding the Haimanta Group / Outer Lesser Himalaya

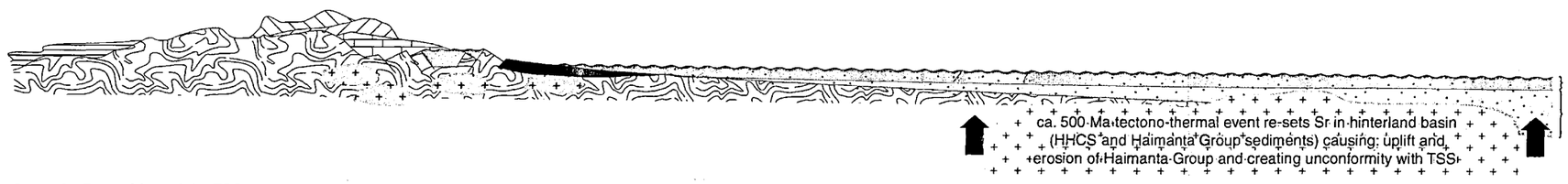

Stage 6 - Deposition of the TSS
- uplift of Haimanta Group results in unconformity with undeformed TSS deposits

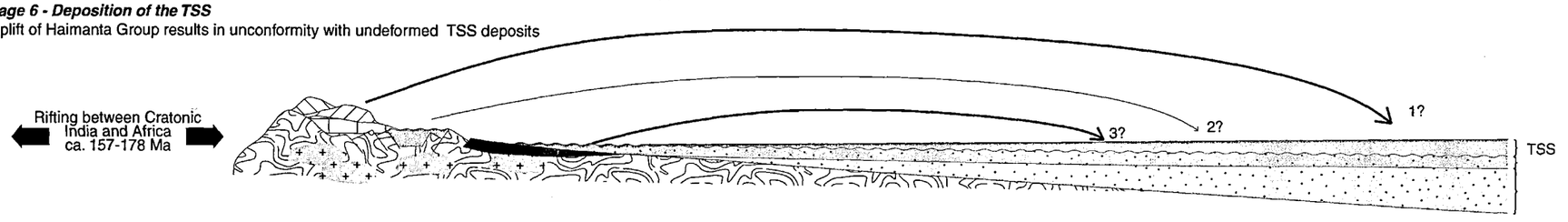

Figure 6.3 Part II:

The subsequent stages are concerned with the tectonic evolution of the Himalayan orogeny:

Stage 7 - Initial thrusting along proto STDS

Estimates for the closure of the Tethys Ocean and beginning of the Himalayan orogenic event range from 65–45 Ma (Beck et al., 1995; Dewey et al., 1988; Rowley, 1996). Sedimentary clastic components in the Subathu Formation (latest Palaeocene to middle Eocene, Sub-Himalaya; Chapter 2) are interpreted as TSS lithic fragments (Najman and Garzanti, 2000) suggesting that TSS sedimentation in the HHCS basin was terminated prior to latest Palaeocene. Compression is accommodated by south-directed thrusting along a proto STDS, with a décollement that exploits the boundary between the Haimanta Group/OLH (hanging wall) and the HHCS (footwall). Southwards thrusting juxtaposes the Haimanta Group/OLH against cratonic Indian type basement material, if this was not already a stratigraphic sedimentary contact.

Stage 8 Duplex formation

South-directed thrusting is accommodated by the formation of a series of thrust stacks/sheets within the ILH creating a duplex that emplaced basement material on top of low-grade ILH sediments (Rampur Formation). In Bhutan, thrusting within the DSG is accommodated by the generation of a series of thrust sheets; basement material *sensu stricto* is not involved.

Stage 8a - Initial thrusting along proto-MCT

Major Himalayan compression during the mid-Miocene is accommodated through the propagation of the MCT and further thickening and folding of the HHCS. The MCT juxtaposes HHCS material against ILH basement material. Syn-tectonic thrusting along the MCT is accommodated by detachment along the STDS resulting in southwards extrusion of the HHCS, as has been modelled from channel flow

(Beaumont et al., 2001; Beaumont et al., 2004; Jamieson et al., 2004); monazite growth ca. 24 Ma within the Vaikrita Group provides constraints on the extrusion of this wedge (Caddick, 2004). Increased metamorphic clastic fragments in the Kasauli Formation (early Miocene, Sub-Himalaya; Chapter 2) are interpreted as reflecting exhumation along the MCT (Najman and Garzanti, 2000). Progressive down thrusting within the MCTZ (Vannay and Grasemann, 1998) may account for isotopic anomalies, as seen for example, in the Barsong Formation.

Stage 8b - Duplex formation along proto-MCT

Rheological contrasts between para and ortho-gneisses (e.g. Jutogh Metasediments and Wangtu Augen Gneiss) within the basement accommodate late thrusting and juxtaposition of these gneisses.

Stage 8c - Duplex formation along proto-MCT

Further late-stage thrusting exploits weaknesses in the basement material (e.g. ancient faults associated with the failed rift formation) juxtaposing the Jutogh Metasediments against the Rampur Formation. Uplift and exposure of the ILH (Stage 8b and c), as suggested by ca. 9 to 12 Ma monazite growth in the Jutogh Group (Caddick, 2004), leads to the extrusion of the ILH after major Miocene movement along the MCT and is recorded in the Sub-Himalayan basins (Najman and Garzanti, 2000 and references within).

Stage 9a - Thrusting along the Jutogh Thrust

Further compression may not be accommodated along the folded MCT due to locking-up of the duplex, and is therefore accommodated to the south of the duplex, resulting in thrusting (post MCT) below the MCT along the Jutogh Thrust (Sutlej). The Tons Thrust (Garhwal; Ahmad et al., 2000) and the Mahabharat Thrust (Nepal; Upreti and Le Fort, 1999) may be lateral equivalents but are interpreted as out-of-sequence thrusting. Out-of-sequence thrusting is also accommodated above the MCT along the Kakhtang Thrust in the eastern Himalaya (Chapter 5). The differing sites of out-of-

sequence thrusting results in different lithological configurations; in the western Himalaya an outer zone of HHCS material is preserved (OLH) whereas in the eastern Himalaya, HHCS material is preserved within the MCTZ. Incision by the Sutlej River through the duplex formed during the Early Miocene with coeval exhumation exposes the Rampur Window (Vannay et al., 2004), resulting in the present-day configuration of the Sutlej traverse (Stage 9b). Rapid uplift and incising of the Kuru Chu in Bhutan exposes large sections of the Daling-Shumar Group.

Figure 6.3 Part II

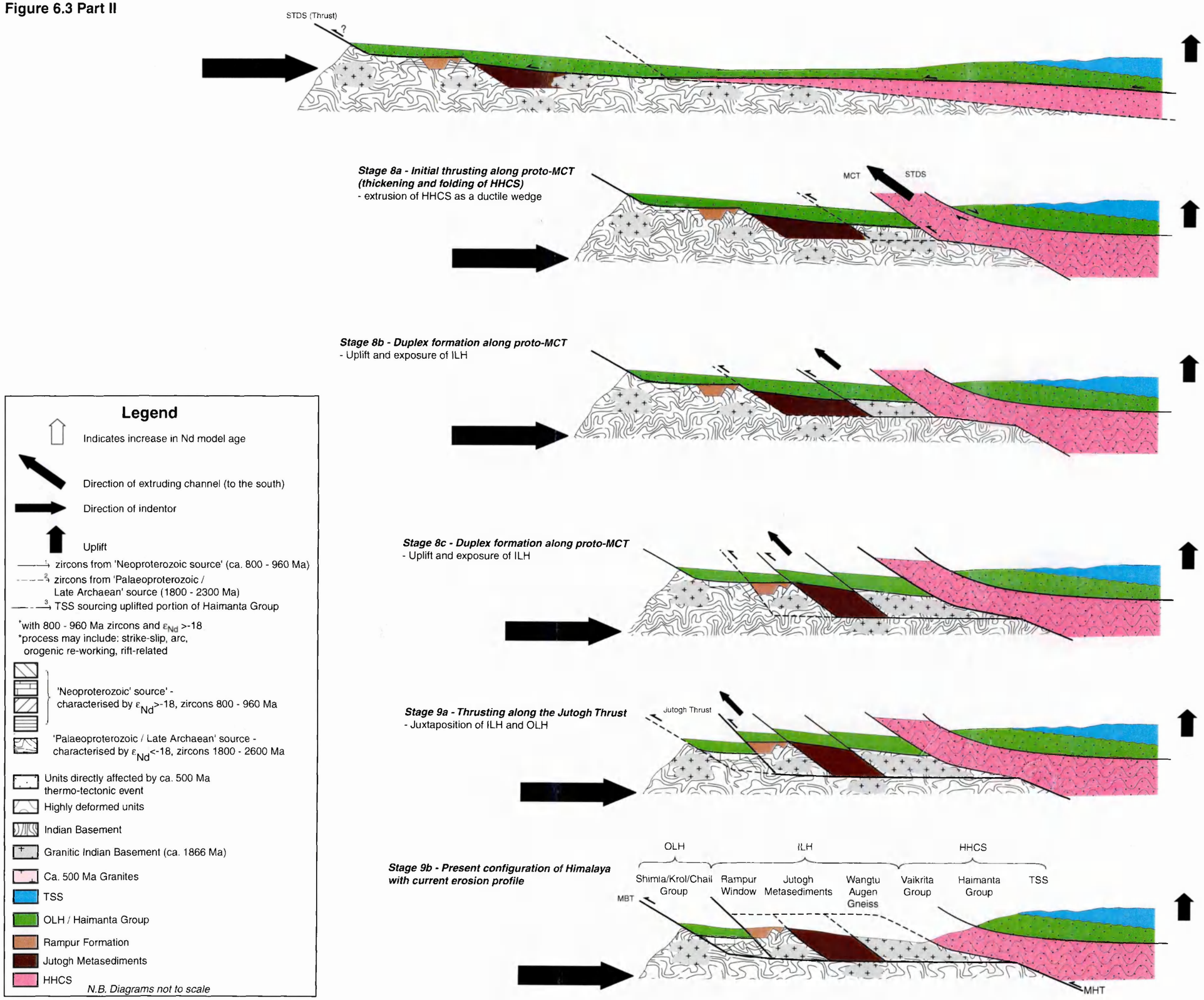

Chapter 7 – Concluding Remarks

7.1 Introduction

Unlike previous attempts to define major tectonic units and structures, combining whole-rock Sr with Nd isotopes and U-Pb zircon geochronology of detrital accessory minerals is an approach that is largely independent of the tectonic orogenic process where lithological constraints, metamorphism or structural deformation are of secondary importance in discriminating different units. It has been shown through the course of this thesis that this combined isotopic approach in the Sutlej Area supports previous isotopic mapping investigations in the western and central Himalaya; furthermore, this technique has been used to demonstrate that isotopes can be used to discriminate between major tectonic units and therefore define structures including the MCT across much of the orogen, from Bhutan to Nanga Parbat.

7.2 Whole-Rock Geochemistry

7.2.1 Sutlej

The combined whole-rock Sr and Nd isotope technique has been used to define the major Himalayan tectonic units in the Sutlej Area. Specifically, the application of these isotope systems has separated the LHS into ILH and OLH (as suggested by Ahmad et al., 2000). The isotope data support the interpretation of Vannay and Grasemann (1998; 2001) and Vannay et al. (2004; 1999) that the MCT lies within a high-grade metamorphic region in the Sutlej Area which therefore consists of both HHCS and Lesser Himalayan basement material (erroneously interpreted as entirely the HHCS by Thakur and Rawat, 1992 and Thakur, 1992, and references therein, Chapter 2). Furthermore this study finds no evidence of tectonic imbrication between the ILH and HHCS (Hodges, 2000). The low-grade Rampur Formation is isotopically

indistinguishable from the ILH basement material and is assigned to the ILH, whereas the Shimla, Chail and Krol Groups are isotopically distinct and similar to the HHCS (Fig. 3.4). These units are assigned to the OLH and may be correlated with the Krol and Chandpur Formations of Ahmad et al. (2000). Indeed, estimates for the sedimentation age suggest that ILH metasediments are much older than the OLH, which supports the interpretation of distinct palaeogeographic source areas for the two units (see below).

The HHCS and OLH define a distinct isotopic field in Sr-Nd space compared to the ILH (Fig. 3.4). However, although many of the Haimanta Group samples appear to have a strong isotopic affinity to the HHCS field, samples stratigraphically younger than the Precambrian – Cambrian boundary lie within the ILH field (Fig. 3.4; summarised in Fig. 3.10), suggesting mixing between the source areas that contributed detritus to the ILH and HHCS/OLH pre-Himalayan depositional basins. The Haimanta Group is terminated at the Cambro-Ordovician boundary, coincident with the intrusion age of the Kinnaur Kailas Granite (459 ± 7.7 Ma U-Pb zircon crystallisation age; Chawla et al., 2000). The Cambro-Ordovician event associated with a number of ca. 500 Ma granite intrusions (Singh and Jain, 2003 and references therein) may be responsible for the Sr isotope homogenisation ca. 500 Ma as observed in the HHCS and OLH. The Haimanta Group was deformed prior to the deposition of the undeformed TSS (Grasemann et al., 1997; Wiesmayr and Grasemann, 2002), which marks the end of the hiatus between the Haimanta Group and the TSS. The early to mid Palaeozoic TSS samples are also isotopically indistinguishable from the HHCS, suggesting that the uplifted portion of the Haimanta Group might be contributing detritus to the TSS basin, which may explain why the TSS samples plot close to the 500 Ma reference line (Fig. 5.3). However, many samples stratigraphically younger than the Late Palaeozoic Panjal Traps have elevated ε_{Nd} values suggesting a contribution from a mantle derived source (such as the Panjal Traps themselves), although not all samples younger than the Panjal Traps share this isotopic anomaly. This suggests that the source area that

contributed detritus to the Early to Mid Palaeozoic TSS basin continued to contribute detritus to the Late Palaeozoic – Mesozoic TSS basin.

7.2.2 Bhutan

Within the Bhutan field area similar broad correlations with the Sutlej Area may be drawn in that the HHCS is isotopically distinct from the LHS. The HHCS is isotopically similar in Bhutan and Sutlej. Although a metamorphic break is observed within the HHCS across the Kakhtang Thrust, metasediments from the footwall and hanging wall are isotopically indistinguishable, suggesting that this thrust is intra-formational within the HHCS of Bhutan (Grujic et al., 2002).

The LHS in Bhutan has isotopic affinities with both the ILH and HHCS field of the Sutlej Area. However, the terms ILH and OLH cannot be extended from the western Himalaya (Sutlej) to Bhutan as in the Sutlej, the OLH lie outward of the orogenic core, whereas in Bhutan the same spatial distribution does not apply (compare Fig. 3.12 and Fig. 4.1), therefore the terms DSG and JBF are used to describe units that have ILH and OLH isotopic affinities, respectively. The geographic position of the JBF may suggest either that it represents an out-of-sequence thrust slice, comparable with the OLH of the Sutlej region, or that it lies within the MCTZ itself. Therefore, if these units demarcate the lower plane of the MCT (as does the Karcham Group in the Sutlej), then the MCT is now mapped below the JBF, supporting the interpretation of Jangpangi (1974) and refuting the interpretation of Dasgupta (1995) that the Jaishidanda Formation forms part of the LHS.

Of particular importance are the similarities of the Karcham Group (incorporated into the Vaikrita Group, Sutlej Area) and the Jaishidanda Formation. Both these units lie in a similar structural position in relation to the MCT, and are isotopically indistinguishable from each other. Indeed it is tempting to relate their structural position to the propagation of the MCT that exploited an unconformable relationship

between these units and the underlying HHCS (Parrish and Hodges, 1996). However, more research is required to asses the validity of this interpretation. Preliminary investigations suggest that there is little or no evidence of tectonic imbrication between the ILH/DSG and the HHCS. However, the small outcrop of the Barsong Formation (compared to the ubiquitous exposures of the Jaishidanda Formation), its location within the MCTZ, and the isotopic similarities with TSS samples suggests that the Barsong Formation may be a small thrust slice with TSS affinities. Furthermore, the Mesozoic palynomorph age requires more research to verify if this age is a true rock age or the result of laboratory contamination.

Gansser (1983) suggests the Chekha Formation marks the base of the TSS. This study confirms they are isotopically similar and tentatively correlates the Chekha Formation with the Haimanta Group; both are intruded by tourmaline-bearing leucogranites, are strongly folded and are of higher metamorphic grade than the overlying low-grade, undeformed TSS. Pebbly horizons in both may correspond to Neoproterozoic Marinoan Glaciations. The Chekha Formation does lack the following features of the Haimanta Group: (i) an overlying unconformity with the TSS; (ii) a 'cap carbonate' observed above the tillite in the Manjir Formation; and (iii) a ca. 500 Ma granite that intrudes the lower Haimanta (Chawla et al., 2000). A larger data set from the Chekha Formation would properly assess a possible correlation between the Chekha Formation and the Haimanta Group.

In comparing the Bhutan and Sutlej sections there are several significant differences. These include the absence of LHS high-grade basement material in Bhutan. However, the thickness of LHS exposure in Bhutan is much less than in other parts of the orogen, and indeed only the Kuru Chu-Shumar Half Window allows reasonable exposure of the LHS, with large sections remaining unsampled due to political reasons. Further differences include the alignment along a 1000 Ma rather than an 1800 Ma reference line for the DSG samples (Fig. 5.3) and a larger separation between this field and the

HHCS/JBF field (Fig. 5.4), which both may reflect either small sample populations or variations in the palaeogeography and location of source areas (see later).

7.3 U-Pb Zircon Geochronology

7.3.1 Sutlej

The zircon populations within the ILH suggest that two Palaeoproterozoic – Late Archaean source areas contributed zircons into ILH basins. The highly concordant and small detrital zircon age spectra within the Rampur Formation lie within error of the crystallisation age of the Wangtu Augen Gneiss, which suggests that this gneiss body is a likely source. However, detrital zircon ages within the Jutogh Metasediments are highly variable and discordant, suggesting a second different source area for the detrital zircons analysed in this study; identification of this source remains elusive. Zircons from the Wangtu Augen Gneiss appear cogenetic and the data suggests a crystallisation age of ca. 1866 Ma. The highly discordant nature of the Wangtu Augen Gneiss compared with the highly concordant nature of the Rampur Formation zircons suggests that the lead loss event suffered by the Wangtu Augen Gneiss post-dates the erosion and deposition of the detritus within the Rampur Formation basin.

Two zircon populations are identified within the Vaikrita Group (HHCS); these are a small Palaeoproterozoic – Late Archaean population (similar to the zircon population in the Jutogh Metasediments) and a younger, dominant Neoproterozoic population. This may reflect the interpretations of the whole-rock Sr and Nd data from the Haimanta Group which suggests that prior to Haimanta Group deposition the source area was dominated by a younger (Neoproterozoic) source that was juxtaposed with (or covered) an older (Palaeoproterozoic – Late Archaean) terrain. As this younger terrain eroded through time depositing detritus into the pre-Himalayan HHCS and Haimanta Group basin, a greater portion of the older underlying terrain was exposed (that had

isotopic characteristics of the ILH) resulting in the balance of sources increasingly favouring the ILH (Palaeoproterozoic – Late Archaean) source.

7.3.2 Bhutan

Zircon age populations within Bhutan broadly correspond to zircon ages in the respective units in the Sutlej region. However, within the HHCS the Palaeoproterozoic – Late Archaean population is absent, suggesting either that the Neoproterozoic source was thicker in this portion of basin, restricting the contribution of the Palaeoproterozoic – Late Archaean population to the basin, or that a smaller Palaeoproterozoic – Late Archaean population (than compared to the Sutlej zircon populations) was the result of dating fewer zircon fractions (discussed in Chapter 6, compare zircon populations in Fig. 6.1 and Fig 1.5).

Metaigneous rocks from the Daling-Shumar Group (a metarhyolite and a biotite orthogneiss) both show strong evidence for inheritance which appears to be reflected in underlying quartzites that have a broad Palaeoproterozoic population with variable amounts of inheritance. This contrasts with the comparable lithology in the Sutlej Area, the Rampur Formation, which has similar whole-rock Sr and Nd isotopic characteristics but zircon discordance is less than 1%.

The Palaeoproterozoic – Late Archaean zircon population from the Mesozoic Barsong Formation (Gansser, 1983) suggests that this sample may have derived its detritus from a highly restricted source. The persistence of the Jaishidanda Formation through the MCTZ in Bhutan, compared to the small exposure of the Barsong Formation suggests that the Barsong Formation may represent a small thrust slice of material comparable to the TSS. However, TSS zircon populations (DeCelles et al., 2000; summarised in Fig. 1.5) suggest that both Neoproterozoic and Palaeoproterozoic – Late Archaean sources contributed detritus into the TSS basin. A further interpretation may be that the sample collected apparently from the Barsong

Formation should be reassigned to the Jaishidanda Formation, although a Neoproterozoic age population is again absent. Dating further zircon fractions could reveal a small as yet unobserved Neoproterozoic population; however, the true nature of the Barsong Formation so far remains elusive.

7.4 Palaeogeography and Source Areas

The palaeogeographic reconstruction of the main Himalayan units is summarised in Figure 6.3 (and accompanying text). Two major sources have been identified on the basis of zircon populations during the course of this project; these are described as a Neoproterozoic source and a Palaeoproterozoic – Late Archaean source. The varying contributions of these sources to the pre-Himalayan depositional basins have enabled discrimination between these sources on the basis of whole-rock Sr and Nd isotopes and U-Pb zircon geochronology. However, it has been shown that the ILH depositional basins contain only the Palaeoproterozoic – Late Archaean source, as expected from the depositional age of these sediments. For the ILH and DSG (equivalent to the ILH in Bhutan) the youngest detrital zircon within the population constrains a maximum depositional age of ca. 1850 Ma, whereas basalts (Sutlej) and rhyolites (Bhutan) probably constrain a minimum depositional age of ca. 1800 Ma. Therefore the ILH is likely to been deposited during the mid-Palaeoproterozoic. Furthermore, the zircon populations in the Rampur Formation strongly suggest a Wangtu Augen Gneiss provenance, whereas source areas for the Jutogh Metasediments are yet to be discovered. Contrastingly metaigneous rocks in the DSG show large amounts of inheritance, which is also observed in detrital zircon fractions from quartzites from the same units, suggesting these metaigneous rocks may be a source of detritus for these sediments. This interpretation of the palaeogeography of the ILH/DSG depositional basins suggests the source areas were in close proximity and were restricted, whereas Upreti & Le Fort (1999) proposed source areas to the north, between the LHS (ILH/DSG) basin and the HHCS basin. However, palaeocurrent indicators observed in

ILH sediments (Valdiya, 1995) support the proposed model that implies the sediments were derived from the southwest.

The metasediments of the HHCS, OLH and TSS contain both Neoproterozoic and Palaeoproterozoic – Late Archaean detritus, with a strong bias towards a Neoproterozoic source. This study invokes a model that during the Neoproterozoic a tectono-thermal event led to the formation of a Neoproterozoic source which was then juxtaposed with, or emplaced onto, the pre-existing Palaeoproterozoic – Late Archaean source. The uplift of the Neoproterozoic source led to preferential erosion and deposition into the pre-Himalayan HHCS sedimentary basin, with only small amounts of detritus derived from the older and underlying Palaeoproterozoic – Late Archaean source. Through time, the balance of eroded detritus favoured the underlying Palaeoproterozoic – Late Archaean source, as observed in the upper portion of the Haimanta Group. The ca. 500 Ma tectono-thermal event led to uplift of the Haimanta Group, OLH and HHCS (protolith) and homogenisation of the Sr isotopes in these units, whereas the ILH remained unaffected. The uplifted portion of the Haimanta Group, and possibly the OLH and HHCS, contributed further detritus to the TSS depositional basin. However, igneous activity during the late Palaeozoic – Mesozoic contributed a significant amount of younger detritus to this basin. Uplift of this basin during the Himalayan orogeny terminated deposition, progressive south directed thrusting led to the separation of the sediments that overlie the HHCS and formation of the OLH and Haimanta Group.

Finally, this study suggests that contrary to McLennan et al. (1989; 1990), ε_{Nd} values from metasedimentary rocks from the Sutlej Area are independent of grain size. For example, ε_{Nd} values of schists from Jutogh Metasediments and quartzites from the Rampur Formation are isotopically more similar than schists from the Vaikrita Group, which supports the work of Goldstein et al (1984) that there is not measurable difference between coexisting sands and muds. However, this study does not directly compare coexisting muds and sands and the studies of McLennan et al. (1989; 1990)

and Goldstein et al (1984) examined samples that were unperturbed by tectonic events.

7.5 Future Work

A number of unresolved issues demonstrate the need for further research into this area. Foremost amongst these are the following.

7.5.1 Investigations into the relationship between the Chail, Shimla and Haimanta Groups

Thakur (1992) assigns the Chail Group to the uppermost portion of the crystalline series. Clearly this group has an isotopic affinity with the HHCS field (Fig. 3.4). However, the metamorphic characteristics of the Chail Group vary considerably when comparing the "Chail Group" exposures south of the Rampur-Larji Window and the "Chail Group" exposures around the village of Chail itself. Thus either the assignment to the crystalline series is inaccurate, or the Chail Group within the Sutlej Area should be separated into first an outlier of the HHCS (to the south of the Rampur Window) and secondly a portion of the OLH. The structural relationship of the Chail and Jutogh Groups south of the Rampur-Larji Window is difficult to resolve with the current small sample population. Clearly there is a need to fully investigate the structures south of the Rampur-Larji Window and sample large portions of both groups to fully map out the boundary between these units. There remains further confusion in the interpretation of the units that crop out surrounding the Chor Granitoid. Isotopically these units have an OLH/HHCS affinity and have therefore erroneously been assigned to the Jutogh Group (Gansser, 1964; Singh et al., 2002; Thakur, 1992). Further investigations in this area may reveal whether these rocks are a portion of the OLH or the HHCS. Interestingly, Gansser (1964) questioned whether intrusions such as the Chor Granitoid have affected susceptible argillaceous units such as the Jutogh and Shimla Groups.

The regional correlation of the Chail Group remains uncertain. In the Lahaul Region, the Lahaul Group is the lateral equivalent to the Chamba Group; they are intruded by the Jispa and Dalhousie 500 Ma Granites respectively. The Chamba Group is interpreted as a westward continuation of the Chail Group, whereas the Lahaul Group is interpreted as a continuation of the Haimanta Group. Thakur (1992) notes that this tectonostratigraphic relationship indicates that the Chail and Haimanta Groups originally belonged to the same tectonic unit but they are now spatially separated.

Frank et al. (1994) correlates the Blaini boulder bed in the OLH (Shimla Group) with the Manjir boulder bed in the Haimanta Group (Draganits et al., 1998). Rb/Sr whole-rock dating indicates a maximum depositional age of 700 Ma for the Blaini Boulder bed; both beds have a similar model Nd age of 1.8-2.3 Ga. Depositional ages are corroborated by detrital muscovite ages of 865 Ma in the Shimla Group (Frank et al., 1994). Clearly, the relationship between the Shimla, Chail and Haimanta Groups needs to be resolved.

7.5.2 Potential correlation between the Haimanta Group and Chekha Formation

As outlined above (section 7.2.2) preliminary investigations into the Chekha Formation (Bhutan) reveals that tentative correlations can be made with the Haimanta Group. However, although the Haimanta Group is stratigraphically well constrained (Fig. 3.10) the Chekha Formation is not. To enable comparisons with the Chekha Formation, a detailed study is required in the northeast Wang Chu Basin (Fig. 4.1), where the most complete section of Chekha Formation crops out (Gansser, 1983). Logistical constraints prevented this project from investigating this area.

7.5.3 Detailed investigations south of the MCT, Bhutan

Political constraints prevented this project from investing and sampling the Duiri and Baxa Formations and the Damudas (located within the LHS of Gansser, 1983). These units require isotopic evaluation to complete the comparison of all the major tectonic

units in eastern and western Himalaya. At present the lateral extent of the OLH, identified in the Sutlej and Garhwal Himalaya, remains undetermined.

7.5.4 Comparative ε_{Hf} zircon study, to asses the validity of source areas

ε_{Hf} values from analysed zircons would enable future work to test the interpretations of sources areas suggested in this study. For example, corresponding ε_{Hf} values from zircon chemistry from the Rampur Formation and the Wangtu Augen Gneiss would establish whether these sediments sourced a Wangtu Augen Gneiss type body.

References

Ahmad, T., Harris, N., Bickle, M., Chapman, H., Bunbury, J. and Prince, C., 2000. Isotopic constraints on the structural relationships between the Lesser Himalayan Series and the High Himalayan Crystalline Series, Garhwal Himalaya. Geological Society of America Bulletin, 112(3): 467-477.

Ahmad, T., Mukherjee, P.K. and Trivedi, J.R., 1999. Geochemistry of Precambrian mafic magmatic rocks of the Western Himalaya, India: petrogenetic and tectonic implications. Chemical Geology, 160(1-2): 103-119.

Aitchison, J.C., Badengzhu, Davis, A. M., Liu, J. B., Luo, H., Malpas, J. G., McDermid, I. R. C., Wu, H. Y., Ziabrev, S. V., Zhou, M. F., 2000. Remnants of a Cretaceous intra-oceanic subduction system within the Yarlung-Zangbo suture (southern Tibet). Earth and Planetary Science Letters, 183(1-2): 231-244.

Amatya, K.M., Jnawali, B.M., Shrestha, P.L., Maske, N.D. and Hoppe, P., 1994. Geological Map of Nepal. Department of Mines and Geology, Kathmandu (Nepal).

Argles, T., Foster, G., Whittington, A., Harris, N. and George, M., 2003. Isotope studies reveal a complete Himalayan section in the Nanga Parbat syntaxis. Geology (Boulder), 31(12): 1109-1112.

Argles, T.W., Prince, C.I., Foster, G.L. and Vance, D., 1999. New garnets for old? Cautionary tales from young mountain belts. Earth and Planetary Science Letters, 172(3-4): 301-309.

Arita, K., 1983. Origin of the Inverted Metamorphism of the Lower Himalayas, Central Nepal. Tectonophysics, 95(1-2): 43-60.

Arndt, N.T. and Goldstein, S.L., 1987. Use and abuse of crust-formation ages. Geology (Boulder), 15(10): 893-895.

Auden, J.B., 1934. The geology of the Krol belt.

Ayres, M., 1997. Trace element behaviour during high-grade metamorphism and anetexis, Open University, Milton Keynes, 354 pp.

Bagati, T.N., 1990. Lithostratigrphy and facies variation in the Spiti nasin (Tethys), Himalchal Pradesh, India. Journal of Himalayan Geology, 1: 35-47.

Beaumont, C., Jamieson, R.A., Nguyen, M.H. and Lee, B., 2001. Himalayan tectonics explained by extrusion of a low-viscosity crustal channel coupled to focused surface denudation. Nature, 414(6865): 738-742.

Beaumont, C., Jamieson, R.A., Nguyen, M.H. and Medvedev, S., 2004. Crustal Channel Flows: 1. Numerical models with applications to the tectonics of the Himalayan-Tibetan Orogen. Journal of Geophysical Research, 109(B06406): 1-24.

Beck, R.A. Burbank, D. W., Sercombe, W. J., Riley, G. W., Barndt, J. K., Berry, J. R., Afzal, J., Khan, A. M., Jurgen, H., Metje, J., Cheema, A., Shafique, N. A., Lawrence, R. D. and Khan, M. A., 1995. Stratigraphic Evidence for an Early Collision between Northwest India and Asia. Nature, 373(6509): 55-58.

Bhanot, V.B., Kwatra, S.K., Kansal, A.K. and Pandey, B.K., 1978. Rb-Sr whole rock age for Chail Series of northwestern Himalaya. Journal of the Geological Society of India, 19(5): 224-225.

Bhargava, O.N., 1972. A reinterpretation of the Krol Belt. Himalayan Geology, 2: 47-81.

Bhatia, M.R., 1983. Plate tectonics and geochemical composition of sandstones. Journal of Geology, 91(6): 611-627.

Blattner, P., Dietrich, V. and Gansser, A., 1983. Contrasting O-18-Enrichment and Origins of High Himalayan and Transhimalayan Intrusives. Earth and Planetary Science Letters, 65(2): 276-286.

Bordet, P., Colchen, M. and Le Fort, P., 1972. Some features of the geology of the Annapurna Range, Nepal Himalaya. Himalayan Geology, 2: 537-563.

Burbank, D.W., Beck, R. A., and Mulder, T., 1996, The Himalayan foreland basin, in Yin, A., and Harrison, T. M., eds., The tectonic evolution of Asia: Cambridge, Cambridge University Press, p. 149–188.

Burchfiel, B.C. Chen, Z., Hodges, K. V., Liu, Y., Royden, L. H., Deng, C. and Xu, J., 1992. The South Tibetan detachment system, Himalayan Orogen; extension contemporaneous with and parallel to shortening in a collisional mountain belt, Special Paper - Geological Society of America. Geological Society of America (GSA), Boulder, CO, (USA).

Burg, J.P., Brunel, M., Gapais, D., Chen, G.M. and Liu, G.H., 1984. Deformation of Leucogranites of the Crystalline Main Central Sheet in Southern Tibet (China). Journal of Structural Geology, 6(5): 535-&.

Burg, J.P. and Chen, G.M., 1984. Tectonics and Structural Zonation of Southern Tibet, China. Nature, 311(5983): 219-223.

Caddick, M., 2004. The Tectonometamorphic Evolution of the Central and Western Himalaya, Cambridge University, Cambridge.

Castelli, D. and Lombardo, B., 1988. The Gophu La and Western Lunana Granites - Miocene Muscovite Leucogranites of the Bhutan Himalaya. Lithos, 21(3): 211-225.

Catlos, E.J. Harrison, T. M., Manning, C. E., Grove, M., Rai, S. M., Hubbard, M. S. and Upreti, B. N., 2002. Records of the evolution of the Himalayan orogen from in situ Th-Pb ion microprobe dating of monazite: Eastern Nepal and western Garhwal. Journal of Asian Earth Sciences, 20(5): 459-479.

Chawla, H.S., Marquer, D., Kramers, J.D., Villa, I.M. and Bussy, F., 2000. Petrology and age of the Kinnar Kailas Granite; evidences for an Ordovician post-orogenic extension in the Higher Himalayan Crystalline, Sutlej, India. The 15th Himalayan-Karakoram-Tibet workshop; study of the Qinghai-Tibet Plateau in the new century Dixue Qianyuan = Earth Science Frontiers, 7: 50-51.

Cohen, A.S., Onions, R.K., Siegenthaler, R. and Griffin, W.L., 1988. Chronology of the Pressure-Temperature History Recorded by a Granulite Terrain. Contributions to Mineralogy and Petrology, 98(3): 303-311.

Colchen, M., Le Fort, P. and Pecher, A., 1986. Annapurna-Manaslu-Ganesh Himal, Centre National de la Recherche Scientique, Paris, 136 pp.

Coleman, M. and Hodges, K., 1995, Evidence for Tibetan Plateau Uplift before 14-Myr Ago from a New Minimum Age for East-West Extension, Nature, 374, 49-52.

Corfield, R.I. and Searle, M.P., 2000. Crustal shortening estimates across the North Indian continental margin, Ladakh, NW India. In: M.A. Khan, P.J. Treloar and M.Q. Jan (Editors), Tectonics of the Nanga Parbat syntaxis and the western Himalaya Geological Society Special Publications. Geological Society of London, London, United Kingdom, pp. 395-410.

Coward, M.P., Butler, R.W.H., Khan, M.A. and Knipe, R.J., 1987. The Tectonic History of Kohistan and Its Implications for Himalayan Structure. Journal of the Geological Society, 144: 377-391.

Cullers, R.L., Barrett, T., Carlson, R. and Robinson, B., 1987. Rare-earth element and mineralogic changes in Holocene soil and stream sediment; a case study in the Wet Mountains, Colorado, U.S.A. Chemical Geology, 63(3-4): 275-297.

Daniel, C.G., Hollister, L.S., Parrish, R.R. and Grujic, D., 2003. Exhumation of the Main Central Thrust from lower crustal depths, eastern Bhutan Himalaya. J. Metamorph. Geol., 21: 317-334.

Darbyshire, D.P.F. and Sewell, R.J., 1997. Nd and Sr isotope geochemistry of plutonic rocks from Hong Kong: implications for granite petrogenesis, regional structure and crustal evolution. Chemical Geology, 143(1-2): 81-93.

Dasgupta, S., 1995. Jaishidanda Formation. In: O.N. Bhargava (Editor), The Bhutan Himalaya: a Geological Account, Special Publication. Geological Survey of India, Calcutta (India), pp. 79-88.

Davidson, C., Grujic, D.E., Hollister, L.S. and Schmid, S.M., 1997. Metamorphic reactions related to decompression and synkinematic intrusion of leucogranite, High Himalayan Crystallines, Bhutan. Journal of Metamorphic Geology, 15(5): 593-612.

Deb, M., Thorpe, R.I., Krstic, D., Corfu, F. and Davis, D.W., 2001. Zircon U-Pb and galena Pb isotope evidence for an approximate 1.0 Ga terrane constituting the western margin of the Aravalli-Delhi orogenic belt, northwestern India. Precambrian Research, 108(3-4): 195-213.

DeCelles, P.G., Gehrels, G.E., Quade, J., LaReau, B. and Spurlin, M., 2000. Tectonic implications of U-Pb zircon ages of the Himalayan orogenic belt in Nepal. Science, 288(5465): 497-499.

DeCelles, P. G., Gehrels, G. E., Quade, J., Ojha, T. P. 1998, Eocene early Miocene foreland basin development and the history of Himalayan thrusting, western and central Nepal, Tectonics, 17, 741-765.

DeCelles, P. G., Robinson, D. M., Quade, J., Ojha, T. P., Garzione, C. N., Copeland, P., Upreti, B. N, 2001, Stratigraphy, structure, and tectonic evolution of the Himalayan fold-thrust belt in western Nepal, Tectonics, 20, 487-509.

Deniel, C., Vidal, P., Fernandez, A., Le Fort, P. and Peucat, J.J., 1987. Isotopic study of the Manaslu granite (Himalaya, Nepal); inference on the age and source of Himalayan leucogranites. Contributions to Mineralogy and Petrology, 96(1): 78-92.

DePaolo, D.J., 1981. Neodymium isotopes in the Colorado Front Range and crust-mantle evolution in the Proterozoic. Nature (London), 291(5812): 193-196.

DePaolo, D.J. and Wasserburg, G.J., 1976a. Inferences about magma sources and mantle structure from variations of Nd-143/Nd-144. Geophysical Research Letters, 3(12): 743-746.

DePaolo, D.J. and Wasserburg, G.J., 1976b. Nd isotopic variations and petrogenetic models. Geophysical Research Letters, 3(5): 249-252.

Dewey, J.F., Shackleton, R.M., Chang, C. and Sun, Y., 1988. The tectonic evolution of the Tibetan Plateau. The geological evolution of Tibet; report of the 1985 Royal Society - Academia Sinica geotraverse of the Qinghai-Xizang Plateau Philosophical Transactions of the Royal Society of London, Series A: Mathematical and Physical Sciences, 327(1594): 379-413.

Dickin, A.P., 1997. Radiogenic isotope geology. Cambridge, Cambridge University Press, United Kingdom, 490 pp.

Dickin, A.P., 2000. Crustal formation in the Grenville Province: Nd-isotope evidence. Canadian Journal of Earth Sciences, 37(2): 165-181.

Dickin, A.P. and McNutt, R.H., 1989. Nd Model Age Mapping of the Southeast Margin of the Archean Foreland in the Grenville Province of Ontario. Geology, 17(4): 299-302.

Dickin, A.P. and McNutt, R.H., 2003. An application of Nd isotope mapping in structural geology: delineating an allochthonous Grenvillian terrane at North Bay, Ontario. Geological Magazine, 140(5): 539-548.

Dietrich, V. and Gansser, A., 1981. The leucogranites of the Bhutan Himalaya (crustal anatexis versus mantle melting). Schweizerische Mineralogische und Petrographische Mitteilungen = Bulletin Suisse de Mineralogie et Petrographie, 61(2-3): 177-202.

Draganits, E., Grasemann, B., Frank, W., Miller, C. and Wiesmayr, G., 1998. The sedimentary protoliths of the HHC in the Chamba-Lahaul area, NW-Himalayas, India. In: S. Hamidullah, R.D. Lawrence and M.Q. Jan (Editors), 13th Himalaya-Karakoram-Tibet international workshop; abstract volume Geological Bulletin, University of Peshawar 31 (1998). University of Peshawar, Department of Geology, Peshawar, Pakistan, pp. 58-60.

Duncan, C., Masek, J. and Fielding, E., 2003. How steep are the Himalaya? Characteristics and implications of along-strike topographic variations. Geology, 31(1): 75-78.

Edwards, M.A. and Harrison, T.M., 1997. When did the roof collapse? Late Miocene north-south extension in the high Himalaya revealed by Th-Pb monazite dating of the Khula Kangri granite. Geology, 25(6): 543-546.

Edwards, M.A., Kidd, W.S.F., Li, J.X., Yu, Y.J. and Clark, M., 1996. Multi-stage development of the southern Tibet detachment system near Khula Kangri. New data from Gonto La. Tectonophysics, 260(1-3): 1-19.

Edwards, M.A., Pecher, A., Kidd, W.S.F., Burchfiel, B.C. and Royden, L.H., 1999. Southern Tibet Detachment System at Khula Kangri, eastern Himalaya: A large-area, shallow detachment stretching into Bhutan? Journal of Geology, 107(5): 623-631.

England, P. and Houseman, G., 1989. Extension During Continental Convergence, with Application to the Tibetan Plateau. Journal of Geophysical Research-Solid Earth and Planets, 94(B12): 17561-17579.

Evans, M.J., Derry, L.A., Anderson, S.P. and France-Lanord, C., 2001. Hydrothermal source of radiogenic Sr to Himalayan rivers. Geology (Boulder), 29(9): 803-806.

Fielding, E., Isacks, B., Barazangi, M. and Duncan, C.C., 1994. How flat is Tibet? Geology (Boulder), 22(2): 163-167.

Foster, G., Kinny, P., Vance, D., Prince, C. and Harris, N., 2000. The significance of monazite U-Th-Pb age data in metamorphic assemblages; a combined study of monazite and garnet chronometry. Earth and Planetary Science Letters, 181(3): 327-340.

Fralick, P.W. and Kronberg, B.I., 1997. Geochemical discrimination of clastic sedimentary rock sources. Sedimentary Geology, 113(1-2): 111-124.

France-Lanord, C., Derry, L. and Michard, A., 1993. Evolution of the Himalaya since Miocene time; isotopic and sedimentological evidence from the Bengal Fan. In: P.J. Treloar and M.P. Searle (Editors), Himalayan Tectonics. Geological Society of London, London, United Kingdom, pp. 603-621.

Frank, W. Bhargava, O. N., Miller, C., Banerjee, D. N., Grasemann, B., and Stuewe, K., (Editors), 2001. A review of the Proterozoic in the Himalaya and the northern Indian Shield. Pergamon, Oxford, United Kingdom, 18 pp.

Frank, W., Grasemann, B., Chowanetz, E. and Miller, C., 1992. Age and Palaeographic setting of Proterozoic rock series in the NW Himalayas, 7th HKT workshop, Oxford, pp. 26.

Frank, W., Miller, C., Grasemann, B. and Thoni, M., 1994. The Haimanta-Simla Slate/Krol Belt sedimentary megacycle (palaeogeographic setting and provenance of sediments). 9th Himalaya-Karakorum-Tibet workshop; abstract volume Journal of Nepal Geological Society, 10: 46-48.

Fuchs, G., 1987. The geology of southern Zanskar (Ladakh); evidence for the autochthony of the Tethys zone of the Himalaya. Jahrbuch der Geologischen Bundesanstalt Wien, 130(4): 465-491.

Fuchs, G. and Frank, W., 1970. The geology of west Nepal between the rivers Kali Gandaki and Thulo Bheri.

Gaetani, M. and Garzanti, E., 1991. Multicyclic History of the Northern India Continental-Margin (Northwestern Himalaya). Aapg Bulletin-American Association of Petroleum Geologists, 75(9): 1427-1446.

Gansser, A., 1964. The geology of the Himalayas, 289 pp.

Gansser, A., 1983. Geology of the Bhutan Himalaya.

Garzanti, E., 1999. Stratigraphy and sedimentary history of the Nepal Tethys Himalaya passive margin. Journal of Asian Earth Sciences, 17(5-6): 805-827.

Garzanti, E., Angiolini, L. and Sciunnach, D., 1996. The mid-carboniferous to lowermost Permian succession of Spiti (Po Group and Ganmachidam Formation; Tethys Himalaya, Northern India): Gondwana glaciation and rifting of Neo-Tethys. Geodinamica Acta, 9(2-3): 78-100.

Garzanti, E., Le Fort, P. and Sciunnach, D., 1999. First report of Lower Permian basalts in South Tibet: tholeiitic magmatism during break-up and incipient opening of Neotethys. Journal of Asian Earth Sciences, 17(4): 533-546.

Gehrels, G.E. DeCelles, P. G., Martin, A., Ojha, T. P., Pinhassi, G., and Upreti, B. N, 2003. Initiation of the Himalayan Orogen as an early Paleozoic thin-skinned thrust belt. GSA Today, 13(9): 4-9.

Godin, L., 2003. Structural evolution of the Tethyan sedimentary sequence in the Annapurna area, central Nepal Himalaya. Journal of Asian Earth Sciences, 22(4): 307-+.

Godin, L., Brown, R.L., Hanmer, S. and Parrish, R., 1999. Back folds in the core of the Himalayan orogen: An alternative interpretation. Geology, 27(2): 151-154.

Godin, L., Parrish, R.R., Brown, R.L. and Hodges, K.V., 2001. Crustal thickening leading to exhumation of the Himalayan Metamorphic core of central Nepal: Insight from U-Pb Geochronology and Ar-40/Ar-39 Thermochronology. Tectonics, 20(5): 729-747.

Godwin-Austen, 1868. Notes on the structure of the country near the foot of Hills in the Western Bhootan Dooars. Journal of the Asiatic Society, Bengal, 37(1): 1-27.

Goldstein, S.L., Onions, R.K. and Hamilton, P.J., 1984. A Sm-Nd Isotopic Study of Atmospheric Dusts and Particulates from Major River Systems. Earth and Planetary Science Letters, 70(2): 221-236.

Gopalan, K., Macdougall, J. D., Roy, A. B., Murali, A. V., Jahn, B. and Moorbath, S. (Editors), 1990. Sm-Nd evidence for 3.3 Ga old rocks in Rajasthan, northwestern India. Elsevier, Amsterdam, International, 287-297 pp.

Gosh, S.C., 1993. Study of Palaeozoic Mesozoic estheriids of India. Extended abstracts of progress reports of the Central Headquarters, AMSE Wing, Coal Wing, Marine Wing, Antarctica Division and Bhutan Unit for the field season 1991-92 Records of the Geological Survey of India, 126: 5.

Grasemann, B., Miller, C., Frank, W. and Draganits, E., 1997. Structural Evidence of Pre-Ordovician Deformation in the Pin Valley (Spiti, India), 12th HKT Workshop, Rome, pp. 143-144.

Gresbach, C.L., 1891. Geology of the Cental Himalaya, 23. Memoirs of the Geological Survey, India, 232 pp.

Grujic, D., Casey, M., Davidson, C., Hollister, L., Kundig, R., Pavlis, T. and Schmid, S., 1996. Ductile extrusion of the Higher Himalayan Crystalline in Bhutan: evidence from quartz microfabrics. Tectonophysics, 260(1-3): 21-43.

Grujic, D., Hollister, L.S. and Parrish, R.R., 2002. Himalayan metamorphic sequence as an orogenic channel: insight from Bhutan. Earth and Planetary Science Letters, 198(1-2): 177-191.

Guillot, S., Cosca, M., Allemand, P. and Le Fort, P., 1999. Contrasting metamorphic and geochronologic evolution along the Himalayan Belt. In: A. Macfarlane, R.B. Sorkhabi and J. Quade (Editors), Himalaya and Tibet; mountain roots to mountain tops Special Paper - Geological Society of America 328 (1999). Geological Society of America (GSA), Boulder, CO, pp. 117-128.

Hager, C., Janda, C., Grasemann, B., Draganits, E. and Vannay, J.C., 2003. Active Extenstion in the Higher Himalaya Crystalline, Sutlej Valley, 18th HKT, Ascona, pp. 55.

Harris, N. and Massey, J., 1994. Decompression and Anatexis of Himalayan Metapelites. Tectonics, 13(6): 1537-1546.

Harris, N.B.W., Gass, I. G., Hawkesworth, C. J., Dewey, J. F., Curry, G. B., and Sengor, A. M. C., (Editors), 1990. A geochemical approach to allochthonous terranes; a Pan-African case study. Royal Society of London, London, United Kingdom, 533-548 pp.

Harrison, T. M., Copeland, P., Kidd,W. S. F., and Yin, A., 1992, Raising Tibet: Science, 255, 1663–1670.

Harrison, T. M., Mahon, K. I., Guillot, S., Hodges, K., Le Fort, P., and Pêcher, A., 1995, New constraints on the age of the Manaslu leucogranite: Evidence for episodic tectonic denudation in the central Himalaya: Discussion and reply, Geology, 23, 478–480.

Harrison, T.M., Grove, M., Lovera, O.M., Catlos, E.J. and D'Andrea, J., 1999. The origin of Himalayan anatexis and inverted metamorphism: Models and constraints. Journal of Asian Earth Sciences, 17(5-6): 755-772.

Hashimoto, S., Ohta, Y. and Akiba, C., 1973. Geology of the Nepalise Himalaya. Saikon Publishing Company Limited, Tokyo (Japan).

Hauck, M.L., Nelson, K.D., Brown, L.D., Zhao, W.J. and Ross, A.R., 1998. Crustal structure of the Himalayan orogen at similar to 90 degrees east longitude from Project INDEPTH deep reflection profiles. Tectonics, 17(4): 481-500.

Hawkesworth, C., Kelley, S., Turner, S., Le Roex, A. and Storey, B., 1999. Mantle processes during Gondwana break-up and dispersal. Journal of African Earth Sciences, 28(1): 239-261.

Hayden, H., 1904. The Geology of the Spiti with parts of the Bashar and Rupshu. Geological Survey of India, 36: 121.

Hayden, H., 1907. The geology of the province of the Tsang and U in Tibet. Geological Survey of India memoirs, 36(2): 122-201.

Heaman, L. and Parrish, R., 1991. U-Pb geochronology of accessory minerals. In: J.N. Ludden (Editor). Mineralogical Association of Canada, [Toronto, ON], Canada, pp. 59-102.

Heim, A. and Gansser, A., 1939. Central Himalaya; geological observations of the Swiss expedition 1936, 245 pp.

Hodges, K.V., 2000. Tectonics of the Himalaya and southern Tibet from two perspectives. Geological Society of America Bulletin, 112(3): 324-350.

Hodges, K.V. Parrish, R. R., Housh, T. B., Lux, D. R., Burchfiel, B. C., Royden, L. H., and Chen, Z., 1992. Simultaneous Miocene Extension and Shortening in the Himalayan Orogen. Science, 258(5087): 1466-1470.

Hodges, K.V., Parrish, R.R. and Searle, M.P., 1996. Tectonic evolution of the central Annapurna Range, Nepalese Himalayas. Tectonics, 15(6): 1264-1291.

Houseman, G., and England, P., 1993, Crustal thickening versus lateral expulsion in the Indian-Asian continental collision, Journal of Geophysical Research, 98, 12233–12249.

Huerta, A.D., Royden, L.H. and Hodges, K.V., 1996. The interdependence of deformational and thermal processes in mountain belts. Science, 273(5275): 637-639.

Hughes, N.C. and Jell, P.A. (Editors), 1999. Biostratigraphy and biogeography of Himalayan Cambrian trilobites. Mountain Roots to Mountain Tops. Geological Society of America (GSA), Boulder, CO, 109-116 pp.

Inger, S. and Harris, N., 1993. Geochemical Constraints on Leukogranite Magmatism in the Langtang Valley, Nepal Himalaya. Journal of Petrology, 34(2): 345-368.

Inger, S. and Harris, N.B.W., 1992. Tectonothermal Evolution of the High Himalayan Crystalline Sequence, Langtang Valley, Northern Nepal. Journal of Metamorphic Geology, 10(3): 439-452.

Jamieson, R.A., Beaumont, C., Medvedev, S. and Nguyen, M.H., 2004. Crustal channel flows: 2. Numerical models with implications for metamorphism in the Himalayan-Tibetan Orogen. Journal of Geophysical Research, 109(B06407): 1-24.

Janda, C., Faber, R., Hager, C. and Grasemann, B., 2003. Tracing of Active Faults in theSutlej Valley (NW-Himalayas, India), 18th HKT, Ascona, pp. 70.

Jangpangi, B.S., 1974. Stratography and tectonics of part of Eastern Bhutan. Himalayan Geology, 4: 117-136.

Jangpangi, B.S. (Editor), 1978. Stratigraphy and structure of Bhutan Himalaya. Today and Tomorrow's Printers & Publ., New Delhi, India, 221-241 pp.

Kishore, N. and Kanwar, R.C., 1986. Source and place of origin of Chor Granitoids of Simla Hills of Himachal Pradesh, India. Bulletin - Indian Geologists' Association, 19(2): 103-107.

Kohn, M.J., Catlos, E.J., Ryerson, F.J. and Harrison, T.M., 2001. Pressure-temperature-time path discontinuity in the Main Central thrust zone, central Nepal. Geology, 29(7): 571-574.

Krogh, T.E., 1982. Improved accuracy of U-Pb zircon ages by the creation of more concordant systems using an air abrasion technique. Geochimica et Cosmochimica Acta, 46(4): 637-649.

Kumar, R. and Brookfield, M.E., 1987. Sedimentary environments of the Simla Group (upper Precambrian), Lesser Himalaya, and their palaeotectonic significance. Sedimentary Geology, 52(1-2): 27-43.

Kwatra, S.K., Bhanot, V.B., Kakar, R.K. and Kansal, A.K., 1986. Rb-Sr radiometric ages of the Wangtu gneissic complex, Kinnaur District, higher Himachal Himalaya. Bulletin - Indian Geologists' Association, 19(2): 127-130.

Lahiri, A., 1941. Geology of Buxa Duars. Quarterly Journal of the Geological, Mining and Metallurgical Society of India, 13(1): 1-62.

Lal, R.K., Mukerji, S. and Ackermand, D., 1981. Deformation and Barrovian metamorphism at Takdah, Darjeeling (Eastern Himalaya). In: P.S. Saklani (Editor), Metamorphic tectonites of the Himalaya. (1981). Publisher Today and Tomorrow's, New Delhi, India, pp. 231-278.

Le Fort, P., 1975. Himalayas; the collided range; present knowledge of the continental arc. American Journal of, Science: 1-44.

Le Fort, P. and Upreti, B.N., 1999. Geology of the Nepal Himalaya; recent advances. Journal of Asian Earth Sciences, 17(5-6): 577-849.

Lombardo, B., Pertusati, P. and Borghi, S., 1993. Geology and tectonomagmatic evolution of the eastern Himalaya along the Chomolungma-Makalu transect. In: P.J. Treloar and M.P. Searle (Editors), Himalayan Tectonics. Geological Society of London, London, United Kingdom, pp. 341-355.

Lombardo, B. and Rolfo, F., 2000. Two contrasting eclogite types in the Himalayas: implications for the Himalayan orogeny. Journal of Geodynamics, 30(1-2): 37-60.

Ludwig, K.R., 2003. User's Manual for Isoplot 3:A Geochronological Toolkit for Microsoft Excel. Berkeley Geochronology Center Special Publication No. 4.

Macfarlane, A.M., Hodges, K.V. and Lux, D., 1992. A Structural-Analysis of the Main Central Thrust Zone, Langtang-National-Park, Central Nepal Himalaya. Geological Society of America Bulletin, 104(11): 1389-1402.

Mallet, F.R., 1875. On the geology and mineral resources of the Darjiling District and the western Duars. Memoirs of the Geological Survey of India, 11: 1-50.

Manickavasagam, R.M., Jain, A.K., Singh, S. and Asokan, A., 1999. Metamorphic evolution of the Northwest Himalaya, India; pressure-temperature data, inverted metamorphism, and exhumation in the Kashmir, Himachal, and Garhwal Himalayas. In: A. Macfarlane, R.B. Sorkhabi and J. Quade (Editors), Mountain Roots to Mountain Tops. Geological Society of America (GSA), Boulder, CO, pp. 179-198.

Marquer, D., Chawla, H.S. and Challandes, N., 2000. Pre-alpine high-grade metamorphism in High Himalaya crystalline sequences: Evidence from Lower palaeozoic Kinnaur Kailas granite and surrounding rocks in the Sutlej Valley (Himachal Pradesch, India). Eclogae Geologicae Helvetiae, 93(2): 207-220.

Massey, J., 1994. Fluid circulation and fault controlled magmatism in the Central Himalayas, Open University, Milton Keynes, lots pp.

Mazumdar, A. and Banerjee, D.M., 2001. Regional variations in the carbon isotopic composition of phosphorite from the Early Cambrian Lower Tal Formation, Mussoorie Hills, India. Chemical Geology, 175(1-2): 5-15.

McDermid, I.R.C., Aitchison, J.C., Davis, A.M., Harrison, T.M. and Grove, M., 2002. The Zedong terrane: a Late Jurassic intra-oceanic magmatic arc within the Yarlung-Tsangpo suture zone, southeastern Tibet. Chemical Geology, 187(3-4): 267-277.

McLennan, S.M., McCulloch, M.T., Taylor, S.R. and Maynard, J.B., 1989. Effects of sedimentary sorting on neodymium isotopes in deep-sea turbidites. Nature (London), 337(6207): 547-549.

McLennan, S.M., Taylor, S.R., McCulloch, M.T. and Maynard, J.B., 1990. Geochemical and Nd-Sr isotopic composition of deep-sea turbidites; crustal evolution and plate tectonic associations. Geochimica et Cosmochimica Acta, 54(7): 2015-2050.

Medlicott, H.B., 1864. On the geological structure and relationship of the southern portion of the Himalayan ranges between the Ganges and Ravee. Memoirs of the Geological Survey of India, 3: 1-212.

Meigs, A.J., Burbank, D.W. and Beck, R.A., 1995. Middle-late Miocene (>10 Ma) formation of the Main Boundary thrust in the western Himalaya. Geology, 23(5): 423-426.

Metcalfe, R.P. (Editor), 1993. Pressure, temperature and time constraints on metamorphism across the Main Central Thrust zone and high Himalayan slab in the Garhwal Himalaya. Himalayan tectonics. Geological Society of London, London, United Kingdom, 485-509 pp.

Mezger, K. and Cosca, M.A., 1999. The thermal history of the Eastern Ghats Belt (India) as revealed by U-Pb and (super 40) Ar/ (super 39) Ar dating of metamorphic and magmatic minerals; implications for the SWEAT correlation. Precambrian Research, 94(3-4): 251-271.

Miller, C., Klotzli, U., Frank, W., Thoni, M. and Grasemann, B., 2000. Proterozoic crustal evolution in the NW Himalaya (India) as recorded by circa 1.80 Ga

mafic and 1.84 Ga granitic magmatism. Precambrian Research, 103(3-4): 191-206.

Miller, C., Thoni, M., Frank, W., Grasemann, B., Klotzli, U., Guntli, P., and Draganits, E., 2001. The early Palaeozoic magmatic event in the Northwest Himalaya, India: source, tectonic setting and age of emplacement. Geological Magazine, 138(3): 237-251.

Molnar, P., England, P. and Martinod, J., 1993. Mantle Dynamics, Uplift of the Tibetan Plateau, and the Indian Monsoon. Reviews of Geophysics, 31(4): 357-396.

Mondal, M.E.A., Goswami, J.N., Deomurari, M.P. and Sharma, K.K., 2002. Ion microprobe 207Pb/206Pb ages of zircons from the Bundelkhand massif, northern India: implications for crustal evolution of the Bundelkhand-Aravalli protocontinent. Precambrian Research, 117(1-2): 85-100.

Mugnier, J.L., Leturmy, P., Mascle, G., Huyghe, P., Chalaron, E., Vidal, G., Husson, L., and Delcaillau, B., 1999. The Siwaliks of western Nepal: I. Geometry and kinematics. Journal of Asian Earth Sciences, 17(5-6): 629-642.

Myrow, P.M., Hughes, N. C., Paulsen, T. S., Willlams, I. S., Parcha, S. K., Thompson, K. R., Bowring, S. A., Peng, S. C., and Ahluwalia, A. D., 2003. Integrated tectonostratigraphic analysis of the Himalaya and implications tor its tectonic reconstruction. Earth and Planetary Science Letters, 212(3-4): 433-441.

Najman, Y., Bickle, M. and Chapman, H., 2000. Early Himalayan exhumation: Isotopic constraints from the Indian foreland basin. Terra Nova, 12(1): 28-34.

Najman, Y., Clift, P., Johnson, M.R.W. and Robertson, A.H.F. (Editors), 1993. Early stages of foreland basin evolution in the Lesser Himalaya, N India. Himalayan Tectonics. Geological Society of London, London, United Kingdom, 541-558 pp.

Najman, Y. and Garzanti, E., 2000. Reconstructing early Himalayan tectonic evolution and paleogeography from Tertiary foreland basin sedimentary rocks, northern India. Geological Society of America Bulletin, 112(3): 435-449.

Najman, Y.M.R., Enkin, R.J., Johnson, M.R.W., Robertson, A.H.F. and Baker, J., 1994. Paleomagnetic Dating of the Earliest Continental Himalayan Foredeep Sediments - Implications for Himalayan Evolution. Earth and Planetary Science Letters, 128(3-4): 713-718.

Najman, Y.M.R., Pringle, M.S., Johnson, M.R.W., Robertson, A.H.F. and Wijbrans, J.R., 1997. Laser Ar-40/Ar-39 dating of single detrital muscovite grains from early foreland-basin sedimentary deposits in India: Implications for early Himalayan evolution. Geology, 25(6): 535-538.

Naqvi, S.M. and Rogers, J.J.W. (Editors), 1987. Precambrian geology of India. Oxford Monographs on Geology and Geophysics No. 6. Oxford Univ. Press, New York, NY, 223 pp.

Nautiyal, S.P. Jangpangi, B. S., Singh, P., Guha S. T. K., Bhate, V. D., Raghavan, M. R. and Sahai, T. N., 1964. A preliminary note on the geology of Bhutan Himalaya, International Geological Congress, [location varies], pp. 1-14.

Ni, J. and Barazangi, M., 1985. Active tectonics of the western Tethyan Himalaya above the underthrusting Indian Plate; the upper Sutlej River basin as a pull-apart structure. Tectonophysics, 112: 277-295.

Noble, S.R., Searle, M.P. and Walker, C.B., 2001. Age and tectonic significance of Permian granites in western Zanskar, High Himalaya. Journal of Geology, 109(1): 127-135.

Noble, S.R., Tucker, R.D. and Pharaoh, T.C., 1993. Lower Paleozoic and Precambrian Igneous Rocks from Eastern England, and Their Bearing on Late Ordovician Closure of the Tornquist Sea - Constraints from U-Pb and Nd Isotopes. Geological Magazine, 130(6): 835-846.

Nutman, A.P., Cordani, U.G. and Sabate, P., 1994. SHRIMP U-Pb ages of detrital zircons from the early proterozoic Contendas-Mirante supracrustal belt, Sao Francisco Craton, Bahia, Brazil. Journal of South American Earth Sciences, 7(2): 109-114.

Pandey, A.K., Sachan, H.K. and Virdi, N.S., 2004. Exhumation history of a shear zone constrained by microstructural and fluid inclusion techniques: an example from the Satluj valley, NW Himalaya, India. Journal of Asian Earth Sciences, 23(3): 391-406.

Pandit, M.K., Carter, L. M., Ashwal, L. D., Tucker, R. D., Torsvik, T. H., Jamtveit, B., and Bhushan, S. K., 2003. Age, petrogenesis and significance of 1Ga granitoids and related rocks from the Sendra area, Aravalli Craton, NW India. Journal of Asian Earth Sciences, 22(4): 363-381.

Pant, C.C. and Shukla, U.K., 1999. Nagthat Formation: An example of a progradational, tide- dominated Proterozoic succession in Kumaun Lesser Himalaya, India. Journal of Asian Earth Sciences, 17(3): 353-368.

Parrish, R.R., 1990. U-Pb Dating of Monazite and Its Application to Geological Problems. Canadian Journal of Earth Sciences, 27(11): 1431-1450.

Parrish, R.R. and Hodges, K.V., 1996. Isotopic constraints on the age and provenance of the Lesser and Greater Himalayan sequences, Nepalese Himalaya. Geological Society of America Bulletin, 108(7): 904-911.

Parrish, R.R. and Krogh, T.E., 1987. Synthesis and Purification of Pb-205 for U-Pb Geochronology. Chemical Geology, 66(1-2): 103-110.

Parrish, R.R. and Noble, S.R., 2003. Zircon U-Th-Pb geochronology by isotope dilution - Thermal Ionization Mass Spectrometry (ID-TIMS). In: J.M. Hanchar and P.W.O. Hoskin (Editors), Zircon. Reviews in Mineralogy & Geochemistry. MINERALOGICAL SOC AMERICA, Washington, pp. 183-213.

Paudel, L.P. and Arita, K., 2000. Tectonic and polymetamorphic history of the Lesser Himalaya is central Nepal. Journal of Asian Earth Sciences, 18(5): 561-584.

Pearson, O.N., 2002. Structural evolution of the central Nepal fold-thrust belt and regional tectonic and structural significance of the Ramgarh Thrust. Doctoral Thesis, University of Arizona, Tucson, AZ, 231 pp.

Pecher, A. and Jest, C. (Editors), 1977. Geology of the Nepal Himalaya; deformation and petrography in the main central thrust zone. Centre National de la Recherche Scientifique, Paris, France, 301-318 pp.

Pilgrim, G.E., 1906. Notes on the geology of a portion of Bhutan. Records of the Geological Survey of India, 34(1): 22-30.

Pilgrim, G.E. and West, W.D., 1928. The structure and correlation of the Simla rocks. Memoirs of the Geological Survey of India, 53: 1-140.

Platt, J.P. and England, P.C., 1994. Convective Removal of Lithosphere beneath Mountain Belts - Thermal and Mechanical Consequences. American Journal of Science, 294(3): 307-336.

Pognante, U. and Spencer, D.A., 1991. 1st Report of Eclogites from the Himalayan Belt, Kaghan Valley (Northern Pakistan). European Journal of Mineralogy, 3(3): 613-618.

Pogue, K.R., Hylland, M.D., Yeats, R.S., Khattak, W.U. and Hussain, A., 1999. Stratigraphic and structural framework of Himalayan foothills, northern Pakistan. In: A. Macfarlane, R.B. Sorkhabi and J. Quade (Editors), Mountain Roots to Mountain Tops. Geological Society of America (GSA), Boulder, CO, pp. 257-274.

Potts, P.J., Tindle, A.G. and Webb, P.C., 1992. Geochemical Reference Material Compositions: Rocks, Minerals, Sediments, Soils, Carbonates, Refractories and Ores Used in Research and Industry. Whittles Publishing, 313 pp.

Prince, C., 1998. Controls on and timing of metamorphism in the Himalaya [abs]. Mineralogical Magazine, 127: 1210-1211.

Prince, C., 1999. The timing of prograde metamorphism in the Garhwal Himalaya, India, Open University, Milton Keynes, 308 pp.

Raha, P.K. and Sastry, M.V.A., 1982. Stromatolites and Precambrian stratigraphy in India. Precambrian Research, 18(4): 293-318.

Raina, B.N., 1981. Need for re-interpretation of the geology of the Simla area: Some suggestions. In: A.K. Sinha (Editor), Contemporary Geoscientific Researches in Hiamalaya. Bishen Singh and Mahender Pal Singh, Dehra Dun (India), pp. 101-108.

Rashid, S.A., 2002. Geochemical characteristics of Mesoproterozoic clastic sedimentary rocks from the Chakrata Formation, Lesser Himalaya: implications for crustal evolution and weathering history in the Himalaya. Journal of Asian Earth Sciences, 21(3): 283-293.

Ratschbacher, L., Frisch, W., Liu, G.H. and Chen, C.S., 1994. Distributed Deformation in Southern and Western Tibet During and after the India-Asia Collision. Journal of Geophysical Research-Solid Earth, 99(B10): 19917-19945.

Ray, S. and Chakraborty, T., 2002. Lower Gondwana fluvial succession of the Pench-Kanhan Valley, India; stratigraphic architecture and depositional controls. Sedimentary Geology, 151(3-4): 243-271.

Ray, S.K., Bandyopadhyay, B.K. and Razdan, R.K., 1989. Tectonics of a Part of the Shumar Allochthon in Eastern Bhutan. Tectonophysics, 169(1-3): 51-58.

Rickers, K., Mezger, K. and Raith, M.M., 2001. Evolution of the continental crust in the Proterozoic Eastern Ghats Belt, India and new constraints for Rodinia reconstruction; implications from Sm-Nd, Rb-Sr and Pb-Pb isotopes. Precambrian Research, 112(3-4): 183-210.

Robinson, D.M., DeCelles, P.G., Patchett, P.J. and Garzione, C.N., 2001. The kinematic evolution of the Nepalese Himalaya interpreted from Nd isotopes. Earth and Planetary Science Letters, 192(4): 507-521.

Rollinson, H.R., 1993. Using geochemical data; evaluation, presentation, interpretation. Harlow, Longman Scientific & Technical, United Kingdom, 352 pp.

Roser, B.P. and Korsch, R.J., 1986. Determination of tectonic setting of sandstone-mudstone suites using SiO (sub 2 content and K (sub 2O/Na (sub 2O ratios. Journal of Geology, 94(5): 635-650.

Roser, B.P. and Korsch, R.J., 1988. Provenance signatures of sandstone-mudstone suites determined using discriminant function analysis of major-element data. Chemical Geology, 67(1-2): 119-139.

Ross, G.M. and Parrish, R.R., 1992. Detrital zircon geochronology of metasedimentary rocks in the southern Omineca Belt, Canadian Cordillera. Precambrian basement of the Canadian Cordillera; isotopic insights--Le sous-sol precambrien de la Cordillere canadienne; techniques isotopiques Canadian Journal of Earth Sciences = Journal Canadien des Sciences de la Terre, 28(8): 1254-1270.

Rowley, D.B., 1996. Age of initiation of collision between India and Asia: A review of stratigraphic data. Earth and Planetary Science Letters, 145(1-4): 1-13.

Royden, L. H., Burchfiel, B. C., King, R. W.,Wang, E., Chen, Z., Shen, F., and Liu,Y., 1997, Surface deformation and lower crustal flow in eastern Tibet, Science, 276, 788–790.

Schelling, D., 1992. The Tectonostratigraphy and Structure of the Eastern Nepal Himalaya. Tectonics, 11(5): 925-943.

Schelling, D. and Arita, K., 1991. Thrust Tectonics, Crustal Shortening, and the Structure of the Far-Eastern Nepal Himalaya. Tectonics, 10(5): 851-862.

Searle, M., Corfield, R.I., Stephenson, B. and McCarron, J., 1997a. Structure of the North Indian continental margin in the Ladakh- Zanskar Himalayas: Implications for the timing of obduction of the Spontang ophiolite, India-Asia collision and deformation events in the Himalaya. Geological Magazine, 134(3): 297-316.

Searle, M.P., 1986. Structural Evolution and Sequence of Thrusting in the High Himalayan, Tibetan-Tethys and Indus Suture Zones of Zanskar and Ladakh, Western Himalaya. Journal of Structural Geology, 8(8): 923-&.

Searle, M., 1995, The rise and fall of Tibet, Nature, 374, 17–18.

Searle, M.P., 1999. Extensional and compressional faults in the Everest-Lhotse Massif, Khumbu Himalaya, Nepal. Journal of the Geological Society of London, 156: 227-240.

Searle, M.P. and Godin, L., 2003. The South Tibetan Detachment and the Manaslu Leucogranite: A structural reinterpretation and restoration of the Annapurna-Manaslu Himalaya, Nepal. Journal of Geology, 111(5): 505-523.

Searle, M.P., Khan, M.A., Fraser, J.E., Gough, S.J. and Jan, M.Q., 1999. The tectonic evolution of the Kohistan-Karakoram collision belt along the Karakoram Highway transect, north Pakistan. Tectonics, 18(6): 929-949.

Searle, M.P., Parrish, R. R., Hodges, K. V., Hurford, A., Ayres, M. W., and Whitehouse, M. J., 1997b. Shisha Pangma leucogranite, south Tibetan Himalaya: Field

relations, geochemistry, age, origin, and emplacement. Journal of Geology, 105(3): 295-317.

Searle, M.P., Simpson, R.L., Law, R.D., Parrish, R.R. and Waters, D.J., 2003. The structural geometry, metamorphic and magmatic evolution of the Everest massif, High Himalaya of Nepal-South Tibet. Journal of the Geological Society, 160: 345-366.

Sharma, K.K., 1998. Geologic and tectonic evolution of the Himalaya before and after the India- Asia collision. Proc. Indian. Acad. Sci. (Earth Planet. Sci.), 107: 265-282.

Sharma, V.P., 1977. Geology of the Kulu Rampur Belt, Himachal Pradesh. Memoirs of the Geological Survey of India, 106: 235-407.

Shaw, R.K., Arima, M., Kagami, H., Fanning, C. M., Shiraishi, K., and Motoyoshi, Y., 1997. Proterozoic events in the Eastern Ghats granulite belt, India; evidence from Rb-Sr, Sm-Nd systematics, and SHRIMP dating. Journal of Geology, 105(5): 645-656.

Simpson, R.L., Parrish, R.R., Searle, M.P. and Waters, D.J., 2000. Two episodes of monazite crystallization during metamorphism and crustal melting in the Everest region of the Nepalese Himalaya. Geology, 28(5): 403-406.

Singh, I.B., 1979. Environment and age of the Tal Formation of Mussorie and Nilkanth areas of Garhwal Himalaya. Journal of the Geological Society of India, 20(5): 214-225.

Singh, P., 1973. A note on the fossiliferous formations in Lesser Himalaya of Nepal and Bhutan. Himalayan Geology, 3: 372-380.

Singh, S., Barley, M.E., Brown, S.J., Jain, A.K. and Manickavasagam, R.M., 2002. SHRIMP U-Pb in zircon geochronology of the Chor granitoid: evidence for Neoproterozoic magmatism in the Lesser Himalayan granite belt of NW India. Precambrian Research, 118(3-4): 285-292.

Singh, S., Claesson, S., Jain, A. K., Sjoberg, H., Gee, D., Manickavasagam, R. M., and Andreasson, P. G., 1994. Geochemistry of the Proterozoic peraluminous granitoids from the Higher Himalayan Crystalline (HHC) and Jutogh Nappe, NW-Himalaya, Himachal Pradesh, India. 9th Himalaya-Karakorum-Tibet workshop; abstract volume Journal of Nepal Geological Society, 10: 125.

Singh, S. and Jain, A.K., 1996. Ductile shearing of the Proterozoic Chor granitoid in the Lesser Himalaya and its tectonic significance. Journal of the Geological Society of India, 47(1): 133-138.

Singh, S. and Jain, A.K., 2003. Himalayan Granitoids. In: S. Singh (Editor), Granitoids of the Himalayan Collisional Belt. Journal of the Virtual Explorer,, pp. 1-20.

Singh, S.K., Trivedi, J.R. and Krishnaswami, S., 1999. Re-Os isotope systematics in black shales from the Lesser Himalaya: Their chronology and role in the Os-187/Os-188 evolution of seawater. Geochimica Et Cosmochimica Acta, 63(16): 2381-2392.

Sinha-Roy, S. and Sen Gupta, S., 1986. Precambrian deformed granites of possible basement in the Himalayas. Precambrian Research, 31(3): 209-235.

Spicer, R.A., Harris, N. B. W., Widdowson, M., Herman, A. B., Guo, S. X., Valdes, P. J., Wolfe, J. A. and Kelley, S. P., 2003. Constant elevation of southern Tibet over the past 15 million years. Nature, 421(6923): 622-624.

Srikantia, S.V. and Bhargava, O.N., 1974. The 'Jaunsar' problem in the Himalaya; a critical analysis and elucidation. Journal of the Geological Society of India, 15(2): 115-136.

Srikantia, S.V. and Razdan, M.L., 1981. Shilakong Ophiolite Nappe of Zanskar Mountains, Ladakh Himalaya. Journal of the Geological Society of India, 22(5): 227-234.

Srikantia, S.V. and Sharma, R.P., 1971. Simla group; a reclassification of the 'Chail series', 'Jaunsar series' and 'Simla slates' in the Simla Himalaya. Journal of the Geological Society of India, 12(3): 234-240.

Srivastava, P. and Mitra, G., 1994. Thrust Geometries and Deep-Structure of the Outer and Lesser Himalaya, Kumaon and Garhwal (India) - Implications for Evolution of the Himalayan Fold-and-Thrust Belt. Tectonics, 13(1): 89-109.

Steck, A., Spring, L., Vannay, J. C., Masson, H., Stutz, E., Bucher, H., Marchant, R., and Tieche, J. C., 1993. Geological Transect across the Northwestern Himalaya in Eastern Ladakh and Lahul (a Model for the Continental Collision of India and Asia). Eclogae Geologicae Helvetiae, 86(1): 219-&.

Steiger, R.H. and Jäger, E., 1977. Subcommission on Geochronology: Convention on the use of decay contants in geo- and cosmochronolgy. Earth and Planetary Science Letters, 36: 359-362.

Stephenson, B.J., Waters, D.J. and Searle, M.P., 2000. Inverted metamorphism and the main central thrust: field relations and thermobarometric constraints from the Kishtwar Window, NW Indian Himalaya. Journal of Metamorphic Geology, 18(5): 571-590.

Stoecklin, J., 1980. Geology of Nepal and its regional frame. Journal of the Geological Society of London, 137: 1-34.

Stuewe, K. and Foster, D., 2001. (super 40) Ar/ (super 39) Ar, pressure, temperature and fission track constraints on the age and nature of metamorphism around the main central thrust in the eastern Bhutan Himalaya. Journal of Asian Earth Sciences, 19(1-2): 85-95.

Swapp, S.M. and Hollister, L.S., 1991. Inverted Metamorphism within the Tibetan Slab of Bhutan - Evidence for a Tectonically Transported Heat-Source. Canadian Mineralogist, 29: 1019-1041.

Termier, G. and Gansser, A., 1974. Les series devoniennes du Tang Chu (Himalaya du Bhoutan). Eclogae Geologicae Helvetiae, 67(3): 587-596.

Tewari, V.C., 1984. Stromatolites and Precambrian-Lower Cambrian biostratigraphy of the Lesser Himalaya, India. In: R.S. Tiwari, N. Awasti and S.C. Srivastava (Editors). Palaeobot. Soc., Lucknow, India, pp. 71-97.

Thakur, V.C., 1992. Geology of Western Himalaya. Physics and Chemistry of the Earth, 19. Pergamon, International, Oxford-New York-Toronto, 366 pp.

Thakur, V.C., 1998. Structure of the Chamba nappe and position of the main central thrust in Kashmir Himalaya. Journal of Asian Earth Sciences, 16(2-3): 269-282.

Thakur, V.C. and Rawat, B.S., 1992. Geological map of Western Himalaya. Wadia Institute of Himalayan Geology, Dehra Dun.

Thimm, K., 2000. Diploma Thesis; Provenance, metamorphism and deformation of the Himalayas: Evidence from U-Pb TIMS dating of samples from the Main Central Thrust and Lesser and Greater Himalayan sequences in Bhutan, eastern Himalayas., Johannes Gutenbeg-Universitat, Mainz, Germany.

Tilmann, F., Ni, James, Hearn, T., Ma, Y. S., Rapine, R., Kind, R., Mechie, J., Saul, J., Haines, S., Klemperer, S., Brown, L., Pananont, P., Ross, A., Nelson, K. D., Guo, J., and Zhao, W., 2003. Seismic imaging of the downwelling Indian lithosphere beneath central Tibet. Science, 300(5624): 1424-1427.

Tiwari, M., 1999. Organic-walled microfossils from the Chert-phosphorite Member, Tal Formation, Precambrian-Cambrian Boundary, India. Precambrian Research, 97(1-2): 99-113.

Tiwari, M., Pant, C.C. and Tewari, V.C., 2000. Neoproterozoic sponge spicules and organic-walled microfossils from the Gangolihat Dolomite, Lesser Himalaya, India. Current Science, 79(5): 651-654.

Turnbull, M.J.M., Whitehouse, M.J. and Moorbath, S., 1996. New isotopic age determinations for the Torridonian, NW Scotland. Journal of the Geological Society, 153: 955-964.

Upreti, B.N., 1999. An overview of the stratigraphy and tectonics of the Nepal Himalaya. Journal of Asian Earth Sciences, 17(5-6): 577-606.

Upreti, B.N. and Le Fort, P., 1999. Lesser Himalayan crystalline nappes of Nepal; problems of their origin. In: A. Macfarlane, R.B. Sorkhabi and J. Quade (Editors), Mountian Roots to Mountian Tops. Geological Society of America (GSA), Boulder, CO, pp. 225-238.

Valdiya, K.S., 1979. An outline of the structural set-up of the Kumaun Himalaya. Field guide to a traverse in the north-western Irish Caledonides Ireland, Geological Survey, Guide Series. Dublin. Journal of the Geological Society of India, 20(4): 145-157.

Valdiya, K.S., 1980. The two intracrustal boundary thrusts of the Himalaya. Tectonophysics, 66(4): 323-348.

Valdiya, K.S., 1995. Proterozoic Sedimentation and Pan-African Geodynamic Development in the Himalaya. Precambrian Research, 74(1-2): 35-55.

Van Schmus, W.R., De Brito Neves, B. B., Williams, I. S., Hackspacher, P. C., Fetter, A. H., Dantas, E. L., and Babinski, M., 2003. The Serido Group of NE Brazil, a late Neoproterozoic pre- to syn-collisional basin in West Gondwana: insights from SHRIMP U-Pb detrital zircon ages and Sm-Nd crustal residence (TDM) ages. Precambrian Research, 127(4): 287-327.

Vance, D. and Harris, N., 1999. Timing of prograde metamorphism in the Zanskar Himalaya. Geology, 27(5): 395-398.

Vance, D. and Mahar, E., 1998. Pressure-temperature paths from P-T pseudosections and zoned garnets: Potential, limitations and examples from the Zanskar Himalaya, NW India. Contributions to Mineralogy and Petrology, 132(3): 225-245.

Vannay, J.C. and Grasemann, B., 1998. Inverted metamorphism in the High Himalaya of Himachal Pradesh (NW India): Phase equilibria versus thermobarometry. Schweiz. Mineral. Petrog. Mitt., 78: 107-132.

Vannay, J.C. and Grasemann, B., 2001. Himalayan inverted metamorphism and syn-convergence extension as a consequence of a general shear extrusion. Geol. Mag., 138(3): 253-276.

Vannay, J.C., Grasemann, B., Rahn, M., Frank, W., Carter, A., Baudraz, V., and Cosca, M., 2004. Miocene to Holocene exhumation of metamorphic crustal wedges in the NW Himalaya: Evidence for tectonic extrusion coupled to fluvial erosion. Tectonics, 23(1): art. no.-TC1014.

Vannay, J.C. and Hodges, K.V., 1996. Tectonometamorphic evolution of the Himalayan metamorphic core between the Annapurna and Dhaulagiri, central Nepal. Journal of Metamorphic Geology, 14(5): 635-656.

Vannay, J.C., Sharp, Z.D. and Grasemann, B., 1999. Himalayan inverted metamorphism constrained by oxygen isotope thermometry. Contributions to Mineralogy and Petrology, 137(1-2): 90-101.

Virdi, N.S., 1976. Stratigraphy and structure of the area around Nirath, district Shimal, Himachal Pradesh. Himalayan Geology, 6: 163-175.

Wetherill, G.W., 1956. Discordant uranium-lead ages. American Geophysical Transactions, 37: 320-326.

Wheeler, J., Treloar, P.J. and Potts, G.J., 1995. Structural and metamorphic evolution of the Nanga Parbat syntaxis, Pakistan Himalayas, on the Indus gorge transect: The importance of early events. Geological Journal, 30(3-4): 349-371.

White, N.M., Pringle, M., Garzanti, E., Bickle, M., Najman, Y., Chapman, H., and Friend, P., 2002. Constraints on the exhumation and erosion of the High Himalayan Slab, NW India, from foreland basin deposits. Earth and Planetary Science Letters, 195(1-2): 29-44.

Whittington, A., Foster, G., Harris, N., Vance, D. and Ayres, M., 1999. Lithostratigraphic correlations in the western Himalaya - An isotopic approach. Geology, 27(7): 585-588.

Wiedenbeck, M., Goswami, J.N. and Roy, A.B., 1996. Stabilization of the Aravalli Craton of northwestern India at 2.5 Ga; an ion microprobe zircon study. Chemical Geology, 129(3-4): 325-340.

Wiesmayr, G. and Grasemann, B., 2002. Eohimalayan fold and thrust belt: Implications for the geodynamic evolution of the NW-Himalaya (India). Tectonics, 21(6): art. no.-1058.

Windley, B.F., 1995. The Evolving Contintents. John Wiley & Sons, 526 pp.

Wu, C.D., Nelson, K. D., Wortman, G., Samson, S. D., Yue, Y. J., Li, J. X., Kidd, W. S. F., and Edwards, M. A., 1998. Yadong cross structure and South Tibetan Detachment in the east central Himalaya (89 degrees-90 degrees E). Tectonics, 17(1): 28-45.

York, D., 1969. Least squares fitting of a straight line with correlated errors. Earth and Planetary Science Letters, 5(5): 320-324.

Zhao, W.J. and Nelson, K.D., 1993. Deep Seismic-Reflection Evidence for Continental Underthrusting beneath Southern Tibet. Nature, 366(6455): 557-559.

Appendix A - Analytical Techniques

A 1 Whole Rock Elemental analyses

A 1.1 Sample Selection

Samples collected were ideally of siltstone/mudstone protolith; sandstones and quartzites were also collected. Carbonate rocks were avoided due to generally perturbed Sr isotope ratios (as suggested by Ahmad et al. 2000); rocks where tested in the field with their reaction to 6M HCL. Samples were later rejected after laboratory tests that included: greater than 4% emission during loss on ignition testing, and $^{147}Sm/^{144}Nd$ ratios greater than 0.14, implying fractionation.

A 1.2 Sample Preparation

Weathered surfaces were removed in the field to reduce shipping costs. The samples were split into <3 cm pieces and crushed in a hardened steel jaw crusher. A representative 100g portion of the crushate was then powdered in an agate Tema mill for between 10-20 minutes until a powder of < 200 µm mesh grain size is achieved. Powders were dried for a minimum of 24 hours prior to any analytical procedure.

A 1.3 Major and Trace Element Analysis

A 1.3.1 X-Ray Fluorescence (XRF)

Whole rock major and trace elements were analysed on an ARL Fisons wavelength-dispersive XRF spectrometer at the Open University. Elemental intensities were corrected for background and known peak interferences, and instrument drift was accounted for using a drift monitor. Count times for most trace elements were selected to achieve 2 sigma precision better than 2 ppm or 2% relative at concentrations >100ppm. Major elements were determined using glass discs prepared by fusing a 5:1 ratio of powdered sample with lithium meta/tetraborate flux

(Spectroflux 105). The mixture was fired in platinum-gold crucibles in a furnace at 1100°C for 20 minutes, stirring every 5 minutes to remove air bubbles. The mixture was poured into a pre-heated mould and formed using a sprung press. 'Loss on ignitions' where calculated by percentage weight loss after igniting the powdered sample at 1000°C in ceramic crucibles for 30 minutes. Trace elements were determined from pressed powder pellets formed by mixing thoroughly 9-10g of sample with 7ml of (PVP)-methyl cellulose binder (using the 'bag technique' developed by J. Watson, at The Open University). The powder pellets were dried overnight at 80-100°C prior to analysis.

A 1.3.2 Inductively Coupled Plasma-Mass Spectrometry (ICP-MS)

Where required, additional trace elements (REE, Ta, Hf, Th and U) were analysed by ICP-MS. ICP-MS solutions were prepared using the method outlined in Table A.1.1. The solutions were analysed using an Agilent 7500s ICP-MS instrument, fitted with a Babington nebuliser operating at a flow rate of 0.4 ml min^{-1}. Internal standards (Be, Rh, In, Tm, Re and Bi) were added on-line using a second peristaltic pump, and residual drift for individual elements was assessed and corrected using repeat analyses of selected sample solutions. Standards used for calibration were AC2/10, AGV-1, BHVO-1, BIR-1, GSP-1 and WS-E; within-run precision was determined using repeat analyses of a standard and sample. In general, within-run precision is better than 2% r.s.d for all elements and often better than 1%. (Accuracy is difficult to assess because of the relatively poor reproducibility of granite reference materials. However, a comparison of the results presented here for AC-E with the compilation from Potts et al. [13], suggests good agreement.)

Table A.1.1 - Flow Chart for digestion of sample for ICP-MS and isotope analysis.

Weigh accurately 0.1g of sample onto weighing paper

↓

Destatic bomb and add 0.1g of sample

↓

add 1ml 15M HNO3

↓

add 4 ml conc. HF

↓

hotplate at 120°C for 48 hours

↓

evaporate to incipient dryness

↓

add 2ml 15M HNO3 & 4ml MQ H2O

↓

hotplate at 120°C for 24 hours

↓

evaporate to incipient dryness

↓

add 3ml 15M HNO3 & 6ml MQ H2O

↓

hotplate for 4 hours (lid on)

↓

weight 125ml labelled bottle (no top)

↓

add dissolved sample to bottle, rinse out Savillex® 3 times

↓

weigh sample and bottle (g)

↓

Calculate weight of water to be added for 100g and add relevant MQ water

You now have a 1000 fold dilution of sample in 2% HNO3 for ICP-MS

↓

Dry down 50 ml of sample in either clean beaker or pre-contaminated

Savillex® bomb

↓

Once dry, convert to chlorides by adding 2 ml of QD 6M HCl and dry down

↓

Once dry add 2 ml of QD 2.5 M HCl

↓

Store 1 ml in micro capsule, use 1 ml for Sr and REE columns

A 1.4 - Isotope Analysis

Rb-Sr and Sm-Nd isotope analysis was performed at the NERC Isotope Geoscience Laboratory (NIGL) and The Open University. The analytical protocol for sample digestion and preparation was different at each laboratory as isotope dilution was

carried out at NIGL, whereas isotope composition was carried out at The Open University. In both procedures, Rb-Sr concentrations where measured by XRF, whereas Sm-Nd concentrations were measured by isotope dilution at NIGL, and ICP-MS at The Open University.

A 1.4.1 - Isotope Analysis: Chemical separation and mass spectrometry at NIGL

Samples for Rb-Sr and Sm-Nd analysis were spiked with ^{150}Nd and ^{147}Sm isotopically enriched tracers and decomposed using HF in sealed Teflon bombs at 120°C. Following treatment with HNO_3 and conversion to the chloride form with 6 M HCL, Sr and the REE were separated by standard ion exchange procedures using Biorad® AG50W-X8 ion exchange resin. Sm and Nd were separated from REE fraction by reversed-phase ion chromatography on a column filled with Biobeads® coated with di-2-ethlyhexyl orthophosphoric acid (HDEHP) (e.g. Darbyshire and Sewell, 1997). Procedural blanks were less that 1.3 ng for Sr and 0.3 ng for Nd.

Isotope ratio measurements were made on a Finnigan-MAT 262 Thermal Ionization Mass Spectrometer (TIMS) at NIGL. Errors are quoted throughout as two standard deviations from the measured or calculated values. Analytical uncertainties are estimated to be ± 0.01% for $^{143}Nd/^{144}Nd$ and $^{87}Sr/^{86}Sr$ ratios and ± 1% for both the $^{147}Sm/^{144}Nd$ and $^{87}Rb/^{86}Sr$ ratios. Measured $^{143}Nd/^{144}Nd$ were corrected for mass fractionation relative to $^{146}Nd/^{144}Nd = 0.7219$, and $^{87}Sr/^{86}Sr$ ratios relative to $^{87}Sr/^{86}Sr = 0.1194$. Replicate analyses (n=43) of Johnson and Matthey® Nd standard made during the period of study yielded a mean $^{143}Nd/^{144}Nd$ ratio of 0.511202 ± 0.000082 (to 2 standard deviations). The average $^{87}Sr/^{86}Sr$ determined for the NBS 987 Sr isotope standard was 0.710230 ± 0.000030 (to 2 standard deviations, n=55).

A 1.4.2 - Isotope Analysis: Chemical separation and mass spectrometry at The Open University

Samples were digested using the technique described in Table A.1.1. (developed by N. Rogers, at The Open University). This technique allows the same digested sample to be used in both ICP-MS and TIMS analysis. Once digested and converted to chlorides (Table A.1.1.) the chemical separation of Sr and Nd is similar to Argles et al. (2003) and Cohen et al. (1988).

Nd and Sr isotope ratios were collected on a Thermo-Finnigan Triton TIMS at the Department of Earth Sciences, Open University. Strontium was loaded in phosphoric acid on single Ta filaments, and the measured $^{87}Sr/^{86}Sr$ ratios were exponentially fractionation corrected within each run to $^{87}Sr/^{88}Sr = 0.1194$. Repeat analyses of the NBS987 Sr standard gave $^{87}Sr/^{86}Sr$ ratios of 0.710234 ± 0.000018 (2 sigma error, n=47) over the analysis period. Total procedural Sr blanks were less than 0.8 ng. $^{87}Rb/^{86}Sr$ ratios were calculated from elemental ratios obtained by XRF.

Neodymium was loaded on Ta filaments (a Re ionisation filament was used) and run as metal ions. $^{143}Nd/^{144}Nd$ ratios were normalised to $^{146}Nd/^{144}Nd = 0.7219$. Repeat analyses of the Johnson-Matthey® internal standard gave 0.511823 ± 0.000018 (2 sigma error, n=54) for a 3 month period during the period of sample analysis. Total procedural Nd blanks were less than 0.5 ng. $^{147}Sm/^{144}Nd$ ratios were calculated from elemental ratios obtained from ICP-MS.

A 1.4.3 - Corrections and constants

$^{87}Rb/^{86}Sr$ and $^{147}Sm/^{144}Nd$ were calculated for each sample using the De Paolo and Wasserburg (1976b) method.

Equation 1:

$$T_{CHUR} = 1/\lambda \cdot \ln \frac{(^{143}Nd/^{144}Nd)^0_{sample} - (^{143}Nd/^{144}Nd)^0_{CHUR}}{(^{147}Sm/^{144}Nd)^0_{sample} - (^{147}Sm/^{144}Nd)^0_{CHUR}} + 1$$

Equation 2:

$$T_{DM} = 1/\lambda \,.\ln \frac{(^{143}Nd/^{144}Nd)^{0}_{sample} - (^{143}Nd/^{144}Nd)^{0}_{DM}}{(^{147}Sm/^{144}Nd)^{0}_{sample} - (^{147}Sm/^{144}Nd)^{0}_{DM}} + 1$$

Equation 3:

$$\varepsilon_{Nd} = \frac{(^{143}Nd/^{144}Nd)_{sample} - (^{143}Nd/^{144}Nd)_{CHUR}}{(^{143}Nd/^{144}Nd)_{CHUR}} \times 10^{4}$$

ε_{Nd} (T) can be calculated, which is the derivation from the value of CHUR at a specified time (T) and is calculated in Equation 4 (appendix A).

Equation 4:

$$\varepsilon_{Nd}(T) = \frac{(^{143}Nd/^{144}Nd)_{sample}(T) - (^{143}Nd/^{144}Nd)_{CHUR}(T)}{(^{143}Nd/^{144}Nd)_{CHUR}(T)} \times 10^{4}$$

The following constants have been used:

$$^{147}Sm/^{144}Nd_{CHUR} = 0.1967$$

$$^{143}Nd/^{144}Nd_{CHUR} = 0.512638$$

A 2 Mineral separates Analysis

A 2.1 Sample Selection

Medium to coarse grained psammites and quartzites were sampled preferentially for single grain zircon analysis, as the average grain size of a sediment is assumed to reflect the size of the zircon crystals within it, coarse grained rocks are used to extract zircons of a size that allows individual crystal analysis.

A 2.2 Sample Preparation

Samples suitable for zircon analysis were crushed and disc milled. After sieving the <250 µm fraction was simultaneously washed and the heavy mineral component was extracted on a Gemeni Shaking table, followed by several runs on a superpanner. Separates where then passed through methylene iodide (di-idomethane) and the

fraction >3.33 g cm^{-3} was removed, washed and dried prior to magnetic separation using a Frantz LB-1 magnetic separator. Zircons from the non-magnetic at 1.8 A fraction were hand picked in pure alcohol and air-abraded in pyrite to remove rims (Krogh, 1982).

A 2.3 Isotope Analysis

Minerals were analysed by ID-TIMS methods on single or small numbers of grains using a ^{205}Pb-^{233}U-^{235}U tracer and a VG354 mass spectrometers using single Re filaments and arrays of both faraday and ion counting detectors. Chemical and mass spectrometric methods were similar to Parrish et al. (1987) and Noble et al. (1993). Pb blanks which averaged less than 30 pg. Decay constants for ^{238}U and ^{235}U used are those recommended by Steiger and Jäger (1978). Off line processing was performed using HTB.

Appendix B – Whole-Rock Geochemical Data

This appendix contains all the geochemical whole rock data from samples collected during the course of this study. This appendix includes XRF, ICP and Rb-Sr and Sm-Nd isotope analysis.

Notes in table:

- Sample numbers with prefix "W" and "B" indicates samples collected from the Sutlej and Bhutan sections respectively.
- Sample numbers with prefix "ED", "LG" and "KD" or "SD" correspond to samples collected by Erich Draganits, Lauren Godin and Nigel Harris, respectively.
- * indicates unrealistic model Nd age due to elevated Sm/Nd ratio, therefore "ND" (not determined).
- Major and trace XRF data from samples with prefix ED courtesy of E. Draganits, analysed at Department of Geological Sciences, University of Vienna, whereas REE and isotope composition determinations were carried out by the author at The Open University.
- $\varepsilon_{(Nd)}t$ = age corrected to 500 Ma.
- (87/86)t = $^{87}Sr/^{86}Sr$, age corrected to 500 Ma

Table B.1 whole-rock geochemical data, Sutlej and Bhutan sections.

Sample No.	W03	W06	W18	W19	W25b	W30.1	W35	W36
Rock type								
Wt %								
SiO_2	76.6	67.7	68.1	77.2	52.3	63.5	75.8	74.8
TiO_2	0.6	0.7	0.4	0.7	0.9	1.0	0.7	0.7
Al_2O_2	10.3	13.8	10.5	9.4	16.3	18.4	11.0	10.8
Fe_2O_2	3.6	5.5	3.2	4.4	9.7	7.6	4.8	4.6
MnO	0.0	0.1	0.1	0.1	0.2	0.2	0.1	0.1
MgO	2.9	3.0	1.4	1.5	8.3	2.3	1.6	2.6
CaO	0.3	2.2	6.4	1.6	8.9	0.9	1.5	2.2
Na_2O	2.0	2.5	3.0	2.0	1.0	1.7	2.4	1.8
K_2O	2.4	2.9	1.6	2.1	1.3	3.8	2.0	2.3
P_2O_5	0.1	0.2	0.1	0.1	0.1	0.2	0.1	0.2
LOI	1.5	1.6	6.2	1.8	1.3	1.1	0.7	0.5
Total	100.5	100.1	101.2	100.9	100.4	100.6	100.7	100.5
ppm								
Rb	183.7	137.2	66.0	91.4	73.2	183.8	92.0	117.6
Sr	46.4	134.6	297.1	99.7	228.5	76.3	120.3	86.0
Y	22.4	25.9	25.1	31.0	29.0	38.6	29.1	25.9
Zr	271.8	151.4	149.5	242.2	87.8	274.5	215.1	230.3
Nb	15.2	13.5	9.0	10.6	7.9	16.4	10.7	11.6
Ba	486.1	1722.8	501.6	407.0	248.5	645.0	447.1	443.3
Pb	8.9	22.7	13.2	11.9	17.7	21.9	23.8	11.2
Th	16.5	13.1	9.5	14.8	4.9	11.9	8.7	13.4
U	3.6	4.7	1.2	1.3	0.0	1.4	2.7	2.0
Sc	7.2	13.9	8.4	9.1	36.9	16.0	7.8	11.4
V	63.4	187.8	52.3	66.9	229.2	114.9	16.9	82.7
Cr	63.4	102.0	52.3	65.6	442.4	69.2	76.1	86.5
Co	1.5	10.5	5.9	6.2	36.6	11.7	6.7	6.6
Ni	21.2	36.4	20.0	23.7	152.6	27.0	25.8	28.7
Cu	2.1	25.7	11.5	12.1	5.4	5.4	4.7	24.2
Zn	28.9	105.3	39.2	40.4	90.6	112.5	36.8	42.8
Ga	11.2	16.1	12.2	10.2	16.9	24.1	11.1	12.9
La		37.6		42.2	12.9		37.2	
Ce		72.0		83.3	26.0		73.6	
Pr		8.2		9.5	3.2		8.4	
Nd	32.7	29.9	25.7	34.0	13.0	47.6	31.2	32.4
Sm	6.1	5.9	5.1	6.6	3.3	9.8	6.2	6.5
Eu		1.2		1.1	0.9		1.1	
Gd		5.1		5.8	4.0		5.5	
Tb		0.7		0.9	0.7		0.8	
Dy		3.8		5.0	4.5		4.5	
Ho		0.7		1.0	1.0		0.9	
Er		1.8		2.8	2.9		2.5	
Yb		1.5		2.5	2.9		2.4	
Lu		0.2		0.3	0.4		0.3	
Hf		0.1		0.2	0.4		0.1	
Pb		21.3		11.8	18.2		24.0	
Th		14.2		15.7	4.6		14.4	
U		4.0		1.7	1.1		2.7	
Isotopic ratios								
$^{87}Sr/^{86}Sr$	0.76461	0.74298	0.73409	0.76387	0.73661	0.77521	0.75006	0.74234
$^{87}Rb/^{86}Sr$	11.46	2.95	0.64	2.65	0.93	6.98	2.21	3.96
$^{143}Nd/^{144}Nd$	0.511672	0.511737	0.511769	0.511919	0.512238	0.512224	0.511829	0.511963
$^{147}Sm/^{144}Nd$	0.1120	0.1186	0.1207	0.1171	0.1542	0.1238	0.1205	0.1202
ε(Nd)t	-13.4	-12.6	-12.1	-8.9	-5.1	-3.4	-10.9	-8.3
T (DM)	2.068	2.110	2.104	1.780	2.083	1.394	1.998	1.769
(87/86)t	0.68292	0.72195	0.72951	0.74496	0.73000	0.72551	0.73428	0.71413

Sample No.	W41	W43	W44	W45	W48	W49	W50	W54
Rock type								
Wt %								
SiO_2	75.5	78.8	82.2	85.1	79.1	73.3	75.9	69.0
TiO_2	0.6	0.6	0.4	0.4	0.6	0.3	0.2	0.6
Al_2O_2	11.6	9.8	8.6	6.9	8.5	13.0	13.8	15.0
Fe_2O_2	4.5	4.2	2.7	3.4	5.2	3.1	1.4	4.2
MnO	0.1	0.1	0.0	0.0	0.1	0.0	0.0	0.0
MgO	1.8	0.9	0.6	0.9	1.5	0.4	0.9	2.8
CaO	1.0	0.7	1.0	0.3	1.3	1.3	1.2	1.1
Na_2O	2.1	0.9	1.8	2.5	1.1	2.4	2.3	1.8
K_2O	2.5	3.2	2.1	0.8	2.2	5.5	3.4	4.7
P_2O_5	0.1	0.1	0.0	0.1	0.1	0.1	0.1	0.1
LOI	0.8	0.9	0.5	0.2	0.6	0.3	1.0	1.0
Total	100.5	100.2	99.9	100.7	100.2	99.8	100.3	100.4
ppm								
Rb	106.1	154.2	85.5	36.1	208.1	335.1	150.1	278.5
Sr	122.4	51.3	120.7	72.7	43.0	97.7	120.0	108.3
Y	22.9	26.2	14.6	17.0	32.4	52.1	27.4	23.4
Zr	191.1	336.3	165.0	145.7	227.4	210.6	101.5	167.0
Nb	10.9	13.3	7.1	7.9	20.4	19.1	12.8	18.1
Ba	606.9	529.8	510.0	422.5	130.5	570.2	286.0	337.7
Pb	18.6	11.2	18.7	5.7	19.3	41.3	39.6	25.4
Th	9.0	17.2	8.7	6.8	22.8	76.2	32.5	30.7
U	2.2	2.8	2.4	1.6	7.0	11.7	9.9	13.0
Sc	7.1	5.6	7.1	6.0	7.3	6.3	3.1	8.2
V	70.3	57.7	34.3	80.3	51.9	12.3	17.8	54.0
Cr	70.0	66.4	33.9	28.8	56.1	11.7	15.3	55.6
Co	6.4	6.3	2.3	3.6	10.0	1.3	1.5	7.8
Ni	27.1	18.4	11.9	10.6	16.5	4.6	6.7	23.4
Cu	7.0	15.8	5.3	0.7	10.6	3.8	2.0	5.8
Zn	52.3	48.4	31.0	32.7	100.2	31.9	14.8	25.3
Ga	12.3	12.3	8.5	9.6	13.5	19.8	15.5	18.3
La				26.4				
Ce				53.9				
Pr				6.0				
Nd	29.7	40.5	23.3	22.2	40.1	99.6	36.4	62.4
Sm	6.0	7.6	4.4	4.6	8.1	17.5	7.3	12.0
Eu				1.0				
Gd				4.1				
Tb				0.6				
Dy				2.8				
Ho				0.5				
Er				1.4				
Yb				1.3				
Lu				0.2				
Hf				0.1				
Pb				5.8				
Th				8.7				
U				1.3				
Isotopic ratios								
$^{87}Sr/^{86}Sr$	0.74319	0.76937	0.74968	0.73110	1.28211	0.96590	0.96384	0.88453
$^{87}Rb/^{86}Sr$	2.51	8.70	2.05	1.44	14.02	9.93	3.62	7.45
$^{143}Nd/^{144}Nd$	0.511977	0.511791	0.511830	0.511809	0.511800	0.511350	0.511512	0.511452
$^{147}Sm/^{144}Nd$	0.1212	0.1130	0.1150	0.1249	0.1224	0.1062	0.1220	0.1160
ε(Nd)t	-8.1	-11.2	-10.6	-11.6	-11.6	-19.4	-17.2	-18.0
T (DM)	1.765	1.905	1.883	2.137	2.092	2.427	2.584	2.516
(87/86)t	0.72531	0.70735	0.73506	0.72085	1.18219	0.89511	0.93802	0.83146

Sample No. Rock type	W58	W59	W60	W61SHA	W63	W64	W64	W65
Wt %								
SiO_2	100.1	63.4	72.4	80.8	74.8	63.2	63.2	68.6
TiO_2	0.1	0.7	0.4	0.4	0.7	0.7	0.7	0.6
Al_2O_2	0.5	18.2	14.5	10.6	15.8	18.5	18.5	15.2
Fe_2O_2	0.7	6.2	3.1	1.0	1.4	6.1	6.1	4.4
MnO	0.0	0.0	0.0	0.0	0.0	0.0	0.0	0.1
MgO	0.5	3.2	0.9	1.1	0.3	2.5	2.5	0.9
CaO	0.0	0.2	1.0	0.3	0.2	0.1	0.1	1.3
Na_2O	0.0	0.4	1.9	2.5	0.1	0.1	0.1	2.8
K_2O	0.0	5.2	4.8	2.4	4.8	5.8	5.8	4.6
P_2O_5	0.0	0.2	0.1	0.1	0.2	0.1	0.1	0.2
LOI	-0.1	2.2	1.0	1.0	2.1	3.4	3.4	1.3
Total	101.8	99.8	100.0	100.3	100.5	100.6	100.6	99.9
ppm								
Rb	0.3	317.0	233.9	50.3	170.8	254.1	254.1	272.1
Sr	0.5	44.8	103.2	52.1	20.6	42.3	42.3	125.0
Y	2.8	29.1	32.1	21.8	20.0	24.1	24.1	35.9
Zr	66.3	154.0	148.2	523.7	376.8	153.1	153.1	222.9
Nb	2.0	18.3	10.2	7.2	12.8	13.6	13.6	18.2
Ba	0.6	726.1	629.1	1643.5	245.0	300.5	300.5	774.1
Pb	2.6	11.5	28.0	10.5	3.0	5.1	5.1	27.7
Th	4.0	20.0	19.8	6.4	11.9	16.1	16.1	45.7
U	1.0	3.6	3.1	2.4	3.8	2.2	2.2	4.7
Sc	0.0	14.4	3.8	3.6	8.2	15.4	15.4	9.5
V	2.9	70.0	31.7	16.6	32.1	109.6	109.6	31.4
Cr	14.8	75.7	28.0	17.3	14.2	97.3	97.3	26.1
Co	0.5	10.3	3.9	1.7	0.9	10.1	10.1	3.2
Ni	0.7	29.6	18.1	7.8	2.5	39.9	39.9	8.1
Cu	0.6	5.8	7.5	1.1	0.9	34.8	34.8	8.7
Zn	2.3	50.1	40.2	5.9	3.2	46.3	46.3	65.6
Ga	1.7	23.4	16.3	10.0	16.3	22.7	22.7	20.5
La						55.0		
Ce						105.7		
Pr						11.9		
Nd	3.5	40.1	30.6	8.0	49.2	41.7	44.5	69.5
Sm	0.7	7.8	6.7	2.8	9.5	6.9	7.3	12.7
Eu						1.3		
Gd						5.4		
Tb						0.8		
Dy						4.2		
Ho						0.9		
Er						2.4		
Yb						2.2		
Lu						0.3		
Hf						2.0		
Pb						6.5		
Th						16.9		
U						1.7		
Isotopic ratios								
$^{87}Sr/^{86}Sr$	0.78242	1.24382	0.87437	0.87047	1.04128	0.94956	0.94567	0.83723
$^{87}Rb/^{86}Sr$	1.74	20.50	6.56	2.80	24.02	17.40	17.40	6.30
$^{143}Nd/^{144}Nd$	0.511446	0.511471	0.511579	0.512502	0.511427	0.511273	0.511193	0.511381
$^{147}Sm/^{144}Nd$	0.1231	0.1173	0.1328	0.2117	0.1166	0.1007	0.0985	0.1104
ε(Nd)t	-18.6	-17.7	-16.6	-3.6	-18.5	-20.5	-21.9	-19.0
T (DM)*	2.736	2.518	2.818	ND	2.574	2.412	2.474	2.485
(87/86)t	0.77004	1.09773	0.82760	0.85054	0.87014	0.82559	0.82169	0.79231

Sample No. Rock type	W70	W77	W78	W79	W80	W83	W87	W88
Wt %								
SiO_2	53.5	64.9	58.6	58.9	84.6	66.7	64.2	64.9
TiO_2	1.6	0.8	0.7	0.8	0.9	1.0	0.8	1.0
Al_2O_2	13.3	17.1	17.4	19.6	20.2	18.0	16.7	14.8
Fe_2O_2	15.1	6.4	8.8	9.0	5.9	4.6	6.9	5.9
MnO	0.3	0.1	0.1	0.1	0.0	0.0	0.1	0.0
MgO	4.5	2.0	3.2	3.4	2.0	0.9	1.9	3.1
CaO	4.9	0.4	3.1	0.2	0.2	0.2	0.9	0.2
Na_2O	1.8	1.8	2.5	0.3	2.2	0.2	1.4	0.2
K_2O	4.0	3.0	3.2	4.0	4.0	4.5	3.7	6.7
P_2O_5	0.2	0.1	0.1	0.1	0.2	0.1	0.2	0.1
LOI	1.1	3.7	2.7	4.4	3.2	3.9	3.4	3.5
Total	100.3	100.3	100.4	100.8	123.5	100.1	100.1	100.3
ppm								
Rb	80.4	112.6	242.6	220.1	177.5	200.3	159.6	129.4
Sr	116.2	84.2	94.5	21.9	76.7	64.4	94.0	35.1
Y	35.6	33.9	32.1	33.7	31.1	41.6	37.5	38.4
Zr	184.6	196.8	150.7	166.9	183.3	261.8	198.8	370.3
Nb	10.1	13.3	16.1	15.8	15.9	19.6	14.1	40.6
Ba	651.0	511.4	265.0	823.9	557.5	830.5	555.7	392.2
Pb	55.4	9.9	6.9	8.9	34.6	3.4	17.9	2.5
Th	5.3	12.6	24.4	26.8	19.3	23.0	16.7	19.3
U	2.3	5.2	3.2	3.2	2.4	5.5	3.1	2.6
Sc	23.2	18.9	20.4	21.1	15.0	16.7	16.4	11.4
V	315.1	118.6	138.6	141.2	102.8	117.4	117.5	83.8
Cr	63.1	81.0	103.8	99.5	75.1	74.7	80.4	64.7
Co	31.0	3.5	15.3	23.1	7.0	6.8	9.5	2.0
Ni	54.1	19.5	26.8	46.5	25.5	28.2	34.8	30.5
Cu	77.6	32.3	56.9	27.2	23.0	4.1	33.1	4.4
Zn	271.4	118.3	38.5	300.1	81.6	46.2	119.1	33.5
Ga	19.4	20.5	21.5	24.9	20.2	22.1	21.3	20.3
La	19.8		49.4					
Ce	45.4		97.8					
Pr	6.0		11.3					
Nd	25.5	33.1	41.4	14.2	32.3	47.6	55.0	43.8
Sm	6.0	6.7	8.4	3.8	6.5	8.0	10.6	8.1
Eu	1.6		1.5					
Gd	6.2		7.4					
Tb	1.0		1.1					
Dy	6.0		6.1					
Ho	1.3		1.2					
Er	3.4		3.3					
Yb	2.9		3.0					
Lu	0.4		0.4					
Hf	1.3		0.1					
Pb	50.5		8.3					
Th	4.3		22.8					
U	1.0		3.9					
Isotopic ratios								
$^{87}Sr/^{86}Sr$	0.77557	0.75265	0.76387	0.94509	0.76961	0.80398	0.76047	0.83029
$^{87}Rb/^{86}Sr$	2.00	3.87	7.43	29.11	6.70	9.01	4.92	10.68
$^{143}Nd/^{144}Nd$	0.511906	0.512099	0.511795	0.512069	0.511936	0.511807	0.512012	0.511951
$^{147}Sm/^{144}Nd$	0.1421	0.1226	0.1230	0.1608	0.1211	0.1017	0.1168	0.1121
ε(Nd)t	-10.8	-5.8	-11.8	-8.8	-8.9	-10.2	-7.1	-8.0
T (DM)	2.460	1.585	2.116	2.905	1.831	1.689	1.628	1.644
(87/86)t	0.76129	0.72506	0.71090	0.73767	0.72186	0.73980	0.72544	0.75421

Sample No. Rock type	W89	W91	W92	W95	W99	W100
Wt %						
SiO_2	56.4	66.7	99.4	69.0	64.6	66.0
TiO_2	0.9	0.9	0.1	0.8	0.7	0.7
Al_2O_2	21.0	18.4	0.8	14.2	15.9	16.1
Fe_2O_2	7.2	4.8	0.8	6.2	5.0	5.7
MnO	0.1	0.0	0.0	0.1	0.1	0.0
MgO	2.1	0.3	0.1	1.0	2.0	2.0
CaO	1.3	0.0	0.0	1.7	3.2	0.3
Na_2O	0.3	0.3	0.0	2.6	2.4	1.7
K_2O	4.6	5.1	0.2	3.7	5.4	3.7
P_2O_5	0.1	0.0	0.0	0.2	0.3	0.1
LOI	5.8	2.9	0.3	1.0	0.5	3.7
Total	99.7	99.6	101.8	100.4	100.1	100.1
ppm						
Rb	223.9	236.3	14.3	140.8	246.8	196.8
Sr	64.1	51.5	2.4	151.0	797.1	48.2
Y	34.4	42.0	2.5	37.3	29.0	33.9
Zr	189.5	426.9	11.9	229.4	289.8	228.4
Nb	19.0	15.0	2.1	16.4	36.1	16.0
Ba	1163.7	602.2	40.3	696.6	2129.7	588.2
Pb	31.7	8.8	3.6	5.9	44.6	23.1
Th	22.9	16.1	0.1	15.6	70.8	24.4
U	2.3	3.9	-0.3	4.5	7.1	4.3
Sc	20.6	11.2	0.9	14.8	11.1	15.4
V	165.7	52.3	6.6	65.8	108.7	94.4
Cr	127.9	55.1	11.5	46.4	50.4	70.9
Co	15.6	1.0	0.9	9.0	6.7	5.4
Ni	55.3	17.6	3.1	41.5	18.9	33.0
Cu	21.3	2.9	0.0	22.4	14.0	18.2
Zn	114.3	30.5	5.0	50.5	43.4	106.0
Ga	25.6	21.0	1.2	16.8	15.8	17.9
La			4.8		238.4	
Ce			7.8		412.8	
Pr			1.0		43.9	
Nd	41.1	28.3	3.4	41.0	140.6	37.1
Sm	7.7	3.8	0.6	8.0	18.2	6.9
Eu			0.1		3.2	
Gd			0.5		11.6	
Tb			0.1		1.2	
Dy			0.5		5.5	
Ho			0.1		1.0	
Er			0.3		2.8	
Yb			0.2		2.5	
Lu			0.0		0.3	
Hf			0.0		0.1	
Pb			0.9		43.5	
Th			1.7		80.3	
U			0.2		6.9	
Isotopic ratios						
$^{87}Sr/^{86}Sr$	0.75325	0.75088	0.75510	0.74425	0.71971	0.81889
$^{87}Rb/^{86}Sr$	10.12	13.29	17.25	2.70	0.90	11.82
$^{143}Nd/^{144}Nd$	0.511973	0.512015	0.511758	0.511966	0.511568	0.511830
$^{147}Sm/^{144}Nd$	0.1134	0.0814	0.1106	0.1182	0.0784	0.1123
ε(Nd)t	-7.7	-4.8	-11.7	-8.1	-13.3	-10.4
T (DM)	1.633	1.190	1.910	1.726	1.668	1.832
(87/86)t	0.68117	0.65620	0.63216	0.72501	0.71332	0.73464

Sample No.	B03	B06	B07	B29a	B29b	B36a	B39	B41
Rock type	Gnt phylite	Slate	Phylite	Phylite	Qzite	Phylite	Ky/Gnt/Sil Paragneiss	Bt/Qz Paragneiss
Wt %								
SiO_2	75.9	58.1	60.9	93.2	68.2	76.9	64.0	70.5
TiO_2	0.5	1.3	0.9	0.2	0.6	0.9	0.9	0.5
Al_2O_2	12.9	23.8	19.0	3.2	16.2	11.5	19.8	14.2
Fe_2O_2	3.9	4.6	7.4	0.4	4.7	2.6	7.9	3.3
MnO	0.1	0.1	0.1	0.0	0.0	0.0	0.2	0.0
MgO	1.1	0.6	2.6	0.4	1.7	1.9	1.8	1.7
CaO	1.0	0.0	0.6	0.0	0.1	0.1	0.3	1.9
Na_2O	0.3	0.6	1.5	0.0	0.2	0.1	0.4	2.7
K_2O	3.6	4.8	4.1	1.2	5.3	4.1	3.9	3.8
P_2O_5	0.1	0.1	0.1	0.0	0.1	0.1	0.1	0.1
LOI	1.7	6.1	3.4	0.7	2.6	1.9	1.5	1.0
Total	101.2	100.1	100.5	99.5	99.6	100.3	100.8	99.8
ppm								
Rb	196.0	255.4	212.4	197.7	42.1	220.4	227.1	182.2
Sr	46.6	253.7	126.5	52.7	10.1	42.8	37.2	118.0
Y	25.7	59.1	33.2	23.2	5.8	44.6	37.2	26.9
Zr	223.3	303.4	167.4	231.9	609.3	3240.9	238.9	141.6
Nb	11.4	28.5	17.8	14.3	4.7	22.0	19.8	14.2
Ba	494.8	871.1	654.8	776.7	304.4	682.1	661.5	571.5
Pb	14.2	100.1	51.5	4.2	4.3	8.5	147.9	6.4
Th	14.6	36.7	26.5	15.9	6.1	78.1	21.2	14.0
U	2.8	7.0	3.1	3.5	3.4	14.2	3.3	3.0
Sc	7.6	23.6	17.8	9.6	0.0	6.9	17.3	11.2
V	48.4	234.1	109.2	68.1	9.3	44.5	128.9	45.7
Cr	57.1	112.8	106.6	70.1	15.0	62.3	121.9	111.5
Co	9.3	3.5	24.2	7.4	1.0	6.5	15.9	4.8
Ni	14.4	36.5	46.5	24.2	1.8	18.3	35.4	10.3
Cu	5.6	2.3	47.0	4.4	1.3	2.8	11.7	7.7
Zn	18.0	68.0	107.3	15.9	4.4	22.1	117.4	18.0
Ga	15.7	31.8	25.3	19.0	3.2	13.4	26.2	15.0
La	27.1	64.2	57.6	7.3	40.7	90.3	55.5	60.0
Ce	49.3	121.1	109.3	14.4	73.1	170.5	105.4	115.2
Pr	6.3	14.7	13.5	1.8	9.1	21.3	13.0	14.3
Nd	22.8	50.2	47.5	6.2	31.9	74.3	45.7	50.7
Sm	4.8	9.3	9.2	1.0	5.7	13.1	9.1	10.2
Eu	1.0	1.5	1.8	0.2	1.0	2.0	1.5	1.4
Gd	4.1	6.3	7.4	0.7	3.9	9.5	7.8	8.1
Tb	0.6	0.8	1.1	0.1	0.5	1.2	1.3	1.2
Dy	3.5	4.0	5.4	0.5	2.0	5.1	7.7	5.4
Ho	0.7	0.7	1.0	0.1	0.3	0.9	1.6	0.9
Er	1.9	1.9	2.6	0.3	0.8	2.1	4.5	1.9
Yb	1.7	1.7	2.0	0.2	0.6	1.6	4.3	1.1
Lu	0.2	0.2	0.2	0.0	0.1	0.2	0.6	0.1
Hf	0.1	1.5	0.2	0.1	0.2	0.4	0.2	0.0
Pb	7.6	52.9	50.5	0.6	2.3	5.2	140.8	8.9
Th	7.1	17.1	26.0	2.6	9.2	84.1	24.7	28.3
U	1.2	2.5	2.4	0.7	1.2	7.8	2.7	4.6
Isotopic ratios								
$^{87}Sr/^{86}Sr$	0.87705	0.72488	0.73381	0.91818	0.88034	0.97145	0.83617	0.77531
$^{87}Rb/^{86}Sr$	12.18	2.92	4.86	10.87	12.07	14.92	17.68	4.47
$^{143}Nd/^{144}Nd$	0.511957	0.511918	0.511769	0.511253	0.511274	0.511238	0.511795	0.511867
$^{147}Sm/^{144}Nd$	0.1266	0.1117	0.1170	0.1016	0.1075	0.1065	0.1202	0.1210
ε(Nd)t	-8.8	-8.6	-11.9	-21.0	-20.9	-21.6	-11.6	-10.2
T (DM)	1.913	1.688	2.022	2.462	2.572	2.601	2.049	1.946
(87/86)t	0.79025	0.70410	0.69917	0.84076	0.79432	0.86517	0.71020	0.74345

Sample No.	B45	B50	B51	B52a	B54	B57	B60	B62a
Rock type	Augen Gneiss	Gnt/Sill Pelite	Mica schist	Bt Schist	Gnt/St/Chld Pelite	Qzte/phylite	Phyllite	Qzite
Wt %								
SiO_2	75.8	74.7	84.0	85.3	70.5	65.1	64.7	91.3
TiO_2	0.3	0.8	0.6	0.5	0.7	0.3	0.8	0.2
Al_2O_2	13.1	12.6	7.9	7.6	12.7	6.3	17.5	4.5
Fe_2O_2	2.3	5.0	3.5	2.8	6.4	2.7	6.5	1.8
MnO	0.0	0.1	0.1	0.0	0.2	0.1	0.1	0.0
MgO	1.2	1.7	1.0	0.7	1.7	1.0	2.0	0.2
CaO	1.7	0.4	0.2	0.1	2.3	12.5	0.3	0.1
Na_2O	3.4	0.3	0.3	0.5	2.9	0.1	0.8	0.0
K_2O	2.1	3.1	2.0	2.2	2.4	2.0	4.5	2.3
P_2O_5	0.2	0.2	0.2	0.0	0.3	0.1	0.1	0.0
LOI	0.6	1.6	1.2	1.1	0.5	10.5	2.9	0.6
Total	100.7	100.5	101.0	100.7	100.5	100.7	99.9	101.0
ppm								
Rb	133.0	162.6	91.6	115.8	206.1	87.7	218.3	84.0
Sr	123.0	45.0	14.9	10.2	103.7	91.6	39.7	11.6
Y	19.2	34.8	26.2	17.3	44.6	18.1	30.7	11.7
Zr	108.2	272.0	250.2	201.3	164.6	120.4	184.0	120.5
Nb	10.9	14.2	11.4	9.7	19.6	6.5	13.0	5.2
Ba	230.7	705.7	260.2	156.7	465.9	385.0	571.4	180.9
Pb	6.9	16.9	11.1	1.5	6.3	14.8	20.1	6.0
Th	13.5	18.6	10.1	10.0	15.1	8.4	16.1	7.5
U	3.6	4.3	3.8	1.5	3.5	2.2	3.2	2.4
Sc	6.0	8.4	7.4	5.6	14.7	7.8	19.6	0.6
V	15.8	92.8	46.3	39.2	76.1	41.3	122.7	12.0
Cr	46.7	82.3	66.3	42.2	71.4	35.1	80.3	19.6
Co	3.8	7.8	6.4	4.7	13.1	3.0	13.7	0.5
Ni	7.4	14.4	12.2	21.5	28.0	11.3	32.9	2.3
Cu	0.7	12.7	14.7	0.0	3.4	11.4	25.1	0.9
Zn	9.4	60.0	30.5	10.8	56.8	38.7	65.2	4.9
Ga	15.6	15.7	10.2	10.3	16.6	7.8	21.3	5.2
La	32.3	44.0	34.4	23.0	43.7	21.7	41.2	15.9
Ce	62.6	85.8	71.1	46.3	98.3	41.5	78.8	32.5
Pr	7.7	10.5	8.4	5.4	13.2	5.1	9.8	3.7
Nd	28.0	37.9	30.3	19.3	54.4	18.4	35.8	13.2
Sm	5.8	7.7	6.1	3.8	13.4	3.8	7.0	2.7
Eu	0.9	1.3	1.1	0.6	2.2	0.7	1.3	0.5
Gd	5.0	7.0	5.3	2.8	12.2	3.5	5.7	2.1
Tb	0.7	1.1	0.8	0.4	1.8	0.5	0.9	0.3
Dy	3.7	5.8	3.8	1.8	9.5	3.0	5.6	1.4
Ho	0.6	1.2	0.7	0.3	1.8	0.6	1.1	0.3
Er	1.5	3.3	2.0	0.7	4.7	1.7	3.0	0.7
Yb	1.0	3.1	1.9	0.6	4.2	1.5	1.9	0.6
Lu	0.1	0.5	0.3	0.1	0.6	0.2	0.2	0.1
Hf	0.0	0.1	0.1	0.1	0.0	0.1	0.4	0.1
Pb	6.5	17.6	10.4	2.3	8.3	14.9	19.1	5.1
Th	22.3	17.6	15.3	10.9	21.1	7.9	14.8	6.7
U	3.0	2.3	2.2	1.3	3.5	1.2	1.5	0.6
Isotopic ratios								
$^{87}Sr/^{86}Sr$	0.75348	0.77506	0.83681	0.83706	0.78299	0.74343	0.81337	0.94429
$^{87}Rb/^{86}Sr$	3.13	10.46	17.80	32.88	5.76	2.77	15.92	20.97
$^{143}Nd/^{144}Nd$	0.511884	0.511873	0.511803	0.511874	0.511788	0.511839	0.511957	0.511805
$^{147}Sm/^{144}Nd$	0.1261	0.1235	0.1218	0.1190	0.1493	0.1252	0.1178	0.1257
ε(Nd)t	-10.2	-10.3	-11.5	-10.0	-13.6	-11.0	-8.3	-11.7
T (DM)	2.033	1.990	2.072	1.892	3.071	2.090	1.733	2.165
(87/86)t	0.73117	0.70050	0.70995	0.60279	0.74198	0.72367	0.69990	0.79484

Sample No.	B66	B68	B70	B71b	B75Z	B81	B83	B85
Rock type	Gnt Pelite	Augen Gneiss	Phylite	Phylite	Qzite (below B35)	Gnt phylite	Gnt/Mica Schist	Gnt/Bt Schist
Wt %								
SiO_2	63.1	74.2	60.4	95.8	97.9	69.1	58.0	71.9
TiO_2	0.7	0.3	0.8	0.1	0.1	0.8	1.1	0.7
Al_2O_2	16.7	13.4	17.9	3.5	2.6	17.8	19.9	14.0
Fe_2O_2	8.0	2.4	4.0	1.3	0.6	5.6	11.4	6.4
MnO	0.1	0.0	0.0	0.0	0.0	0.1	0.2	0.1
MgO	2.4	1.0	3.2	0.3	0.5	1.2	2.0	1.9
CaO	2.1	1.1	2.9	0.0	0.0	0.2	1.1	1.0
Na_2O	1.6	3.0	0.2	0.0	0.0	0.7	1.6	1.0
K_2O	3.5	3.8	5.7	2.0	0.8	4.3	4.2	3.5
P_2O_5	0.7	0.1	0.1	0.0	0.0	0.1	0.3	0.1
LOI	1.9	0.8	4.8	0.4	0.5	2.1	2.6	1.6
Total	100.9	100.2	100.0	103.5	103.2	102.0	102.4	102.3
ppm								
Rb	186.5	165.9	226.4	77.2	32.6	283.0	247.0	144.0
Sr	88.9	102.1	98.8	17.1	3.8	38.3	165.9	40.4
Y	81.0	34.9	30.1	10.1	5.4	35.4	49.8	34.9
Zr	183.3	127.5	210.6	66.6	113.2	238.3	210.1	331.5
Nb	13.5	12.7	17.6	2.6	1.7	16.6	22.3	15.4
Ba	473.6	541.0	538.0	230.2	76.0	712.3	641.5	794.0
Pb	27.9	7.4	16.4	6.1	5.6	16.3	106.0	13.6
Th	17.7	16.7	29.1	5.1	3.9	16.5	26.9	21.1
U	5.2	3.0	5.9	1.8	0.7	14.6	5.6	4.8
Sc	16.7	5.3	15.5	1.0	1.1	10.5	14.0	9.9
V	113.6	15.7	109.0	9.5	3.8	84.7	126.5	72.1
Cr	91.1	44.7	86.2	32.9	11.0	80.8	95.6	98.0
Co	13.0	3.7	12.9	3.2	1.0	6.9	35.0	8.3
Ni	36.2	6.3	30.6	3.9	0.3	10.8	54.9	19.0
Cu	23.7	0.7	53.9	10.4	0.7	15.3	16.8	27.1
Zn	110.5	12.4	25.7	5.2	7.8	59.0	110.6	58.1
Ga	21.0	14.8	23.0	4.3	3.2	23.3	28.8	17.2
La	50.8	37.2	56.8	13.6	11.8	55.2	78.2	51.0
Ce	102.3	70.8	106.4	28.0	23.4	104.3	149.5	95.9
Pr	13.8	8.8	13.1	3.3	2.6	13.2	18.7	11.7
Nd	56.6	31.6	45.9	11.8	9.2	47.1	67.7	41.7
Sm	15.7	6.7	8.3	2.4	1.7	9.6	13.8	8.2
Eu	2.2	0.9	1.3	0.5	0.3	1.4	2.2	1.2
Gd	17.3	6.1	6.4	2.3	1.3	8.1	11.4	6.7
Tb	2.8	1.0	1.0	0.3	0.2	1.2	1.6	1.0
Dy	14.4	5.7	5.4	1.7	0.8	6.0	8.3	5.0
Ho	2.6	1.2	1.1	0.3	0.2	1.1	1.5	1.0
Er	6.2	3.2	2.9	0.7	0.4	3.2	4.1	2.6
Yb	4.3	2.8	2.2	0.6	0.3	3.6	4.1	2.5
Lu	0.5	0.4	0.3	0.1	0.0	0.6	0.6	0.4
Hf	0.1	0.0	0.2	0.0	0.1	0.1	0.1	0.1
Pb	28.5	7.5	16.3	6.3	0.9	15.0	101.3	13.2
Th	16.9	18.3	25.4	4.9	3.5	22.1	29.2	24.3
U	2.1	3.2	3.0	1.8	0.5	12.4	3.4	2.6
Isotopic ratios								
$^{87}Sr/^{86}Sr$	0.78164	0.76448	0.73319	0.92056	1.05902	0.80052	0.72775	0.78961
$^{87}Rb/^{86}Sr$	6.08	4.71	6.64	13.08	24.85	21.40	4.31	10.32
$^{143}Nd/^{144}Nd$	0.512202	0.511877	0.511656	0.511738	0.511312	0.511932	0.512017	0.511801
$^{147}Sm/^{144}Nd$	0.1673	0.1279	0.1087	0.1224	0.1102	0.1237	0.1229	0.1195
ε(Nd)t	-6.6	-10.5	-13.5	-12.8	-20.4	-9.1	-7.4	-11.4
T (DM)	2.863	2.089	2.027	2.198	2.585	1.893	1.731	2.022
(87/86)t	0.73835	0.73095	0.68591	0.82739	0.88195	0.64805	0.69703	0.71606

Sample No.	B87	B88	ed96/12	ed96/16	ed96/18	ed96/21	ed96/31	ed96/32
Rock type	Gneiss	Gnt/Mica Schist						
Wt %								
SiO_2	69.3	65.6	64.3	66.3	65.5	72.4	69.8	70.0
TiO_2	0.8	0.8	0.7	0.7	0.7	0.6	0.6	0.6
Al_2O_2	16.0	17.3	15.8	14.6	14.7	12.0	13.5	14.0
Fe_2O_2	6.5	6.3	6.5	5.2	7.0	4.8	4.9	4.6
MnO	0.1	0.1	0.1	0.1	0.1	0.1	0.1	0.1
MgO	1.7	1.6	2.4	2.4	3.0	2.2	2.4	2.0
CaO	0.8	1.0	0.5	1.1	0.5	0.7	0.7	1.3
Na_2O	1.7	2.6	1.2	1.9	2.2	1.3	2.1	1.5
K_2O	3.9	3.0	3.8	3.4	2.4	3.3	2.6	3.4
P_2O_5	0.1	0.1	0.1	0.2	0.2	0.2	0.2	0.1
LOI	0.7	1.6	3.3	2.6	3.0	1.6	2.1	1.5
Total	101.6	99.8	98.7	98.4	99.2	99.1	98.9	99.1
ppm								
Rb	163.9	162.8	166.0	126.0	117.0	134.0	116.0	147.0
Sr	182.0	156.5	36.0	93.0	94.0	40.0	97.0	93.0
Y	31.5	34.8	30.0	28.0	42.0	21.0	25.0	31.0
Zr	230.1	207.7	201.0	259.0	211.0	195.0	246.0	227.0
Nb	15.1	15.7	17.0	16.0	15.0	12.0	13.0	14.0
Ba	881.9	549.2	682.0	744.0	579.0	793.0	683.0	541.0
Pb	26.6	28.8	9.0	14.0	23.0	20.0	14.0	23.0
Th	13.0	14.1	17.0	19.0	14.0	13.0	14.0	14.0
U	2.5	1.9	4.0	3.0	3.0	3.0	4.0	3.0
Sc	14.6	11.7	14.0	13.0	14.0	12.0	11.0	12.0
V	101.9	90.0	90.0	85.0	83.0	80.0	70.0	84.0
Cr	99.7	78.9	81.0	74.0	83.0	66.0	79.0	51.0
Co	10.4	10.6	23.0	19.0	26.0	14.0	13.0	10.0
Ni	20.9	15.3	38.0	34.0	52.0	29.0	53.0	22.0
Cu	10.2	27.2	82.0	11.0	40.0	32.0	24.0	33.0
Zn	170.6	82.0	98.0	58.0	115.0	73.0	69.0	86.0
Ga	18.7	21.3	21.0	18.0	18.0	16.0	17.0	17.0
La	54.3	47.7	41.5	45.9	48.7	34.8	36.8	39.5
Ce	103.8	90.9	77.3	86.6	89.2	66.5	70.5	75.9
Pr	12.8	11.2	9.6	10.6	11.0	8.1	8.6	9.3
Nd	45.8	40.4	34.5	38.0	40.0	28.8	31.3	33.7
Sm	8.8	8.2	6.7	7.5	8.0	5.6	6.2	6.8
Eu	1.6	1.5	1.2	1.4	1.6	1.1	1.2	1.3
Gd	7.3	6.9	5.7	6.1	7.2	4.8	5.1	6.0
Tb	1.0	1.0	0.8	0.9	1.1	0.7	0.7	0.9
Dy	5.2	5.3	4.3	4.6	6.1	3.9	4.1	5.1
Ho	1.0	1.0	0.9	0.9	1.3	0.8	0.8	1.0
Er	2.7	2.9	2.4	2.6	3.5	2.1	2.1	2.7
Yb	2.7	2.9	2.3	2.6	3.2	1.7	1.7	2.2
Lu	0.4	0.4	0.4	0.4	0.5	0.2	0.2	0.3
Hf	0.1	0.1	2.0	1.8	1.0	0.2	0.4	1.0
Pb	25.6	27.1	6.7	11.1	23.9	19.1	13.5	24.6
Th	20.0	19.4	20.8	21.8	17.5	13.9	15.3	15.0
U	1.3	2.5	3.0	2.9	2.5	2.0	2.3	1.5
Isotopic ratios								
$^{87}Sr/^{86}Sr$	0.74394	0.75981	0.79002	0.75271	0.75083	0.77038	0.75171	0.76311
$^{87}Rb/^{86}Sr$	2.61	3.01	13.35	3.92	3.60	9.70	3.46	4.58
$^{143}Nd/^{144}Nd$	0.511780	0.511908	0.511734	0.511684	0.511644	0.511728	0.511489	0.511903
$^{147}Sm/^{144}Nd$	0.1166	0.1227	0.1179	0.1188	0.1214	0.1177	0.1206	0.1217
ε(Nd)t	-11.6	-9.5	-12.6	-13.7	-14.6	-12.7	-17.6	-9.6
T (DM)	1.996	1.914	2.098	2.202	2.334	2.105	2.581	1.900
(87/86)t	0.72535	0.73834	0.69487	0.72476	0.72515	0.70125	0.72703	0.73050

Sample No. Rock type	ed96/33	ed96/57	ed96/58	ed96/74	ed96/83	ed96/91	ed96/99	ed98/226
Wt %								
SiO_2	54.9	71.7	71.2	67.2	64.9	66.1	66.7	
TiO_2	0.8	0.6	0.5	0.6	0.7	0.6	0.8	
Al_2O_2	20.7	12.0	13.5	13.6	14.6	15.6	15.6	
Fe_2O_2	7.0	3.5	3.4	5.8	6.3	4.2	5.6	
MnO	0.1	0.1	0.0	0.1	0.1	0.1	0.1	
MgO	4.0	2.7	2.2	4.6	4.3	1.9	1.9	
CaO	0.5	1.7	1.1	0.5	0.8	1.2	0.7	
Na_2O	0.7	2.1	2.5	2.0	1.9	1.2	1.3	
K_2O	6.2	2.2	2.9	2.1	2.9	3.7	3.1	
P_2O_5	0.2	0.1	0.1	0.2	0.1	0.1	0.1	
LOI	3.8	1.7	1.1	2.3	3.1	4.0	3.3	
Total	98.9	98.4	98.6	99.0	99.7	98.7	99.2	
ppm								
Rb	232.0	84.0	107.0	100.0	117.0	135.0	137.0	142.4
Sr	38.0	61.0	87.0	67.0	53.0	63.0	85.0	68.1
Y	19.0	17.0	28.0	29.0	27.0	27.0	37.0	
Zr	177.0	258.0	212.0	179.0	160.0	214.0	384.0	
Nb	16.0	10.0	13.0	12.0	14.0	12.0	16.0	
Ba	1128.0	422.0	579.0	281.0	838.0	595.0	412.0	
Pb	19.0	6.0	10.0	11.0	4.0	25.0	22.0	
Th	16.0	15.0	13.0	11.0	11.0	11.0	18.0	
U	4.0	3.0	3.0	3.0	4.0	3.0	4.0	
Sc	22.0	10.0	11.0	9.0	15.0	12.0	15.0	
V	200.0	52.0	65.0	78.0	101.0	84.0	103.0	
Cr	139.0	53.0	37.0	75.0	108.0	45.0	143.0	
Co	22.0	8.0	5.0	23.0	23.0	9.0	20.0	
Ni	51.0	22.0	17.0	45.0	47.0	17.0	24.0	
Cu	5.0	< 2	6.0	87.0	4.0	17.0	18.0	
Zn	106.0	55.0	69.0	104.0	102.0	72.0	94.0	
Ga	30.0	10.0	14.0	15.0	20.0	18.0	20.0	
La	57.8	28.6	40.1	27.9	31.4	37.1	52.5	49.6
Ce	107.1	57.5	74.0	54.0	58.5	71.4	102.2	95.8
Pr	12.9	7.1	9.4	6.8	7.2	8.9	12.9	11.5
Nd	43.6	25.7	33.3	25.0	25.7	32.3	46.8	40.9
Sm	6.6	5.1	6.5	5.5	5.2	6.3	9.0	7.9
Eu	1.5	0.9	1.3	1.1	1.0	1.1	1.3	1.4
Gd	4.8	4.1	5.6	5.7	4.5	4.7	5.9	6.3
Tb	0.6	0.6	0.9	0.9	0.7	0.6	0.8	0.9
Dy	3.0	2.8	4.8	5.2	3.5	2.8	3.3	4.4
Ho	0.6	0.6	1.0	1.1	0.7	0.5	0.5	0.8
Er	1.6	1.5	2.7	2.8	1.8	1.4	1.2	2.3
Yb	1.5	1.3	2.3	2.2	1.5	1.2	0.9	2.1
Lu	0.2	0.2	0.3	0.3	0.2	0.2	0.1	0.3
Hf	0.2	0.2	0.3	0.6	0.6	1.0	0.5	1.2
Pb	19.8	5.4	9.6	9.3	2.8	24.5	21.3	14.6
Th	20.6	15.2	11.9	11.7	12.4	12.2	19.7	22.1
U	3.2	1.4	0.9	1.8	3.2	1.1	1.2	2.9
Isotopic ratios								
$^{87}Sr/^{86}Sr$	0.79369	0.77770	0.75598	0.77902	0.78082	0.77180	0.75920	0.76297
$^{87}Rb/^{86}Sr$	17.68	3.99	3.56	4.32	6.39	6.21	4.67	6.05
$^{143}Nd/^{144}Nd$	0.511766	0.511796	0.512023	0.511946	0.511841	0.511941	0.511919	0.511627
$^{147}Sm/^{144}Nd$	0.0920	0.1190	0.1172	0.1335	0.1222	0.1185	0.1161	0.1167
ε(Nd)t	-10.3	-11.5	-6.9	-9.5	-10.8	-8.6	-8.9	-14.6
T (DM)	1.605	2.021	1.617	2.103	2.017	1.773	1.764	2.246
(87/86)t	0.66771	0.74928	0.73060	0.74822	0.73527	0.72758	0.72595	0.71985

Sample No. Rock type	lg94/166b	lg94/56	lg94/73	sd14	kd13	sd9
Wt %						
SiO_2						
TiO_2						
Al_2O_2						
Fe_2O_2						
MnO						
MgO						
CaO						
Na_2O						
K_2O						
P_2O_5						
LOI						
Total						
ppm						
Rb	208.7	1.9	81.7	146.3	149.2	54.6
Sr	328.9	11.2	63.1	498.4	201.0	119.8
Y						
Zr						
Nb						
Ba						
Pb						
Th						
U						
Sc						
V						
Cr						
Co						
Ni						
Cu						
Zn						
Ga						
La	139.9	3.1	110.1	57.2	20.6	45.1
Ce	275.6	6.7	224.2	111.0	40.0	87.2
Pr	31.4	0.9	30.7	13.5	4.8	10.8
Nd	109.0	3.7	118.9	47.9	17.3	40.7
Sm	21.1	1.1	23.0	8.8	3.9	8.6
Eu	3.3	0.2	3.7	1.5	0.7	2.4
Gd	14.9	1.2	18.0	5.7	3.5	7.8
Tb	1.9	0.2	2.6	0.6	0.5	1.2
Dy	8.9	0.8	13.0	2.6	2.1	6.2
Ho	1.6	0.2	2.4	0.4	0.4	1.2
Er	4.0	0.4	6.2	0.9	1.0	3.2
Yb	3.3	0.4	5.0	0.7	0.9	2.9
Lu	0.5	0.1	0.7	0.1	0.1	0.4
Hf	0.4	0.6	19.2	0.3	0.6	5.9
Pb	53.7	1.1	13.0	22.2	51.7	9.8
Th	50.3	4.3	11.9	22.6	18.3	7.3
U	2.3	0.4	2.2	0.6	0.9	1.7
Isotopic ratios						
$^{87}Sr/^{86}Sr$	0.72699	0.71528	0.71504	0.71142	0.71695	0.71242
$^{87}Rb/^{86}Sr$	1.84	0.49	3.75	0.85	2.15	1.32
$^{143}Nd/^{144}Nd$	0.511765	0.511702	0.512385	0.511889	0.511996	0.512704
$^{147}Sm/^{144}Nd$	0.1168	0.1809	0.1171	0.1115	0.1361	0.1280
ε(Nd)t	-11.9	-17.3	0.2	-9.2	-8.7	5.7
T (DM)*	2.024	ND	1.047	1.729	2.073	0.626
(87/86)t	0.71390	0.71177	0.68833	0.70536	0.70164	0.70301

Appendix C – Zircon Data

This appendix contains all the zircon data collected during the course of this study.

Notes:

i refers to fractions prior to abrasion.

ii refers to fractions after abrasion.

Figure C.1 - Photomicrographs of zircons in Batch 091.

a (W49Z)

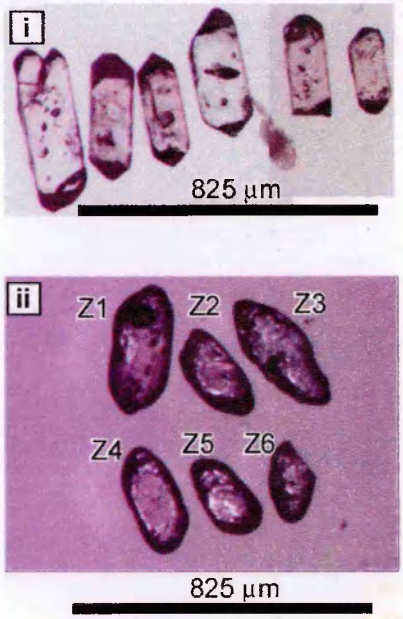

b (W34Z)

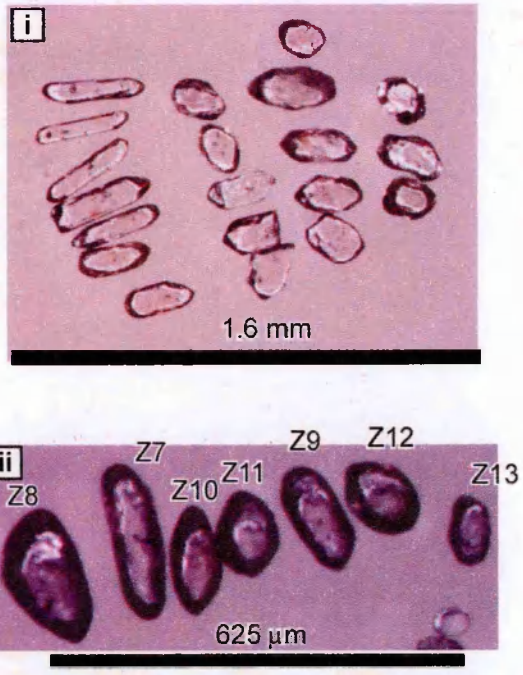

c (W60Z)

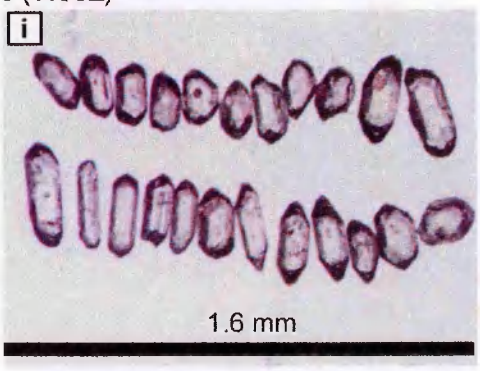

d (W58Z)

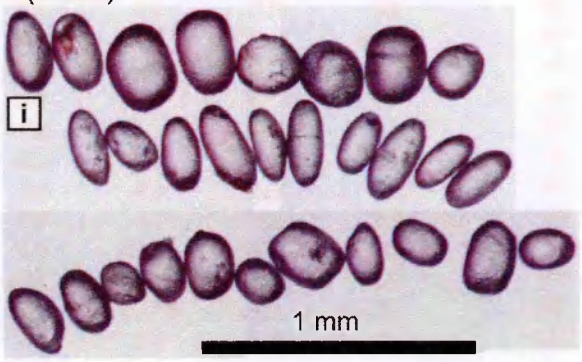

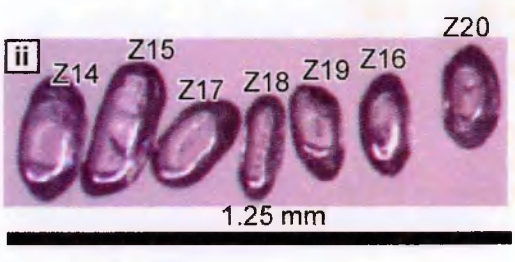

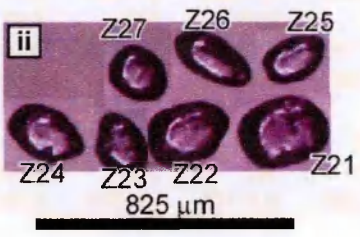

C.2 - Photomicrographs of zircons in Batch 124.

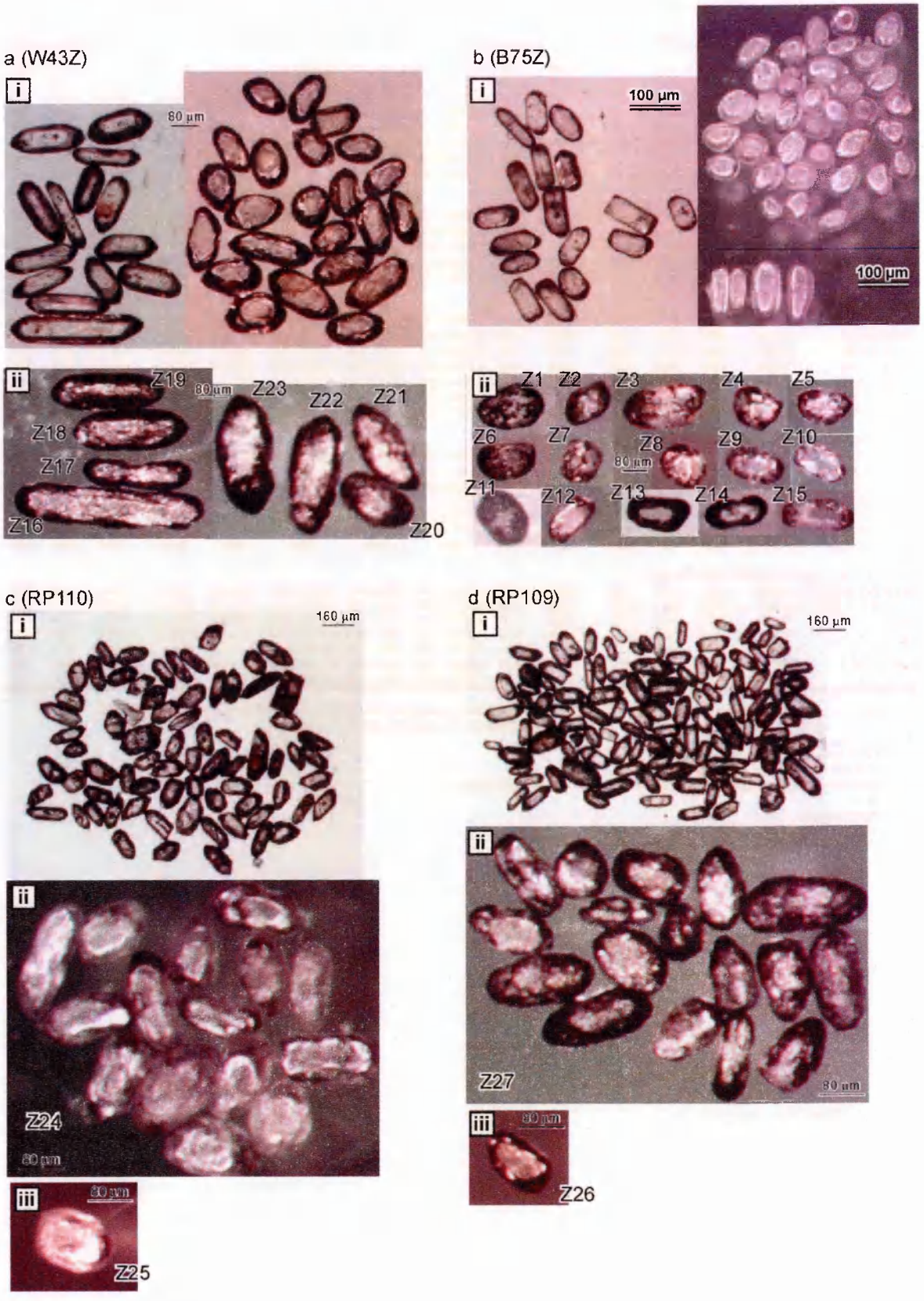

Table C.1 - U-Pb isotopic data from analysed zircons the Sutlej Valley:

Fraction Number[a]	Fraction weight (mg)	U (ppm)	Pb (ppm)	Blank Pb pg)[b]	$^{206}Pb/^{204}Pb$[c]	Th/U[d]	$^{206}Pb/^{238}U$[e]	$^{207}Pb/^{235}U$[e]	$^{207}Pb/^{206}Pb$[e]	$^{206}Pb/^{238}U$ age[f]	$^{207}Pb/^{235}U$ age[f]	$^{207}Pb/^{206}Pb$ age[f]	Cc[g]	% dis[h]
W43z - Metasediment, Vaikrita Group														
z16 (L,D,CL)*	0.0123	262.0	36.5	21.6	1285	0.37	0.1370 ± 0.19	1.290 ± 0.23	0.0683 ± 0.11	828 ± 3	841 ± 3	877 ± 5	0.87	6.00
z17 (L,D,CL)*	0.0049	1188	145.0	11.6	3805	0.31	0.1219 ± 0.17	1.133 ± 0.18	0.0674 ± 0.07	741 ± 2	769 ± 2	850 ± 3	0.92	13.5
z18 (L,D,CL)*	0.0091	459.4	61.0	13.3	2589	0.33	0.1320 ± 0.23	1.233 ± 0.24	0.0677 ± 0.07	799 ± 3	816 ± 3	861 ± 3	0.96	7.60
z19 (L,D,CL)*	0.0070	453.7	63.6	13.6	2081	0.23	0.1428 ± 0.29	1.358 ± 0.27	0.0690 ± 0.08	861 ± 4	871 ± 3	897 ± 3	0.95	4.40
z20 (E,D,CL)*	0.0061	674.6	228.3	9.76	8938	0.08	0.3415 ± 0.12	6.078 ± 0.13	0.1291 ± 0.04	1894 ± 4	1987 ± 2	2085 ± 1	0.96	10.6
z21 (E,D,CL)*	0.0087	489.4	242.2	15.2	7809	0.39	0.4487 ± 0.14	10.62 ± 0.15	0.1716 ± 0.03	2389 ± 6	2490 ± 3	2574 ± 1	0.97	8.60
z22 (E,D,CL)*	0.0128	82.2	10.4	20.6	306	1.71	0.0912 ± 0.28	0.839 ± 0.58	0.0667 ± 0.45	563 ± 3	619 ± 5	830 ± 19	0.66	33.6
z23 (E,D,CL)*	0.0157	629.3	81.0	21.9	3735	0.14	0.1330 ± 0.25	1.229 ± 0.26	0.0670 ± 0.07	804 ± 4	814 ± 3	839 ± 3	0.96	4.40
W49z - Augen Gneiss, Wangtu Gneiss Complex, Jutogh Group														
Z1 (M,U,CR,I)	0.0136	214.6	74.7	26.6	2224	0.52	0.3194 ± 0.08	5.002 ± 0.25	0.1136 ± 0.21	1787 ± 3	1820 ± 4	1858 ± 8	0.61	4.40
Z2 (M,U,CR,OP)	0.0106	357.9	120.4	23	3324	0.51	0.3094 ± 0.10	4.815 ± 0.12	0.1129 ± 0.06	1738 ± 3	1788 ± 2	1846 ± 2	0.89	6.70
Z3 (M,U,I,CR,)	0.0131	16.6	5.9	30.9	1484	0.59	0.3217 ± 0.10	5.032 ± 0.15	0.1134 ± 0.09	1798 ± 3	1825 ± 3	1855 ± 3	0.78	3.50
Z4 (M,U,CR,I)	0.0104	281.9	98.3	66.4	928.5	0.54	0.3185 ± 0.08	4.984 ± 0.16	0.1135 ± 0.12	1783 ± 2	1817 ± 3	1856 ± 4	0.73	4.50
Z6 (M,U,CR)	0.0033	320.1	121.4	6.2	3615	0.82	0.3255 ± 0.10	5.099 ± 0.17	0.1136 ± 0.12	1816 ± 3	1836 ± 3	1858 ± 4	0.74	2.60
W34z - Metasediment, Vaikrita Group														
Z7 (D,E,CL,I,R)	0.0087	424.6	60.1	10.8	3048	0.26	0.1434 ± 0.16	1.352 ± 0.18	0.0684 ± 0.07	864 ± 3	869 ± 2	880 ± 2	0.92	2.00
Z8 (D,R,PI,CL)	0.0130	554.3	81.5	11.6	5805	0.26	0.1480 ± 0.06	1.575 ± 0.10	0.0772 ± 0.07	890 ± 1	961 ± 1	1126 ± 3	0.77	22.5
Z9 (D,CL,R,S)	0.0060	206.4	29.1	9.35	1076	0.73	0.1268 ± 0.11	1.173 ± 0.50	0.0671 ± 0.5	769 ± 2	788 ± 5	842 ± 19	0.53	9.10
Z10 (D,CL,R,I)	0.0056	368.7	183.6	20.9	2708	0.62	0.4315 ± 0.07	9.895 ± 0.09	0.1663 ± 0.05	2313 ± 3	2425 ± 2	2521 ± 2	0.88	9.80
Z11 (D,R,E,CL)	0.0062	988.5	451.2	12.4	13610	0.2	0.4346 ± 0.06	9.931 ± 0.08	0.1657 ± 0.03	2327 ± 2	2428 ± 1	2515 ± 1	0.94	8.90
Z12 (D,R,CL,E)	0.0062	521.7	74.7	7.78	3491	0.61	0.1325 ± 0.08	1.228 ± 0.20	0.0672 ± 0.17	802 ± 1	814 ± 2	845 ± 7	0.56	5.30
Z13 (D,R,CL,E)	0.0024	478.3	65.8	24.9	391.4	0.57	0.1288 ± 0.22	1.191 ± 0.69	0.0671 ± 0.57	781 ± 3	796 ± 8	840 ± 24	0.66	7.40
W60z - Jutogh Metasediment, Jutogh Group														
Z14 (D,E,R,I,CL)	0.0135	305.7	137.1	9.99	10170	0.67	0.3903 ± 0.06	7.656 ± 0.08	0.1423 ± 0.03	2124 ± 2	2191 ± 1	2255 ± 1	0.91	6.80
Z15 (D,L,S,CL)	0.0141	410.9	145.4	6.11	20860	0.19	0.3489 ± 0.23	5.980 ± 0.23	0.1238 ± 0.03	1930 ± 8	1970 ± 4	2012 ± 1	0.99	4.80
Z16 (D,S,CL,I)	0.0073	417.1	163.7	19.9	3700	0.17	0.3829 ± 0.06	7.506 ± 0.09	0.1422 ± 0.04	2090 ± 2	2174 ± 2	2254 ± 2	0.88	8.50
Z17 (D,R,E,I,CL)	0.0080	471.1	210.5	3.88	23670	0.7	0.3861 ± 0.09	7.593 ± 0.10	0.1426 ± 0.03	2105 ± 3	2184 ± 2	2260 ± 1	0.95	8.00
Z18 (D,R,E,CL)	0.0082	600.1	138.7	6.57	10380	0.3	0.2194 ± 0.17	4.209 ± 0.18	0.1391 ± 0.04	1279 ± 4	1676 ± 3	2217 ± 1	0.97	46.50
Z19 (D,R,E,CL)	0.0053	407.0	154.0	4.52	10980	0.25	0.3648 ± 0.09	6.784 ± 0.12	0.1349 ± 0.05	2005 ± 3	2084 ± 2	2163 ± 2	0.91	8.50
Z20 (D,E,R,CL,I)	*failed*	*failed*	*failed*	*failed*	*failed*	*failed*	*failed*	*failed*	*failed*	*failed*	*failed*	*failed*	*failed*	*failed*
W58z - Quartzite, Rampur Formation, Rampur Window														
Z21 (D,R,E,CL,CR)	0.0444	452.7	164.4	12.9	34540	0.27	0.3524 ± 0.10	5.809 ± 0.11	0.1196 ± 0.03	1946 ± 13	1948 ± 2	1950 ± 1	0.97	0.20
Z22 (D,R,E,CL,I,PI)	0.0325	851.0	302.3	7.57	76920	0.42	0.3341 ± 0.84	5.252 ± 0.84	0.1140 ± 0.03	1858 ± 27	1861 ± 14	1864 ± 1	1.00	0.40
Z23 (D,R,CL,CR)	0.0206	317.5	119.4	7.73	17860	0.66	0.3349 ± 0.07	5.275 ± 0.09	0.1142 ± 0.03	1862 ± 3	1865 ± 2	1868 ± 1	0.94	0.40
Z24 (D,R,CL)	0.0156	351.4	134.0	4.87	23680	0.74	0.3336 ± 0.12	5.244 ± 0.13	0.1140 ± 0.04	1856 ± 4	1860 ± 2	1864 ± 1	0.96	0.50
Z25 (D,R,CL,E)	0.0139	775.0	281.2	4.19	54170	0.5	0.3345 ± 0.06	5.267 ± 0.08	0.1142 ± 0.03	1860 ± 2	1864 ± 1	1867 ± 1	0.94	0.40
Z26 (D,EL,R,CL)	0.0084	313.3	116.6	4.77	11660	0.61	0.3349 ± 0.08	5.281 ± 0.11	0.1144 ± 0.05	1862 ± 3	1866 ± 2	1870 ± 2	0.87	0.50
Z27 (D,R,CL,I)	0.0108	307.8	112.7	4.78	14700	0.54	0.3348 ± 0.06	5.280 ± 0.09	0.1144 ± 0.05	1862 ± 2	1866 ± 2	1870 ± 2	0.88	0.50

[a] Single grain analysis unless statated; fraction identifiers; MG;n, multigrain analysis;n; number of grains; D, detrital; M, magmatic; U, euhedral; S, subhedral; A, anhedral; P, prismatic; E, equant; L, elongate; O, oval; CR, cracks; T, tabular; I, inclusions; PI, pitted; OP, opaque; CL, clear; R, rounded.
[b] Calculated assuming all ^{204}Pb in analysis is blank.
[c] Corrected for spike contribution and instumental bias.
[d] Determined based on measured ^{206}Pb.
[e] Determined ratios corrected for instrumental biases, spike, blank, and common lead. Errors are 1σ.
[f] Errors are 2σ.
[g] Correlation coefficient.
[h] % Discordance, discordant calculated with respect to the origin.
* Fractions analyised in second chemistry batch with Bhutan zircons

Table C.2 - U-Pb isotopic data from analysed zircons from Bhutan.

Fraction Number[a]	Fraction weight (mg)	U (ppm)	Pb (ppm)	Blank Pb pg)[b]	$^{206}Pb/^{204}Pb$[c]	Th/U[d]	$^{206}Pb/^{238}U$*	$^{207}Pb/^{235}U$*	$^{207}Pb/^{206}Pb$*	$^{206}Pb/^{238}U$ age†	$^{207}Pb/^{235}U$ age†	$^{207}Pb/^{206}Pb$ age†	Cc [e]	% dis[h]
RP109 - Metarhyolite, Daling-Shumar Group, LHS														
Z26 (U)	0.0016	295.1	95.9	19.8	488	0.25	0.3188 ± 1.08	4.912 ± 1.38	0.1117 ± 0.94	1784 ± 34	1804 ± 23	1827 ± 34	0.74	2.7
Z27 (U,MG;12)	0.0388	4.9	1.43	22.9	14780	0.25	0.2847 ± 0.23	4.3635 ± 0.24	0.1111 ± 0.04	1619 ± 7	1705 ± 4	1819 ± 1	0.99	12.7
Z1 (U,MG;2)*	0.0122	370.09	116.3	2.9	1874	0.3	0.3039 ± 0.35	4.8431 ± 0.38	0.1156 ± 0.10	1711 ± 11	1792 ± 6	1889 ± 4	0.97	10.8
Z2 (U,MG;3)*	0.0107	280.87	89.45	3.1	1710	0.44	0.2990 ± 0.25	4.5843 ± 0.27	0.1112 ± 0.08	1686 ± 8	1746 ± 5	1819 ± 3	0.96	8.3
Z3 (U,MG;3)*	0.0113	264.56	90.35	0.4	13436	0.32	0.3289 ± 0.13	5.1068 ± 0.15	0.1126 ± 0.05	1833 ± 4	1837 ± 3	1842 ± 2	0.95	0.6
Z4, (U)*	0.0015	320.72	101.7	3.3	1756	0.27	0.3082 ± 0.26	4.6635 ± 0.28	0.1097 ± 0.10	1732 ± 8	1761 ± 5	1795 ± 4	0.93	4
Z5, (U)*	0.0018	306.13	95.56	2.8	2150	0.16	0.3138 ± 0.22	4.7277 ± 0.24	0.1093 ± 0.90	1759 ± 7	1772 ± 4	1788 ± 3	0.93	1.8
M1*	0.0269	4019.6	50.1	4.7	341	-	0.0031 ± 0.23	0.0199 ± 0.62	0.0460 ± 0.50	20 ± 0	20 ± 0	neg.	0.67	neg.
M2(T)*	0.0025	5566.5	61.07	24.2	70	10.54	0.0028 ± 0.92	0.0186 ± 3.29	0.0478 ± 2.74	18 ± 0	19 ± 0	-	0.68	-
M3(L)*	0.0005	865.32	336.5	2.5	246	37.65	0.0370 ± 0.52	0.5400 ± 0.84	0.1057 ± 0.58	234 ± 2	438 ± 6	1727 ± 21	0.73	73
M4(A)*	0.0018	467.14	199.6	1.9	791	12.54	0.1034 ± 0.32	1.5409 ± 0.43	0.1055 ± 0.28	634 ± 4	930 ± 5	1724 ± 10	0.79	66.3
RP110 - Biotite augen gneiss, Daling-Shumar Group, LHS														
Z24 (U)	0.0034	374.8	148.9	25.4	1589.0	0.41	0.3657 ± 0.10	7.166 ± 0.13	0.1421 ± 0.08	2009 ± 3	2132 ± 2	2253 ± 3	0.81	12.6
Z25 (U,MG;11)	0.0376	438.0	137.2	87.2	3831.6	0.35	0.2998 ± 0.37	4.574 ± 0.35	0.1106 ± 0.16	1691 ± 11	1744 ± 6	1810 ± 6	0.90	7.50
Z1 (U,O)*	0.0111	438.77	156.7	1.7	3299	0.24	0.3467 ± 0.24	6.1214 ± 0.26	0.1280 ± 0.12	1919 ± 8	1993 ± 5	2071 ± 4	0.88	8.5
Z2 (U,MG;4)*	0.0131	323.74	113.3	1	5455	0.29	0.3378 ± 0.28	5.5935 ± 0.28	0.1200 ± 0.13	1876 ± 9	1915 ± 5	1958 ± 5	0.9	4.8
Z3 (U,MG;6)*	0.0089	289.43	78.86	5.5	712	0.31	0.2624 ± 0.24	4.2520 ± 0.38	0.1175 ± 0.30	1502 ± 6	1684 ± 6	1919 ± 11	0.62	24.3
Z4 (U,MG;6)*	0.0076	282.33	76.6	0.2	5908	0.23	0.2676 ± 0.17	4.1442 ± 0.18	0.1123 ± 0.08	1529 ± 5	1633 ± 3	1837 ± 3	0.9	18.9
Z5 (U,MG;7)*	0.0065	57.48	19.48	4.08	1408	0.25	0.3303 ± 0.27	5.4619 ± 0.29	0.1200 ± 0.08	1840 ± 9	1895 ± 5	1956 ± 3	0.96	6.8
Z6 (U)*	0.0024	478.72	143.5	1.8	3215	0.33	0.2887 ± 0.33	4.4280 ± 0.34	0.1113 ± 0.12	1635 ± 10	1718 ± 6	1820 ± 4	0.94	11.5
Z7 (U,CR,MG;2)*	0.0073	136.78	42.99	13.3	390	0.26	0.3084 ± 0.38	4.6561 ± 0.53	0.1095 ± 0.31	1733 ± 12	1759 ± 9	1791 ± 11	0.82	3.7
Z8 (U)*	0.0035	343.3	120.1	0.9	6551	0.46	0.3257 ± 0.21	5.0947 ± 0.22	0.1135 ± 0.06	1817 ± 7	1835 ± 4	1856 ± 2	0.97	2.4
Z9 (U,T)*	0.0021	343.93	109.9	2	2812	0.55	0.2934 ± 0.28	4.2493 ± 0.29	0.1050 ± 0.09	1659 ± 8	1684 ± 5	1715 ± 3	0.96	3.7
Z10 (U,O)*	0.0013	865.09	318.6	2.6	2086	0.35	0.3453 ± 0.23	6.7107 ± 025	0.1409 ± 0.08	1912 ± 8	2074 ± 4	2239 ± 3	0.94	16.8
B75z - Quartzite, Daling-Shumar Group														
z1 (D,A,E,CL)	0.0067	94.76	36.21	50.3	283.5	0.60	0.3428 ± 0.19	5.755 ± 0.43	0.1218 ± 0.34	1899 ± 6	1939 ± 7	1982 ± 12	0.66	4.8
z2 (D,A,E)	0.0044	160.42	91.01	375	71.28	0.76	0.4780 ± 0.98	11.01 ± 2.09	0.1672 ± 0.97	2518 ± 41	2524 ± 25	2529 ± 33	0.7	5
z3 (D,A,L)	0.0107	201.8	75.50	50.3	283.5	0.46	0.3470 ± 0.24	5.742 ± 0.28	0.1200 ± 0.11	1920 ± 8	1938 ± 5	1956 ± 4	0.91	2.1
z4 (D,A,E,CL)	0.0042	41.40	15.20	43.1	853.9	0.53	0.3354 ± 0.13	5.494 ± 0.19	0.1188 ± 0.11	1865 ± 4	1900 ± 3	1938 ± 4	0.8	4.4
z5 (D,A,E)	0.0045	309.2	110.80	56	557.2	0.21	0.3521 ± 0.31	5.970 ± 0.36	0.1223 ± 0.17	1944 ± 10	1972 ± 6	2000 ± 6	0.88	3.2
z6 (D,A,E)	0.0050	328.6	105.1	47.5	696.5	0.2	0.3176 ± 0.12	4.995 ± 0.22	0.1141 ± 0.15	1778 ± 4	1818 ± 4	1865 ± 5	0.76	5.3
z7 (D,A,E)	0.0050	*failed*	*failed*	*failed*	*failed*	*failed*	*failed*	*failed*	*failed*	*failed*	*failed*	*failed*	*failed*	*failed*
z8 (D,CL,A,E)	0.0039	209.2	77.3	12.2	1422	0.5	0.3395 ± 0.15	5.575 ± 0.18	0.1191 ± 0.08	1884 ± 5	1912 ± 3	1943 ± 3	0.89	3.5
z9 (D,A,E)	0.0037	189.2	97.8	7	2764	0.69	0.4436 ± 0.16	9.749 ± 0.17	0.1594 ± 0.06	2366 ± 9	2411 ± 3	2449 ± 2	0.93	4
z10 (D,A,E)	0.0038	140.7	51.28	4.9	283.5	0.51	0.3351 ± 0.17	5.452 ± 0.18	0.1180 ± 0.01	1863 ± 5	1893 ± 3	1926 ± 4	0.84	3.8
z11 (D,A,E)	0.0048	423	139.8	60.9	283.5	0.14	0.3308 ± 1.06	5.537 ± 1.08	0.1214 ± 0.21	1842 ± 34	1906 ± 19	1977 ± 8	0.98	7.8
z12 (D,A,E)	0.0046	391	129.2	8.5	4203	0.27	0.3210 ± 0.11	5.175 ± 0.12	0.1169 ± 0.05	1795 ± 4	1849 ± 2	1910 ± 2	0.93	6.9
z13 (D,A,L)	0.0048	179.8	63.3	10.4	1718	0.42	0.3309 ± 1.16	5.179 ± 1.16	0.1135 ± 0.09	1843 ± 37	1849 ± 20	1856 ± 3	1	0.8
z14 (D,A,E)	0.0041	113.9	39.9	8.85	1073	0.5	0.3234 ± 0.18	5.055 ± 0.20	0.1134 ± 0.10	1806 ± 6	1829 ± 3	1854 ± 4	0.86	3
z15 (D,A,L)	0.0037	209.7	72.6	9.01	1715	0.51	0.3183 ± 0.11	5.067 ± 0.13	0.1154 ± 0.08	1782 ± 3	1831 ± 2	1887 ± 3	0.8	6.4
RP 52 - Quartzite, Barsong Formation, LHS.														
Z1(D,E)*	0.0046	295.89	125	0.5	10657	0.21	0.4069 ± 0.17	8.2842 ± 0.18	0.1477 ± 0.06	2201 ± 6	2263 ± 3	2319 ± 2	0.94	6
Z2 (D,R)*	0.0039	114.96	43.6	2.7	1773	1.13	0.3065 ± 0.44	4.5000 ± 0.44	0.1065 ± 0.13	1723 ± 13	1731 ± 7	1741 ± 5	0.96	1.1
Z3 (D,E,CR)*	0.003	597.1	225.4	0.4	14651	0.41	0.3541 ± 0.17	5.8556 ± 0.18	0.1199 ± 0.06	1954 ± 6	1955 ± 3	1955 ± 2	0.94	0.1
Z4 (D,E)*	0.0042	461.22	103.5	1	6050	0.16	0.2300 ± 0.18	2.7737 ± 0.20	0.0875 ± 0.07	1334 ± 4	1349 ± 3	1371 ± 3	0.94	3
Z5 (D,L)*	0.0018	153.59	49.19	6.5	788	0.77	0.2805 ± 0.46	3.8346 ± 0.48	0.0992 ± 0.16	1594 ± 13	1600 ± 8	1608 ± 6	0.95	1
Z6 (D,O)*	0.0018	1780.2	779.3	0.4	13474	0.43	0.3964 ± 0.18	8.8980 ± 0.19	0.1628 ± 0.05	2153 ± 7	2328 ± 3	2485 ± 2	0.97	15.7
Z7 (D,T)*	0.0013	333.32	117.5	3.5	1461	0.89	0.2997 ± 0.28	4.4392 ± 0.30	0.1074 ± 0.11	1690 ± 8	1720 ± 5	1756 ± 4	0.93	4.3
Z8 (D,O)*	0.006	110.81	61.06	16.3	296	0.54	0.4850 ± 1.28	11.361 ± 1.30	0.1699 ± 0.22	2549 ± 54	2553 ± 24	2557 ± 7	0.99	0.4
Z9 (D,L)*	0.0011	1871.3	890	0.2	32576	0.43	0.4307 ± 0.18	9.6688 ± 0.19	0.1628 ± 0.45	2309 ± 7	2404 ± 4	2485 ± 2	0.97	8.4
RP 51 - Mica schist from the upper MCT zone, Jaishidanda Formation.														
M1(A)*	0.0032	4218.5	61.87	14.8	111	-	0.0037 ± 0.57	0.0220 ± 3.33	0.0430 ± 3.03	24 ± 0	22 ± 2	-	0.58	neg.
M2(A)*	0.0012	1351.7	21.79	20.3	71	13.51	0.0035 ± 1.14	0.0222 ± 7.08	0.0466 ± 6.44	22 ± 1	22 ± 3	-	-	neg.
M3(A)*	0.0017	5962.9	75.58	14.4	121	-	0.0035 ± 0.48	0.0217 ± 1.92	0.0452 ± 1.65	22 ± 0	22 ± 1	-	0.66	neg.
M4(A)*	0.001	3349.6	49.62	20.2	79	-	0.0036 ± 0.72	0.0219 ± 4.20	0.0437 ± 3.77	23 ± 0	22 ± 2	-	0.65	neg.
M5(A)*	0.0007	4854.6	58.4	24	73	9.75	0.0033 ± 0.78	0.0220 ± 4.10	0.0479 ± 3.62	22 ± 0	22 ± 2	-	-	neg.
RP 69 - Augen gneiss, Takhtsang Formation above Kakhtang thrust, Thimphu Group, HHCS.														
Z1 (U,L)*	0.0038	533.22	67.06	2.4	2517	0.23	0.1286 ± 0.14	1.193 ± 0.18	0.0673 ± 0.01	780 ± 2	797 ± 2	847 ± 4	0.84	8.5
Z2 (U,L)*	0.0092	432.99	52.09	2.9	2085	0.24	0.1227 ± 0.16	1.1289 ± 0.20	0.0667 ± 0.12	741 ± 2	767 ± 2	829 ± 5	0.81	10.6
Z3 (U)*	0.0085	304.74	37.18	2	2998	0.42	0.1860 ± 0.17	1.0898 ± 0.19	0.0666 ± 0.10	723 ± 2	748 ± 2	827 ± 10	0.86	13.3
Z4 (U,MG;2)*	0.0036	424.19	37.45	7.3	813	0.25	0.0899 ± 0.31	0.8235 ± 0.39	0.0664 ± 0.23	555 ± 3	610 ± 4	820 ± 10	0.81	33.7
M1(A)*	0.0044	1571.2	1393	0.1	2897	61.41	0.0512 ± 0.54	0.4617 ± 0.56	0.0654 ± 0.20	322 ± 3	385 ± 4	788 ± 9	0.93	60.7
M2(A)*	0.056	2097.2	865.1	0.1	4789	42.53	0.0336 ± 1.13	0.3036 ± 1.18	0.0655 ± 0.15	213 ± 5	269 ± 6	791 ± 6	0.99	74.3
M3(A)*	0.0046	5788.3	254.3	0.45	1449	32.16	0.0045 ± 025	0.0349 ± 0.32	0.0557 ± 0.21	29 ± 0	35 ± 0	439 ± 10	0.74	93.5
M4(A)*	0.0022	50526	401.7	2.4	754	9.29	0.0023 ± 0.67	0.0145 ± 0.71	0.0461 ± 0.23	15 ± 0	15 ± 0	-	0.95	neg.
M5*	0.0086	5080.6	37.32	4.7	402	-	0.0023 ± 0.24	0.0142 ± 0.65	0.0457 ± 0.56	15 ± 1	14 ± 0	-	0.55	neg.
M6*	0.0025	5452.3	40.24	3.5	532	8.66	0.0022 ± 0.28	0.0142 ± 0.62	0.0463 ± 0.50	14 ± 0	14 ± 0	-	0.6	neg.
M7, (T)*	0.0013	5781.4	43.88	6.7	266	-	0.0022 ± 0.81	0.0134 ± 2.69	0.0445 ± 2.50	14 ± 0	14 ± 0	-	0.38	neg.

RP 71 - Quartzite, Naspe Formation, Thimphu Group, HHCS.

Th(E,L)*	0.0022	16339	8146	3.17	12904	42.53	0.0406 ± 0.44	0.3658 ± 0.44	0.0653 ± 0.15	257 ± 2	317 ± 2	785 ± 6	0.94	68.7
Z1 (D,U)*	0.002	517.34	87.86	7.9	671	0.62	0.1566 ± 0.44	1.5668 ± 0.50	0.0726 ± 0.30	938 ± 8	957 ± 6	1001 ± 72	0.8	6.8
Z2 (D,U)*	0.0018	326.74	53.61	4.9	1211	0.32	0.1630 ± 0.23	1.6120 ± 0.31	0.0717 ± 0.20	974 ± 4	975 ± 4	978 ± 8	0.75	0.4
Z3 (D,E)*	0.0046	324.66	94.75	0.71	8464	0.2	0.2898 ± 0.33	4.4557 ± 0.34	0.1115 ± 0.06	1641 ± 10	1723 ± 6	1824 ± 2	0.98	11.4
Z4(D,O,pink)*	0.003	415.46	74.99	5.6	1011	0.45	0.1732 ± 0.23	1.8114 ± 0.28	0.0759 ± 0.16	1030 ± 4	1050 ± 4	1091 ± 7	0.82	6.1
Z5 (D,L,pink)*	0.0041	311.5	57.34	2.4	2255	0.71	0.1651 ± 0.19	1.8947 ± 0.23	0.0832 ± 0.13	985 ± 3	1079 ± 3	1275 ± 5	0.82	24.5
Z6 (D,O,pink)*	0.0058	458.99	106.2	12.8	399	0.45	0.2178 ± 024	2.5788 ± 0.44	0.0859 ± 0.32	1270 ± 5	1295 ± 6	1336 ± 12	0.71	5.4
Z7 (D,E,pink)*	0.0029	193.1	40.91	7.1	753	0.54	0.1964 ± 0.23	2.5382 ± 0.27	0.0937 ± 0.13	1156 ± 5	1283 ± 4	1503 ± 5	0.87	25.2
Z8 (D,O)*	0.0018	459.02	120.9	5.9	897	0.57	0.2462 ± 0.23	3.3206 ± 0.26	0.0978 ± 0.14	1419 ± 6	1486 ± 4	1583 ± 5	0.84	11.6
Z9 (D,O)*	0.0025	241.82	66.22	3.9	1377	0.69	0.2444 ± 0.22	3.2868 ± 0.25	0.0975 ± 0.12	1410 ± 6	1478 ± 4	1578 ± 4	0.89	11.9

[a]Single grain analysis unless statated; fraction identifiers; MG, multigrain analysis;n; number of grains; D, detrital; T, magmatic; U, euhedral; S, subhedral; A, anhedral; P, prismatic; E, equant; L, elongate; O, oval; CR, cracks; T, tabular.

[b]Calculated assuming all ^{204}Pb in analysis is blank.

[c]Corrected for spike contribution and instumental bias.

[d]Determined based on measured ^{206}Pb.

[e]Determined ratios corrected for instrumental biases, spike, blank, and common lead. Errors are 1σ.

[f]Errors are 2σ.

[g]Correlation coefficient.

[h]% Discordance, discordant calculated with respect to the origin.

* Fraction analyised by K. Thimm

Appendix D – Sample Catalogue

This appendix contains a comprehensive list of rock samples collected from the both the Sutlej and Bhutan sections.

Notes:

Location maps for samples from the Bhutan section follow, samples locations are included in Figure 2.2 for the Sutlej section.

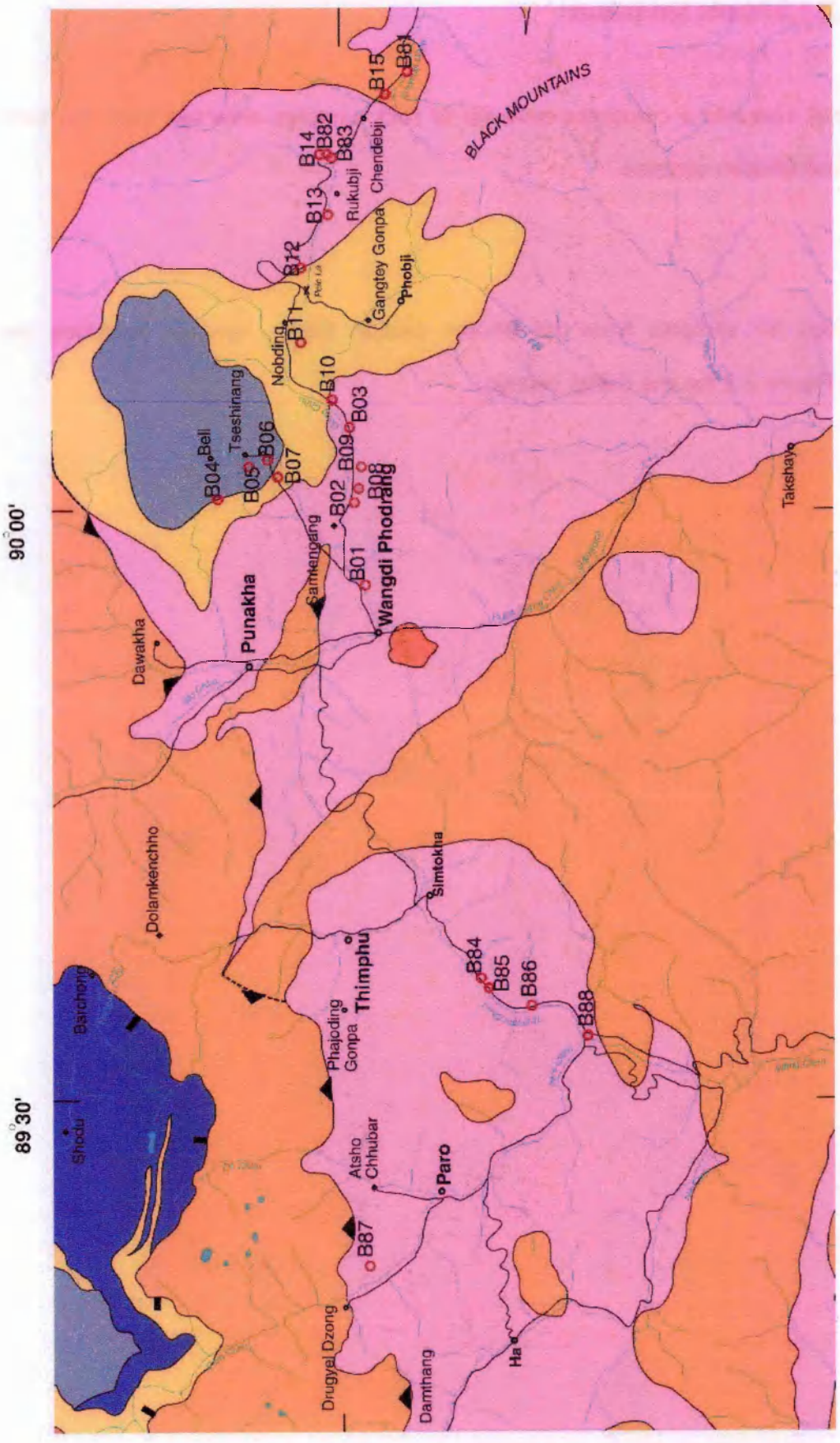
90°00'
89°30'
27°30'
BLACK MOUNTAINS
B15
B81
B14
B82
B83
Chendebji
Rukubji
B13
B12
Gangtey Gonpa
Phobji
Nobding
B11
B10
B03
B09
B08
B02
B01
Wangdi Phodrang
Samtengang
B04
Bell
Tseshinang
B05
B06
B07
Punakha
Dawakha
Takshaya
Dolamkenchho
Simtokha
Thimphu
B84
B85
B86
B88
Phajoding Gonpa
Barchong
Shodu
Atsho Chhubar
Paro
B87
Drugyel Dzong
Damthang
Ha

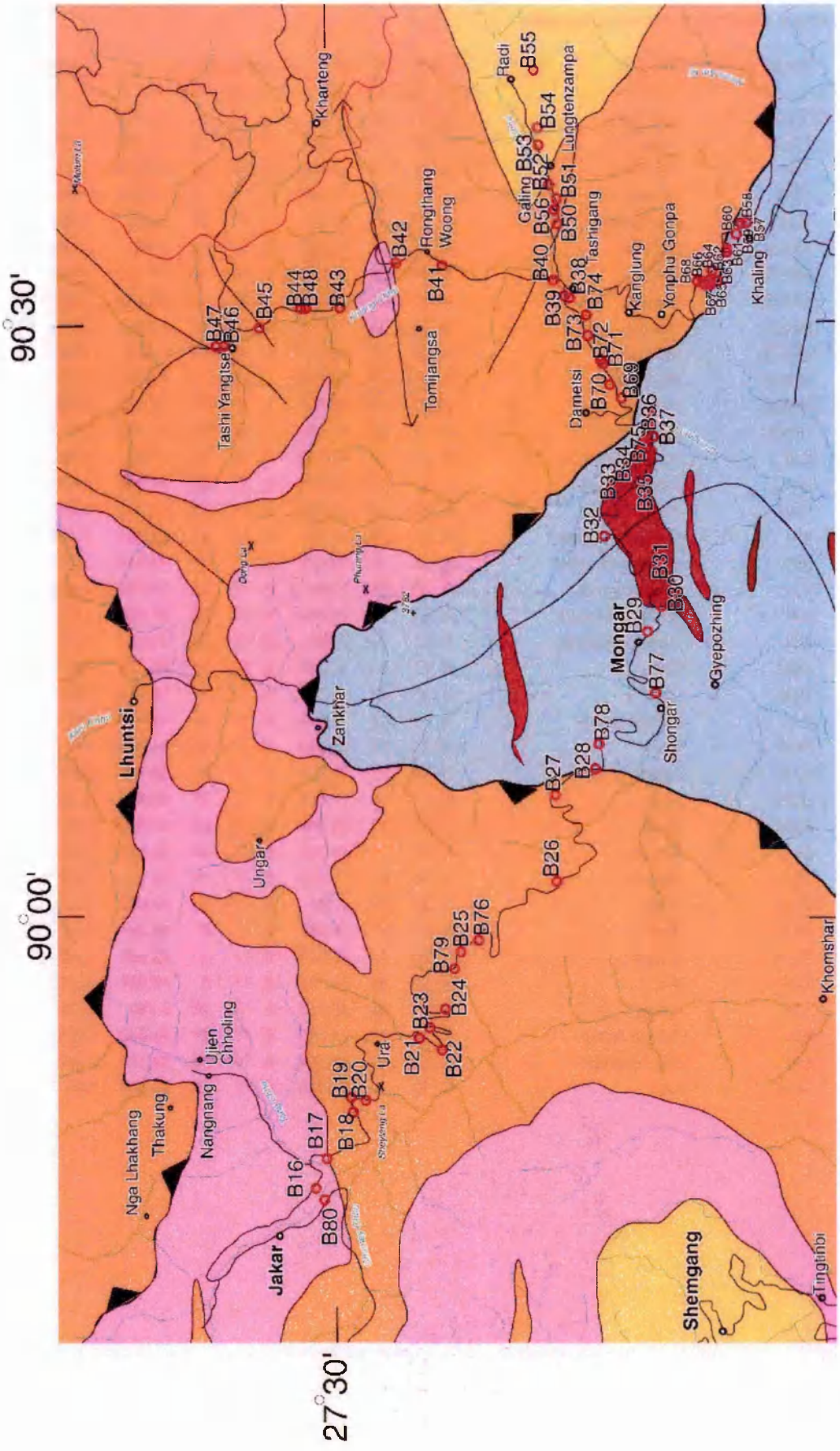
90°30'
90°00'
27°30'
Lhuntsi
Jakar
Shemgang
Mongar
Khomshar
Tingtibi
Gyepozhing
Shongar
Zankhar
Ungar
Nga Lhakhang
Thakung
Nangnang
Ujien Chholing
Ura
Tashi Yangtse
Tomijangsa
Rongthang
Woong
Kharteng
Radi
Lungtenzampa
Tashigang
Kanglung
Yonphu Gonpa
Khaling
Dametsi
B17
B16
B80
B18
B19
B20
B21
B23
B22
B24
B79
B25
B76
B26
B27
B28
B78
B77
B29
B30
B31
B32
B33
B35
B36
B37
B70
B69
B71
B72
B73
B74
B39
B38
B40
B56
B53
B52
B51
B50
B54
B55
B41
B42
B43
B44
B48
B45
B46
B47

Table D.1 – Sample Catalogue for Sutlej samples.

Sample No.	Tectonic Unit	Fm/Grp	Latitude				Longitude				Elevation
				deg	min	sec		deg	min	sec	
W03	TSS	Hiamanta	N	31	35	7.332	E	78	26	32.460	2302
W06	HHCS	Vaikrita	N	31	35	7.332	E	78	22	17.724	2313
W18	TSS	Hiamanta	N	31	48	24.408	E	78	24	34.272	3109
W19	TSS	Haimanta	N	31	42	27.900	E	78	32	10.500	2362
W25b	TSS	Haimanta	N	31	37	8.760	E	78	26	5.028	2288
W30.1	HHCS	Viakrita	N	31	35	23.784	E	78	22	6.420	2140
W35	HHCS	Vaikrita	N	31	35	52.476	E	78	18	11.160	2093
W36	HHCS	Viakrita	N	31	35	33.972	E	78	17	29.868	2168
W41	HHCS	Viakrita	N	31	33	12.636	E	78	16	47.964	2638
W43	HHCS	MCT Zone	N	31	30	19.872	E	78	14	5.640	1847
W44	HHCS	MCT Zone	N	31	29	54.384	E	78	12	9.576	1930
W45	HHCS	Vaikrita	N	31	29	46.464	E	78	11	51.180	1818
W48	HHCS	MCT Zone	N	31	29	47.832	E	78	10	56.568	1841
W49	ILH	Jutogh Group	N	31	30	42.120	E	78	10	5.700	1885
W50	ILH	Jutogh Group	N	31	33	46.728	E	77	58	31.080	1608
W54	ILH	Jutogh Group	N	31	33	57.060	E	77	49	43.536	1693
W58	ILH	Rampur Window	N	31	29	6.720	E	77	41	22.560	1199
W59	ILH	Rampur Window	N	31	30	39.672	E	77	47	43.044	2169
W60	ILH	Jutogh Group	N	31	31	6.564	E	77	45	15.768	2199
W61SHA	ILH	Rampur Window	N	31	27	31.464	E	77	39	57.024	1107
W63	ILH	Rampur Window	N	31	24	7.920	E	77	38	3.624	1035
W64	OLH	Chail	N	31	23	14.964	E	77	37	32.124	996
W64	OLH	Chail	N	31	23	14.964	E	77	37	32.124	996
W65	ILH	Jutogh Group	N	31	22	51.420	E	77	32	53.448	926
W70	OLH	Chail	N	31	22	55.992	E	77	42	54.540	1434
W77	ILH	Jutogh Group	N	31	16	12.720	E	77	26	38.148	2464
W78	OLH	Chail	N	31	15	17.856	E	77	27	26.604	2722
W79	OLH	Chail	N	31	12	24.048	E	77	23	47.940	2427
W80	OLH	Shimla	N	31	7	44.112	E	77	20	58.020	2335
W83	OLH	Shimla	N	31	6	23.472	E	77	12	31.752	2252
W87	OLH	Chail	N	30	58	3.144	E	77	11	42.072	2135
W88	OLH	Krol	N	30	57	35.568	E	77	6	45.360	1423
W89	OLH	Subathu	N	30	57	28.944	E	77	0	42.660	1297
W91	OLH	Krol	N	30	58	58.152	E	77	8	49.668	1252
W92	ILH	Jutogh	N	30	48	48.132	E	77	26	2.796	2125
W95	ILH	Jutogh Group	N	30	47	25.080	E	77	27	41.040	1985
W99	ILH	Chor Granite	N	30	49	20.964	E	77	26	32.172	1992
W100	OLH	Krol	N	30	33	33.048	E	77	38	59.028	680

Table D.2 – Sample Catalogue for Bhutan samples.

Sample No.	Tectonic Unit	Fm/Grp	Latitude				Longitude				Elevation
				deg	min	sec		deg	min	sec	
B03	Tethys	Checkha	N	27	30	24.8	E	90	4	53.4	2027.1
B06	Tethys	Checkha	N	27	34	8.9	E	90	3	7.3	2133.5
B07	Tethys	Checkha	N	27	33	24.2	E	90	2	46.1	2082.3
B29a	LH	Daling-Shumar Group	N	27	16	19.4	E	91	14	52.1	1732.9
B29b	LH	Daling-Shumar Group	N	27	16	19.4	E	91	14	52.1	1732.9
B36a	LH	Daling-Shumar Group	N	27	15	54.6	E	91	23	49.3	991.5
B39	HHCS	Tashigang Crystaline Unit	N	27	20	18.3	E	91	32	45.7	788.6
B41	HHCS	Tashigang Crystaline Unit	N	27	25	55.6	E	91	34	11	929
B45	HHCS	Takhsang Crystaline Unit	N	27	35	1.5	E	91	29	51.8	1804.7
B50	HHCS	Tashigang Crystaline Unit	N	27	20	50.2	E	91	37	4.6	906.6
B51	HHCS	Tashigang Crystaline Unit	N	27	20	49.2	E	91	37	37.1	979
B52a	Tethys	Checkha	N	27	21	3.7	E	91	38	11.3	998.7
B54	Tethys	Checkha	N	27	21	35.1	E	91	41	14.9	1323.9
B57	LH	Daling-Shumar Group	N	27	12	5	E	91	36	3.4	2078
B60	LH	Daling-Shumar Group	N	27	12	58.6	E	91	34	44.2	2220
B62a	LH	Daling-Shumar Group	N	27	13	33.6	E	91	33	44.4	2169.6
B66	LH	Daling-Shumar Group (Barsor	N	27	13	57.2	E	91	32	59.8	2331.1
B68	HHCS	Tashigang Crystaline Unit	N	27	14	12.3	E	91	33	6.9	2369.3
B70	LH	Daling-Shumar Group	N	27	17	39.6	E	91	27	16.1	820.6
B71b	LH	Daling-Shumar Group	N	27	17	53.4	E	91	28	28.6	763.4
B75Z	LH	Daling-Shumar Group	N	27	16	6.1	E	91	23	44.4	894.6
B81	HHCS	Paro Meta seds (Candebi mel	N	27	27	24.7	E	90	22	3.9	2490.6
B83	HHCS	Paro Meta seds (Candebi mel	N	27	30	54.7	E	90	17	44.2	2690.4
B85	HHCS	Paro metaseds	N	27	23	24	E	89	35	14.5	2247.2
B87	HHCS	Takhsang Crystaline Unit	N	27	28	49.9	E	89	21	14.8	2585.1
B88	HHCS	Paro metaseds	N	27	18	52.7	E	89	32	55.3	2141.4

Appendix E – Conference Abstracts

Parts of this thesis have been presented at various international conferences during the course of this study and are listed below:

Richards, A.; Argles, T.; Harris, N.; Parrish, R.; Ahmad, T., Mapping the Himalaya: an integrated isotopic approach, 18th Himalayan-Karakoram-Tibet Workshop, Abstracts from the meeting held in Monte Verita, Switzerland, 2 – 4 April 2003.

Richards, A.; Argles, T.; Harris, N.; Parrish, R.; Ahmad, T., Isotopic mapping of major Himalayan structures, EGS - AGU - EUG Joint Assembly, Abstracts from the meeting held in Nice, France, 6 - 11 April 2003.

Reproduced with permission of copyright owner. Further reproduction prohibited without permission.